STUDY OF A WIDEBAND PROBE

Peter Alexander
Howard Salwen
SIGNATRON, Inc.,
27 Hartwell Avenue
Lexington, Massachusetts 02173

July 1972

Final Report

Prepared for

GODDARD SPACE FLIGHT CENTER
Greenbelt, Maryland, 20771

A-134

TECHNICAL REPORT STANDARD TITLE PAGE

1. Report No.	2. Government Accession No.	3. Recipient's Catalog No.

4. Title and Subtitle	5. Report Date
STUDY OF A WIDEBAND PROBE	July 1972
	6. Performing Organization Code

7. Author(s)	8. Performing Organization Report No.
Dr. Peter Alexander and Howard Salwen	A-134

9. Performing Organization Name and Address	10. Work Unit No.
SIGNATRON, INC. 27 Hartwell Ave. Lexington, Mass. 02173	11. Contract or Grant No. NAS5-21683
	13. Type of Report and Period Covered FINAL REPORT

12. Sponsoring Agency Name and Address	14. Sponsoring Agency Code
NASA Goddard Space Flight Center Greenbelt, Maryland 20771	L.Kleinberg/Code 750

15. Supplementary Notes

16. Abstract

This study analyzes the design of an experiment to measure communication characteristics of wideband satellite-to-ground links. Of special concern are the effects of rainstorms and atmospheric turbulence on path attenuation and phase fluctuation. Multi-tone and pulse probing are considered. A multi-tone technique which is a modification of ATS-5 and ATS-F hardware is recommended. Data extraction and data processing techniques and key hardware requirements for the experiment are reviewed.

17. Key Words (Selected by Author(s))	18. Distribution Statement
wideband communications, satellite-to-ground links, channel measurements, wideband channel probing	

19. Security Classif. (of this report)	20. Security Classif. (of this page)	21. No. of Pages	22. Price*
Unclassified	Unclassified	267 + viii	

*For sale by the Clearinghouse for Federal Scientific and Technical Information, Springfield, Virginia 22151.

PREFACE

This study analyzes the design of an experiment to measure communication characteristics of wideband satellite-to-ground links. Of special concern are the effects of rainstorms and atmospheric turbulance on path attenuation and phase fluctuation. The proposed experiments are to aid substantially in the accurate determination of the tolerance of typical communication systems to the various interference producing mechanisms.

The study estimates the expected range of channel parameters such as delay-Doppler scattering functions, range and frequency resolution requirements and dynamic range. Key hardware requirements are considered and data collection and analysis methods are investigated.

The study concludes with the recommendation of a modification of multi-tone techniques used in the ATS-5 and ATS-F experiments. Hardware analysis indicates advantages to the in-phase/quadrature approach of measurement implementation.

Recommendations include development of key components such as space-qualified, stable reference oscillators, IMPATT oscillators capable of operation above 20 GHz, and an efficient frequency synthesizer for the prober.

The authors of this report are Howard Salwen who was project engineer and Dr. Peter Alexander who was concerned with the analytic portions of the study. Contributing to this investigation was Dr. P.A. Bello. The Goddard Space Flight Center technical monitor was Leonard Kleinberg. Dr. Julian J. Bussgang and John N. Pierce edited the final report.

TABLE OF CONTENTS

Section		Page
1	INTRODUCTION	1-1
	1.1 Millimeter Wave Communications Systems	1-1
	1.2 Phenomena to be Observed	1-5
	1.3 State of Knowledge Summary	1-7
	1.4 Experimental Technique	1-9
	1.5 Organization of the Report	1-15
	Section 1 References	1-18
2	CHANNEL CHARACTERIZATION AND MEASUREMENT PHILOSOPHY	2-1
	2.1 General Channel Characteristics	2-1
	2.1.1 Description of the Model	2-1
	2.1.2 Discussion of Terminal Characteristics	2-4
	2.2 An Equivalent Filter Channel Model	2-6
	2.3 Statistical Properties of the Received Signal	2-10
	2.3.1 Definition of Parameters	2-10
	2.3.2 Correlation Function Properties	2-13
	2.3.3 Channel Properties for Low Scattered Signal Levels	2-15
	2.4 Channel Measurement Philosophy	2-19
	2.4.1 Extraction of Coherent Filter Parameters	2-20
	2.4.2 Measurement of Scattered Signal Properties	2-23
	Section 2 References	2-28
3	CHANNEL MEASUREMENT USING COHERENT TONES	3-1
	3.1 Form of the Transmitted Signal	3-1
	3.1.1 Phase Instabilities	3-6
	3.2 Basic Receiver Structure	3-8
	3.2.1 Carrier Tracking and Incremental Phase Correction Schemes	3-18
	3.2.2 Analysis of the Incremental Phase Correction Receiver	3-26

TABLE OF CONTENTS (Cont.)

Section		Page
	3.3 Application of Phase Locked Loops for Incremental Phase Correction	3-38
	Section 3 References	3-46
4	CHANNEL MEASUREMENT USING PULSES	4-1
	4.1 Basic Approach	4-1
	4.2 IF Signal to Noise Ratio Estimates	4-10
	4.3 Incoherent Pulse Measurements	4-11
	4.4 Coherent Pulse Processing	4-19
	4.5 Summary for Pulse Probing Techniques	4-22
5	EQUIPMENT CONFIGURATION	5-1
	5.1 Transmitter Configuration	5-1
	5.2 Receiver Design	5-7
	5.3 Compatibility with the ATS-F System	5-12
6	DATA PROCESSING REQUIREMENTS	6-1
	6.1 Processing of the Tone Responses	6-1
	6.1.1 Estimation Performance	6-6
	6.1.2 Summary of Tone Processing	6-13
	6.2 Collection and Processing of Auxiliary Data	6-16
	6.2.1 Meteorological Parameters of Interest	6-16
	6.2.2 Verification of Link Parameters Using Rainfall Data	6-21
	Section 6 References	6-22
7	CONCLUSIONS	7-1
	7.1 Channel Characterization and Measurement Approach	7-1
	7.2 Measurement Techniques	7-2
	7.3 Hardware and Data Processing Considerations	7-4
	7.4 Summary of Results and Recommendations	7-6

TABLE OF CONTENTS (Cont.)

	Page
APPENDIX A	
RAIN SCATTERING EFFECTS FOR THE LOS MILLIMETER WAVE SATELLITE LINK	A-1
APPENDIX B	
PREDICTION OF CHANNEL CHARACTERISTICS	B-1
APPENDIX C	
DELAY POWER SPECTRUM ESTIMATES FOR INTERFERING BEAMS	C-1
APPENDIX D	
INTERFERENCE EXPERIMENT CONFIGURATION DESIGN	D-1

LIST OF ILLUSTRATIONS

Figure		Page
1.1	Frequency Domain Channel Response to a Multi-Tone Spectrum	1-12
1.2	Incremental Phase Correction Procedure	1-13
2.1	Typical Path Geometry	2-2
2.2	Idealized Scattering Model	2-3
2.3(a)	Equivalent Filter Model	2-8
2.3(b)	Simplified Filter Model for the Channel	2-9
2.4	Vector Sum of Random and Coherent Signals	2-17
3.1	Transmitter	3-4
3.2	General Receiver Structure	3-9
3.3a	Phase Difference References	3-11
3.3b	Phase Sum Reference	3-13
3.4	Representation of Satellite Motion and Oscillator Instabilities	3-19
3.5	Complete Channel Model	3-20
3.6	Phase Locked Loop Structure	3-22
3.7	Simplified Phase Locked Loop Structure	3-23
3.8	Phase Locked Loop Design	3-25
3.9	Demodulator Design	3-27
3.10	Phase-Frequency Characteristics	3-28
3.11	Vector Sum of Scattered and Coherent Signal Showing Phase Correction Error	3-34
3.12	Phase Locked Loop Configuration	3-39
4.1	Pulse Modulation	4-2
4.2	Pulse Transmission and Response	4-5
4.3	Channel Response to a Sequence of Pulses	4-7
4.4	Pulse Probe Receiver	4-9
4.5	Incoherent Pulse Receiver	4-18
4.6	Coherent Pulse Receiver	4-21
4.7	Pulse Response Averaging	4-25

LIST OF ILLUSTRATIONS

Figure		Page
5.1	Transmitter Block Diagram	5-2
5.2	Approximate Transmitted Spectrum	5-4
5.3	Receiver Block Diagram	5-8
5.4	Receiver Frequency Synthesizer	5-11
5.5	20 GHz System Synthesizer	5-14
5.6	30 GHz System Synthesizer	5-15
6.1	Data Collection	6-2
6.2	Processing of In-Phase and Quadrature Data	6-3
6.3	Rain Gauge Configuration	6-18
6.4	Rain Gauge Data Acquisition	6-19
A.1	Coordinate System for Scattering from a Sphere	A-6
A.2	Single Scattering Model for Rain	A-7
A.3	Equivalent Propagation Medium for Rain	A-10
A.4	One-dimensional Scattering Model	A-17
A.5	Integral Weighting Functions	A-18
B.1	Rain Scattering Geometry	B-3
C.1	Beam Intersection Geometry	C-2
C.2	Delay Shell Intersection	C-4
C.3	Integration Geometry	C-5
C.4	Parameters for Evaluation of Ψ	C-8
C.5	Differential Attenuation	C-9
C.6	Path Loss vs Scan Coordinate R (Atmospheric Scattering)	C-15
C.7	Path Loss vs Scan Coordinate R (Rain Scattering)	C-16
C.8	Common Volume Dimensions	C-18
C.9	Antenna Beam Configuration	C-20

Figure		Page
C.10	ES Beam Pattern	C-21
C.11	Turbulence - Rain Storm Geometry	C-23
C.12	Ducting - Rain Storm Geometry	C-24
D.1	Intersection Geometry	D-2
D.2	Proposed Configuration	D-8
D.3	Antenna Pointing Coordinate System	D-10
D.4	Current RIPP Configuration	D-11
D.5	Common Volume Geometry	D-12
D.6	Intersection Geometry	D-15
D.7	Scan Patterns	D-18
D.8	Great Circle Paths	D-19
D.9	Orthogonal Mode	D-29
D.10	Orthogonal Configuration	D-31

SECTION 1
INTRODUCTION

1.1 Millimeter Wave Communications Systems

It is rapidly becoming evident that the expanding spectrum requirements of various radio communication services will soon stimulate the development of millimeter wave communication links. The millimeter wave portion of the spectrum, particularly the band from 30 GHz to 90 GHz, offers the use of potentially wide bandwidths and high gain antennas, and appears eminently suitable for high data rate satellite-to-ground links. This is especially true when one considers the performance gains and communication efficiency which may be realized by the use of time division multiplexing (TDM). Typically this approach results in very wide signal bandwidths thus necessitating a reexamination of the link characteristics, to determine whether or not such bandwidths can be supported.

Visions of the ultimate role of millimeter wave communications systems have been outlined in the literature for both synchronous satellite-to-ground and terrestrial links [1.1,1.2]. In both situations the overriding concern is that of attenuation due to intervening rain storms. For line of sight terrestial links this necessitates the use of reduced repeater spacings down to several miles to ensure adequate signal strengths. As a consequence wideband digital modulation with repeater regeneration becomes desirable if not necessary, to alleviate effects of interference and repeater noise.

Satellite systems must also be designed to take into account high attenuation levels due to rain in the atmosphere. In most instances the beam center-lines subtend an angle of 10^{o} or more with the horizon. so that the path traverses the atmosphere for only a few kilometers. Generally speaking this results in less severe scattering and attenuation effects than would be encountered over terrestial links, but nevertheless a substantial deterioration over free space propagation conditions takes place. This report is concerned exclusively with the modeling and analysis of satellite-to-ground data links.

There are several new problems encountered with the use of both higher carrier frequencies and wider bandwidths. For example, the move to higher frequency bands involves substantial increases in path attenuation and antenna beam diffraction effects, while the frequency dependence of the medium and multipath scattering result in an effective band limiting of the channel. The basic objective of this study is to investigate the link parameters which determine communication performance, and to outline various measurement techniques which might be used to evaluate such parameters in a millimeter wave experiment. Typical parameter values and their range of variation, are to be estimated from the experiment and related to the local climatological conditions where possible. The link characteristics of interest, which must be examined to allow prediction of communication link performance, can be grouped in the following way.

(a) Signal Fades

These will occur on a short time scale (seconds) due to multipath scattering, and on a larger time scale due to gross variations in the intervening medium. The depth and frequency of fades must be determined so that an adequate fade margin can be specified in the link design.

(b) Pulse Distortion

Because the signal transmitted between satellite and ground station traverses various layers which have frequency dependent refractive index properties, wide bandwidth signals are subject to an effective filtering and distortion. This will be particularly evident when a short pulse is transmitted. When the pulse length is reduced sufficiently, the original transmitted pulse becomes smeared in time. This effect severely limits the transmission of wideband data primarily because of intersymbol interference.

(c) Multipath Spread

When the medium has random structure, (e.g., atmospheric turbulence and rainstorms) the transmitted energy is scattered, thus attenuating the incident field. More importantly, the receiving system can then acquire signal components from other than the direct path. These scattered signals arrive with a variance of diverse time delays and contribute to further smearing of the signal as in topic (b). The principal difference here is that the scattered components are random in their behavior, hence requiring a characterization based on statistical properties.

(d) Doppler Spread

The scattering of energy from inhomogeneities along its path gives rise to a time varying distortion of the transmitted signal. The scattering medium is continually in motion so that individual scattering elements impose Doppler frequency shifts on the received components. The resultant spectral properties of the signal are thus determined by bulk and turbulent motion of the medium. Gross spectral parameters such as RMS Doppler spread of a transmitted sine wave are important to the communication engineer, since certain communication techniques are more susceptible to Doppler spreading than others.

It is apparent therefore that before the millimeter wave region can be seriously considered for high rate data links, a carefully designed characterization experiment must be implemented. Although such an experiment is closely coupled to studies of the physics of the atmosphere, it is essential that certain parameters which are important from the point of view of the communication problem, be measured.

A second area of research which will ultimately be of great importance is that of co-channel interference. By taking advantage of PCM modulation techniques, which are inherently less sensitive to interfering signals then conventional analog methods [1.3], and by utilizing the narrow antenna beamwidths in the millimeter wave region, it appears that dense communication networks will be feasible. Such networks, which will involve considerable overlapping of the frequency band assignments, are likely to be interference

rather than noise limited. There are various ways that energy from co-channel transmitters can be coupled into a given link, and the prediction of the resulting interference levels is obviously of an important problem. Some attention is given in Appendices C and D to interference which arises due to coupling of antenna beams.

1.2 Phenomena to be Observed

The transmission medium between satellite and receiver will be subject to marked variations due to changing weather conditions. Two of the most important atmospheric effects which distort the signal are associated with rainstorms and atmospheric turbulence. The former will be the one determining the worst case system performance but the latter is important because it will be the dominant propagation mechanism most of the time.

The channel characteristics are determined by the nature of the propagation medium and geometrical factors such as antenna pointing angles and beamwidths.

The received field for the millimeter wave channel can conveniently be thought of in terms of the sum of two components; a scattered incoherent signal, and a coherent but time invariant component. This can be clearly demonstrated for scattering by raindrops, since the exact solution for the field scattered by dielectric spheres can be stated explicitly [1.4]. Similarly, many theoretical analyses have been presented on the scattering effects of atmospheric inhomogeneities [1.5,1.6]. In both cases we are primarily concerned with a

statistical description of the field which results when a plane wave is incident on the medium. The total channel effect can be conveniently summarized by the use of a time varying transfer function H(f,t) such that,

$$H(f,t) = T_c(f)[1 + T_R(f,t)]$$

i.e., the response at time t to a sinusoid of frequency f.

The function $T_c(f)$ represents attenuation and phase shift characteristics of the medium as it affects the coherent transmitted component. It appears as a function of frequency because the clear atmosphere and rain storms both behave as dielectric material with a refractive index which is frequency dependent over very wide frequency bands. This gives rise to distortion of the broadband signals [1.7,1.8]. Note that pure constant attenuation or linear phase shift characteristics with frequency do not introduce any distortion effects; the received signal is a delayed, attenuated version of that transmitted.

The time varying filter $T_R(f,t)$ represents the scattered signal components. Its behavior as a function of t is determined by movement of the scattering elements with time (e.g., downward or turbulent motion of raindrops). The spectral width of T_R is usually referred to as the Doppler spread. The frequency dependence of T_R is related to the geometrical properties of the scatterer distribution, which also determine the multipath spread of the channel [1.9]. Note that $T_R(f,t)$ is a random function of both f and t. From a two dimensional

correlation analysis, both multipath spread and Doppler spread parameters can be obtained [1.10].

Provided sufficient information can be extracted about H(f,t), the communication link performance for any arbitrary signaling scheme can be computed. In general H(f,t) is a complex process, i.e., it contains both phase and amplitude information; therefore channel measurement techniques based on incoherent processing are often inappropriate.

1.3 State of Knowledge Summary

The current body of knowledge pertaining to millimeter wave propagation can be separated into three distinct areas: theoretical, related terrestrial experiments, and satellite-to-ground experiments.

The theoretical area has been the most active one. The basic theory of propagation through a random medium has long been a subject of interest, particularly for dielectric sphere scattering [1.4] and propagation through a turbulent atmosphere [1.5,1.6]. Application of these stochastic wave propagation theories to the specifics of millimeter wave links has also been pursued [1.7,1.8,1.11-1.15] with major emphasis placed on relating attenuation characteristics to meteorological conditions. This is true also for the second category which covers experimental programs [1.16,1.17]. However several experiments have been developed with the objective of obtaining data which would be useful from a communication theory point of view [1.19-1.21].

The direct measurement of satellite to ground links has received only secondary attention. Most of the effort has been associated with the ATS-5 and ATS-F millimeter wave experiments [1.22-1.24].

At this date the total available data relevant to millimeter wave communication system design is much too sparse. Furthermore the link characteristics above 30 GHz can only be obtained by extrapolating this sketchy data, clearly pointing to the need for the implementation of a pilot experiment which can be easily adapted to a range of frequency bands. In designing an experiment it is useful to know at least the broad range of parameters to be encountered, so the following numerical values which have been extracted from the literature, are listed to help establish design guidelines.

Attenuation:

Atmosphere (Zenith)	$\simeq$ 0.3 dB (total)
Rain Storm (1 inch/hr)	$\simeq$ 8 dB/km
Multipath Spread	< 1 nanosec.
Bandwidth of $T_c(f)$	> 1 GHz
Doppler Spread	< 1 Hz
Scattered Signal/Coherent Signal	$\simeq$ -40 dB (6"/hr rain, 30 GHz)

The parameters of course vary with antenna beamwidths and pointing angles so that the values given above must be used with caution. They were obtained for narrow beam receiving

antenna (0.2^{o}) pointed at the zenith. The multipath and Doppler spread parameters increase with increasing antenna beamwidth.

1.4 Experimental Technique

In Section 1.2 an equivalent filter model for the link was presented. The design of the experiment is based on this model and its relationship to the basic physical phenomena. The filter characteristics which must be determined are phase and amplitude for $T_c(f)$ and two dimensional correlation properties for $T_R(f,t)$.

The principal difficulty involved with such measurements is the very large bandwidth required for the probing signal. There are two different philosophies that one could adopt: either measure channel characteristics with a signal of bandwidth comparable to that available for present day data modulation techniques, or alternatively probe with signal whose bandwidth is well in excess of the expected channel bandwidth even though the full band may not be utilized in contemporary communication systems. The former simply gives a verification that the channel properties will be suitable for immediate needs, while the latter will demonstrate constraints for future systems, and perhaps provide useful scientific data about propagation through the atmosphere.

The choice of probing signals lies mainly between a frequency domain approach, i.e., the use of several tones centered about some nominal carrier frequency (multitone signal), and a time domain approach, i.e., the use of a short pulse or pseudo random noise phase modulating sequence [1.25, 1.26]. The objective of covering at least 1 GHz bandwidth is difficult to achieve using the time domain methods. On the other hand, the multitone spectrum is easily generated and can be processed as a set of narrowband signals at the receiver. However, some problems do arise in connection with phase stability of the transmitter and movement of the satellite as will be discussed subsequently.

Consider a transmitted waveform consisting of a set of tones $\{s_n(t)\}$;

$$s_n(t) = a_n \sin(\omega_n t + \theta_n) \qquad n=0,\pm1,\ldots,\pm N \qquad (1.1)$$

This type of signal structure is employed in the ATS-5 and ATS-F propagation experiment.

After phase and amplitude distortion by the channel, the received signals essentially represent the transfer function $H(f,t)$ sampled at frequencies $\{\omega_n/2\pi\}$ i.e.,

$$r_n(t) = \left|H\left(\frac{\omega_n}{2\pi}, t\right)\right| \sin\left(\omega_n t + \theta_n + \angle H\left(\frac{\omega_n}{2\pi}, t\right)\right) \qquad (1.2)$$

Thus the required properties of $T_c(f)$ and $T_R(f,t)$ can be extracted from the phase and amplitude behavior of the received

set of signals $\{r_n(t)\}$. The received spectrum is a set of Doppler broadened spectral lines as shown in Fig. 1.1.

Unfortunately the phase processes $\{\theta_n\}$ do not remain constant due to transmitter oscillator instabilities and satellite motion. It can easily be demonstrated that oscillator instabilities give rise to phase errors which increase linearly across the band, and hence are indistinguishable from a variable propagation delay. The satellite also suffers from systematic and random perturbations in its position thereby introducing an additional variable delay component. These two effects can be lumped together as in Fig. 1.2. Thus the filter $T_c(f)$, representing coherent effects, is related to path delay perturbations in the line of sight propagation.

It has been shown that the usual carrier phase locking procedure is inadequate for this kind of wideband measurement. That is to say, the correction for phase variations at center frequency leaves significant residual phase errors in the other received tones, and the magnitude of these errors is large enough to obscure the true phase properties of $H(f,t)$. It is desirable to separate out the phase instability effects from channel induced perturbations so that the data is applicable to other satellite configurations.

The time varying delay τ introduces a phase shift versus frequency expressed as;

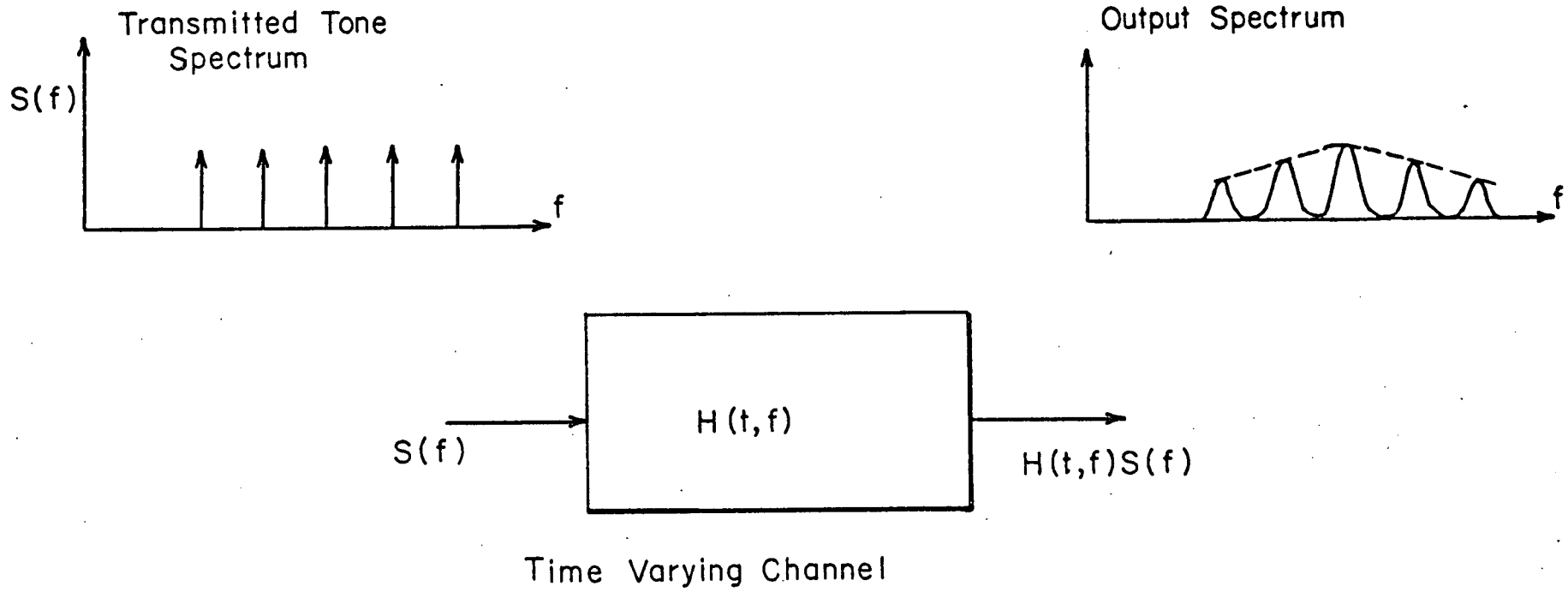

Figure 1.1 Frequency Domain Channel Response to a Multi-Tone Spectrum

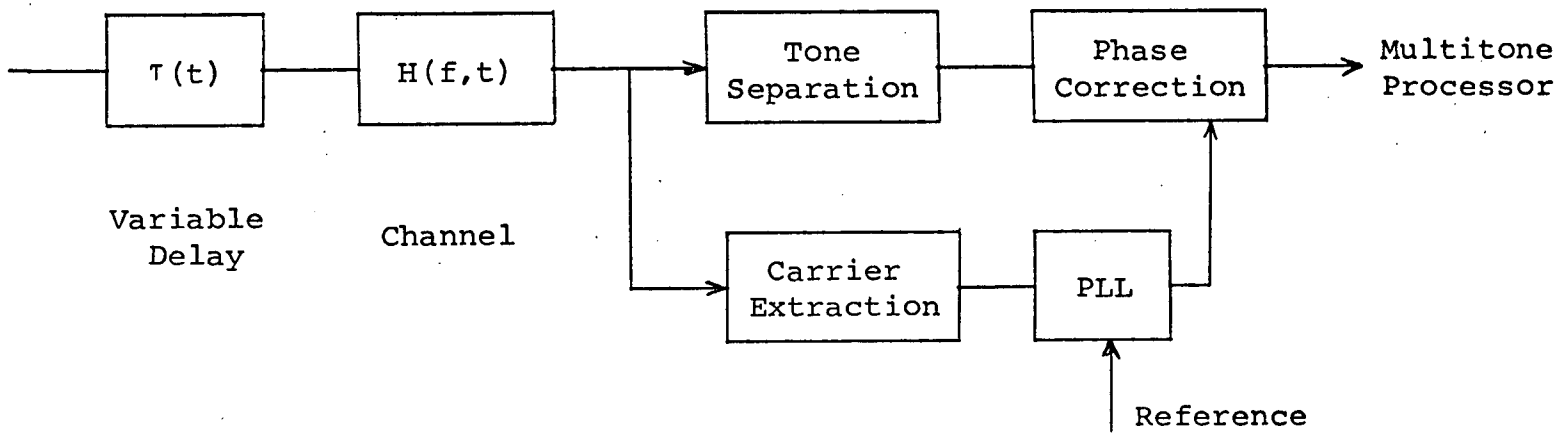

Fig. 1.2 Incremental Phase Correction Procedure

$$\theta(f) = 2\pi f\tau$$

$$= 2\pi(f_0 + \Delta f)\tau$$

$$= \theta_0\left(1 + \frac{\Delta f}{f_0}\right) \qquad (1.3)$$

where θ_0 is the phase at the carrier (center) frequency. Thus knowledge of θ_0 allows the receiver to make the required phase correction as depicted in Fig. 1.2. However the transfer functions T_R and T_c both distort the phase characteristics further, so that θ_0 is never observed directly. This aspect of the measurement has been studied in detail in Chapter 3. In particular the following points are relevant;

(a) When the scattered signal level is sufficiently low it can be shown that a suitable estimate of θ_0 can be obtained. The detailed performance and precise region of validity must be studied further for various link configurations.

(b) The phase instabilities and channel phase characteristics have different spectral properties in general. Our experience in the design of phase locked loop receivers leads us to believe that the two effects can be separated by suitable choice of filters within the loop structure.

Returning to Eq. (1.2) it can be seen that a phase correction scheme as discussed above, allows us to remove the phase parameters $\{\theta_n\}$ by suitable receiver design (see Fig. 1.2). Hence phase and amplitude characteristics of H(f,t) are obtained directly. These quantities provide a complete description of

the instantaneous transfer function H(f,t) sampled in frequency. If the samples are taken close enough together, the complete function can be reconstructed. Since H(f,t) is a random process, its statistical properties are of interest rather than its instantaneous values. This aspect of the measurement is discussed more fully in Chapter 2, while Chapter 6 contains information on the required form of processing for the tone responses.

1.5 Organization of the Report

As just noted Section 2 contains a discussion of the channel characteristics and measurement philosophy. The discussion emphasizes the communication aspects of the channel's characteristics rather than the physical mechanisms that give rise to those characteristics. The discussion of Section 2 leads to the expression of channel characteristics in terms of parameters that can be measured or derived from an experimental configuration.

Chapter 3 discusses one candidate for a channel measurement configuration, namely a multi-tone channel prober. This technique is currently employed in ATS-5 and ATS-F K-Band experimental equipment. The discussion of Section 3 reviews the characteristics of such channel probing equipment and shows that the capabilities of such equipment can be augmented by the use of an incremental phase correction technique. The phase correction technique allows for measurement of the channel parameters in a manner which is more easily related to the channel characterization parameters in Section 2.

Section 4 discusses an alternate probing technique, namely the pulsed probing technique. Several variations of the pulsed probing technique are described and discussed. Although at first

glance the pulsed probing techniques appear to offer advantages over the multi-tone techniques,it is found that component limitations make this technique less desirable. The pulsed techniques are desirable because the data derived through their use is in a form more suitable for deducing communication properties of the channel.

Section 5 presents detailed block diagrams for a multi-tone probing transmitter and receiver system. The system is designed to capitalize upon advances in the state-of-the-art of component technology which have occurred since the initial design of the ATS experimental package. The design furthermore, incorporates some of the data processing features derived in this report--namely, incremental phase correction and some minor modifications in the data detection circuitry. Assuming that it is undesirable at this time to make any modification to the spacecraft hardware for the ATS-F flight experiment, a modified receiver configuration is suggested which is compatible with the ATS-F K-Band multi-tone transmission, but which provides incremental phase correction at the receiver. Thus, if such an approach were taken, additional data could be extracted from the existing K-Band downlink signal.

Section 6 contains a discussion of data processing requirements for a K-Band satellite-to-ground link channel measurement experiment. A data processing technique which deals with in-phase and quadrature components of the received tones rather than amplitude and phase components is presented and analyzed in detail. After describing the data processing algorithms to be employed, a statistical analysis of expected performance using the in-phase and quadrature algorithms is carried out. Finally, the measured parameters are related to the simplified channel model which was derived in Section 2. Section 6 goes on to consider meteorological

data collection and processing. Rainfall rate, atmospheric turbulence and refractive index profiles are considered.

Section 7 presents a brief summary of the results of this study effort. In summary, the report concludes that the multi-tone channel probing method remains the most desirable candidate technique at this time in spite of the great advances in the state-of-the-art since the ATS experimental configuration was first conceived. The report suggests minor modifications in data extraction and processing techniques which will provide additional data about the channel. Block diagrams of a new transmitter and receiver are presented which incorporate these minor design advantages and which capitalize on the advances in the state-of-the-art in component technology which have occurred in recent years. The discussion of Section 7 includes some recommended development areas which will ensure success of future programs in this area.

SECTION 1

REFERENCES

[1.1] Tillotson, L. C., "A Model of a Domestic Satellite Communication System," BSTJ, December 1968, Vol. 47, No. 10, pp. 2111-2138.

[1.2] Tillotson, L. C., "Use of Frequencies Above 10 GHz for Common Carrier Applications," BSTJ, July 1969, Vol. 48, No. 6, pp. 1563-1576.

[1.3] Hult, J. L., and E. E. Reinhart, "Satellite Spacing and Frequency Sharing for Communication and Broadcast Services," Proc. IEEE, Vol. 59, No. 2, February 1971, pp. 118-121.

[1.4] VanderHulst, H. C., Light Scattering by Small Particles, Wiley, New York, 1957, Chapter 4.

[1.5] Tatarski, V. I., Wave Propagation in a Turbulent Medium, McGraw-Hill, New York, 1961, Chapter 4.

[1.6] Strohbehn, J. W., "Line of Sight Wave Propagation Through the Turbulent Atmosphere," Proc. IEEE, Vol. 56, pp. 1301-1318, August 1968.

[1.7] Crane, R. K., "Coherent Pulse Transmission Through Rain," IEEE Trans. AP, Vol. AP-15, No. 2, March 1967, pp. 252-256.

[1.8] Brookner, E., "Characterization of Millimeter Wave Wave Earth Space Link Communication Channels," IEEE Conf. on Communications, June 11, 1969, (Revised version June 25, 1969).

[1.9] Application of Wideband Signals for Propagation Interference Measurement, NASA Final Report, SIGNATRON, Inc., July 1970, p. 4.4.

[1.10] Gallager, R., "Characterization and Measurement of Time and Frequency-Spread Channels," MIT Lincoln Lab. Tech. Report 352, April, 1964.

[1.11] Crane, R. K., "Propagation Phenomena Affecting Satellite Communication Systems Operating in the Centimeter and Millimeter Wavelength Bands," Proc. IEEE, Vol. 59, No. 2, February 1971, pp. 176-184.

[1.12] Altschuler, E. E., et al, "Atmospheric Effects of Propagation at Millimeter Wavelengths," IEEE Spectrum, July 1968, pp. 83-90.

[1.13] Evans, H. W., "Attenuation on Earth-Space Paths at Frequencies up to 30 GHz," ICCC 1971 Conf. Proc., pp. 27-1 to 27-5.

[1.14] Kerr, D. E., Propagation of Short Radio Waves, Rad. Lab. Series, McGraw-Hill, New York, 1951, Vol. 13.

[1.15] Lane, J. A., "Scintillation and Absorption Fading on Line of Sight Links at 35 and 100 GHz," IEE Conf. on Tropospheric Wave Propagation, Pub. No. 48, 1968.

[1.16] Janes, H. B., et al, "Comparison of Simultaneous Line of Sight Signals at 9.6 and 34.52 GHz," IEEE Trans. AP, Vol. AP-18, pp. 447-451, July 1970.

[1.17] Straiton, A. W., et al, "Amplitude Variations of 15 GHz Radio Waves Transmitted Through Clear Air and Through Rain," Radio Science, Vol. 5, No. 3, pp. 551-557, March 1970.

[1.18] Weibel, G. E., and H. O. Dressel, "Propagation Studies in Millimeter Wave Link Systems," Proc. IEEE, Vol. 55, No. 4, April 1967, pp. 497-513.

[1.19] Vignali, J. A., "Overwater Line of Sight Fade and Diversity Measurements at 37 GHz," IEEE Trans. AP, Vol. AP-18, No. 4, July, 1970.

[1.20] Mondre, E., "Correlation Analysis and Scintillation for 15 GHz Line of Sight Propagation," Tech. Note NASATND-5613, April 1970.

[1.21] Roche, J. F., et al, "Radio Propagation at 27-40 GHz", IEEE Trans. AP, Vol. AP-18, No. 4, July 1970.

[1.22] Ippolito, L. J., "Effects of Precipitation on 15.3 and 31.65 GHz Earth Space Transmissions With the ATS-V Satellite," Proc. IEEE, Vol. 59, No. 2, February, 1971.

[1.23] Bellini, A., and G. Bianchi, "Experimental SHF Transponder for Italian SIRIO Satellite," Paper presented at the AGARD Space Communications Seminar, MIT.

[1.24] Ippolito, L. J., "The ATS-F Millimeter Wave Propagation Experiment," NASA X Document, X-751-71-460, October, 1971.

[1.25] Bello, P. A., "Measurement of the Complex Time-Frequency Channel Correlation Function," Radio Science, Vol. 68D, No. 10, October 1964, p. 1161.

[1.26] Green, P. E., "Radar Astronomy Measurement Techniques," Lincoln Lab Tech. Report No. 282, December 1962, pp. 24-42.

SECTION 2

CHANNEL CHARACTERIZATION AND MEASUREMENT PHILOSOPHY

2.1 General Channel Characteristics

The statistical characteristics of the millimeter wave channel are determined by the nature of the propagation medium and geometrical parameters such as antenna beamwidths. In the sections that follow two specific media will be considered in detail, i.e., rain and turbulent atmosphere. These will illustrate the general nature of the channel characterization task and with slight modification the analysis can be used directly for other meteorological conditions.

2.1.1 Description of the Model

The medium, which gives rise to scattering and absorption of millimeter waves, can not be characterized too accurately because of the natural inhomogeneous structure of rain, fog and other atmospheric phenomena. Instead an idealized model must be employed to gain insight into the general behavior. Figures 2.1 and 2.2 indicate distinctions between the real and the ideal satellite-to-ground communication links. The following assumptions are also necessary to simplify the description.

(a) The distance R_0 is much greater than the altitude of the scattering medium. (Typically the latter is 0 - 15 Km for atmospheric effects.) Moreover, the receiving beam is sufficiently narrow and the transmitting beam on the satellite so broad, that the field incident at the top of the layer can be approximated by a plane wave over the region which will ultimately be of interest (several receiving beamwidths).

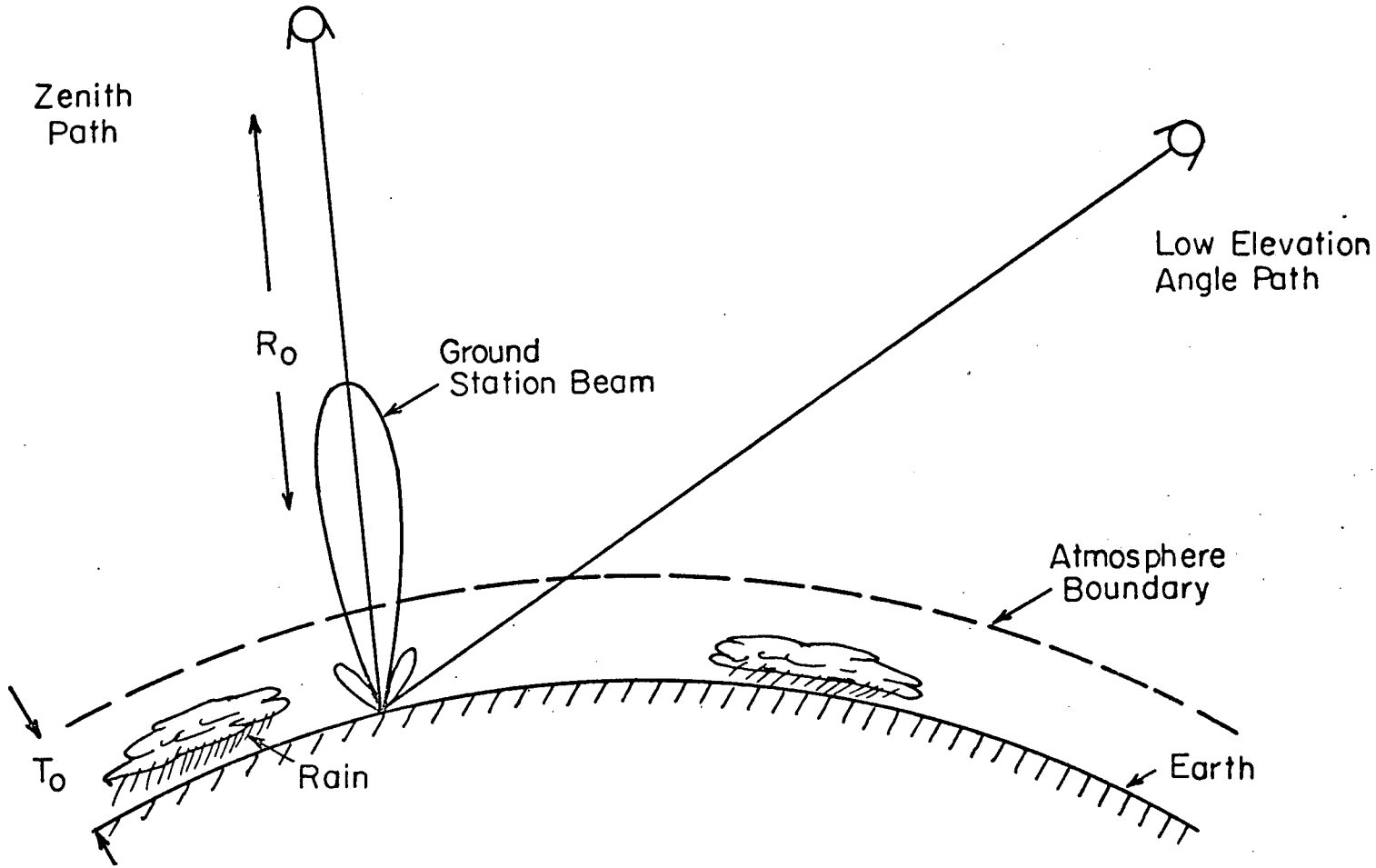

Fig. 2.1. Typical Path Geometry.

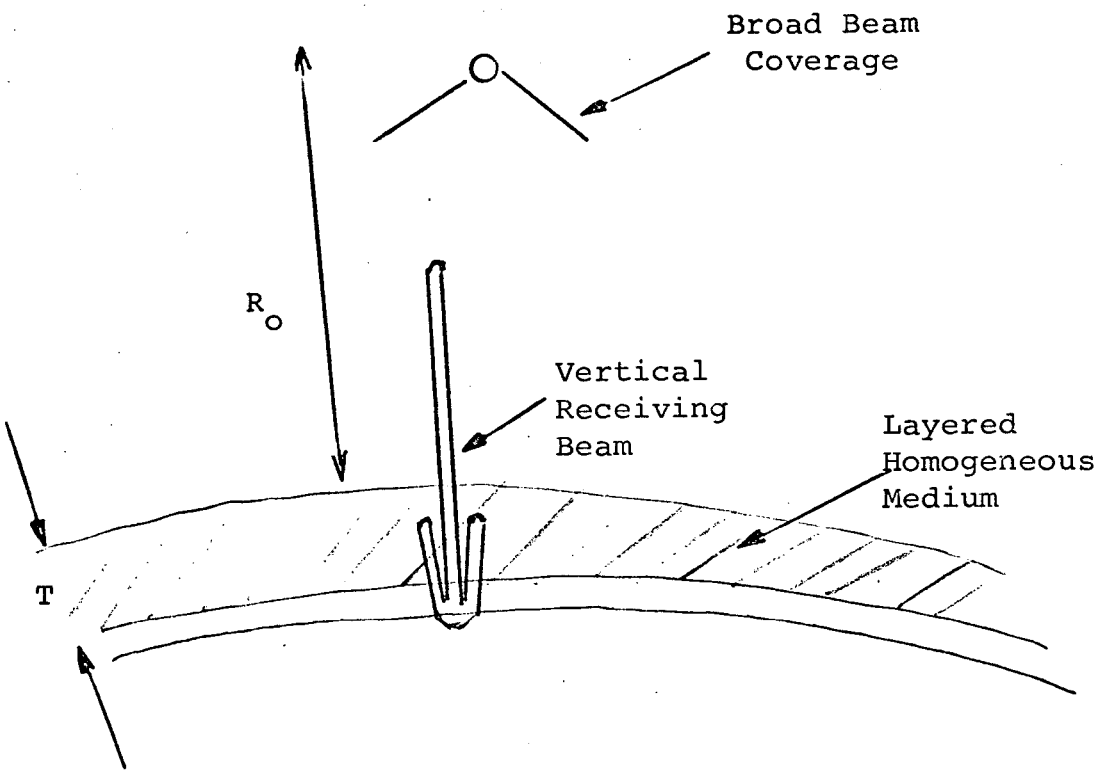

Fig. 2.2. Idealized Scattering Model.

(b) Oblique pointing angles may be of interest. These will be accounted for by increasing the effective thickness of the layer using an appropriate factor, i.e.,

$$T = \frac{T_0}{\sin \theta} \tag{2.1}$$

where T_0 is the physical thickness of the layer and θ is the elevation angle. Hence we need only consider the zenith pointing angle in this discussion.

2.1.2 Discussion of Terminal Characteristics

The received field for the millimeter wave channel can conveniently be thought of in terms of the sum of two components; a scattered incoherent signal, and a coherent time invariant component.This is clearly demonstrated in Appendix A for scattering by raindrops, where the exact solution for the field scattered by dielectric spheres can be stated explicitly. This is true also for scattering by atmospheric inhomogeneities, where the coherent field is simply the time invariant statistical average field. In both cases we are primarily concerned with a statistical description of the field which results when a plane wave is incident on the medium. In particular typical parameters describing the antenna terminal voltage are obtained as a function of various atmospheric conditions and link geometries.

Of additional interest are the effects of multipath spreading, i.e., the time smearing of a short transmitted pulse, and temporal fading characteristics. Both of these are determined by scatterer properties and system geometry, and some details are available in the Appendices. The total channel effect is conveniently summarized by the use of a time varying impulse response $h(t, \tau)$, the response at time t to an impulse τ seconds earlier. This function will always provide a valid description

of the channel since it is founded only on the assumption of linearity between input and output; this assumption is in turn assured by the linearity of Maxwell's equations which describe the received field.

The channel can be described equally well by the time varying system function H(f,t) which is related to h(t,τ) by Fourier transformation on τ, i.e.,

$$H(f,t) = \int_{-\infty}^{\infty} h(t,\tau)e^{-j2\pi f\tau}\, d\tau \qquad (2.2)$$

H(f,t) then, is the complex time varying response to a tone of frequency f. Note that variation of H(f,t) with respect to t will be quite slow (tens of Hz or less) compared with the data rate, so that H is easily visualized in terms of conventional system functions, except that it is randomly varying in time.

The measurement of channel properties can be approached at several different levels. We could attempt to measure the complete function H(f,t) over particular time and frequency bands. However such knowledge would generally provide an overly detailed description of the channel: To provide data useful in predicting communication performance we need broad trends rather than detailed sample function behavior. Generally a sufficient description of the channel is provided from the average properties of H(f,t). When the channel statistics are Gaussian it is only necessary to measure certain underlying correlation functions, but even if the channel is non-Gaussian, correlation functions may still be appropriate for most purposes. Note that a given correlation function describing statistical properties of H(f,t) will only be valid over time periods for which the bulk medium properties are fixed.

2.2 An Equivalent Filter Channel Model

The effect of the atmosphere and discrete scattering particles (such as raindrops) on the transmitted signal, can be viewed in terms of equivalent filters. In particular we need to consider a model with two different kinds of filters, one corresponding to the effect of the medium on the coherent signal, and the other corresponding to the scattered signal. Consider the former which will be denoted by $T_c(f)$. As the number and shape of constituent scattering elements within the coherent scattering zone changes, so does the equivalent refractive index of the medium, but as we have seen in Appendix A the effect is small. If the medium scattering properties were invariant with the frequency of the incident field, we could assume that the equivalent refractive index was constant with frequency. Hence $T_c(f)$ would have a constant amplitude and linear phase shift across the band. A refined model would allow variable attenuation and quadratic or higher order phase shifts across the band. These characteristics, which have been investigated for rain in a theoretical study by Crane [2-1], can be expected to give rise to pulse distortion if a wide enough bandwidth is used. Note that if $T_c(f)$ was expanded as a function of frequency using a Taylor's series for phase and amplitude, the sample calculations of Appendix B suggest that only the first few terms would be required.

With a single scattering model the energy received from a collection of scatterers is computed using only the original field incident on each scatterer (i.e., the field which would exist in the absence of other scatterers). One can visualize that this incident field, before reaching the scatterer, initially passes through a region which imposes its attenuation and phase characteristics in the same way as previously discussed for the coherent field. Similarly the field originating

from a single scatterer must traverse the medium between the scatterer and the antenna. Thus we can use a random time varying filter $T_R'(f,t)$ to represent the total influence of the incoherent scattered signal as in Fig. 2.3(a), or alternatively separate out the coherent distortion effects which result from propagation through the medium, as in Fig. 2.3(b). A channel model which is frequently of use in describing communications links when scattering is involved, is the Wide Sense Stationary Uncorrelated Scattering (WSSUS) model of Bello [2-2]. As indicated in Appendix A it is not necessarily valid to assume that the scattered component represented by $T_R(f,t)$, fits into this category. The use of the WSSUS model requires system functions which are statistically stationary in both the f and t variables, and it is therefore clear that the product $T_R(f,t)\ T_C(f)$ does not fit this category.

In the material that follows we shall generally refer to the model given in Fig. 2.3(b) without assuming T_R to be a WSSUS filter. The overall input-output relationships can be described in terms of a composite transfer function H(f,t);

$$H(f,t) = T_C(f)[1 + T_R(f,t)] \qquad (2.3)$$

Measurements of phase and amplitude or in-phase and quadrature components can be made using either tones or wideband signals and these provide data for the subsequent compilation of statistical properties. Because the transfer function $T_R(f,t)$ has been defined as a zero mean process (see Appendix A for details), it is possible to extract information about $T_C(f)$ by directly averaging the in-phase and quadrature components of a given tone response. Second order properties of H(f,t) are also of interest, but are more difficult to obtain, so that this subject will be left for a more complete development in later sections.

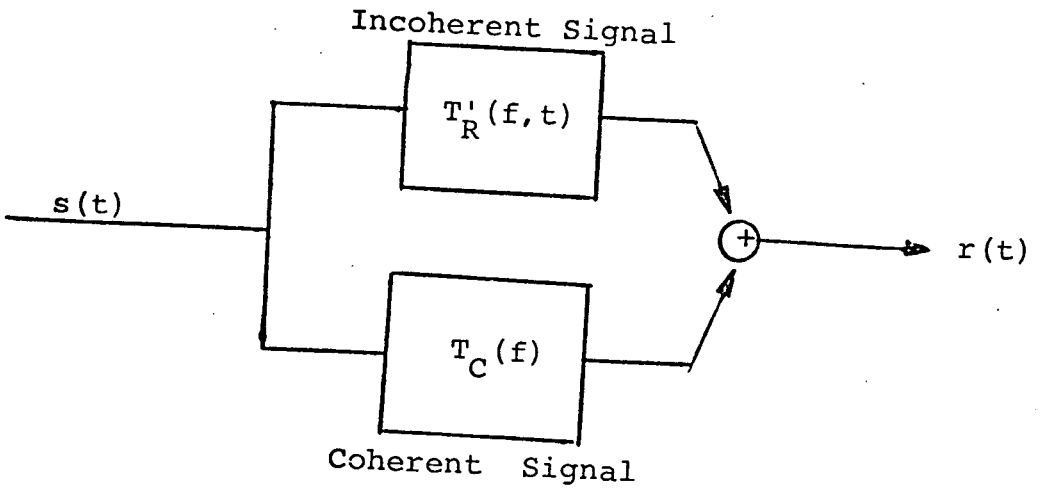

Fig. 2.3(a). Equivalent Filter Model.

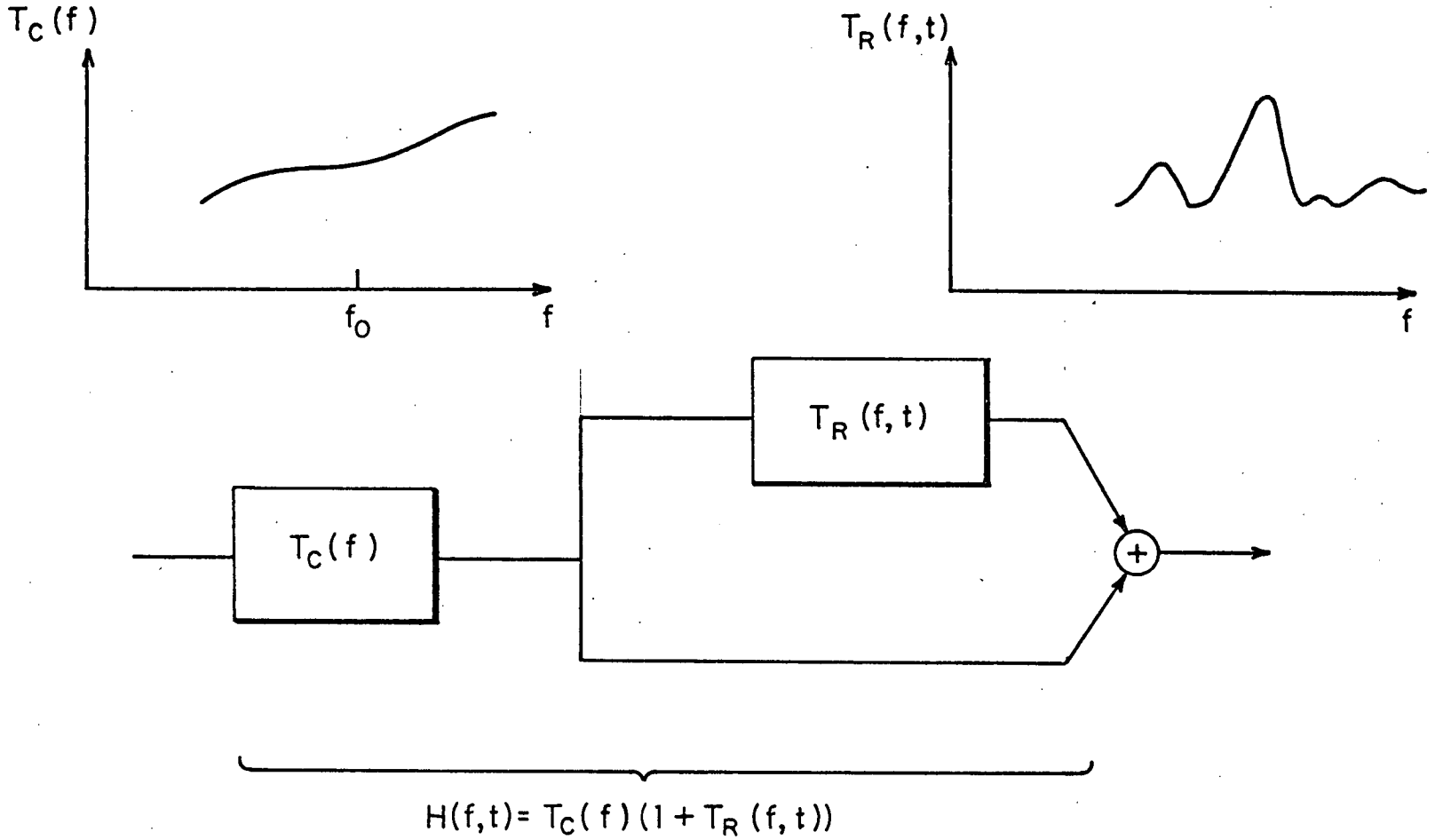

Fig. 2.3(b). Simplified Filter Model for the Channel.

2.3 Statistical Properties of the Received Signal

2.3.1 Definition of Parameters

The time varying impulse response $h(t,\tau)$ is derived from the super-position of many scattered signals for each t and τ. The scattering elements may be phase coherent, but there is randomness associated with their scattering properties, e.g., because of variations in shape and diameter. This leads to the assumption of a Gaussian statistical description for the impulse response $h(t,\tau)$, its transform on τ, $H(f,t)$, or for that matter the response to any deterministic waveform. The response to a tone of frequency f can be expressed as;

$$\begin{aligned} r(f,t) &= A(f,t)\cos(2\pi ft + \gamma(f,t)) \\ &= X(f,t)\cos 2\pi ft - Y(f,t)\sin 2\pi ft \end{aligned} \tag{2.4}$$

where

$$\begin{aligned} X(f,t) &= x(f,t) + \bar{X}(f) \\ Y(f,t) &= y(f,t) + \bar{Y}(f) \end{aligned} \tag{2.5}$$

Thus the quadrature components $X(f,t)$ and $Y(f,t)$ have been defined as the sum of a frequency dependent mean and a zero mean random term which is consistent with previous definitions in terms of specular and scattered signals.

The time varying transfer function $H(f,t)$ can be related to $r(f,t)$ using,

$$r(f,t) = \mathrm{Re}\{H(f,t)e^{j2\pi ft}\} \tag{2.6}$$

$T_c(f)$, $T_R(f,t)$ and hence $H(f,t)$ have been implicitly defined for $-\infty < f < \infty$ (although generally only $H(f,t)$ $f > 0$ will be required since $H(f,t) = H^*(f,t)$), which implies that,

$$X(f,t) = \text{Re}\ \{H(f,t)\}$$

$$Y(f,t) = \text{Im}\ \{H(f,t)\} \tag{2.7}$$

Thus

$$H(f,t) = X(f,t) + jY(f,t) \tag{2.8}$$

In much of the material which follows, the properties of H(f,t) will be examined at a particular value of t. However for the present it is convenient to define the following statistical properties in terms of the complete time-frequency function r(f,t). The in-phase and quadrature components, which are assumed to be stationary in time, have mean and correlation properties denoted;

$$E\{X(f,t)\} = \bar{X}(f) \tag{2.9}$$

$$E\{Y(f,t)\} = \bar{Y}(f) \tag{2.10}$$

$$E\{x(f_1,t_1)x(f_2,t_2)\} = R_x(f_1,f_2,t_1-t_2) \tag{2.11}$$

$$E\{y(f_1,t_1)y(f_2,t_2)\} = R_y(f_1,f_2,t_1-t_2) \tag{2.12}$$

$$E\{x(f_1,t_1)y(f_2,t_2)\} = R_{xy}(f_1,f_2,t_1-t_2) \tag{2.13}$$

Referring to the original definitions (Eqs. (2.4) and (2.5)) it is apparent that one can define a pair of covariance functions for the complex process H(f,t) and express them in terms of the quadrature component correlations above. For example define,

$$K_H(f_1,f_2,t_1-t_2) \triangleq E\{[H(f_1,t_1) - \bar{H}(f_1,t_1)][H^*(f_2,t_2) - \bar{H}^*(f_2,t_2)]\}$$

(2.14)

$\bar{H}$ denotes mean value. Using Eq.(2.8) and subtracting out the mean values we find;

$$\begin{aligned} K_H(f_1,f_2,t_1-t_2) &= E\{[x(f_1,t_1) - jy(f_1,t_1)][x(f_2,t_2) + jy(f_2,t_2)]\} \\ &= R_x(f_1,f_2,t_1-t_2) + R_y(f_1,f_2,t_1-t_2) \\ &\quad + j[R_{xy}(f_1,f_2,t_1-t_2) - R_{xy}(f_2,f_1,t_2-t_1)] \end{aligned}$$

(2.15)

Similarly without the conjugate in Eq. (2.14) we get;

$$\begin{aligned} \tilde{K}_H(f_1,f_2,t_1-t_2) &\triangleq E\{[H(f_1,t_1) - \bar{H}(f_1,t_1)][H(f_2,t_2) - \bar{H}(f_2,t_2)]\} \\ &= E\{[x(f_1,t_1) - jy(f_1,t_1)][x(f_2,t_2) - jy(f_2,t_2)]\} \\ &= R_x(f_1,f_2,t_1-t_2) - R_y(f_1,f_2,t_1-t_2) \\ &\quad - j[R_{xy}(f_1,f_2,t_1-t_2) + R_{xy}(f_2,f_1,t_2-t_1)] \end{aligned}$$

(2.16)

Thus if the quadrature and in phase covariances (Eqs.(2.11) - (2.13)) are known, both K_H and $\tilde{K}_H$ can be reconstructed. Conversely, these two functions alone provide sufficient information to allow the extraction of R_x R_y and R_{xy} uniquely.

In the next section we examine more closely the various correlation functions which have been defined and relate their properties to certain physical properties of the millimeter wave channel.

2.3.2 Correlation Function Properties

It is clear that estimates of the functions $R_x R_y$ and R_{xy} along with knowledge of T_c, allow one to predict the performance of any potential communication scheme. For the present we shall be concerned only with measurement of the above functions, and in order to capitalize on any simplifying channel properties, we need to study them further.

Consider first the question of stationarity in time. It can be shown that the response r(f,t) at a single frequency, which will be denoted by r(t) has a covariance function,

$$K_r(t_1,t_2) = \frac{1}{2} \mathrm{Re}\{K_H(f_1,f_2,t_1-t_2)e^{j2\pi f(t_1-t_2)} + K_H(f_1,f_2,t_1-t_2)e^{j2\pi f(t_1+t_2)}\} \tag{2.17}$$

Here we see that the bandpass process r(t) will be a function of (t_1+t_2) and hence nonstationary unless $\tilde{K}_H$ is zero, despite the fact that the in-phase and quadrature components were themselves assumed stationary. Returning to Eq. (2.16) which defines $\tilde{K}_H$ it is seen that stationarity of r(t) (for fixed f) requires;

$$R_x(f,f,t_1-t_2) = R_y(f,f,t_1-t_2) \tag{2.18}$$

and

$$R_{xy}(f,f,t_1-t_2) = -R_{xy}(f,f,t_2-t_1) \tag{2.19}$$

These constraints have frequently been observed and satisfied in certain other problems concerned with bandpass stochastic processes. In particular they hold when r(t) is bandpass noise or when we can associate with r(t) a random initial phase component γ_o which is uniformly distributed over $[-\pi,\pi]$. This latter approach must be applied with care however. If the parameter is in fact constant over a given measurement interval (0,T), then subsequent processing of the data for that interval will not effectively average over γ_o. Generally speaking it can be shown [2-3] that a large number of channels, e.g., tropospheric and ionospheric scatter channels, do give rise to a signal r(t) such that the above conditions are satisfied. These channels can be characterized in terms of K_H only, since $\tilde{K}_H = 0$.

A further simplification can often be made if the spectrum of the process r(t) is symmetrical about the carrier frequency. It can then be demonstrated that; [2-4]

$$R_{xy}(f,t,t_1-t_2) = 0$$

so that r(t) is completely characterized by a single correlation function R_x. Suitable extensions can be made to the above conclusions for a pair of responses $r(f_1, t_1)$ and $r(f_2, t_2)$, but the necessary symmetry properties (i.e. symmetrical delay power spectrum) are rarely satisfied in practice.

For the millimeter wave link it is expected that the channel characteristics will preclude the assumptions of true stationarity for the response to a single tone, because the requirements of Eqs. (2.18) and (2.19) will not hold. The in-phase and quadrature components will in general be strongly correlated and may have different variances. Evidence to support these statements is contained in Appendix A for rain scattering while the effects of

atmospheric turbulence have been covered in detail by Bello Ref. [2-5]. Broadly speaking we can expect the in-phase and quadrature components to be correlated and of unequal variance whenever the majority of the scattered energy originates from the first few Fresnel zones. As a consequence of this coupling, the resultant tone responses cannot be classified simply as having Ricean amplitude distributions; the behavior of the channel is instead determined by the complete set of functions given in Eqs. (2.9) to (2.13) (see Ref. [2-6] for an evaluation of the resultant amplitude distribution).

These channel characteristics, which arise because of the extremely narrow beamwidths envisioned for millimeter wave links, obviously make the required measurement program more complex, and underline the need for coherent (in-phase and quadrature) receiver processing. The subject of channel measurement is broached in Section 2.4, while Sections 3 and 4 give a more detailed description of two different schemes.

In Section 2.3.3 we present a discussion concerning the channel behavior for situations where the random signal component is much smaller in strength than the coherent signal.

2.3.3 Channel Properties for Low Scattered Signal Levels

The existence of a low level scattered signal allows the use of certain approximations in the determination of a suitable measurement strategy. The composite time varying transfer function is,

$$H(f,t) = (1 + T_R(f,t))T_c(f) \qquad (2.20)$$

where T_R is the transfer function corresponding to the scattered signal component, and T_c which includes the gross path loss

characteristics, is representative of the average medium behavior. When the ratio of unscattered power to scattered power is high (say greater than 20 dB) we have,

$$|T_R|^2 << 1 \tag{2.21}$$

and from the phasor diagram of Fig. 2.4 we see that,

$$\phi(f,t) = \text{Tan}^{-1}\left[\frac{|T_C T_R| \sin \eta}{|T_C| + |T_C T_R| \cos \eta} \right]$$

$$= \text{Tan}^{-1} \left[\frac{|T_R| \sin \eta}{1 + |T_R| \cos \eta} \right] \tag{2.22}$$

Using Eq. (2.21) this expression can be approximated by;

$$\phi(f,t) \simeq \frac{|T_R| \sin \eta}{1 + T_R \cos \eta}$$

$$\simeq |T_R| \sin \eta \tag{2.23}$$

The phase angle ν has been left as a parameter to allow the discussion to proceed in terms of an arbitrary reference. In practice, the receiver phase reference may be locked to the received carrier using a phase locked loop. In addition the observable amplitude $|H(f,t)|$ can be written as;

$$|H(f,t)| = |T_C| + |T_C T_R| \cos \eta$$

$$= |T_C|(1 + |T_R| \cos \eta) \tag{2.24}$$

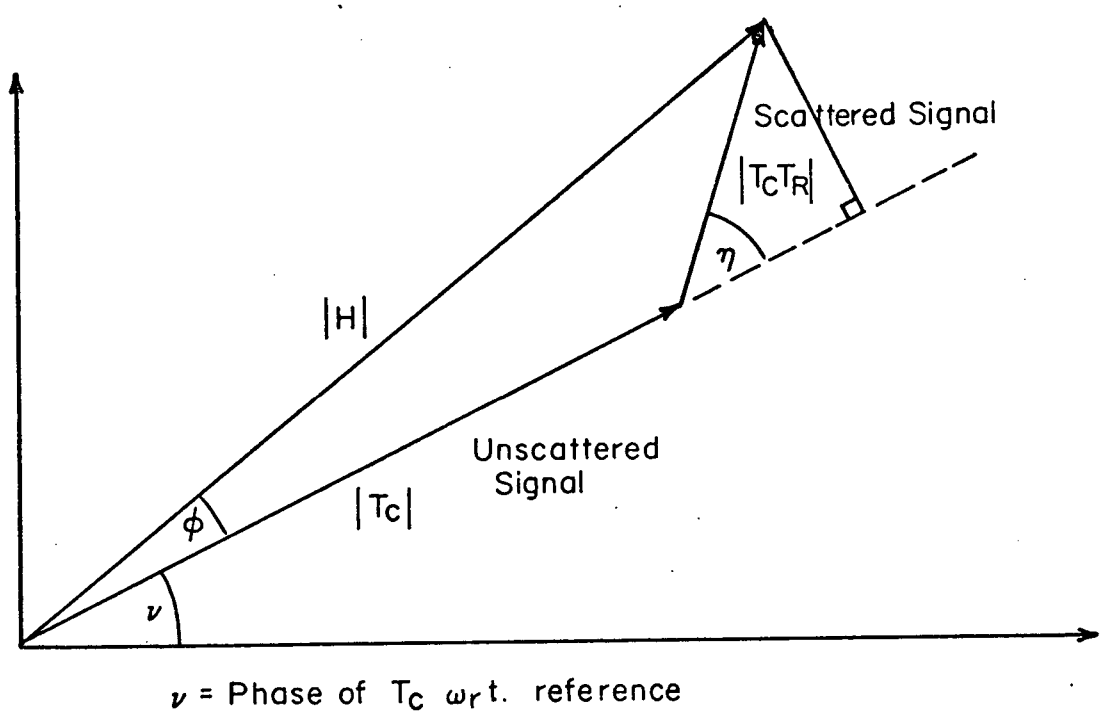

Fig. 2.4. Vector Sum of Random and Coherent Signals

Thus it is seen from Eqs. (2.23) and (2.24) that the observed phase and amplitude fluctuations of the tone response correspond directly to the components of the scattered signal in phase and in quadrature to the time invariant component T_c. Phase measurements will of necessity be relative to a reference, so that the actual observed phase will be $\nu + \phi$ rather than ϕ alone. However ν can easily be removed after averaging the phase processes.

The discussion above is useful in providing insight as well as specific approaches to measurement of the channel parameters. For example the phase fluctuation properties are of interest in developing designs for pilot tone phase locked loops. Eq. (2.23) suggests that the phase of a narrowband signal can be described as a zero mean Gaussian random process, since it represents the quadrature component of a random vector.

The approximations used here are of further interest in establishing the utility of certain measurement procedures as will be seen for example in Section 3.2.2.

2.4 Channel Measurement Philosophy

The composite channel filter $H(f,t)$ can be examined using either a time domain or frequency domain approach. In particular the time varying impulse response $h(\tau,t)$, which is the Fourier transform of $H(f,t)$, can be examined directly using periodic signals having narrow autocorrelation properties. The period must be chosen smaller than the inverse Doppler rate which determines the time variation of $h(\tau,t)$, and yet large enough to exceed the duration of the impulse response. To satisfy both of these constraints we require that the delay spread - Doppler spread product be less than unity (see Ref. [2.8]). This is easily satisfied for the millimeter wave channel.

There are three prime candidate techniques which might be suitable for millimeter wave channel measurement. (see Refs. [2.9, 2.10]).

(a) Sampling of $H(f,t)$ using tones spaced in frequency.

(b) Probing of the channel in the time domain using a periodic pseudo random phase modulated carrier.

(c) Time domain probing using a sequence of short pulses.

Note that in all cases the required bandwidth of the signal must be of the same order or larger than the effective bandwidth of $H(f,t)$.

In the material which follows we shall assume that the complete impulse response $g(t,\xi)$ or its transform $H(f,t)$ is available. The former can be most easily obtained using coherent

processing of a sequence of pulse responses (see Chapter 4) while H(f,t) is available in sampled form from a multitone probing signal (see Chapter 3).

2.4.1 Extraction of Coherent Filter Parameters

The term $T_R(f,t)$ contained in the expression for the channel transfer function has been defined as a zero mean process. The obvious way of establishing estimates of $T_c(f)$ then, is to average the quantity H(f,t) over a long time interval (see Section 6 for a discussion of averaging times). Then we can proceed on the assumption that,

$$\langle H(f,t) \rangle \simeq T_c(f)$$

where <> denotes time average. In this section we discuss the characteristics of $T_c(f)$ and their relationship to the physical properties of the link.

For a total path length x through the medium which has a frequency dependent refractive index $n(\omega)$, the phase angle, ϕ of $T_c(f)$ is found from

$$\phi = -kx \tag{2.25}$$

where

$$k = \frac{\omega}{c} n(\omega)$$

n = refractive index

c = velocity of light in free space

For this discussion we will assume a lossless medium.

Expanding about the center frequency ω_0;

$$n(\omega) \simeq a_0 + a_1(\omega-\omega_0) + a_2(\omega-\omega_0)^2 \tag{2.26}$$

Thus

$$\phi(\omega) = -\frac{\omega}{c} x[a_0 + a_1(\omega-\omega_0) + a_2(\omega-\omega_0)^2] \tag{2.27}$$

Upper and lower sidetones at $\pm\omega_m$ therefore have phase parameters;

$$\phi_1 = \frac{-(\omega_0+\omega_m)x}{c} [a_0 + a_1\omega_m + a_2\omega_m^2] \tag{2.28}$$

and

$$\phi_2 = \frac{-(\omega_0-\omega_m)x}{c} [a_0 - a_1\omega_m + a_2\omega_m^2] \tag{2.29}$$

Note that terms linear in frequency give rise to delay effects only. At the center frequency, $\omega=\omega_0$, we have

$$\phi_0 = \frac{-\omega_0 x}{c} a_0 \tag{2.30}$$

Then

$$\phi_1 = \phi_0 - \frac{x}{c}[\omega_m(a_0+a_1\omega_0) + \omega_m^2(a_1+a_2\omega_0) + a_2\omega_m^3] \tag{2.31}$$

$$\phi_2 = \phi_0 - \frac{x}{c}[-\omega_m(a_0+a_1\omega_0) + \omega_m^2(a_1+a_2\omega_0) - a_2\omega_m^3] \tag{2.32}$$

Thus it can be seen that the currently proposed ATS-F processor will give a phase measurement;

$$\Delta\phi = \phi_1 + \phi_2 - 2\phi_0$$
$$= \frac{-2x}{c}\,\omega_m^2\,(a_1 + a_2\omega_0) \qquad (2.33)$$

i.e., in the general case only terms in the phase expansion which are even functions with respect to the carrier are retained. To relate the parameters a_0, a_1, a_2 and the corresponding frequency dependent attenuation characteristic to spreading of a pulse envelope, one must represent the pulse by its spectrum, multiply by the equivalent channel filter (using the phase characteristic of eq. (2.27)) and transform back to the time domain. The details will not be carried out here, but we can note the following points;

(a) The parameter a_0 is related to delay effects only and is not generally of interest in characterizing the channel.

(b) Parameters a_1 and a_2 are directly related to pulse distortion effects and they can be used to predict bandwidth limitations due to dispersion [2.1]. Thus the quantity $\Delta\phi$ provides useful experimental data for this channel characteristic.

Although the role of amplitude variations $|T_c(f)|$ has not been fully discussed, it is clear that amplitude variations across the band also give rise to pulse distortions. However the required measurement technique is straightforward and needs no elaboration.

Note that the coherent channel function $T_c(f)$ is time invariant provided that the bulk medium properties are fixed. Hence knowledge of $T_c(f)$ allows equalization of the channel to counteract intersymbol interference effects which are likely to occur.

2.4.2 Measurement of Scattered Signal Properties

This section describes the rationale behind a measurement technique for the scattered signal properties. The technique is presented in detail in Section 6 below. The method relies on detection and processing of in-phase and quadrature components of the complex envelope of the received tones, rather than their amplitudes and phases.

First, let us consider the statistical characterization of the amplitude and phase processes $A(f,t)$ and $\gamma(f,t)$ (see Eq. (2-4)) in terms of quadrature component properties. Clearly A and γ will not be Gaussian processes, so that a complete description would entail substantially more than the specification of correlation functions. However some useful relationships between in-phase-quadrature process correlation functions and phase-amplitude correlation functions can be established.* The results available are applicable only to wide sense stationary processes (i.e., satisfying Eqs. (2.21) and (2.22)), and often only for symmetrical spectra (i.e., satisfying Eq. (2.23)). The conclusions may be summarized as follows;

*See for example the treatment of this subject given in Davenport and Root, p. 158 or in Middleton, p. 396. These authors are primarily concerned with the statistics of a deterministic signal plus narrow band Gaussian noise after passage through various nonlinear devices such as detectors. The narrowband noise can be shown to have equal variance quadrature components and be wide sense stationary in character.

(a) When $K_H = 0$ and the channel function $H(f,t)$ is stationary in time and frequency, we have a complete characterization in terms of

$$K_H(f_1-f_2, t_1-t_2) = 2[R_x(f_1-f_2, t_1-t_2) + j\, R_{xy}(f_1-f_2, t_1-t_2)]$$

(from Eq. (2.18)). (2.34)

(b) The amplitude process $A(f,t)$ has a correlation function R_A which is a complicated function of the magnitude squared of K_H, i.e.,

$$|K_H|^2 = 4(R_x^2 + R_{xy}^2) \tag{2.35}$$

(c) The phase process $\theta(f,t)$ similarly has a correlation function R_θ which is a complicated function of both phase and amplitude of K_H. (Note the simplifications which arise when the spectrum is symmetrical and $R_{xy} = 0$.)

(d) It is difficult to use the relationships provided in (b) and (c) to estimate R_x and R_{xy} from R_A and R_θ. For the millimeter wave channel it would be necessary to generalize these results to include three parameters R_x, R_y and R_{xy} so that the two functions R_A and R_θ would obviously not provide sufficient information even if closed form relationships could be found.

The real motivation for pursuing this particular topic is related to the following question. Suppose that correlation functions for the phase and amplitude were available. Could these be used to determine the complete correlation properties of the process $r(f,t)$ over a given frequency band? Furthermore it is important to know how the phase and amplitude correlation

functions relate to the communication performance, particularly whether or not they provide enough information to determine the bit error rate.

Of course it is not necessary to restrict attention to the phase process correlation function. Any suitable statistic such as moments of the observed phase quantity, could be estimated. For example if the measurement was

$$\hat{\theta} = \theta(f_1,t_1) - \theta(f_2,t_2) \tag{2.36}$$

then $E\{\hat{\theta}^2\}$ can be related (with some difficulty) to the parameters R_x, R_y and R_{xy}. Note however that a phase measurement of the form,

$$\theta' = \theta(f_1,t) + \theta(f_2,t) - 2\theta(f_0,t)$$

$$\triangleq \theta_1 + \theta_2 - 2\theta_0$$

is even more difficult to handle because it must be related to R_x, R_y and R_{xy} at three different frequency pairs.

In summary we can say that the measurement of channel parameters using directly observed in-phase and quadrature components appears to eliminate many of the difficulties inherent in the task of interpreting phase and amplitude measurements. We should note that the implementation of a phase difference measurement of the form

$$\hat{\theta} = \theta(f_1,t_1) - \theta(f_2,t_2)$$

requires the use of delay lines for on-line processing, or alternatively $\theta(f_1,t_1)$ and $\theta(f_2,t_2)$ must be measured individually with respect to a stable reference and recorded for off-line processing.

In a recent paper, Mondre [2.7], established some useful bounds on the behavior of a complex covariance function in terms of the covariance function for the transfer function amplitude $|H(f,t)|$. Although a Ricean channel model was assumed, the analysis yields useful insight. Briefly, the result was obtained that the covariance function for the amplitude process was always bounded by the magnitude of the complete complex correlation function. Furthermore as the ratio of coherent non-fading power to average random power increases, the bound tends to become tighter, and in fact leads to true equality in the case of symmetrical spectral properties (i.e., $R_{xy} = 0$; see Section 2.3.2). This latter result is easily explained in terms of the material given in Section 2.3.3 where the case of low power scattered signals was discussed. When the cross-covariance function R_{xy} is zero we can express the random signal in terms of a pair of independent equal variance in-phase and quadrature components for any arbitrary reference. Thus when the coherent signal is relatively large, amplitude measurements yield an approximation to the sum of T_c and the co-phasal T_R component. Hence the amplitude covariance is simply the correlation function for the in-phase random component which provides a complete characterization for $R_{xy} = 0$. When this latter condition is not satisfied, as will be the case for reasons given previously, it is obvious that amplitude information will not be sufficient even for high coherent/random signal

power ratio, although the bound is still valid. This is even more true for a non-Ricean channel which will frequently occur in millimeter wave systems. (see Section 2.3.2 and Appendix A).

CHAPTER 2

REFERENCES

[2.1] Crane, R.K., "Coherent Pulse Transmission Through Rain," IEEE Trans. AP, Vol. AP-15, No. 2, March 1967, pp.252-256.

[2.2] Bello, P.A.,"Characterization of Randomly Time-Variant Linear Channels," IEEE Trans. Comm. Syst., Vol. CS-11 pp. 360-393, Dec. 1963.

[2.3] Kennedy, R.S., Fading Dispersive Communications Channels, Wiley-Interscience, N.Y., 1969, Ch. 1.

[2.4] Middleton, D., Introduction to Statistical Communication Theory, McGraw-Hill, New York, 1960, Chapter 7.

[2.5] Bello, P.A., "A Study of the Relationship Between Multipath Distortion and Wavenumber Spectrum of Refractive Index in Radio Links", Proc. IEEE, Vol.59, No.1, January 1971, pp 47-75.

[2.6] Beckman, P. and A. Spizzichino, The Scattering of Electromagnetic Waves from Rough Surfaces, Macmillan, New York, 1963, Chapter 7.

[2.7] Mondre, E., "Complex and Envelope Covariance for Ricean Fading Communication Channels", IEEE Trans. on Communication Technology, February 1971, pp 80-84.

[2.8] Kailath, T., "Measurements on Time-Variant Communication Channels", IEEE Trans. IT, September 1962, pp 231-233.

[2.9] Bello, P.A., "Measurement of the Complex Time-Frequency Channel Correlation Function", Radio Science Vol. 68D, No. 10, October 1964, p 1161.

[2.10] Gallager, R., "Characterization and Measurement of Time and Frequency-Spread Channels", MIT Lincoln Lab Tech Report 352, April 1964.

Section 3

CHANNEL MEASUREMENT USING COHERENT TONES

The basic idea behind this scheme is the sampling of $H(f,t)$ using a set of spaced coherent tones. If the spacing is sufficiently small, the complete function $H(f,t)$ can be reconstructed and processed to obtain its correlation properties. Generally speaking it is only necessary to correlate individual tone responses thus obtaining an estimate of the sampled correlation function. It will be seen that a major difficulty in this method is in maintaining phase stability for the tones. In fact the true channel response will be masked by,

(a) Instabilities in the transmitter oscillator.

(b) Movement of the spacecraft giving rise to Doppler shifts in the received signal.

(c) Instabilities in the receiver oscillator output.

One could argue that (a) and (b) will be part of any ultimate communications system anyway and should be measured as part of the channel. However the choice of oscillator for an initial experiment may be somewhat restricted and not entirely representative so that it would appear better to try and separate the effects of oscillator and propagation medium.

Alternatively it can be shown that for certain configurations both (a) and (b) give rise to a phase error which is linear with frequency. Careful processing at the receiver will eliminate this variable linear term, but also unfortunately introduce certain errors in the estimation of the medium induced linear phase component. A linear phase shift with frequency corresponds to an instantaneous delay in the time domain,

and constitutes quite an important aspect of the millimeter wave channel. It would be desirable to know the typical or RMS delay fluctuation and its rate of variation.

Thirdly, we can consider the use of averaging times that are short compared with the oscillator instabilities and satellite induced phase drifts [3.1]. For the millimeter wave channel, the probing bandwidths of interest do not allow this kind of approach, as will be seen subsequently.

The individual channel probing schemes will now be examined in more detail beginning with the approach that looks the most promising to date, which is based on the multitone signal.

3.1 Form of the Transmitted Signal

The basic transmitted waveform consists of several coherently phased tones. These will be denoted by,

$$S_n(t) = a_n \sin(\omega_n t + \theta_n) \qquad n=0,\pm 1,\ldots,\pm N \qquad (3.1)$$

After phase and amplitude distortion by the channel, the received tones are processed so as to yield estimates of the desired channel properties.

The tones must be generated from a single low frequency reference oscillator to ensure coherency. The reference is multiplied up to the desired RF band using a synthesizer. In addition the reference can be used to phase modulate a carrier so that a constant amplitude signal is made available to the final stages of the transmitter.

The following analysis pertains to the latter technique which is to be used to generate the ATS-F satellite millimeter wave probing signal.

Consider for example the 20 GHz signal. Starting with a reference oscillator of frequency $f_s \simeq 5$ MHz, a carrier is obtained by multiplying up to 10 GHz i.e., using a multiplication of K = 2000 we have,

$$c(t) = \sin (K\omega_s t + K\theta_s) \tag{3.2}$$

where ω_s and θ_s are the frequency and phase of the reference and,

$$\frac{K\omega_s}{2\pi} = 10 \text{ GHz}.$$

The carrier is phase modulated in such a way that 65% of the output is in the multitone spectrum. The phase modulator is driven by the output of a multitone processor which is in turn driven by a harmonic of the oscillator. The multitone processor consists of an amplifier and matching network and provides a sinusoidal drive to the modulator, i.e.,

$$m(t) = \beta_1 \sin (k\omega_s t + k\theta_s), \; k = 36 \tag{3.3}$$

Hence the transmitter output after x2 multiplication is;

$$s(t) = \sin (2K(\omega_s t + \theta_s) + \beta \sin (k\omega_s t + k\theta_s))$$

$$\beta = 2\beta_1 \tag{3.4}$$

Figure 3.1 shows the basic transmitter structure.

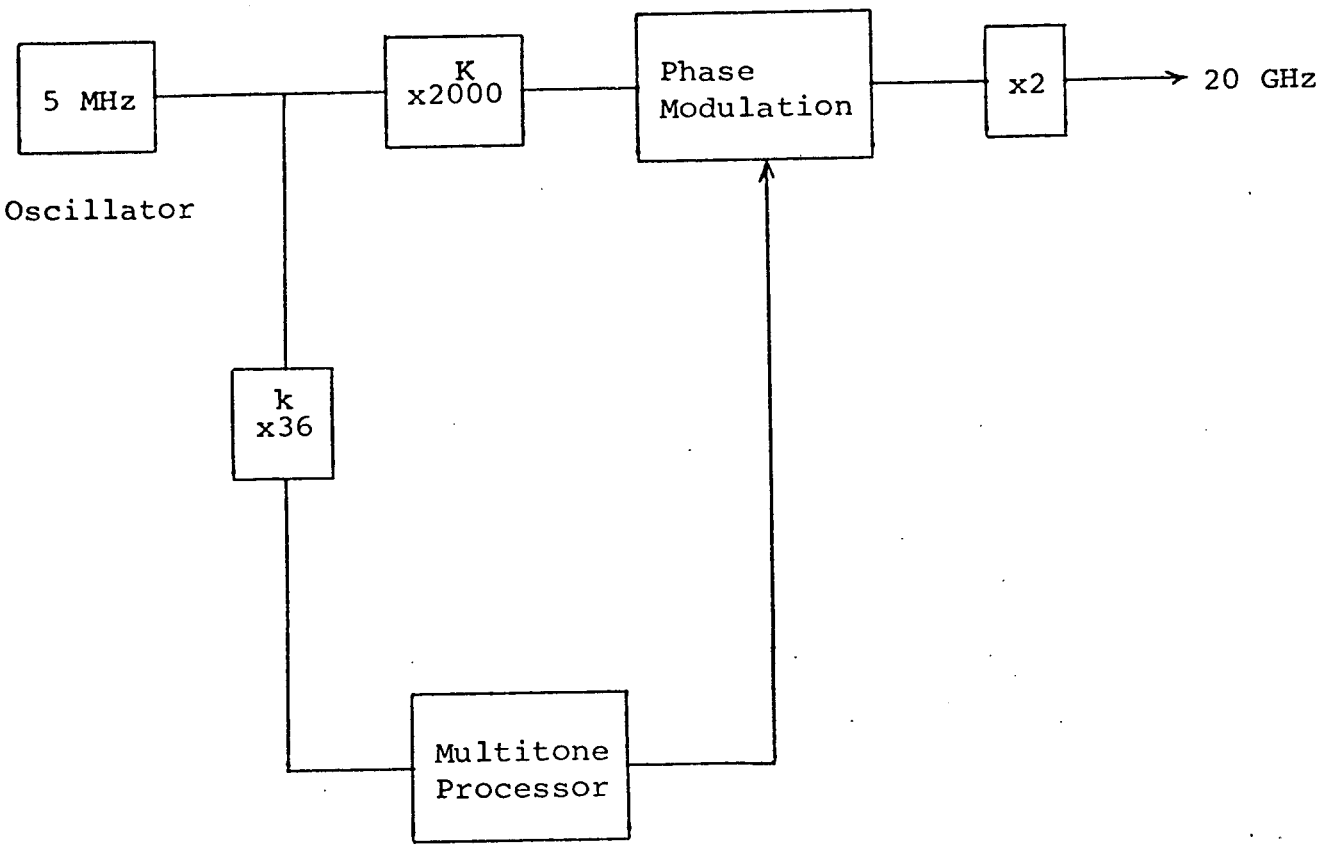

Fig. 3.1 Transmitter

In terms of a carrier frequency ω_0 and modulation frequency ω_m;

$$s(t) = \sin (\omega_0 t + \theta_0 + \beta \sin (\omega_m t + \theta_m)) \qquad (3.5)$$

which results in sidetone expansion of the form;

$$s(t) = \mathrm{Im}\{e^{j(\omega_0 t + \theta_0 + \beta \sin (\omega_m t + \theta_m))}\}$$

$$= \mathrm{Im}\{e^{j(\omega_0 t + \theta_0)} \sum_n a_n e^{jn\omega_m t}\}$$

where

$$a_n = \frac{1}{2\pi} \int_{-\pi/\omega_m}^{\pi/\omega_m} e^{j(\beta \sin (\omega_m t + \theta_m) - n\omega_m t)} \, dt$$

$$= \frac{1}{2\pi} e^{jn\theta_m} \int_{-\pi + \theta_m}^{\pi + \theta_m} e^{j(\beta \sin x - nx)} \, dx$$

$$= e^{jn\theta_m} J_n(\beta)$$

Thus

$$s(t) = \sum_{n=-\infty}^{\infty} J_n(\beta) \sin (\omega_0 t + \theta_0 + n(\omega_m t + \theta_m)) \qquad (3.6)$$

Thus if we represent the composite signal s(t) as the sum of tones,

$$s(t) = \Sigma\, a_n s_n(t) = \sum_{-\infty}^{\infty} a_n \sin(\omega_n t + \theta_n) \tag{3.7}$$

we see that,

$$a_n = J_n(\beta) \tag{3.8}$$

$$\omega_n = \omega_0 + n\omega_m = (2K + kn)\omega_s \tag{3.9}$$

$$\theta_n = (2K + kn)\,\theta_s \tag{3.10}$$

The index β_1 can be chosen so that the desired coefficients $\{a_n\}$ are similar in magnitude and negligible outside the desired band. Differential amplitude effects can easily be accounted for provided that the system is correctly calibrated.

We now proceed with a discussion of the tone instabilities induced by oscillator variability and satellite motion.

3.1.1 Phase Instabilities

The following areas are of importance in this discussion.

(a) The effect of satellite oscillator instabilities.

(b) Phase shifts due to satellite movement.

(c) Receiver local oscillator instabilities and their relationship to derived references.

It will be demonstrated that (a) and (b) induce a phase deviation which is linear across the band, while the influence of the receiver local oscillator depends on the precise nature of the processing employed.

Let us assume that the satellite reference phase is

$$\omega_s t + \theta_s(t)$$

where $\theta_s(t)$ is a random time varying term which accounts for the oscillator drift. From Eq. 3.10 it is seen that the individual tones are affected also,

$$\theta_n(t) = (2K + kn)\ \theta_s(t) \tag{3.11}$$

Alternatively in terms of the carrier phase θ_o,

$$\theta_n(t) = \left(1 + \frac{kn}{2K}\right)\ \theta_o(t) \tag{3.12}$$

Thus for a phase reference (or equivalently frequency) perturbation, we experience a corresponding linear phase perturbation across the band.

Similarly movement of the satellite causes phase errors. If the total transmitter-receiver path length is x, the phase shift at the carrier corresponding to this free space path is,

$$\psi_o = kx \qquad\qquad k = \frac{\omega_0}{c}$$

Hence for a variable path length,

$$\psi_n(t) = \frac{\omega_n}{c}\ x(t) = \left(1 + \frac{nk}{2K}\right)\frac{\omega_0 x(t)}{c}$$

$$= \left(1 + \frac{nk}{2K}\right)\psi_o(t) \tag{3.13}$$

i.e. a linear phase variation with frequency. Because the form of $\psi_n(t)$ is identical with the transmitted phase processes $\theta_n(t)$ of Eq. (3.12), we will not distinguish between the two effects in future, and simply lump ψ_n variations in with those caused by oscillator instability. Equations (3.12) and (3.13) indicate that provided the carrier phase $\theta_o(t)$ is tracked, the incremental phase effects at the sidetones can be accounted for. In other words the carrier phase contains complete phase information for the total spectrum. An incremental phase correction procedure of this kind will be discussed in later sections. For the moment we merely add the warning that transmitted signals must also pass through a dispersive medium which does not have linear phase frequency properties, and hence any correction scheme based on received carrier phase will in fact introduce phase errors.

The discussion of item (c), instabilities in the receiver reference oscillator, will be postponed until the next section which deals with the basic receiver structure.

3.2 Basic Receiver Structure

The total bandwidth of the transmitted spectrum must be greater than 1 GHz, thus dictating the use of individual tone processors i.e. each of the tones must be supplied with a reference such that after mixing, individual tones are contained in separate but similar channels at a second IF of about 10 MHz. At this frequency they can easily be manipulated and processed to yield the desired phase and amplitude information. Figure 3.2 shows the general receiver structure of interest.

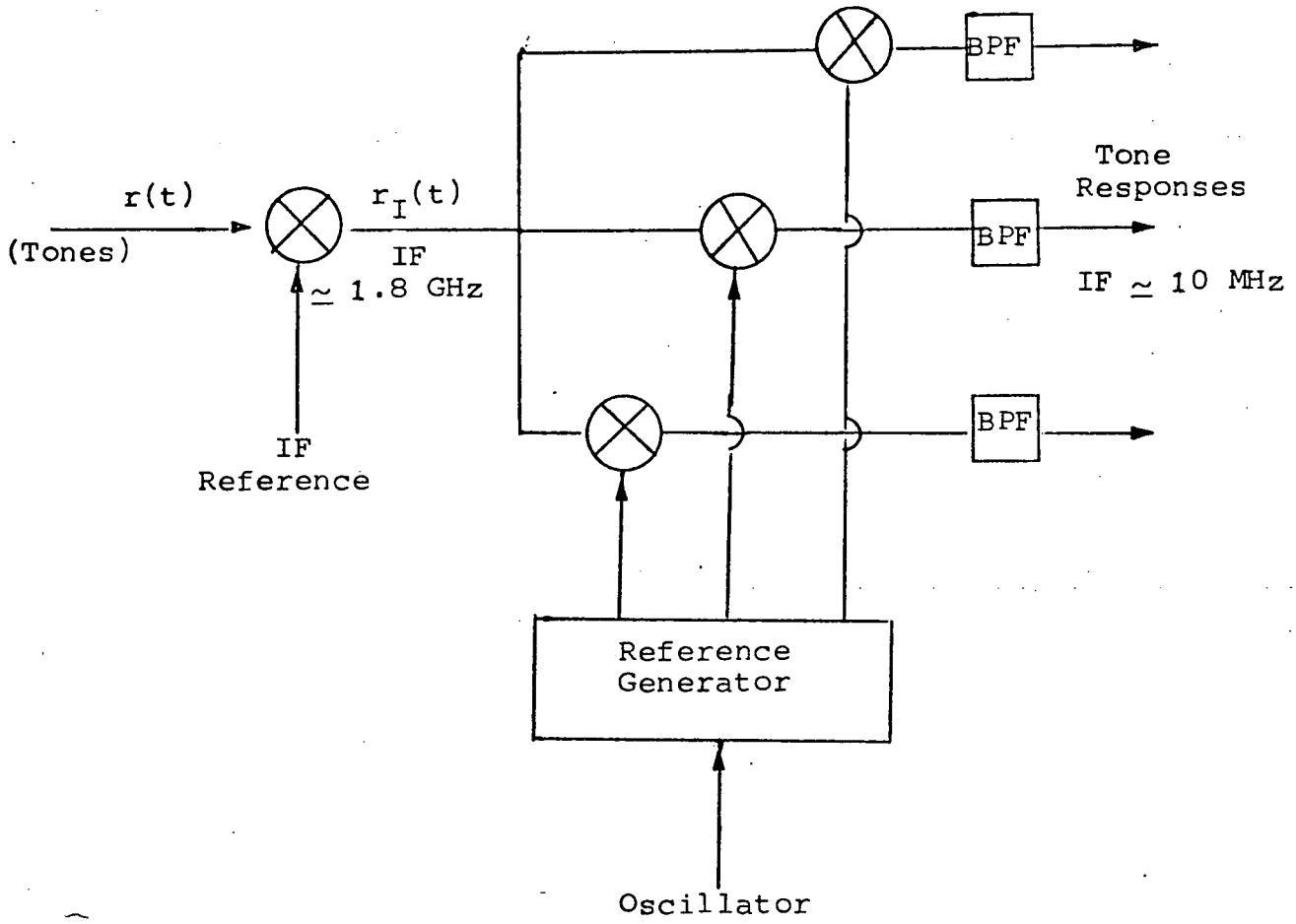

Fig. 3.2. General Receiver Structure

The signals which would exist at the receiver for a free space path can be written as,

$$s_n(t) = \sin(\omega_n t + \theta_n) \qquad n=0, \pm1 \cdots \pm4 \tag{3.14}$$

Note that unity amplitude has been assumed to simplify the notation. These tones are received subject to phase and amplitude distortions due to randomness of the propagation medium;

$$r_n(t) = \alpha_n \sin(\omega_n t + \theta_n + \phi_n) \tag{3.15}$$

where ϕ_n and α_n are the channel induced phase and amplitude fluctuations (relative to the free space response).

The received signals are first mixed down to a convenient IF band.

The resulting IF signals can be represented as,

$$r_{In}(t) = \alpha_n \sin(\omega_{In} t + \theta_n + \phi_n + \theta_I) \tag{3.16}$$

where ω_{I0} is the center IF frequency and θ_I is the phase of the IF reference. Typically the IF frequency will need to be a few GHz to accommodate the total spectrum bandwidth. For the proposed ATS-F system it is 1.8 GHz. The radian frequency of the n-th tone at the first IF is ω_{In}.

To reduce each tone to the second (10 MHz) IF, two possibilities exist.

(a) Use individual references offset by ω_{IF} <u>below</u> each tone frequency. (See Fig.3.3a). ω_{IF} here denotes the second IF frequency.

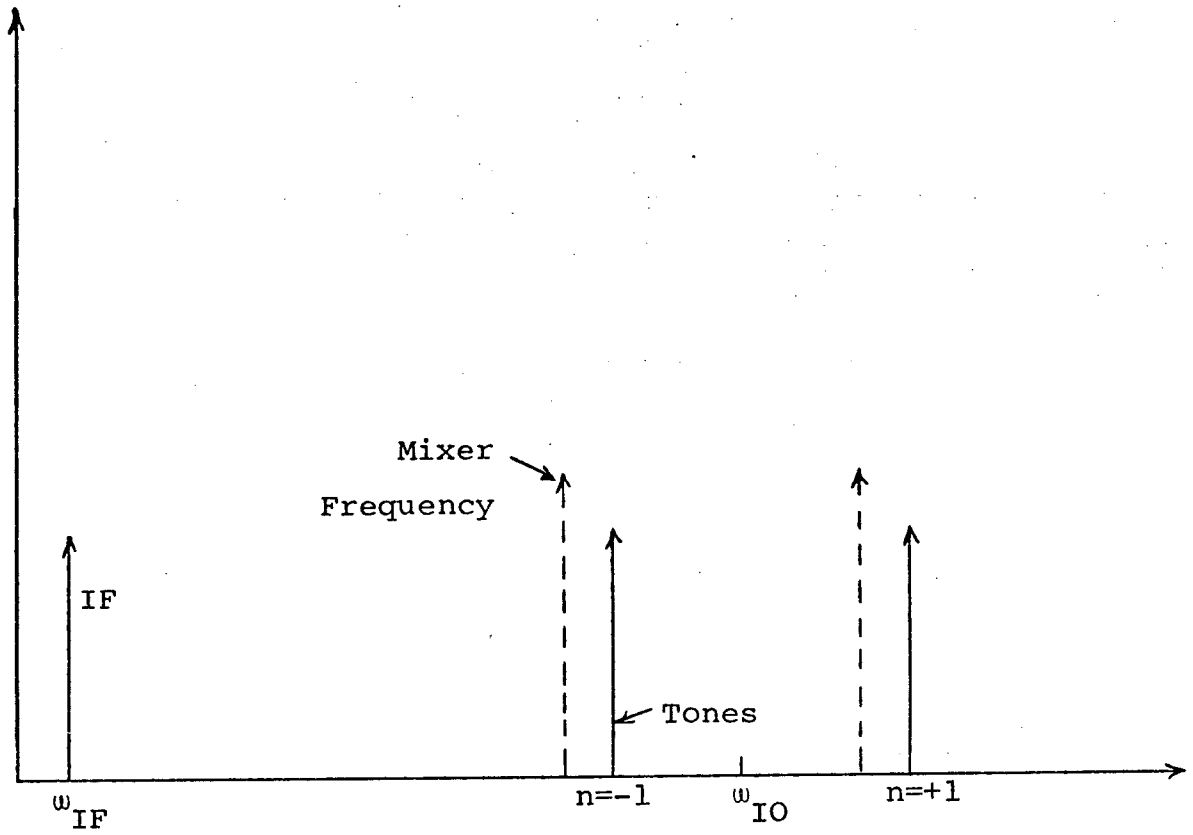

Fig. 3.3a. Phase Difference References

(b) Use a reference between the upper and lower sidetones of interest. (See Fig.3.3b) with subsequent translation to ω_{IF}.

Figures 3.3a and b show these two alternatives in terms of a pair of tones n = ±1.

For the processing outlined in (a) the signals represented by Eq. (3.16) become;

$$\tilde{r}_n(t) = \alpha_n \sin(\omega_{IF}t + \theta_n + \phi_n + \theta_I + \theta_{IF}) \qquad (3.17)$$

θ_{IF} is the phase introduced by the references. At this point it should be noted that the references will be synthesized from a stable reference oscillator with frequency and phase denoted by ω_* and θ_* respectively. Hence θ_{IF} will depend on n, although the precise nature of this dependence will vary with the method used to derive the references. For example the references could be obtained directly from the receiver oscillator,

$$\omega_{Rn} = (2K+kn)\omega_* - N\omega_*$$

$$\theta_{Rn} = (2K+kn)\theta_* - N\theta_*$$

where $\omega_* \simeq \omega_s$ and N is chosen so that the desired second IF ω_{IF} results.

Alternatively using a phase locked loop to track the carrier at the 1st IF (ω_{IO}), we could derive references of the form;

$$\omega_{Rn} = \omega_{IO} + kn\omega_* - N\omega_*$$

$$\theta_{Rn} = \theta_{IO} + kn\theta_* - N\theta_*$$

Again N is chosen so that a second IF at ω_{IF} results.

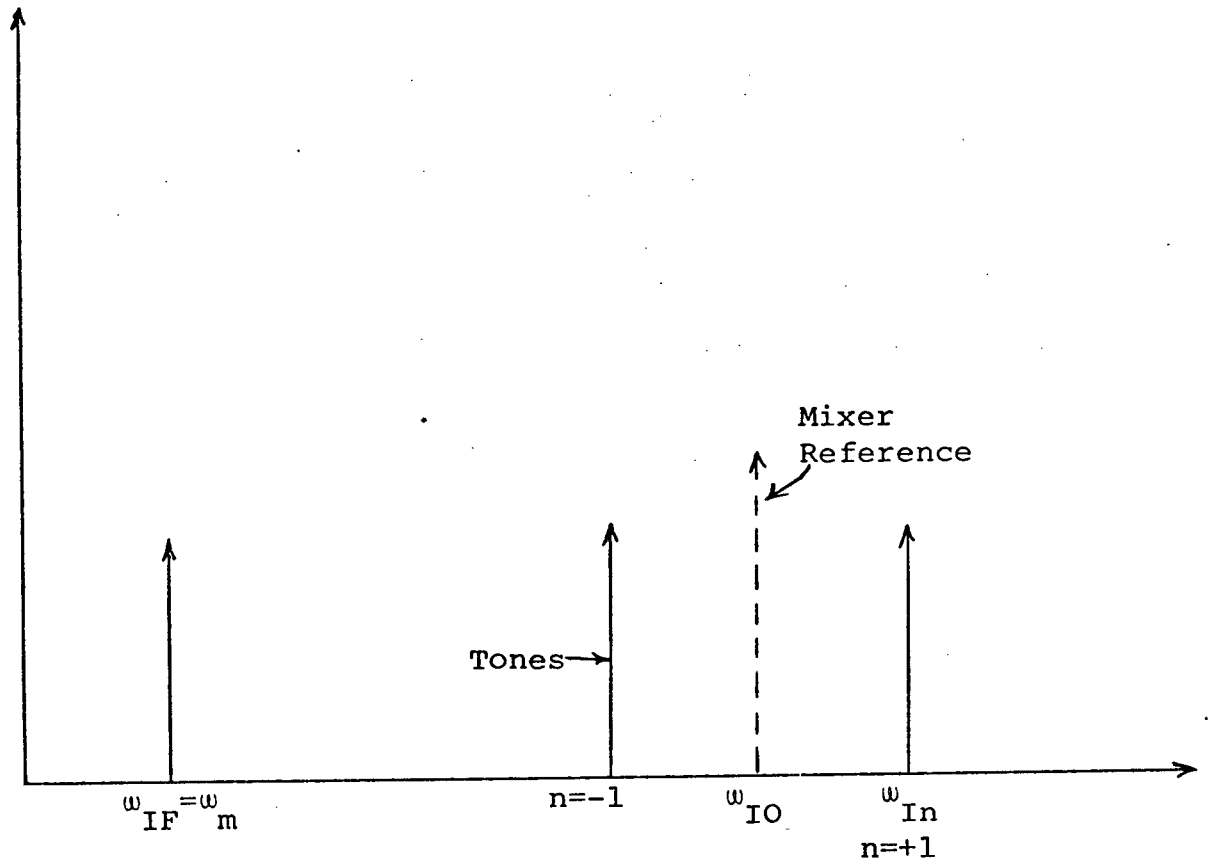

Fig. 3.3b. Phase Sum Reference

For this latter situation it can be shown that the resulting phase difference between tone n and tone -n can be expressed as;

$$\tilde{\phi}_n = \theta_n - \theta_{-n} + \phi_n - \phi_{-n} - 2nk\theta_*$$

$$= \phi_n(t) - \phi_{-n}(t) + 2nk(\theta_s(t) - \theta_*(t)) \qquad (3.18)$$

The difference $\theta_n - \theta_{-n}$ was obtained using Eq. (3.11). Note that;

(i) The usefulness of such a measurement over a total interval (0,T), depends on the stability of both transmitter and receiver oscillators.

(ii) θ_s and θ_* will always be unknown parameters; at best it can be hoped that they will be constant over the measurement interval, thus introducing only a fixed unknown path delay.

(iii) Similar results are obtained for phase differences between say tone n and the carrier with an obvious alteration of the factor 2nk to nk.

(iv) The phase θ_I introduced by the first mixer reference is removed by the phase differencing process, since it is not a function of n.

It is immediately apparent from Eq. (3.18), that the difficulties suggested in (i) will be alleviated by locking θ_* to θ_s. It is not possible to do this exactly since neither θ_s nor θ_0 can ever be observed directly, but estimates of θ_s obtained by tracking the center frequency phase could, in principle, be obtained. This is the substance of material presented in Sections 3.2.1 and 3.2.2 where we describe an effective phase tracking scheme, referred to as the incremental phase correction approach.

Let us now return to item (b), which suggests an alternative processing scheme using a central reference.

Assume that a reference locked to the carrier at IF, is available to the second mixer. i.e. the reference is represented by,

$$\sin\ (\omega_{IO}t + \theta_0 + \phi_0 + \theta_I) \tag{3.19}$$

After mixing with tone n we choose the frequency difference signal,

$$\tilde{r}_n = \alpha_n \sin\left[(\omega_{IO} - \omega_{In})\ t \pm(\theta_n-\theta_0 + \phi_n-\phi_0)\right] \tag{3.20}$$

The plus sign applies to tones above the IF center frequency ω_{IO}, while the negative sign applies to those below. Subsequent translation down to ω_{IF} introduces an arbitrary phase constant which need not be considered, provided we are only interested in the phase relationship between $\tilde{r}_n$ and $\tilde{r}_{-n}$. Their phase difference will be;

$$\Delta\phi_n = \theta_n + \theta_{-n} + \phi_n + \phi_{-n} - 2\ (\theta_0 + \phi_0)$$

From Eq. (3.12) it is seen that

$$\theta_n + \theta_{-n} - 2\theta_0 = 0$$

Hence

$$\Delta\phi_n = \phi_n + \phi_{-n} - 2\phi_0 \tag{3.21}$$

Thus it appears that $\Delta\phi_n$ is not influenced by either satellite or receiver oscillator instabilities and it removes the effect of total path delay. Unfortunately it also eliminates any linear phase vs frequency trends in the channel phase parameter ϕ. In effect this measurement removes the instantaneous linear phase variation across the band. More generally it can be shown to remove <u>all</u> terms with odd exponents in a Taylor's series expansion of the phase process. To conclude we note that there is no difficulty in making amplitude measurements once the signals are available at the second IF.

In phase and quadrature components can easily be extracted from each of the IF tones. The resulting in-phase and quadrature processes will be directly related to $\tilde{r}_n(t)$ of Eq.(3.17) mixed with the tracked carrier at the second IF. The demodulator will have a reference signal;

$$\sin(\omega_{IF}t + \theta_0 + \phi_0 + \theta_I + \theta_{IF}) \tag{3.22}$$

and after mixing tone n will yield in-phase and quadrature components $X_n(t)$ and $Y_n(t)$ respectively;

$$X_n = \alpha_n \cos (\theta_n - \theta_0 + \phi_n - \phi_0 - nk\theta_*)$$

$$Y_n = \alpha_n \sin (\theta_n - \theta_0 + \phi_n - \phi_0 - nk\theta_*)$$

or using Eq. (3.11) we get,

$$X_n(t) = \alpha_n(t) \cos \left[\phi_n(t) - \phi_0(t) + nk(\theta_s(t) - \theta_*(t))\right]$$

$$Y_n(t) = \alpha_n(t) \sin\left[\phi_n(t) - \phi_0(t) + nk(\theta_s(t) - \theta_*(t))\right] \quad (3.23)$$

Unless the reference oscillators are highly stable, the in-phase and quadrature components will be inadvertently phase modulated. For example consider an oscillator stability of 1 part in 10^9 averaged over 10 msec. The expected phase error over this interval for n=4, k=36 and ω_s=5 MHz can be computed from,

$$\epsilon = \text{stability} \times kn\omega_s T$$
$$= 10^{-9}\ 7200 \times 10^6\ 10^{-3}$$
$$= 7.2 \times 10^{-3} \text{ cycles.}$$

While this is not excessive for the short time interval and high oscillator stability specified, it indicates that serious difficulties will arise for realistic averaging times on the order of 10-100 seconds. Furthermore it demonstrates that an oscillator of high quality is mandatory. The consequences of processing over time intervals using a poor quality oscillator may be seen by representing the introduced phase error

in terms of a random variable uniformly distributed over 2π. Averaging in an ensemble sense or time averaging as in the actual measurement, the result will approach zero.

3.2.1 Carrier Tracking and Incremental Phase Correction Schemes

In this section we explore whether a receiver structure is capable of correcting for the effects of satellite mostion and system oscillator instabilities. Eq. (3.18) and (3.23) indicate explicitly the consequences of transmitter and receiver oscillator phase fluctuations from the point of view of both direct phase comparison measurements and quadrature and in-phase measurements. The satellite motion introduces phase variations similar in effect to transmitter instabilities so that they can be included in $\theta_s(t)$. The basic idea of this section is to extend the concept of the phase lock loop in its role of tracking the carrier phase. In the absence of any scattering effects the channel can be represented as a time invariant filter $T_c(f)$, (See Section 2.2) coupled with a variable delay. Figures 3.4 and 3.5 illustrate this simplified channel model. The delay accounts for all linear phase vs frequency characteristics introduced by oscillator and satellite variations. Since the dispersive medium is physically separated from these effects, it can be dealt with independently in the system model.

The phase locked loop essentially establishes the phase at the carrier frequency. An incremental phase correction based on Eq. (3.12) can then be implemented. i.e. using the relationship;

$$\theta_n(t) = \left(1 + \frac{kn}{2K}\right) \theta_0(t)$$

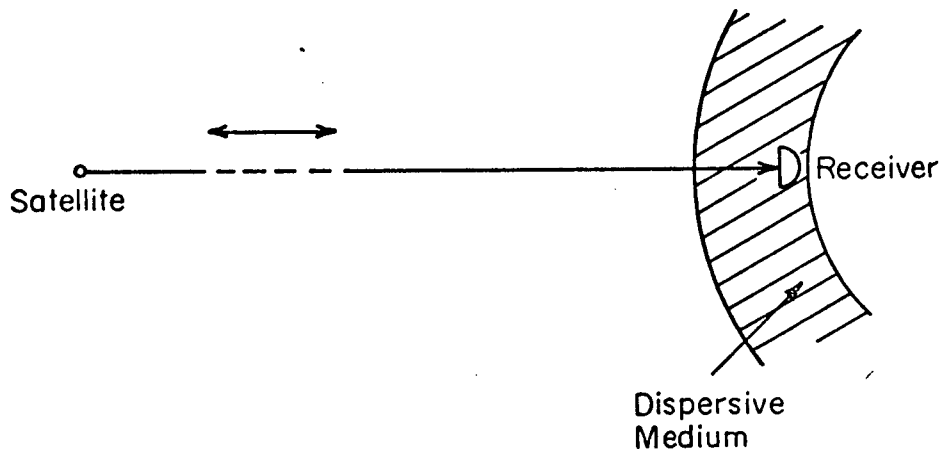

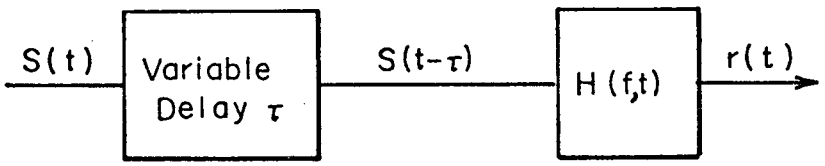

Figure 3.4 Representation of Satellite Motion and Oscillator Instabilities

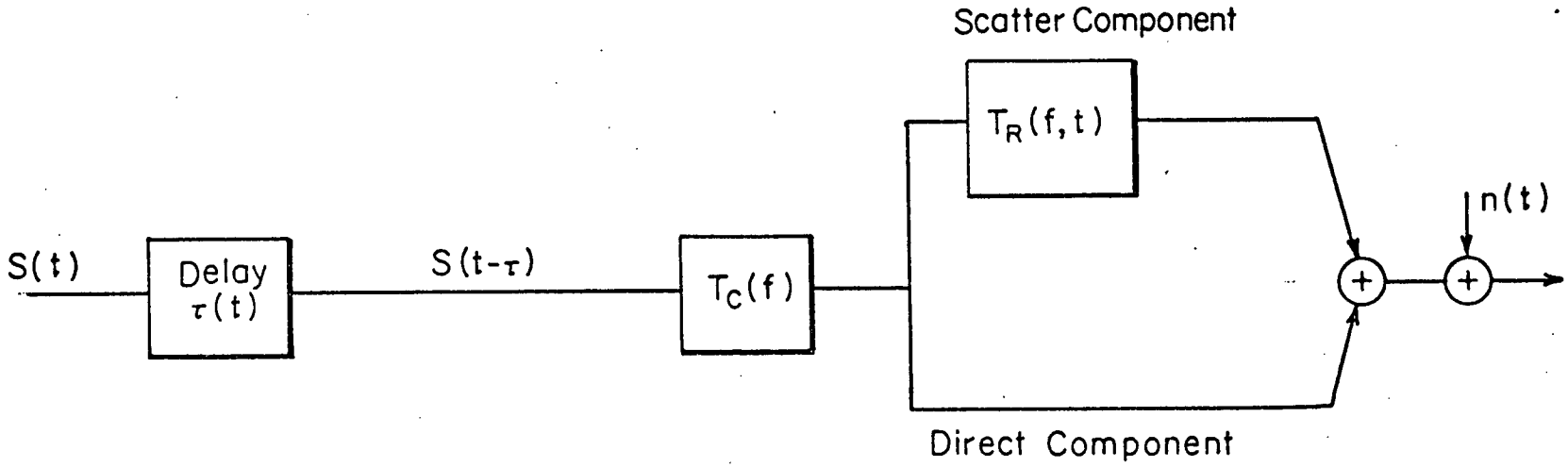

Figure 3.5 Complete Channel Model

If $\theta_0(t)$ is available at the reference synthesizer, corrections can be made. Figure 3.6 shows the structure of a phase locked loop which would be compatible with the currently proposed ATS-F receiver.

It is important to note that the first mixer reference must be generated from the reference ω_*. The use of an independent oscillator at the first mixer introduces phase fluctuations, so that the incremental correction scheme would respond incorrectly.

While the configuration shown in Fig. 3.6 is desirable from a practical point of view, it is instructive to first analyze the operation of the incremental correction scheme in terms of a simplified structure. Let us assume, as shown in Fig. 3.7, that the loop encompasses the first mixer so that all of the loop frequency translations can be combined using a single mixing operation. Under locked conditions both inputs to the phase detector have the same phase, and at the mixer, (ω_1 and θ_1 relate to the VCO-multiplier output)

$$\omega_0 t + \theta_0 - (\omega_1 t + \theta_1) = \omega_* t + \theta_* \tag{3.24}$$

By providing the offset ω_* between the mixer and the VCO we are able to choose $\omega_{v0} \simeq \omega_s$. Hence the VCO output has phase,

$$\omega_{v0} t + \theta_{v0} = \frac{1}{2K} (\omega_1 t + \theta_1 + \omega_* t + \theta_*)$$

$$= \frac{1}{2K} (\omega_0 t + \theta_0) \tag{3.25}$$

The latter relationship follows from Eq. (3.24). Then from Eqs. (3.9) and (3.10) we see that

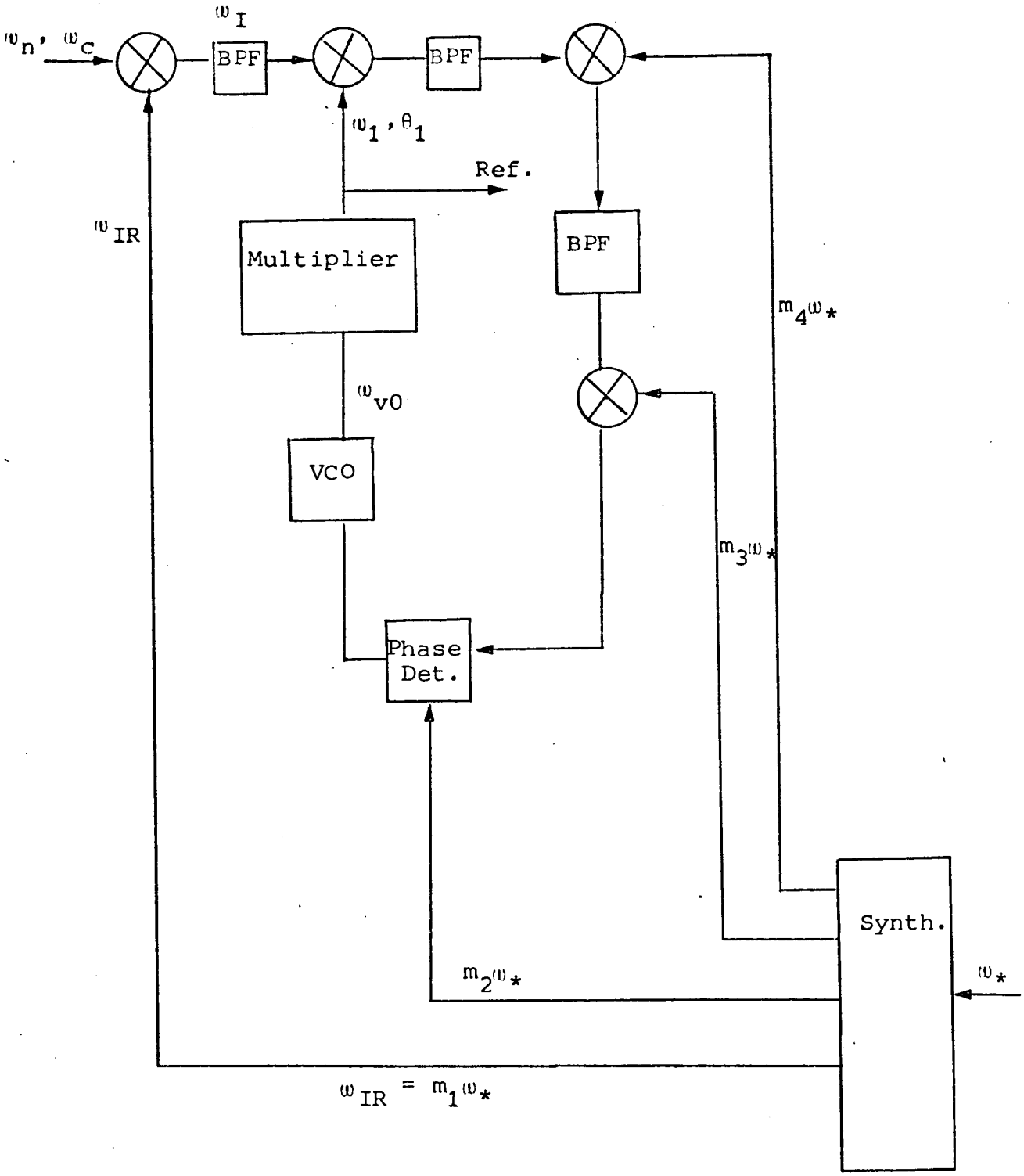

Fig. 3.6 Phase Locked Loop Structure

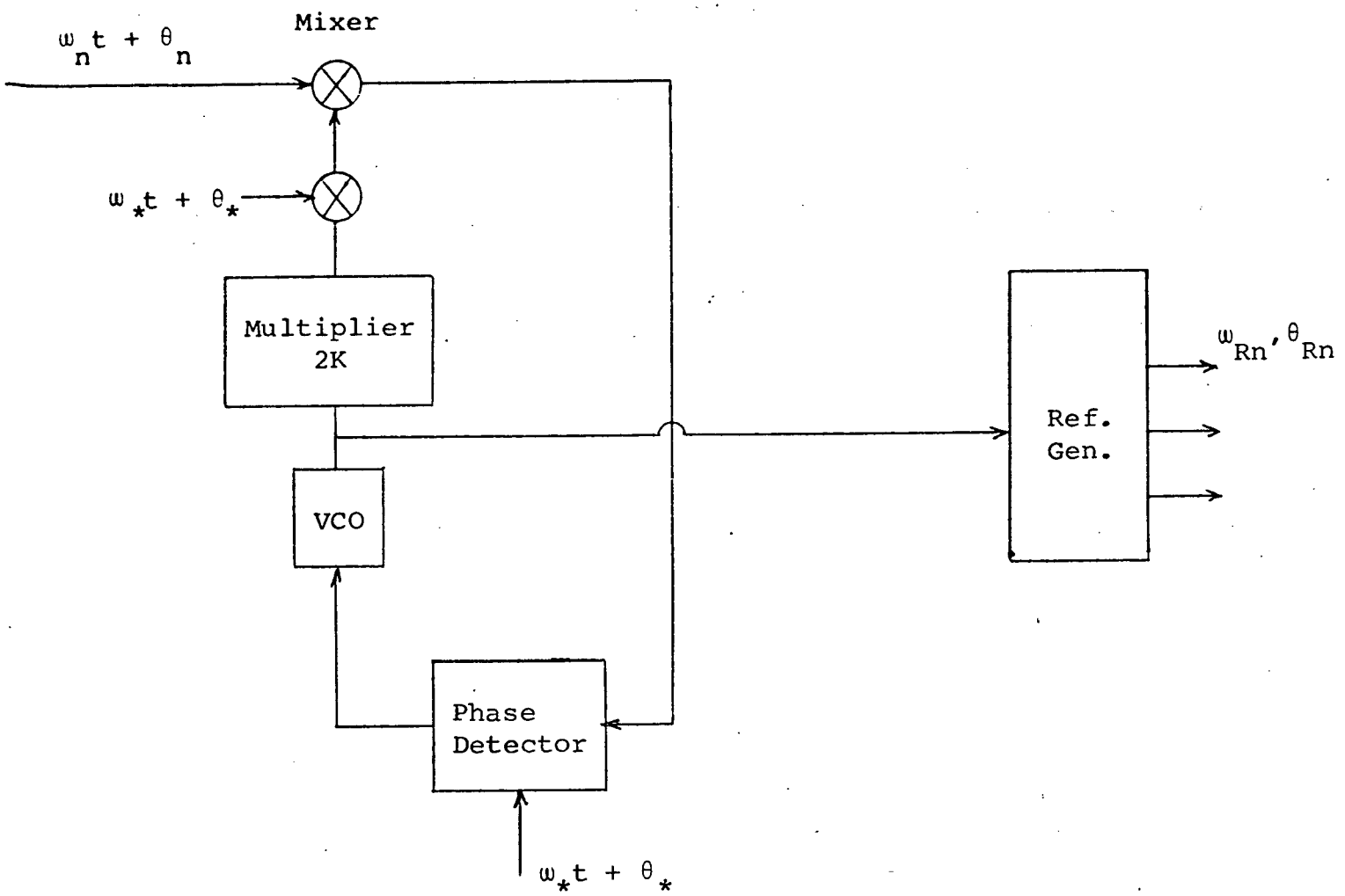

Fig. 3.7 Simplified Phase Locked Loop Structure

$$\omega_{v0}t + \theta_{v0} = \omega_s t + \theta_s \tag{3.26}$$

and the references can be generated using the relationships,

$$\omega_{Rn} = (2K + nk)\ \omega_{v0}$$

$$\theta_{Rn} = (2K + nk)\ \theta_{v0} \tag{3.27}$$

When the references specified by Eq. (3.27) are employed, the individual tones are mixed down to baseband, which is desirable if in-phase and quadrature components are to be measured. Alternatively the references can be offset by some nominal IF frequency ω_{IF}.

The simple minded approach depicted by Fig. 3.7 can be expanded to avoid various impracticalities but the basic procedure remains the same. For example Fig. 3.8 indicates the way in which the signal can mixed down to an IF for easy processing, without destroying the phase tracking properties of the receiver. In addition the phase detection is carried out after a further reduction in frequency to 100 kHz. The choice of K_1 and K_2 is governed only by practical considerations subject to the condition that;

$$K_1 + K_2 = 2K$$

where

$2K = 2000$ in the proposed experiment.

In general it would not be desirable to have the first IF lower that about 2 GHz because of the wide signal bandwidth, hence

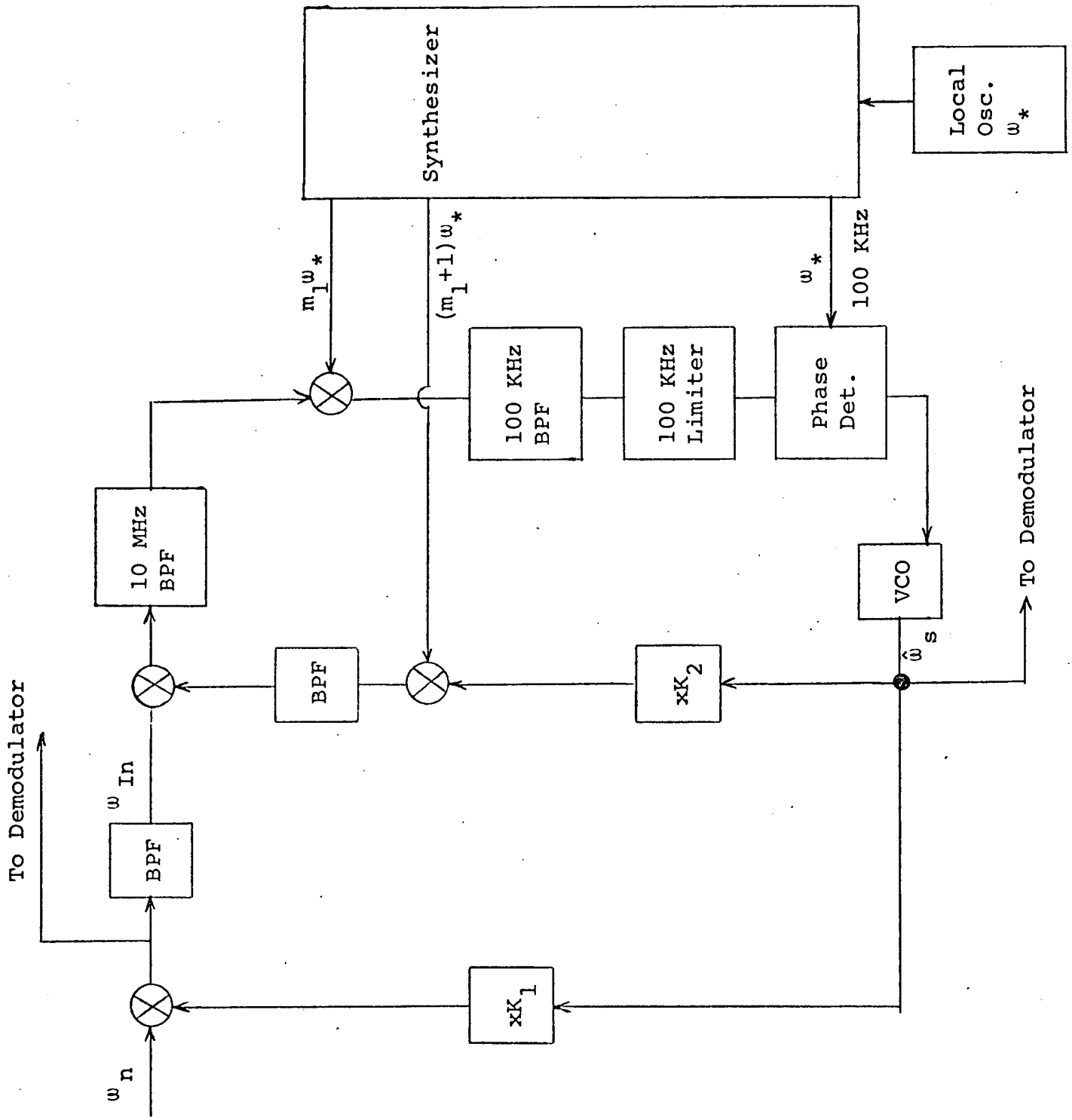

Fig. 3.8 Phase Locked Loop Design

$K_1 \simeq 200$

$K_2 \simeq 1800$

The extraction of in-phase and quadrature tone components must be carried out at a second IF band to avoid complications associated with the 90^{o} phase shifting of the references. Figure 3.9 illustrates one possible method of implementing this measurement.

At this point it would seem that the procedures involved with an incremental phase correction, are not too difficult to realize. However we have not yet broached the question of the utility of such measurements when the channel exhibits arbitrary phase characteristics due to the presence of a scattered signal component. This topic will be investigated in the next section.

3.2.2 Analysis of the Incremental Phase Correction Receiver

For the simplified channel model shown in Fig. 3.5 which involved free space propagation, the incremental phase correction procedure completely removes time variations in the free space path delay. Furthermore when the actual medium can be represented by an equivalent (possibly time varying) refractive index, the same conclusions follow. In these cases all of the tone phases are coherently related to the carrier phase $\theta_0(t)$. However when the signal received is the sum of scattered plus direct energy, no such relationship exists. Thus a linear phase correction scheme incorrectly interprets changes in the mid-band phase by assuming that the linear portion of the composite phase response is in fact proportional to $\theta_0 + \phi_0$. Fig. 3.10 depicts the various phase processes involved, while

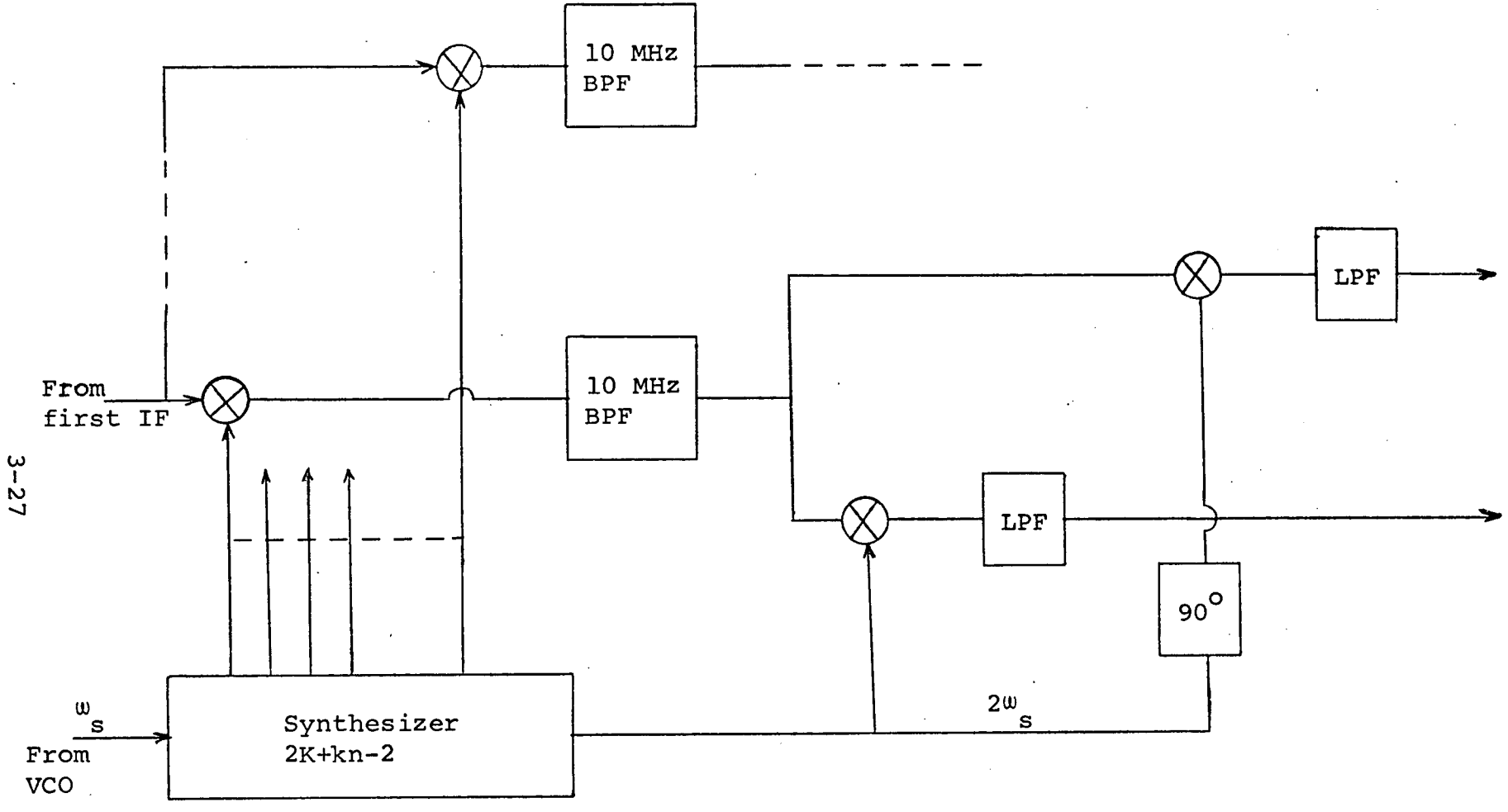

Fig. 3.9 Demodulator Design

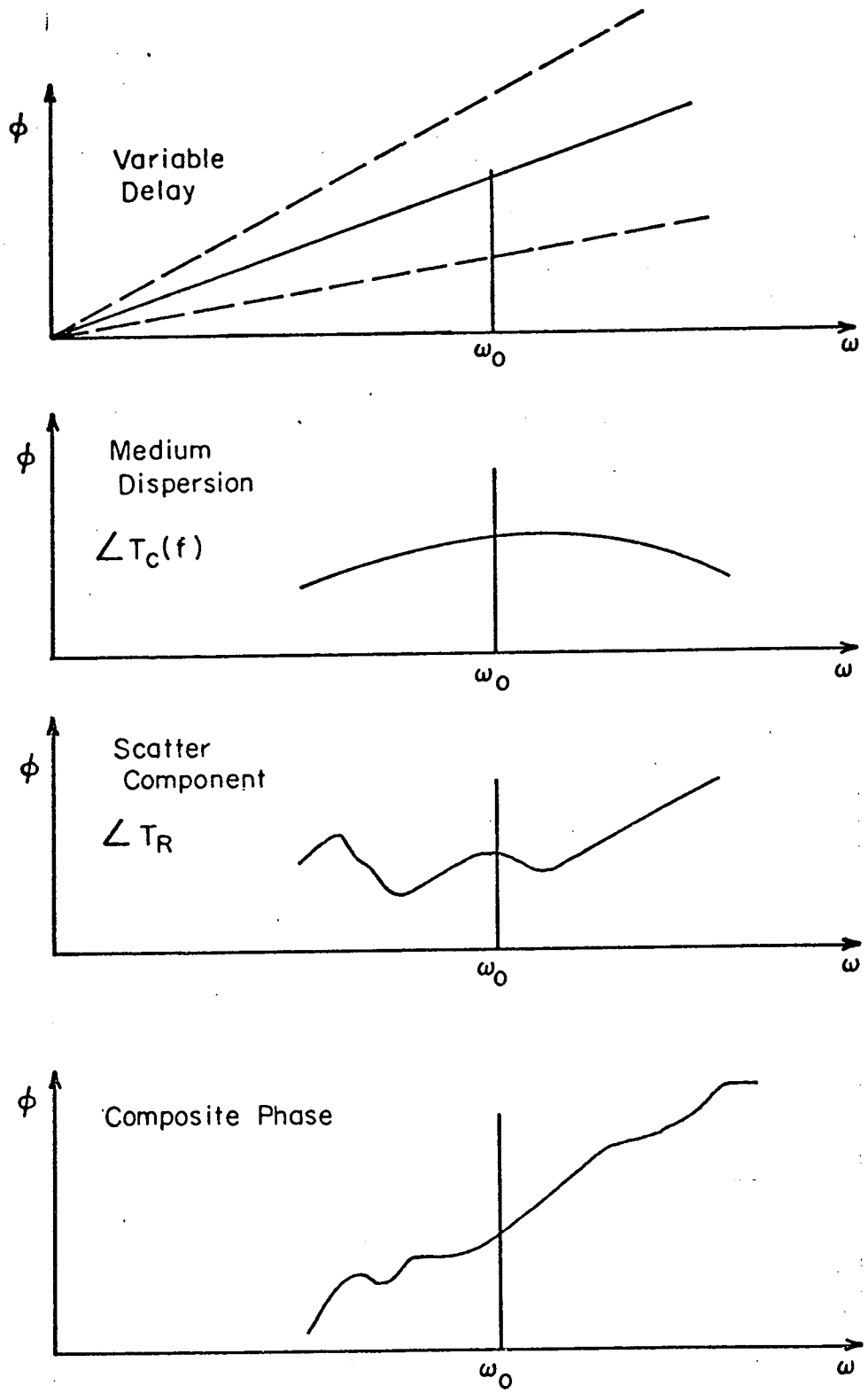

Figure 3.10 Phase-Frequency Characteristics

Fig. 3.11 indicates the complete channel model. (See Section 2). Note that the correction scheme does not actually eliminate the instantaneous linear phase component as one might suppose. This would only occur if $\phi_0 + \theta_0$ was deterministically related to the linear phase term, which is not necessarily true when the filters $T_R(f,t)$ or $H(f,t)$ are involved.

To best illustrate the performance of the phase correction technique, we first examine a continuous model for the phase process. The instantaneous received phase expressed as a function of both time and frequency is,

$$\gamma(t,t) = \phi(f,t) + \theta(f,t) \tag{3.28}$$

where $\theta(f,t)$ represents the time varying phase shift corresponding to the model shown in Fig. 3.5 (i.e. filter T_c plus a variable delay). $\theta(f,t)$ will generally deviate from a linear function of frequency because of the frequency dependent nature of the medium equivalent refractive index. (See Appendix B). However its time variation originates almost entirely from the variable delay. In any case $\theta(f,t)$ can be expressed as,

$$\theta(f,t) = \theta_0(t)\left[1 + \frac{\Delta f}{f_0}\right] + \epsilon(f) \tag{3.29}$$

where $\theta_0(t)$ = phase at carrier
$\Delta f = f - f_0$, deviation from carrier
ϵ = remainder in phase expansion

$\phi(f,t)$ on the other hand is the phase perturbation introduced by the scattered signal contributions (See Fig. 3.5). It can be expressed in terms of the real and imaginary components of the filter T_R as,

$$\phi(f,t) = \tan^{-1}\left[\frac{\mathrm{Im}\{T_R(f,t)\}}{1 + \mathrm{Re}\{T_R(f,t)\}}\right] \tag{3.30}$$

However one should note that

$$|T_R| << 1$$

(See Appendix B); thus we have the approximation,

$$\phi(f,t) \simeq \frac{\mathrm{Im}\{T_R(f,t)\}}{1 + \mathrm{Re}\{T_R(f,t)\}}$$

$$\simeq \mathrm{Im}\{T_R(f,t)\} \tag{3.31}$$

These approximations can be justified because the strength of the scattered signal is expected to be at least 20 dB below the attenuated direct component assuming narrow beamwidth earth station antennas. Consequently we can conclude that $\phi(f,t)$ can be quite small, perhaps less than 10^{-2} radians on the average (for a 20 dB unscattered/scattered power ratio).

Consider an expansion of $\phi(f,t)$ about the carrier frequency;

$$\phi(f,t) \simeq \phi_0(t) + a_1(t)\Delta f + \delta(f,t) \tag{3.32}$$

where $\Delta f = f - f_0$

Then the total observed phase is,

$$\gamma(f,t) = \phi(f,t) + \theta(f,t) = \phi_0(t) + a_1(t)\Delta f$$

$$+ \theta_0(t)\left[1 + \frac{\Delta f}{f_0}\right] + \epsilon(f) + \delta(f,t) \tag{3.33}$$

The phase locked loop (PLL) tracks the carrier phase

$$\gamma_0(t) = \theta_0(t) + \phi_0(t)$$

In discussing phase processes such as this, we are implicitly dealing with the phase relative to some fictional reference. By representing oscillator and satellite instability effects in terms of an equivalent delay as in Fig. 3.5, we can assume this reference to be some ideal, perfectly stable oscillator on board the satellite. Note that $\gamma_0(t)$ is the true carrier phase observed at the receiver; $\theta_0(t)$ includes the free space phase shift corresponding to a large number of wavelengths separating transmitter and receiver. The receiver phase locked loop supplies an estimate $\hat{\gamma}_0(t)$, or more exactly, a reference with phase $\hat{\gamma}_0(t)$, i.e.,

$$A \cos\left(\omega_0(t) + \hat{\gamma}_0(t)\right) \tag{3.34}$$

$$\hat{\gamma}_0(t) = \theta_0(t) + \phi_0(t) \tag{3.35}$$

Let us now consider the phase corrected demodulator references which, as discussed in Section 3.2.1 are generated from the PLL output. Although this procedure is to be implemented in the receiver IF sections, the principles are identical regardless of the frequency band, and for simplicity we carry out the details in terms of the RF signals.

The references are generated with a phase of the form;

$$\theta_R(f,t) = \left(1 + \frac{\Delta f}{f_0}\right) \hat{\gamma}_0(t) \tag{3.36}$$

and this is essentially subtracted from $\gamma(f,t)$. Ideally $\hat{\gamma}_0(t) = \gamma_0(t)$ in which case;

$$\tilde{\gamma}(f,t) \triangleq \gamma(f,t) - \theta_R(f,t)$$

$$= \phi_0(t) + a_1(t)\Delta f + \theta_0(t)\left(1 + \frac{\Delta f}{f_0}\right) + \varepsilon(f) + \delta(f,t)$$

$$- \left(1 - \frac{\Delta f}{f_0}\right)\left(\theta_0(t) + \phi_0(t)\right) \qquad (3.37)$$

Therefore

$$\tilde{\gamma}(f,t) = \left(a_1(t) - \frac{\phi_0(t)}{f_0}\right)\Delta f + \delta(f,t) + \varepsilon(f) \qquad (3.38)$$

In Eq. (3.38) we see that aside from the possibility of errors in the estimate of $\gamma_0(t)$, there is a time varying phase error present. i.e. the desired form of $\tilde{\gamma}(f,t)$ is, (from Eq. (3.32) and (3.29))

$$\gamma(f,t) = \phi(f,t) - \phi_0(t) + \varepsilon(f)$$

$$= a_1(t)\Delta f + \delta(f,t) + \varepsilon(f) \qquad (3.39)$$

while the measurement phase given by Eq. (3.36) contains an additional term,

$$\phi_e(f,t) = \frac{\phi_0(t)}{f_0}\ \Delta f \qquad (3.40)$$

The severity of this error depends on the nature of the channel characteristics and the information we are trying to extract from the received data. In general it can be seen that the factor

$$\frac{\Delta f}{f_0} \leq 0.036 = \frac{720 \text{ MHz}}{20 \text{ GHz}}$$

ensures that the error is small whenever $\phi_0(t)$ and the phase process of interest $\phi(f,t)$, are not strongly correlated. At the other extreme it is clear that when $T(f,t)$ corresponds to a simple time varying delay, the error component reduces the phase $\phi(f,t)$ to zero.

For situations between these two extremes we need to examine some specific measurements. Consider the true in-phase and quadrature components of the scattered signal relative to the so called specular component represented by T_c. (See Fig. 3.11). These quantities will be referred to as

$$x = |T_C T_R| \cos \eta$$

and

$$y = |T_C T_R| \sin \eta \tag{3.41}$$

respectively. Following the spirit of previous approximations we note that,

$$|H(f,t)| \simeq |T_c(f)| + x(f,t) \tag{3.42}$$

and

$$\phi(f,t) \simeq y(f,t) \tag{3.43}$$

However the measured quadrature component will be in error by an amount,

$$\begin{aligned} y_e(f,t) &\simeq \phi_e(f,t) \\ &= \frac{\Delta f}{f_0} \phi_0(t) \\ &\simeq \frac{\Delta f}{f_0} y(f_0,t) \end{aligned} \tag{3.44}$$

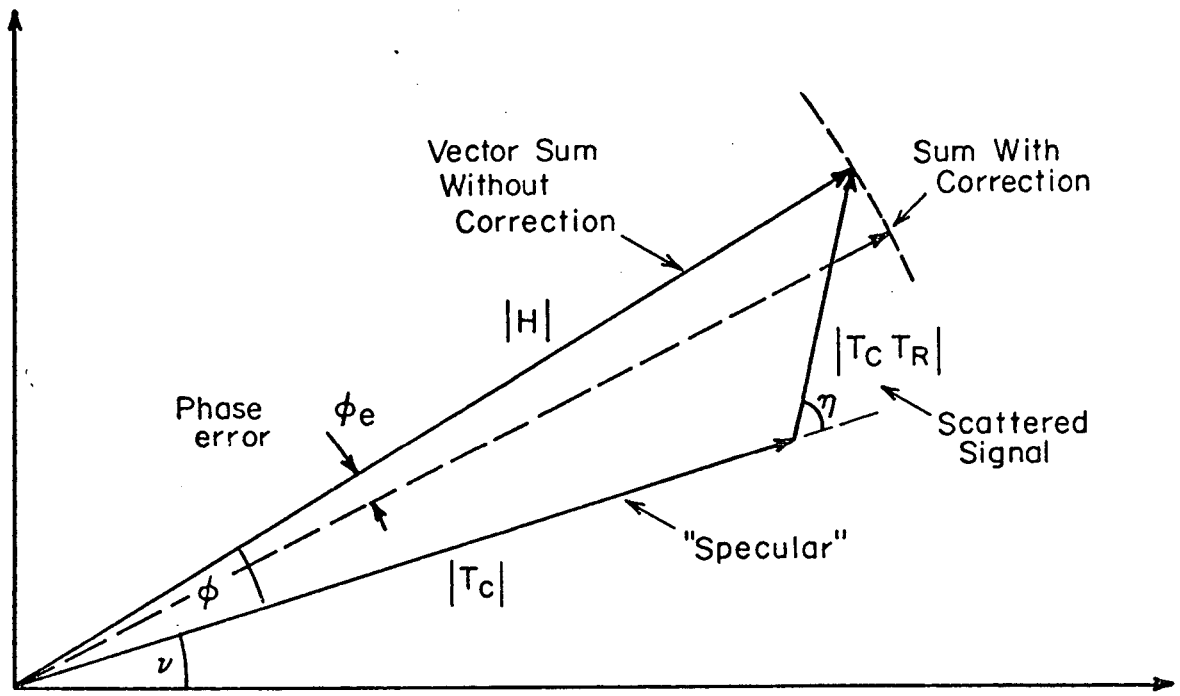

Figure 3.11 Vector Sum of Scattered and Coherent Signal Showing Phase Correction Error

Since the scattered signal is Gaussian in nature and zero mean by definition (See Section 2.2), y(f,t) is characterized by the function,

$$R_y(f_1, f_2; t_1 - t_2) = \overline{y(f_1, t_1)\, y(f_2, t_2)}$$

If we were to try and measure this quantity by averaging the product of two tone responses, we would obtain an estimate which approached,

$$\hat{R}_y(f_1, f_2; t_1 - t_2) = \overline{\hat{y}(f_1, t_1)\, \hat{y}(f_2, t_2)} \qquad (3.45)$$

where

$$\hat{y}(f_1, t_1) = y(f_1, t_1) - y_e(f_1, t_1)$$

etc. Thus

$$\hat{R}_y(f_1, f_2; t_1 - t_2) =$$

$$= \overline{\left[y(f_1,t_1) - \frac{\Delta f}{f_0}\, y(f_0,t_1)\right]\left[y(f_2,t_2) - \frac{\Delta f}{f_0}\, y(f_0,t_2)\right]} =$$

$$= R_y(f_1,f_2;t_1-t_2) + \left(\frac{\Delta f}{f_0}\right)^2 R_y(f_0,f_0;t_1-t_2)$$

$$- \frac{\Delta f}{f_0}\left[R_y(f_0,f_2;t_1-t_2) + R_y(f_1,f_0;t_1-t_2)\right]$$

(3.46)

This relationship clearly indicates the way errors are introduced in a correlation function measurement. To be more specific let

$$R_y(f_1,f_2;t_1-t_2) = R_y(f_1-f_2,\ t_1-t_2)$$

and

$$f_1 = f_0 - \Delta f$$

$$f_2 = f_0 + \Delta f, \text{ so that } f_1 - f_2 = 2\Delta f$$

$$\Delta t = t_1 - t_2$$

Then

$$\frac{\hat{R}_y(2\Delta f,\ \Delta t)}{R_y(2\Delta f,\ \Delta t)} = 1 + \left[\frac{\left(\frac{\Delta f}{f_0}\right)^2 R_y(0,\ \Delta t) - \frac{2\Delta f}{f_0} R_y(\Delta f,\ \Delta t)}{R_y(2\Delta f,\ \Delta t)}\right] \tag{3.47}$$

The fractional error contained in the brackets is insignificant if,

$$\left|\frac{R_y(2\Delta f,\ \Delta t)}{R_y(0,\Delta t)}\right| \geq \left(\frac{\Delta f}{f_0}\right)^2 \tag{3.48}$$

and

$$\left|\frac{R_y(2\Delta f,\ \Delta t)}{R_y(\Delta f,\Delta t)}\right| \geq \frac{2\Delta f}{f_0} \tag{3.49}$$

It can be seen that because $\Delta f/f_0$ is at most 0.04 (for the ATS-F system, these conditions do not pose serious problems. Note that for increasing Δf we would normally expect $R_y(2\Delta f,\Delta f)$ to approach zero. In addition the error parameter $\Delta f/f_0$ becomes larger, so it is clear that the fractional error will be most severe in the tails of $\hat{R}_y$, i.e. for large Δf. Similar conclusions can be drawn for estimates of the in-phase and cross correlation functions R_x and R_{xy}, which were discussed in Chapter 2.

This concludes discussion of the incremental phase correcting receiver. Subject to the limitations imposed by Eqs. (3.48) and (3.49), the method appears feasible. Further study is however required to ascertain whether available receiver components will support the ideal assumptions implicitly made in previous discussions. In particular it must be verified that the receiver does not superimpose any delay distortion on the signal.

From this and previous sections we can intuitively see that if the true channel correlation functions are to be measured, some form of phase correction to eliminate oscillator instabilities is a mandatory requirement. The technique outlined here appears to provide a valid approach only if the actual channel-induced phase fluctuations $\phi(f,t)$ are quite small, and this in turn is due to the presence of a large specular signal. If the phase variations due to the scattered component were in fact larger, it might not be possible to achieve such good separation of the channel from terminal instabilities. An exception occurs if the spectral characteristics of each are such that judicious choice of phase lock loop filter parameters allows separation on a frequency domain basis. This possibility is discussed next.

3.3 Application of Phase Locked Loops for Incremental Phase Correction

It may be possible under certain conditions to separate the phase effects due to satellite motion and oscillator drift from the phase effects due to scattering in the channel. This is possible, for example, when the scattering fluctuations are fast and the phase fluctuations due to satellite motion and oscillator drift are slow. In this case a phase locked loop can be employed to separate the two phase effects.

Specifically, assume that the instantaneous received phase is defined as shown in Eq. (3.28), repeated here for convenience.

$$\gamma(f,t) = \phi(f,t) + \theta(f,t) \tag{3.50}$$

Where $\theta(f,t)$ includes the phase shifts due to oscillator instability and satellite motion and also includes the phase characteristic of the time invariant portion of the channel's transfer function. $\phi(f,t)$ represents the phase perturbation induced by the scatter signal contributions at the receiver. Now, if the bandwidth of $\theta(f,t)$ is much less than the bandwidth of $\phi(f,t)$ then a phase locked tracking loop can be used to separate the two effects at a particular frequency.

A simplified block diagram for this purpose is shown in Fig. 3.12. The transfer function of the phase locked loop, from the input to the output at point A, H(s), is typically a simple low-pass filter of the form given in Eq. (3.51).

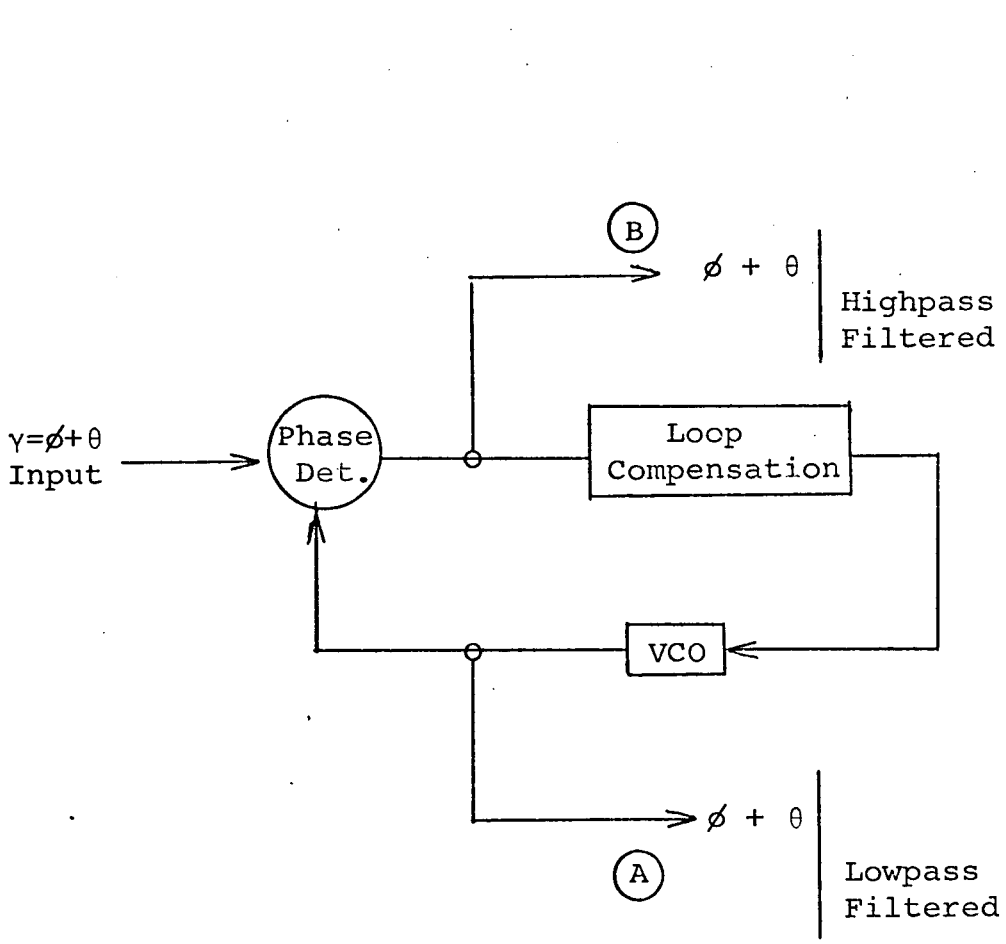

Fig. 3.12 Phase Locked Loop Configuration

$$H(s) = \frac{k(\tau s + 1)}{s^2 + k\tau s + k} \qquad (3.51)$$

That is the transfer function is unity from DC to roughly k rad/s and then the transfer function rolls off at 6 dB per octave. The transfer function from the input to the error point, point B in Fig. 3.12 is given by 1-H(s). Thus from the input to the error point, the loop highpass filters the phase data.

In order to determine the applicability of the phase locked loop technique, the dynamics of the phase variations due to scattering and the phase variations due to oscillator stability and satellite motion must be defined. Appendix A shows that phase variations due to scattering create a doppler spread process whose bandwidth is on the order of 1 Hz, maximum. It is not expected that the Doppler spread will exceed this value by very much. However it is possible that considerably smaller Doppler spreads will be encountered. The large Doppler spread cases are the ones which are of more interest because they involve heavy weather conditions. The dynamics of the phase variations due to oscillator stability and satellite motion are not usually defined in terms of a bandwidth. Instead they are usually specified in terms of power series expansion coefficients. For example, in the case of an oscillator the predominant source of instability may be defined as an aging rate. Of course, for satellites the dynamics are defined in terms of maximum velocity and maximum acceleration along the line of site path. It is reasonable to assume that phase variations due to satellite motion will predominate over

those due to oscillator instability. Therefore let us investigate the bandwidths required by a PLL to accomodate a given amount of satellite dynamics.

Three system configurations will be considered. First a digitally compensated second order loop will be presented. Then a digitally compensated third order loop will be discussed. Finally the use of rate aiding with either of these loops will be described.

The loop compensation for a second order loop is

$$F_2(s) = \frac{\tau s + 1}{s} \tag{3.52}$$

The overall closed loop transfer function with such compensation is of the form

$$H_2(s) = \frac{k(\tau s + 1)}{s^2 + k\tau s + k} \tag{3.53}$$

Where k is the overall loop gain and τ is a coefficient set by the specific digital design. For the loop to be critically damped,

$$k\tau^2 = 2 \tag{3.54}$$

and the 3 dB bandwidth of the closed loop response of Eq. (3.53) is

$$BW_{3dB} = \frac{\sqrt{k}}{2\pi} \text{ Hz} \tag{3.55}$$

The dynamic capabilities of tracking loops are typically expressed in terms of steady state errors due to position, velocity, and acceleration inputs. The steady state error of the second order loop just defined is zero for both position and velocity inputs. However the steady state error due to an acceleration input is not zero. In particular

$$\Delta\phi = \frac{\dot{\omega}}{k} = \frac{\dot{\omega}}{(2\pi BW_{3dB})^2} \tag{3.56}$$

where $\Delta\phi$ is the phase error at the phase detector and $\dot{\omega}$ is the doppler rate caused by satellite motion (and, perhaps, oscillator drift).

It is clear that the 3 dB bandwidth of the loop cannot be made indefinitely small. The lower bound in this case is set by the doppler rate caused by satellite motion. In particular the phase error at the phase detector must remain small so that the loop remains in its linear region. Typically an upper bound on the loop steady state phase error is set at 0.2 rad. From Eq. (3.56) it is seen that this constraint creates a lower bound on the 3 dB loop bandwidth given by

$$BW_{3dB} > \frac{1}{2\pi}\sqrt{\frac{\dot{\omega}}{0.2}} \tag{3.57}$$

In terms of satellite acceleration, a, the lower bound on 3 dB bandwidth can be recast as

$$BW_{3dB} > \sqrt{\frac{a\,f}{0.4\pi c}} \tag{3.58}$$

where f is the carrier frequency to be tracked (in Hz), a, is the radial acceleration of the satellite as seen at the receiver (in ft/sec^2) and c is the speed of light(in ft/sec).

At 20 GHz the maximum tolerable acceleration which permits a 3 dB bandwidth of 1 Hz using a second order loop is 0.0628 ft/sec^2.

A third order loop provides a significant increase in dynamic performance for a given bandwidth. Thus higher vehicle dynamics can be tolerated. The loop compensation for a third order loop is of the form

$$F_3(s) = \left(\frac{\tau s + 1}{s}\right)^2 \tag{3.59}$$

and the closed loop response is given by

$$H_3(s) = \frac{k(\tau s + 1)^2}{s^3 + k\tau^2 s^2 + 2k\tau s + k} \tag{3.60}$$

The equivalent of critical damping is achieved with the third order loop by setting

$$k\tau^3 \approx 4 \tag{3.61}$$

The loop 3 dB bandwidth under the constraint given in Eq. (3.61) is approximately

$$BW_{3dB} = \frac{3.2}{5\tau} \tag{3.62}$$

The third order loop has zero steady state error for position, velocity ,and acceleration inputs. The first non-trivial steady state dynamic error is produced by a rate of change of acceleration, J. Specifically the error due to a jerk,J, is given by

$$\Delta\phi = \frac{8.4\ \dddot{\omega}}{125\ (BW_{3db})^3} \tag{3.63}$$

Thus,

$$BW_{3dB} > \left[\frac{8.4\ \dddot{\omega}}{(125)\ (0.2)}\right]^{1/3} = \left[\frac{2.1\ fJ}{c}\right]^{1/3} \tag{3.64}$$

This implies that the maximum tolerable rate of change of acceleration at 20 GHz for a 1 Hz 3 dB bandwidth is roughly 0.024 ft/sec^3.

Usually rates of change of acceleration on the order of 0.02 ft/sec^3 are not experienced with satellites in synchronous orbit, thus it may be possible using a third order loop to track the satellite motion using a loop 3 dB bandwidth on the order of 1 Hz.

It is desired that even lower tracking bandwidths be used. This would provide capability for separating out phase fluctuations due to scatter under conditions when the Doppler spread associated with such processes is less than 1 Hz. Under these conditions it would be necessary to add rate aiding to the phase locked loop. Implementation of rate aiding requires a good estimate of the satellite ephemeris. The ephemeris data is processed to derive an estimate of the expected Doppler as a function of time at the receiver. This estimate is added to

the PLL loop compensation network output at the input to the loop VCO. Thus the loop need not track the satellite dynamics per se. In this case the loop need only track the difference between the estimated dynamics and the actual dynamics. In this way the use of rate aiding can reduce the dynamics to be tracked by at least an order of magnitude.

In summary the brief discussion above has shown that the use of phase locked loop techniques for separating out the phase effects due to satellite motion and oscillator instability from phase variations due to scattering are marginal. To accommodate narrower Doppler spreads relatively sophisticated equipment would be required. Detailed evaluation of the technique requires specific orbit characteristics.

SECTION 3

REFERENCES

[3.1] Bello, P.A., "Measurement of the Complex Time-Frequency Channel Correlation Function", Radio Science, Vol. 68D, No. 10, October 1964, p 1161.

[3.2] Gallager, R., "Characterization and Measurement of Time and Frequency-Spread Channels", MIT Lincoln Lab. Tech Report 352, April 1964.

SECTION 4

CHANNEL MEASUREMENT USING PULSES

It can be seen that frequency domain channel measurement techniques discussed in the previous section, involve certain difficulties with respect to oscillator stability. Because of the additional receiver complexity required to circumvent these problems, it is natural to investigate the potential of more direct measurement strategies. In particular we will consider certain alternative approaches which involve the transmission of pulse trains.

4.1 Basic Approach

In the following sections we shall examine the use of two different kinds of pulse trains;

(a) Coherent pulses, i.e., individual members of the pulse sequence are phase coherent at least over time intervals large compared with the repetition period.

(b) Incoherent pulses, i.e., because of the method of generation, adjacent pulses in the sequence are unrelated in phase.

Both of these signals, when processed correctly, sample the complete channel impulse response at a given instant of time. With (a), the coherent pulse train, we must take the same precautions as with the multitone spectrum to suppress the phase instabilities introduced primarily by transmitter oscillator effects.

The basic pulse modulation approach is illustrated in Fig. 4.1. It will be assumed for the purposes of analysis that the pulse is perfectly rectangular, of length Δ, amplitude A, and is to be repeated every T secs.

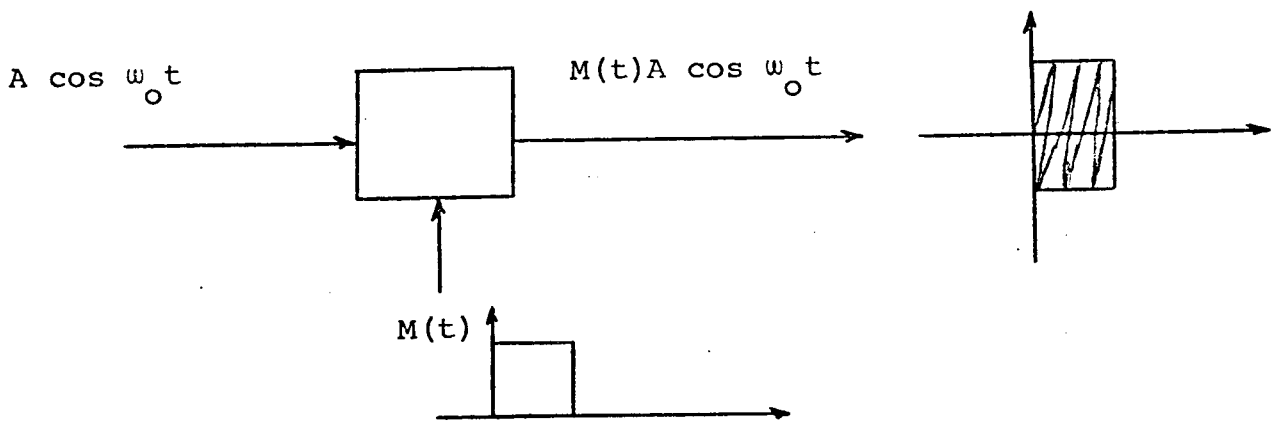

Fig. 4.1 Pulse Modulation

Before discussing the two methods we first define the general time domain measurement problem. Using complex low pass notation as in Ref. [2.2] to symbolically represent the bandpass processes, we have a channel input-output relationship of the form,

$$r(t) = \int g(t,\xi)\ z\ (t-\xi)\ d\xi + n(t) \qquad (4.1)$$

where $g(t,\xi)$ is the complex time varying channel impulse response at time t to an impulse ξ seconds earlier, and $z(t)$ is the complex envelope of the transmitted signal. $n(t)$ is additive receiver noise. An ideal channel measurement would yield in-phase and quadrature components of the channel impulse response as functions of time for each value of delay ξ. These correspond to the real and imaginary components of $g(t,\xi)$. From such measurements all of the necessary statistical characteristics can be estimated as discussed in Section 2.2.

The rate of change of $g(t,\xi)$ with respect to t, indicates the Doppler spreading properties of the channel, while the variation with ξ indicates the delay spreading properties. Generally the degree of delay spread will be discussed in terms of parameters such as L_{max}, the maximum extent of the delay dispersion, or L, the RMS delay spread width. Similarly for Doppler spread we shall use B_{max} and B to denote maximum and RMS spectral widths. (See Ref. [2.2] for a more precise definition of these quantities in terms of statistical properties of $g(t,\xi)$). It should be apparent after the discussion presented in earlier sections, that the measurement of $g(t,\xi)$ is limited in resolution by the signal bandwidth. In essence we require that

$$\frac{1}{W} \simeq \Delta < L$$

where Δ is the pulse duration, and W is the corresponding signal bandwidth. To satisfy this relationship for the millimeter wave channel we need bandwidths on the order of 1 GHz, but because of equipment constraints these conditions may be difficult or impossible to satisfy.

A suitable signal for estimating the impulse response $g(t,\xi)$ is a short pulse of width Δ, which is narrow compared with the delay spread L. Consider the signal,

$$z(t) = Ap(t)$$

$$p(t) = \begin{cases} 0 & |t| > \Delta/2 \\ 1 & |t| \leq \Delta/2 \end{cases} \qquad (4.2)$$

$\Delta \leq$ delay spread L (See Fig. 4.2).

Provided the variation of $g(t,\xi)$ is slow <u>in the t variable</u> over an interval of length L, the response to a pulse at time t_0 can be approximated using Eq. (4.1) as:

$$r(t) = A \int g(t_0,\xi)\, p(t-\xi-t_0)\, d\xi + n(t)$$

We can relate the observed sequence of responses directly to the function of interest, i.e., $g(t,\xi)$. Thus let

$$\tilde{g}_{t_0}(\tau) = \int g(t_0,\xi)p(\xi-\tau)\, d\xi \qquad (4.3)$$

then

$$r(t) = A\, \tilde{g}_{t_0}(t-t_0) + n(t) \qquad (4.4)$$

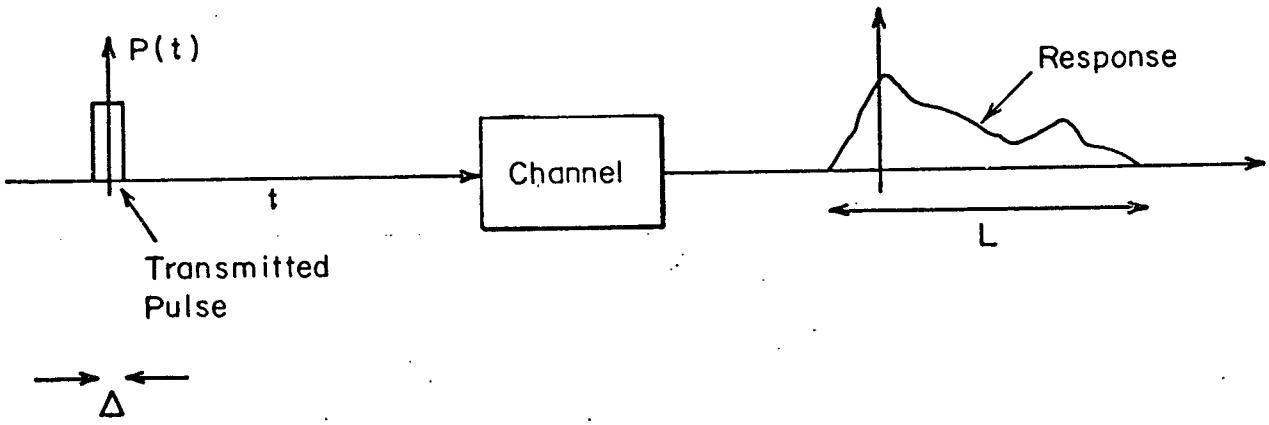

Fig. 4.2 Pulse Transmission and Response

Eq. (4.3) can be interpreted as a smoothing of the instantaneous impulse response $g(t_0,\xi)$ by the transmitted pulse. If a sequence of pulses is transmitted with an interpulse spacing of T secs, the resulting sequence of responses resembles the quantity $g(t,\xi)$ sampled at $t=nT$, except for the convolution with $p(t)$. (See Fig. 4.3.) Obviously the period T needs to be chosen so that, $T \gg L$ while we also require the pulse sampling rate to be higher than the Doppler rate; $T < 1/B$. Various statistical properties of the impulse response $g(t,\xi)$ can therefore be extracted directly from the sequence of pulse responses. Note that the coupling between the transmitted signal and channel impulse response demonstrated in Eq. (4.3) precludes the possibility of obtaining useful channel data when the pulse width exceeds the delay spread L. Consequently we need, $\Delta \ll L$.

The sequence of pulse responses illustrated in Fig. 4.2 allows direct measurement of the channel delay spread properties, i.e., the behavior of $g(t,\xi)$ with respect to ξ. Doppler information can also be extracted from the variation along the pulse sequence or alternatively by transmitting an auxiliary C.W. carrier either adjacent to or superimposed on the pulse spectrum.

Most of this discussion has been concerned with the basic channel measurement theory involved; we now examine some of the difficulties involved in producing the required hardware for an incoherent pulse probing experiment.

The most severe problem facing the system designer is that of obtaining the 1 GHz or so video bandwidth. This

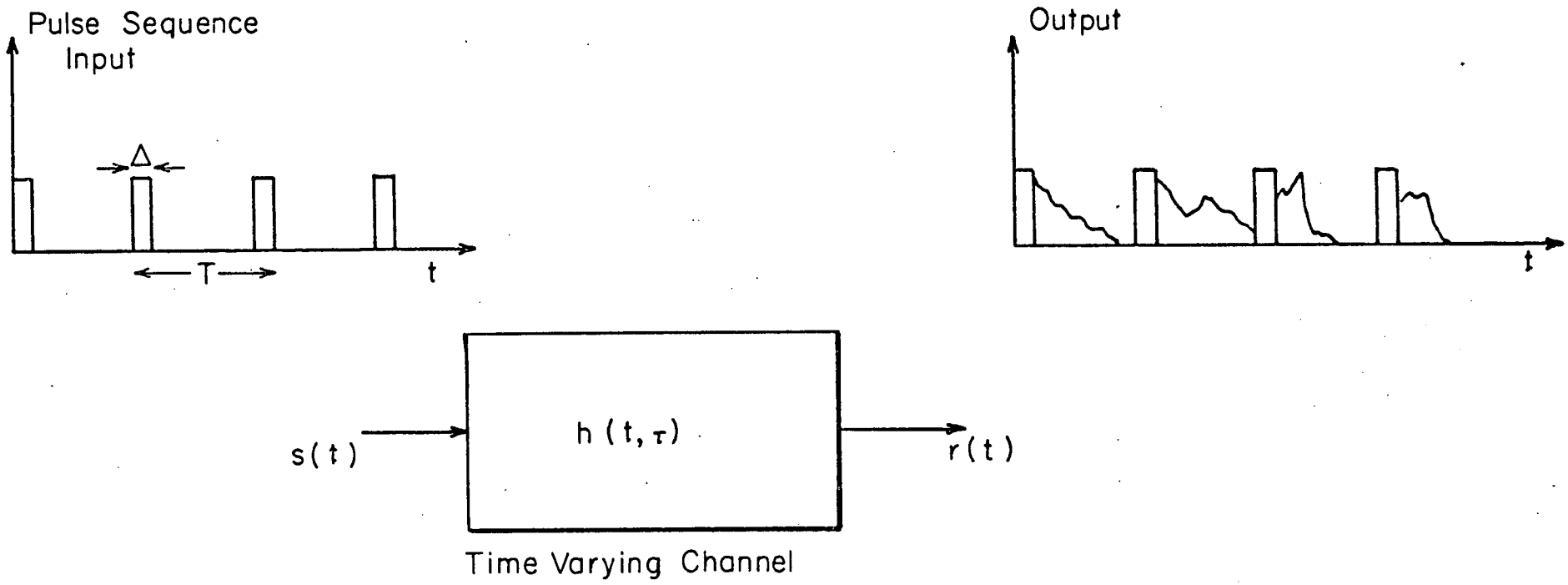

Fig. 4.3 Channel Response to a Sequence of Pulses

aspect can be partially sidestepped by the use of a delay line processor shown in Fig. 4.4.

The response r(t) propagates along the delay line after translation to an IF band. At the delay line taps, which are spaced by Δ seconds, we observe the processes $\{r(t-n\Delta)\}$, so that each tap output is a 1 GHz bandwidth process around the IF center frequency. Following the detection of these waveforms, which can either be coherent or incoherent depending on our ability to realize the required equipment, the resultant low pass processes are sampled*. The sampling rate for each tap must be locked in with the pulse repetition frequency so that the same point on the pulse responses is sampled each time. i.e., the n^{th} tap is sampled for the k^{th} time at

$$t = k(K_0 T) + n\Delta$$

T = interpulse period

Δ = delay line tap spacing

K_0 = arbitrary integer

There are various ways the sampler can be shared amongst the delay line outputs as long as the period T is much shorter than the inverse Doppler bandwidth 1/B, so that no information is lost. For example each T secs. a different tap could be sampled in sequence, resulting in the n^{th} tap

---

* High speed samplers are currently available with rise times on the order of 30 picosecs.

B

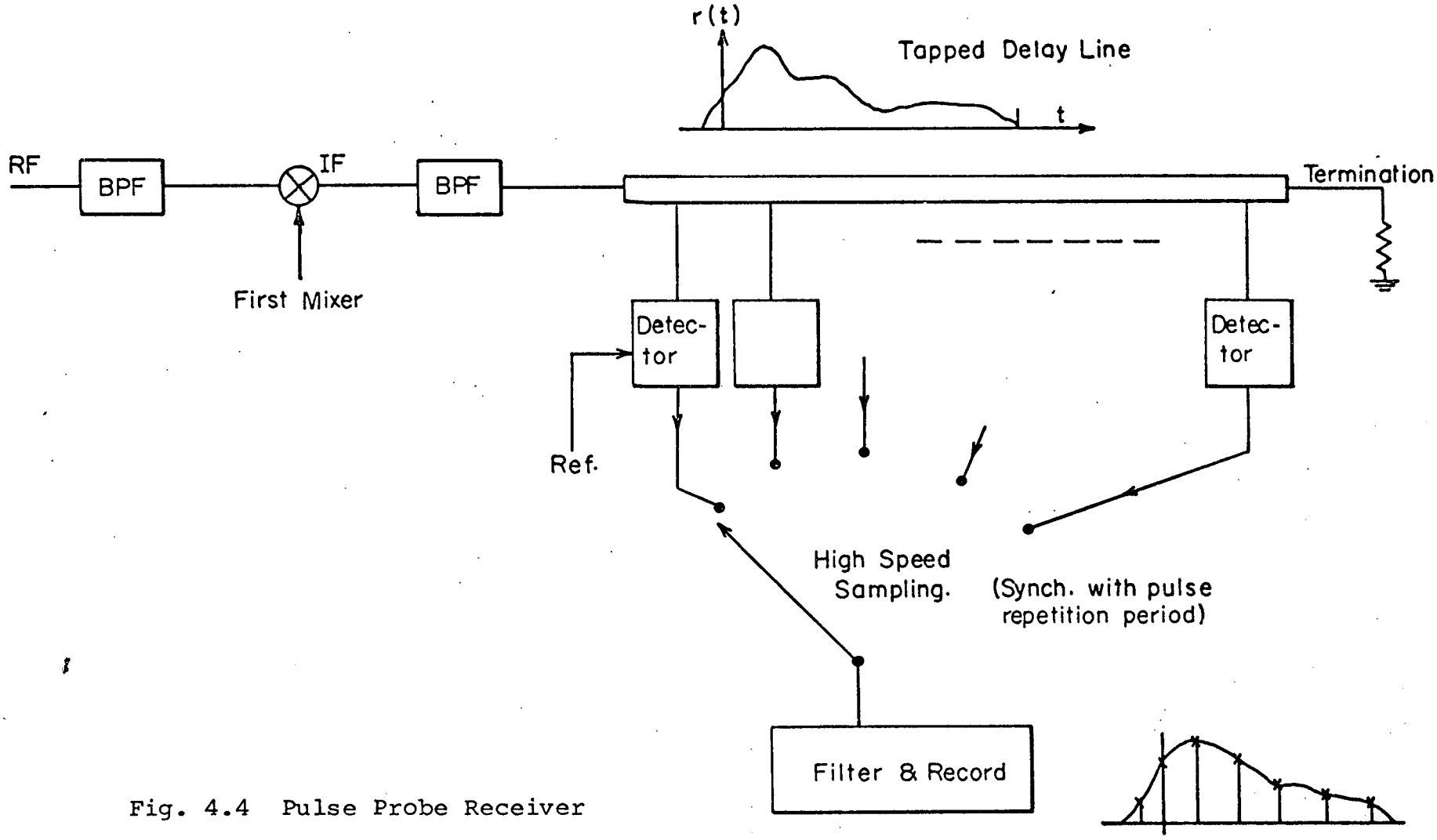

Fig. 4.4 Pulse Probe Receiver

being sampled, for the k^{th} time at an instant,

$$t = (kN+n)T + n\Delta$$
$$n = 0, 1, \ldots N-1$$
$$N = \text{total number of taps.}$$

Thus at time zero we sample tap zero, time $T + \Delta$ tap 1, $2T + 2\Delta$ tap 2, etc. The sampling trigger signals can be generated from a clock reference with period T connected to a switched delay line of length $n\Delta$. Note that the original sequences of output samples from each tap are of low bandwidth (i.e., the Doppler bandwidth), so that conventional digital filtering can be implemented, or a D/A converter can be used to regenerate analog signals. The IF processes have a noise bandwidth on the order of 1 GHz which means that the samples will be quite noisy. The post detection filtering suggested above helps to alleviate this situation as will be demonstrated subsequently.

4.2 IF Signal to Noise Ratio Estimates

Before continuing with implementation details for the pulse probe technique, it would be prudent to compute the SNR to be expected.

The impulse response $g(t,\xi)$ used in Eq.(4.1) to relate channel input and output quantities can be represented as the sum of two functions;

$$g(t,\xi) = g_c(\xi) + g_R(t,\xi) \qquad (4.5)$$

where $g_c(\xi)$ is the time invariant coherent response, and $g_R(t,\xi)$ is the time varying scatter component.*

Consider the transmission of a single pulse of amplitude A at t = 0. From Eqs. (4.3) and (4.4) we have,

$$r(t) \simeq A\int[g_c(\xi) + g_R(0,\xi)]\, p(t-\xi)d\xi + n(t)$$

$$\triangleq A\, \tilde{g}_0(t) + n(t) \qquad (4.6)$$

First we compute the IF signal to noise ratio choosing the ATS-F experiment as an example. At 20 GHz the following parameters are typical;

Transmitting antenna gain	37 db
System and free space loss	212 db
Receiving antenna gain	56 db
Noise power/Hz	-159.1dbm.

Hence relative to a milliwatt transmitted, we have for a 1 GHz bandwidth, an IF carrier to noise power ratio,

$$\gamma = -212 + 37 + 56 - 90 + 159.1$$
$$= -49.9 \text{ db}$$

Referring to Eq.(4.6), we see also that a transmitted pulse is spread in time by the channel, hence resulting in an even lower SNR at the delay line taps. Let us assume that $\tilde{g}_0(t)$ is a factor of 10 wider than the pulse p(t)

---

* In terms of previously defined transfer functions g_c is the transform of T_c while g_R is the transform of $T_c T_R$.

(resulting in N = 10 active taps on the delay line). This implies a 10 db drop in signal to noise ratio. Consequently a zero db γ can only be obtained by transmitting a pulse which is approximately 60 db above 1 mW in power. Thus,

$$P_T = 10^3 \text{ watts.}$$

where P_T is the transmitted pulse power level. The energy of each pulse is on the order of

$$E_T = P_T \Delta$$

$$\leq 10^{-6} \text{ Joules.}$$

Note also that for a pulse repetition rate in the range of 10^6 pps, we require an average transmitted power of approximately

$$P_{AV} \simeq E_T \, 10^6$$

$$\simeq 1 \text{ watt}$$

The use of post detection filtering allows substantial improvement in the effective signal to noise ratio however. and this aspect will be discussed in the following sections.

4.3 Incoherent Pulse Measurements

In this section we assume that the pulse waveform p(t) has associated with it a phase angle which is random from pulse to pulse. This necessitates the use of incoherent detection. Here we consider the use of a square law detector.

Referring to Eq. (4.6) we can form an estimate of the quantity,

$$P(t) = E\{|\tilde{g}_0(t)|^2\} \tag{4.7}$$

by computing,

$$\hat{P}(t) = |A\,\tilde{g}_0(t) + n(t)|^2 - \sigma_n^2 \tag{4.8}$$

where $\sigma_n^2 = E\{|n(t)|^2\}$

and E denotes statistical expectation.

This function indicates the estimated average power profile of the channel impulse response and as shown, is constructed from a single pulse response. In practice the estimate is of course refined by repetition of the pulse and superposition of the responses. For the above one shot estimator it can be shown that the estimate has the following properties. The average is computed to be;

$$E\{\hat{P}(t)\} = A^2P(t) + E\{|n(t)|^2\} - \sigma_n^2$$

$$= A^2P(t) \tag{4.9}$$

while the estimate variance is,

$$E\{(\hat{P}(t) - A^2P(t))^2\} = E\{(|A\tilde{g}_0(t) + n(t)|^2 - \sigma_n^2)^2\}$$

$$-A^4P^2(t)$$

$$= \sigma_n^2(A^2P(t) + \sigma_n^2) \tag{4.10}$$

This result was obtained using the assumption that the composite impulse response $\tilde{g}_0(t)$ is approximately time invariant, and hence non-random, i.e.,

$$g(t,\xi) \simeq g_c(\xi) \tag{4.11}$$

The more general case which includes the random response $g_R(t,\xi)$ can be obtained if desired, but leads to more complicated expressions. Roughly speaking the variance is increased over that due to noise alone because we are trying the estimate the average strength of a random process. As an example consider the situation where

$$g(t,\xi) \simeq g_R(t,\xi) \tag{4.12}$$

i.e., the scattered signal component dominates the direct signal. If in addition we assume that $g_R(t,\xi)$ has the properties*,

$$\begin{aligned} E\{g_R(t,\xi_1)g_R^*(t,\xi_2)\} &= \delta_0(\xi_1-\xi_2)\, Q(\xi_1) \\ E\{g_R(t,\xi_1)g_R(t,\xi_2)\} &= 0 \end{aligned} \tag{4.13}$$

then the channel is defined by the function $Q(\xi)$ which is estimated as in Eq. (4.8), i.e.,

$$\hat{Q}(t) = |A\tilde{g}_0(t) + n(t)|^2 - \sigma_n^2 \tag{4.14}$$

---

* See section 2.3 for an interpretation of these conditions.

where from Eq. (4.6) we have,

$$\tilde{g}_0(t) \simeq \int g_R(0,\xi)\ p(t-\xi)\ d\xi \tag{4.15}$$

Note that,

$$\begin{aligned} E\{|\tilde{g}_0(t)|^2\} &= \iint E\{g_R(0,\xi_1)g_R^*(0,\xi_2)\}p(t-\xi_1)p(t-\xi_2) \\ &\qquad d\xi_1\ d\xi_2 \\ &= \int Q(\xi)|p(t-\xi)|^2\ d\xi \\ &\simeq Q(t)\int|p(t-\xi)|^2\ d\xi \\ &= Q(t)\ \Delta \end{aligned} \tag{4.16}$$

Eq. (4.16) results from the use of Eq. (4.13) and the assumption that $Q(\xi)$ is smooth compared with the pulse envelope. The estimate $\hat{Q}(t)$ given in Eq. (4.14) has the property;

$$E\{\hat{Q}(t)\} = A^2\Delta\ Q(t) \tag{4.17}$$

and variance,

$$\begin{aligned} \mathrm{Var}\{\hat{Q}(t)\} &= E\{(\hat{Q})^2\} - [E\{\hat{Q}\}]^2 \\ &= E\{[|A\tilde{g}_0(t) + n(t)|^2 - \sigma_n^2]^2\} - A^4\Delta^2Q^2(t) \\ &= E\{|\tilde{A}g_0(t) + n(t)|^4\} - 2\sigma_n^2(\sigma_n^2 + A^2\Delta Q(t)) \\ &\qquad + \sigma_n^4 - A^4\Delta^2Q^2(t) \\ &= [A^2\Delta Q(t) + \sigma_n^2]^2 \end{aligned} \tag{4.18}$$

To summarize we note that in both cases, i.e., the pure specular and the pure scatter channels, the estimates $\hat{P}(t), \hat{Q}(t)$ (Eqs. (4.8) and (4.14)) converge to within a constant of the desired quantity (Eqs. (4.9) and (4.17)). Hence they can be made unbiased by renormalization. The variance in each case is better expressed as a fractional standard deviation; i.e.,

$$\mu = \frac{\text{st. dev. of estimate}}{\text{mean of estimate}} \tag{4.19}$$

$$= \begin{cases} \left[\left(\dfrac{\sigma_n^2}{A^2 P(t)}\right)\left(1 + \dfrac{\sigma_n^2}{A^2 P(t)}\right)\right]^{\frac{1}{2}} \\ \qquad \text{pure specular (Eqs. (4.9) and (4.10))} \\ \left[1 + \dfrac{\sigma_n^2}{A^2 \Delta Q(t)}\right] \\ \qquad \text{pure scatter (from Eqs. (4.17) and (4.18))} \end{cases}$$

Note that we are generally interested in situations where the IF signal-to-noise ratio is low. The parameter γ previously defined as the IF signal to noise ratio for a CW signal, can be expressed here as;

$$\gamma = A^2/\sigma_n^2$$

It should be noted that the function Q(t) has the dimensions of power per unit time while P(t) has units of power.

Consider the consequences of averaging the estimate by filtering the samples as in Fig. 4.5. The effective standard deviation index μ given by Eq. (4.19) is reduced in a manner which depends on the time constant of the filter. For a sequence of samples spaced in time by T_0 seconds, and a filter bandwidth W_0 such that,

$$W_0 > B \qquad\qquad B = \text{Doppler BW.}$$

we average over a total of N samples each perturbed with independent noise components. N is given by,

$$N = \frac{1}{W_0 T_0}$$

It can be shown that the effective index μ becomes,

$$\mu' \simeq \begin{cases} (W_0T_0)^{\frac{1}{2}} \left(\frac{1}{\gamma P(t)}\right) \quad ; \quad \frac{\sigma_n^2}{A^2 P(t)} \ll 1 \\ \qquad\qquad \text{pure specular} \\ 1 + (W_0T_0)^{\frac{1}{2}} \left(\frac{1}{\gamma \Delta Q(t)}\right) \\ \qquad\qquad \text{pure scatter} \end{cases} \tag{4.20}$$

Generally speaking the estimates involved will not be of any value unless μ' can be made much less than unity. In the case of a pure specular signal this is achieved by making $\left(\frac{W_0}{\gamma}\right)$ very small. Similarly for the pure scatter signal. In this latter instance however we obviously require,

$$W_0 < B$$

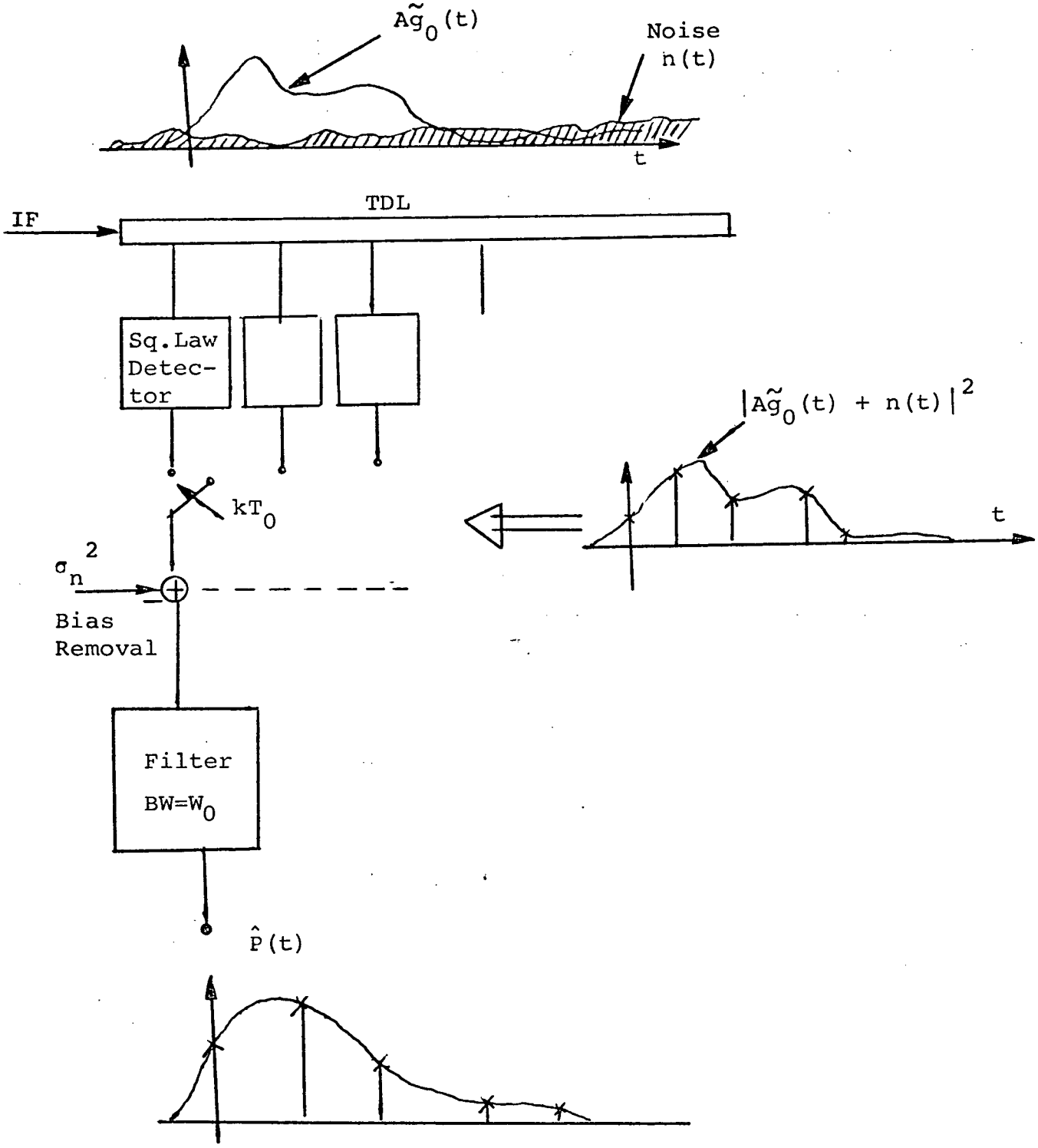

Fig. 4.5 Incoherent Pulse Receiver

and the performance is approximately,

$$\mu' = \left(\frac{W_0}{B}\right)^{\frac{1}{2}} + (W_0T_0)^{\frac{1}{2}} \left(\frac{1}{\gamma\Delta Q(t)}\right) \qquad (4.21)$$

If we require $\mu'<1/10$ and assume a unity SNR, i.e., $\gamma=1$, it can be seen that when P(t) and Q(t) are 10 times wider than the pulse p(t), we require on the order of

$$W_0T_0 \geq 10^4$$

samples for the pure specular case and,

$$W_0T_0 \geq 10^4$$

with

$$W_0 \leq 10^{-2}B$$

for the pure scatter signal case.

Figure 4.5 shows the structure of the receiver required. Note that the square law detection can be implemented using wideband microwave diodes biased correctly, although the square law characteristic could be replaced by some alternative non-linearity with little change in performance. The high speed sampler is required to have a gate time of between 30 and 100 ps, performance which can be readily achieved using off the shelf samplers. Note that the 10 GHz or so bandwidth of this device provides the dual function of low pass filtering, thus eliminating the higher order harmonics from the detector output.

4.4 Coherent Pulse Processing

Now we take the case where phase coherence is retained between pulses in the transmitted pulse train. Such a signal could be generated by chopping a coherent CW source at the transmitter. The receiver is now required to extract in-phase and

quadrature signal components from the delay line taps, and can take the form shown in Fig. 4.6. The IF signal must first be mixed with in-phase (I) and quadrature (Q) references. The references are obtained from a transmitted pilot tone.

The IF signal at each tap can be expressed as;

$$A(t) \cos (\omega t + \theta)$$

The mixing operation then gives a signal part of the form,

$$m_I(t) = A(t) \cos (\omega t + \theta) \cos \omega t$$

$$m_Q(t) = A(t) \cos (\omega t + \theta) \sin \omega t$$

The high speed sampler again acts as a low pass filter (BW $\simeq$ 10 GHz) which results in sampled versions of the processes,

$$X(t) = A(t) \cos \theta(t)$$

$$Y(t) = A(t) \sin \theta(t)$$

at the sampler output. Along the delay line we therefore observe in-phase and quadrature samples of the process r(t), the response to a single pulse. Repetition of the pulse gives a sequence of sample pairs at each tap. (See Fig. 4.6.) Each sample contains an additive noise component which can be suppressed by filtering. If a filter of bandwidth B is employed, the channel function g(t,ξ) will be approximately constant over the filter time constant, and the RMS noise level will be reduced by a factor;

$$(T_0 B)^{\frac{1}{2}}$$

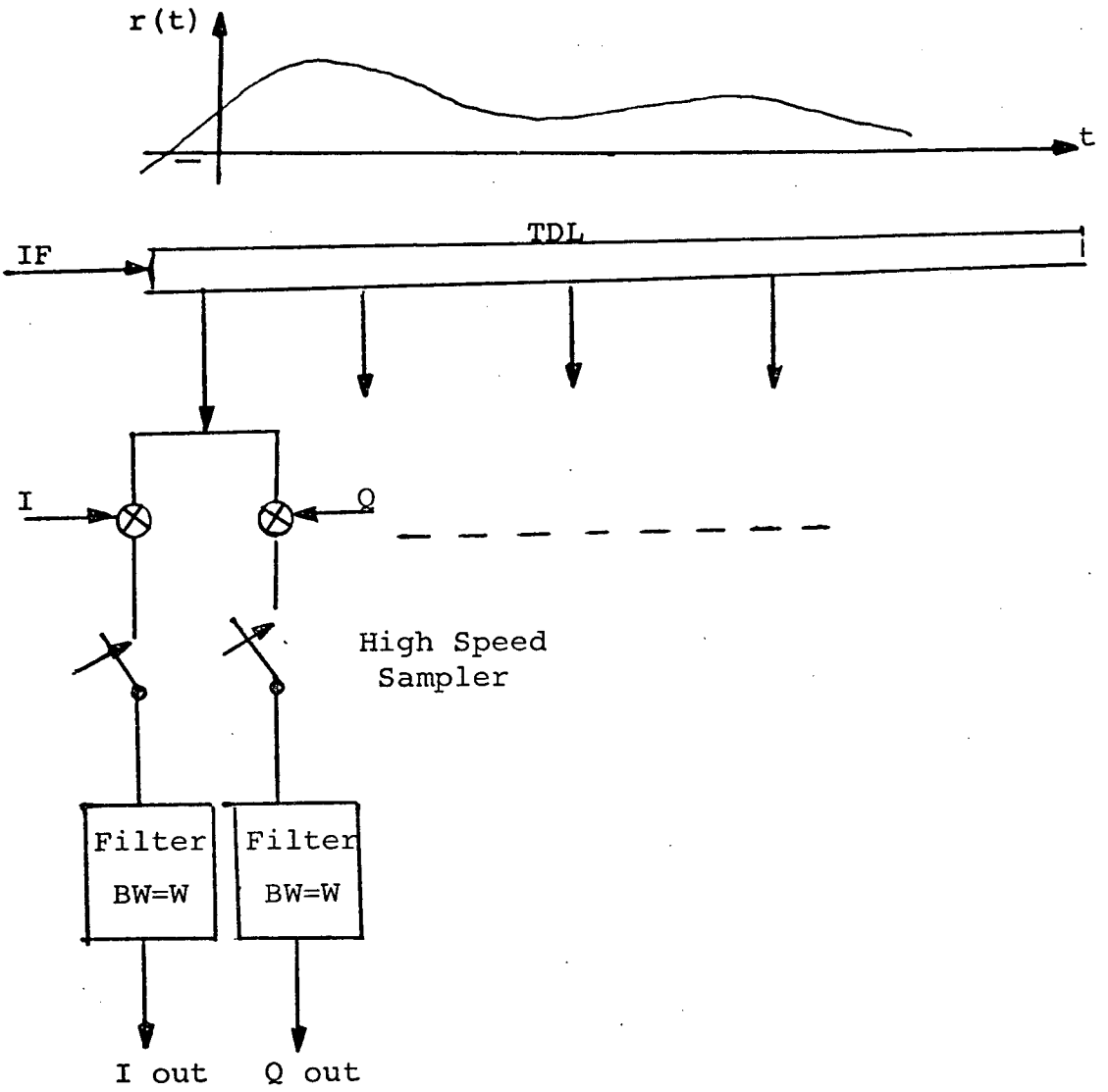

I = in-phase reference
Q = quadrature reference

Fig. 4.6 Coherent Pulse Receiver

Hence the real and imaginary components of the impulse response will be observable directly with a signal to noise ratio obtained using an equivalent noise power

$$\tilde{\sigma}_n^2 = \sigma_n^2 (T_0 B)$$

Pulse repetition rates on the order of 10^6 should be easily obtainable, while a conservative estimate for the Doppler spread B would be 10 Hz. Hence the equivalent noise power is in the vicinity of;

$$\tilde{\sigma}_n^2 = 10^{-4} \sigma_n^2$$

Considering the expected IF signal to noise ratio computed in Section 4.2, it appears that this method of directly obtaining in-phase and quadrature components of the channel impulse response will be feasible. The impulse response estimate is then processed further to obtain the complete mean, Doppler and delay characteristics.

4.5 Summary for Pulse Probing Techniques

The basic difficulty with this and most other millimeter wave channel measurements is that tremendous bandwidths are required to obtain useful data. The figure of 1 GHz has been arbitrarily chosen to be the signal bandwidth objective as a result of theoretical predictions and data from related experiments. Such bandwidths make video signal processing very difficult and require state of the art components for generation of the transmitted millimeter wave signal. The main non-idealities and problem areas which must be considered in conjunction with the previous analysis are;

(a) Generation of sub-nanosecond pulses at relatively high power levels.

(b) Arrival time jitter due to transmitter oscillator instabilities and motion of the satellite.

(c) Accurate tracking of the pulse response arrival times which is necessary for extraction of average properties by overlapping the sequence of responses.

The first two topics mentioned above will be discussed briefly.

The state of sub-nanosecond switching technology is changing very rapidly, being stimulated to some extent by the prospect of high data rate communications systems. The fundamental requirement is the availability of a high speed switch which must be used in amplitude and phase modulators and also in baseband data switching circuits. A wide variety of microwave semiconductor switching devices can be obtained with sub-nanosecond rise times. In particular we can consider the following performance guidelines;

Tunnel diodes	20-100 ps
Common Emitter Transistor	~ 150 ps
Step recovery diode	50-150 ps

The primary difficulty is that of obtaining reasonably high power levels in conjunction with fast switching. However as we have seen in the previous sections, the use of high pulse repetition rates allows somewhat lower power levels to be employed.

Arrival time jitter is a manifestation of the oscillator drift and satellite movement (See Section 3.2.2). It is easy to see that for multipath spreads on the order of nanoseconds,

the accurate estimation and tracking of the pulse response sequence either using leading edge or center of gravity techniques, constitutes a critical receiver operation. Figure 4.7 shows the consequences of incorrectly lining up a sequence of pulse responses used to form the impulse response estimate. Clearly the result is an over-estimate of the channel delay spread. Note that when the satellite moves only one foot during the averaging interval, a differential delay of 1 nanosecond is introduced thus producing a relatively large error in the measurement of delay spread.

Similarly the transmitter reference oscillator is not perfectly stable. Using the oscillator output

$$f(t) = \cos\ (\omega_s t + \theta_s)$$

the pulse train can be triggered by counting down to a repetition rate of 1/T.

i.e. $$\frac{2\pi}{T} = \frac{\omega_s}{k}$$

The pulse generation reference is determined by the zero crossings of

$$f_T(t) = \cos \frac{1}{k}\ (\omega_s t + \theta_s)$$

$$= \cos \left(\frac{2\pi t}{T} + \frac{\theta_s(t)}{k}\right)$$

Following along the lines of previous discussion it is apparent that the properties of timing jitter Δ defined as,

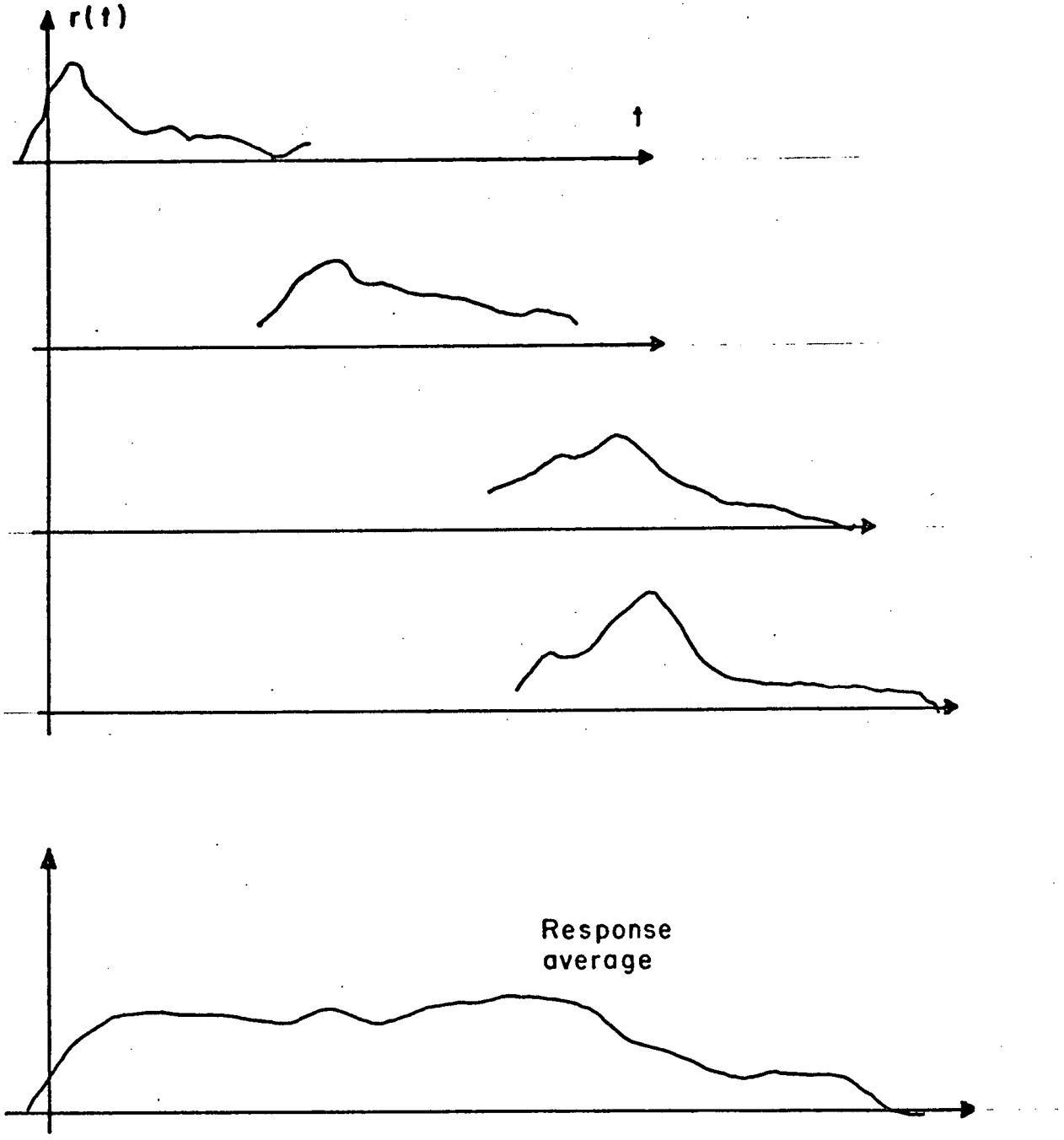

Fig. 4.7 Pulse Response Averaging

$$\Delta(t) \triangleq \frac{\theta_s(t)\ T}{2\pi k} = \frac{\theta_s(t)}{\omega_s}$$

can be found using the phase stability characteristics of the local oscillator. For example an oscillator stability of 1 part in 10^9 averaged over 1 second implies

$$\Delta_e = \frac{(10^{-9} \times 1 \text{ sec})\ \omega_s}{\omega_s} = 1 \text{ nanosecond}$$

where Δ_e is the change in $\Delta(t)$ due to phase drift (over 1 sec). This indicates the need for either a highly stable oscillator or some form of arrival time tracking. The one second averaging time relates to the time constant of the post detection filter which might typically be used to smooth the estimates derived in Sections 4.3 and 4.4.

To conclude it can be seen that although the pulse probing technique appears promising, there are many areas which would require substantial investigation and development effort.

SECTION 5

EQUIPMENT CONFIGURATION

This section discusses the equipment configuration for measurement propagation characteristics of a 20-30 GHz satellite to ground link. The equipment includes a satellite-borne transmitter and a ground-based receiver and demodulator. The equipment described is basically similar to that employed in the ATS-5 and ATS-F experiments. The emphasis in the discussion below is placed on modifications of the current designs. These modifications are based on the experience obtained by NASA personnel with the current equipment, on improvements in the state-of-the-art of solid state components, and, in part, based on the results derived in this study. The proposed incremental phase correcting receiver is configured to be compatible with existing ATS-F satellite 20-30 GHz experiment.

5.1 Transmitter Configuration

Figure 5.1 shows a suitable transmitter for generation of a multi-tone channel probing signal. The design takes full advantage of the current state of the art of solid state microwave signal sources.

As shown in Fig. 5.1 the transmitter is controlled by two feedback loops. The inner loop is a phase locked loop which synchronizes the phase of the transmitted carrier component with a suitably multiplied reference signal. The second loop feeds back a demodulated tone which is compared against a reference tone. The difference between the two is used to modulate the microwave signal source.

For the purposes of illustrating the operation of the transmitter, assume that the transmitted output is of the form given in Eq. 5.1.

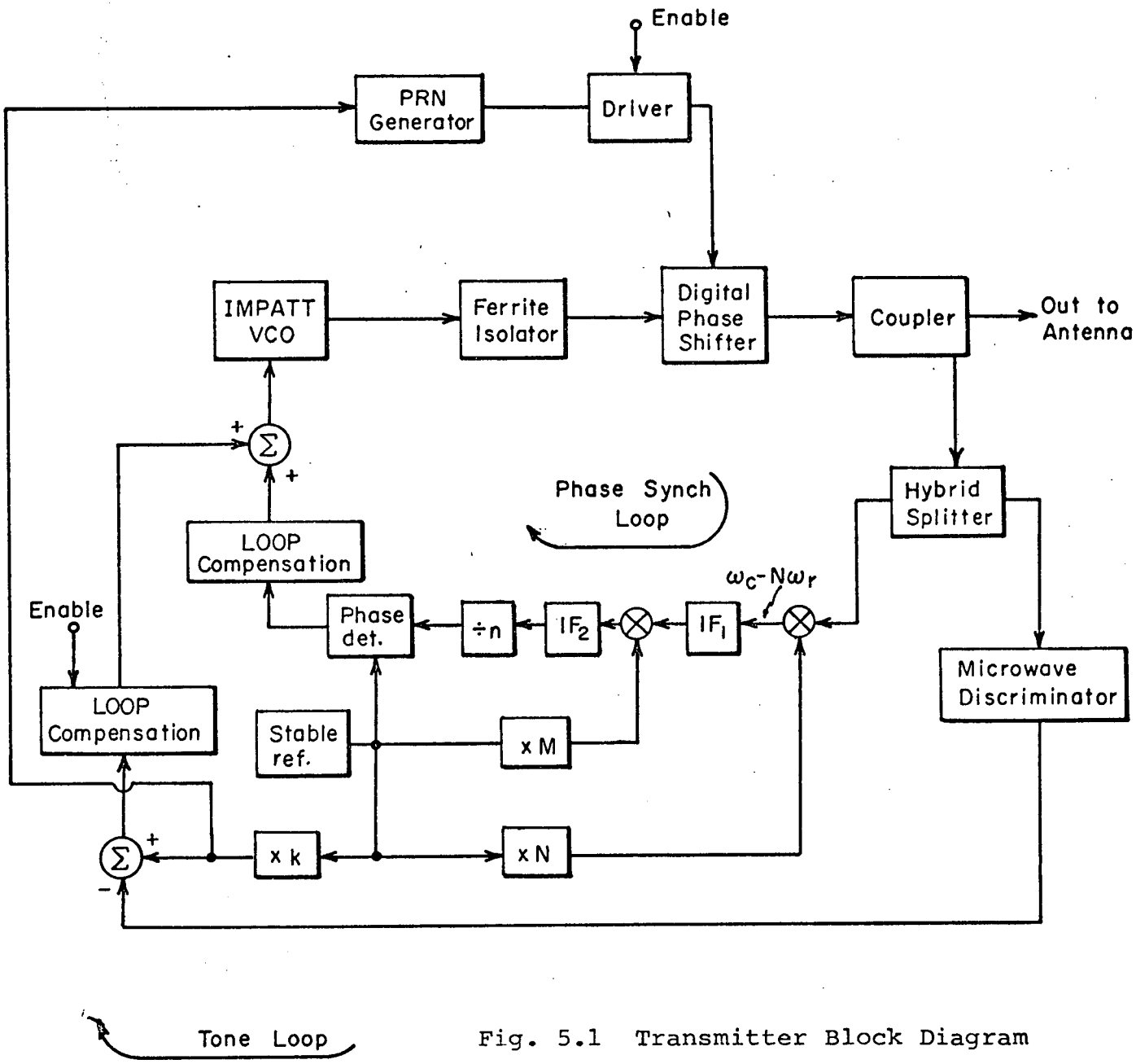

Fig. 5.1 Transmitter Block Diagram

$$S(t) = A \sin (\omega_c t + \delta \sin \omega_m t) \qquad (5.1)$$

Where ω_c is the microwave carrier frequency (say 20 GHz) and ω_m is the tone frequency (say 180 MHz). The deviation, δ, is set at roughly, $\delta = 3.0$, in order to produce four reasonably large-amplitude spectral components on either side of the carrier. The spectrum of the transmitted signal is approximately as shown in Fig. 5.2. It is noted that for the purposes of the propagation measurement experiment the power in each of the probing tones need not be the same. It is only necessary that there be sufficient power in each of the tones so that a considerable margin is available above the receiver noise level. The transmitted power spectrum with the deviation set at 3.0 yields three tones with almost equal power and a fourth tone which is not too far down.

Part of the transmitted output is coupled to the feedback loops using a microwave coupler. The signal is then split between the tone loop and the phase sync.loop. The part of the transmitted output which is fed to the phase sync. loop is mixed with a carrier reference signal. This latter signal is derived by carefully multiplying up a stable reference signal which is say 5 MHz. Thus the multiplication factor, N, is on the order 4,000. The result of the mixing process is filtered in an IF amplifier. The output of the first IF amplifier is mixed with a second reference at M x 5 MHz. The output is then filtered in a second IF amplifier. This IF filter is designed to select the carrier component at the output of the mixer and to reject those components which are associated with the tone modulation. The output of the IF amplifier is thus the down-converted microwave carrier component. This carrier is then divided by n in a frequency divider and the results compared directly against the

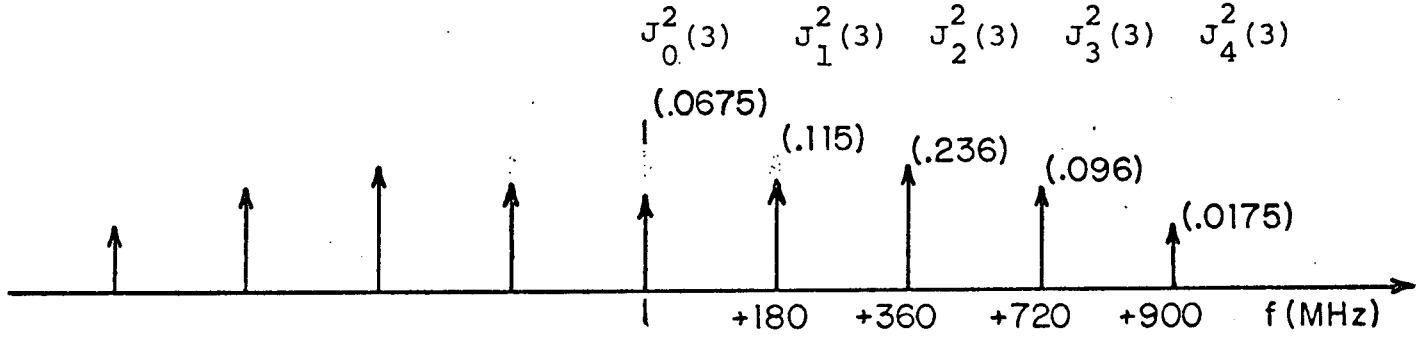

Fig. 5.2 Approximate Transmitted Spectrum

stable reference standard to create a phase error signal.

Assuming that the transmitter output center frequency is higher than N x the stable reference frequency, then the 1^{st} IF frequency in the phase synchronization loop is defined as

$$\omega_{IF1} = \omega_c - N\omega_{ref} \tag{5.2}$$

Where ω_{IF1} is the IF center frequency, ω_c is the K-band carrier output center frequency and ω_{ref} is the stable reference frequency, The second IF is similarly defined as

$$\omega_{IF2} = \omega_{IF1} - M\omega_{ref} = \omega_c - (N+M)\,\omega_{ref} \tag{5.3}$$

The phase detector lock condition is defined by

$$\omega_{ref} = \frac{\omega_{IF2}}{n} = \frac{\omega_c - (N+M)\omega_{ref}}{n} \tag{5.4}$$

Thus the output center frequency is defined in terms of the phase synchronizer loop parameters as follows:

$$\omega_c = (N+M+n)\omega_{ref} \tag{5.5}$$

The phase stability of the output produced by the phase synchronizer loop is strongly dependent on the quality of the loop reference signals. In fact the stability of the output will be almost equal to the stability of the RF reference i.e. the stable reference carrier multiplied by N.

The modulation of the output signal is also controlled by a feedback loop. Again a small sample of the output signal is coupled into a microwave discriminator. The discriminator demodulates the frequency modulated waveform and produces a tone at the output whose amplitude is proportional to the modulation

deviation and whose frequency is equal to a tone reference frequency. This latter signal is derived directly from the stable reference standard by multiplying the stable reference carrier by k. The demodulated tone signal is compared against the tone reference and the difference is amplified in a loop compensation system. The loop compensation system actually employs in-phase and quadrature demodulation of the tone to produce in-phase and quadrature base band error signals. These signals are low-pass filtered and then are used to modulate the tone reference signal. The results are applied to the VCO control input.

The transmitter subsystem also provides a means for transmitting a sample digital message. This message is modulated directly onto the output carrier produced by the VCO. A microwave phase shifter is used for that purpose. The phase shifter is driven from a pseudo-random sequence generator which produces the sample data stream. For convenience the bit rate is chosen to be equal to the tone modulating frequency, 180 MHz. Digital logic which works at this rate is available off the shelf. Similarly a K-band digital phase shifter with sufficiently fast switching time is also readily available. Of course it would be more interesting to transmit at a significantly higher rate but components are not available at the present time for this purpose. It is possible to increase the chip rate to 500 MHz with a moderate effort.

The transmitter configuration just discussed performs the same function for the most part as previously implemented systems. Basic changes included in the configuration presented in Fig. 5.1, take advantage of new technology. The resulting device would be all solid state. The system of Fig. 5.1 relies heavily on the use of feedback techniques to assure that the desired output signal is being generated. This approach somewhat reduces component performance requirements. For example,

the use of a microwave discriminator relaxes the specifications on the IMPATT VCO. In particular it is simpler to make a stable wide range linear microwave frequency demodulator than it is to make a stable microwave frequency modulator. The demodulator can be used to determine the output frequency with the aid of feedback. Similarly the inner phase synchronizing loop uses feedback so that a low power carefully generated reference signal can be used to lock up the high power IMPATT oscillator thus transfering the stability from the low power signal to the high power signal.

5.2 Receiver Design

This section describes a receiver which is compatible with the transmitter described above and which provides incremental phase correction. The receiver is also compatible with the transmitter configuration currently employed in the ATS-F system.

A block diagram of the receiver is shown in Fig. 5.3. The operation of the system is as follows. The received RF signal is converted to the first IF by mixing with a local oscillator reference. The local oscillator reference is generated in a frequency synthesizer subsystem which will be described in more detail below. For the moment it is noted that the first local oscillator frequency is coherently related to a fundamental reference frequency denoted by ω_r^*. In particular the local oscillator frequency is $N\omega_r^*$. This down conversion is exactly the same as that performed in the phase synchronizer loop of the transmitter. Thus the first IF in the receiver is equal to the first IF in the transmitter's phase synchronizer loop. Adequate performance is achieved if this stage is wideband. To this end the first IF should be around 2 GHz. This choice is

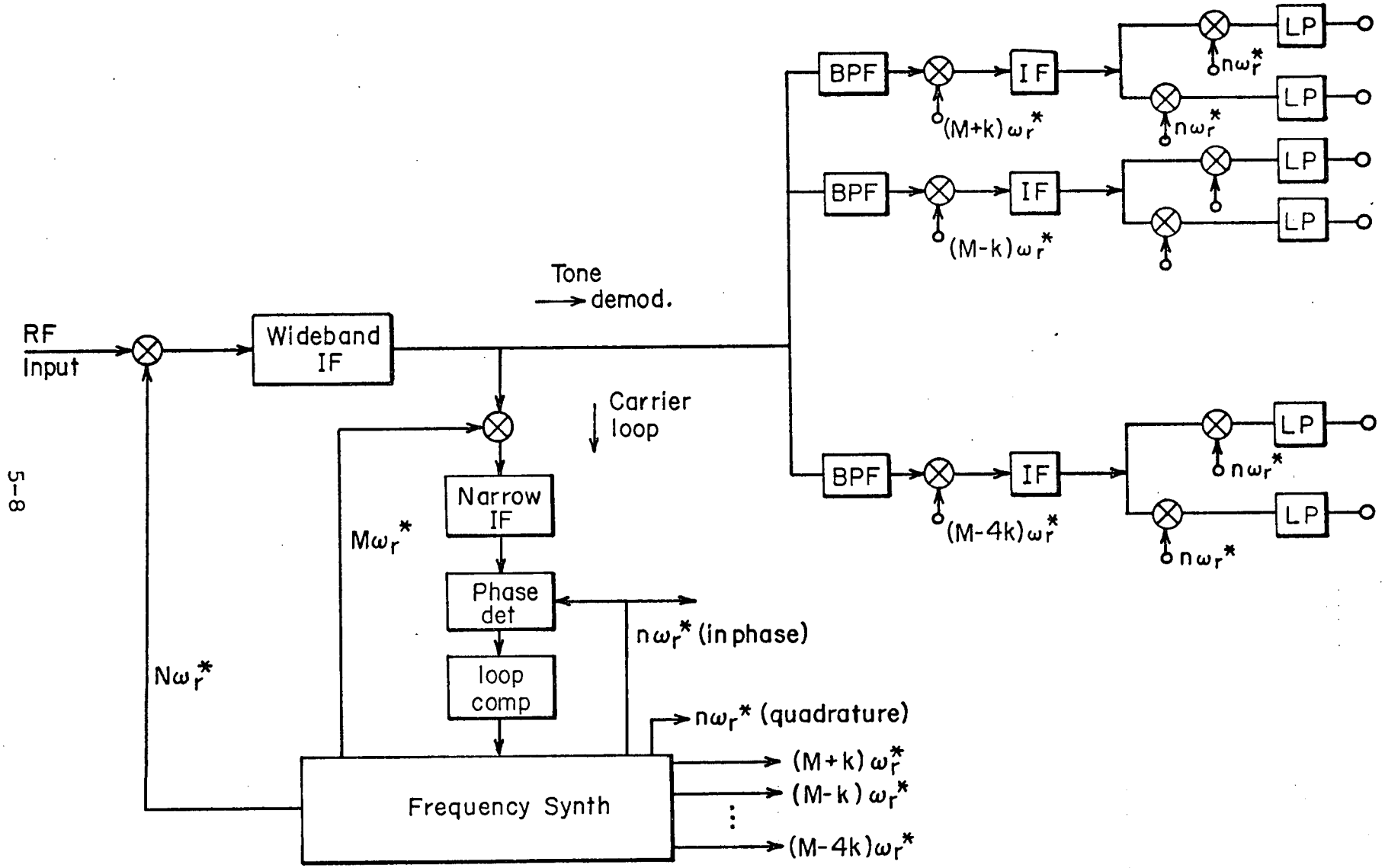

Figure 5.3 Receiver Block Diagram

similar to that exercised for the ATS-F receiver. The output of the wideband IF is used to drive a carrier loop and a series of tone demodulation circuits. The carrier loop extracts the carrier from the modulated signal and coherently demodulates to baseband. This operation is carried out in a series of down conversions. First the output of the wideband IF is mixed with a second coherent reference signal generated by the frequency synthesizer subsystem. This signal is at $M\omega_r^*$. The carrier component at the output of this mixing process is filtered in a narrow band IF and the results are phase detected against a third coherent reference, at $n\omega_r^*$. Note that these operations are essentially equivalent to those carried out in the phase synchronizer loop of the transmitter. Except that in the case of the transmitter the IF signal is divided by n whereas for the receiver it is better to multiply the phase detector reference by n. It is noted that in the transmitter we desire a wide pull-in range for the synchronizer loop and we are not specifically concerned with sensitivity of the phase detector since we are not dealing with a signal plus noise process. On the other hand, in the receiver we have a potentially fading weak signal with noise and we are interested in sensitivity. Furthermore, division of the fading process could lead to extra zero crossings which would upset the phase locked condition.

The results of the phase detector process are used to control the VCO in the frequency synthesizer subsystem after suitable loop compensation as discussed in Section 3.3.

The carrier tracking loop provides two functions for the receiver. First it centers the received signal on all the filters in the tone demodulator system. More important, it provides a stable reference signal, ω_r^*, which is incrementally phase corrected. This reference signal is multiplied up to create conversion references for the carrier loop. It is also multiplied up in the frequency synthesizer subsystem to provide incrementally phase corrected tone demodulation references. This operation is shown in the tone demodulation portion of the receiver in Fig. 5.3.

Specifically, the output of the wideband IF is split eight ways. Each component is then bandpass filtered in an appropriately tuned circuit to select a specific line in the received spectrum. The output of the bandpass filter is then mixed with a specific reference frequency which is produced in the frequency synthesizer subsystem. The resulting frequency is $n\omega_r^*$. This component is further filtered in an IF amplifier. Then the signal is synchroneously demodulated again using references generated by the frequency synthesizer subsystem to produce video signals which are proportional to the in-phase and quadrature complex envelope components of the received tones. These outputs, sixteen video signals, contain the propagation data.

A block diagram of the receiver frequency synthesizer is shown in Fig. 5.4. The operation of this device is straight forward. A VCO is controlled from the carrier loop compensation network. This VCO operates at the reference frequency, $n\omega_r^*$. In order to be able to establish exceedingly narrow carrier tracking loop bandwidths the VCO must provide high inherent stability. It would not be surprising to find on further analysis that this VCO's instabilities place the lower limit on loop noise bandwidth. In other words it

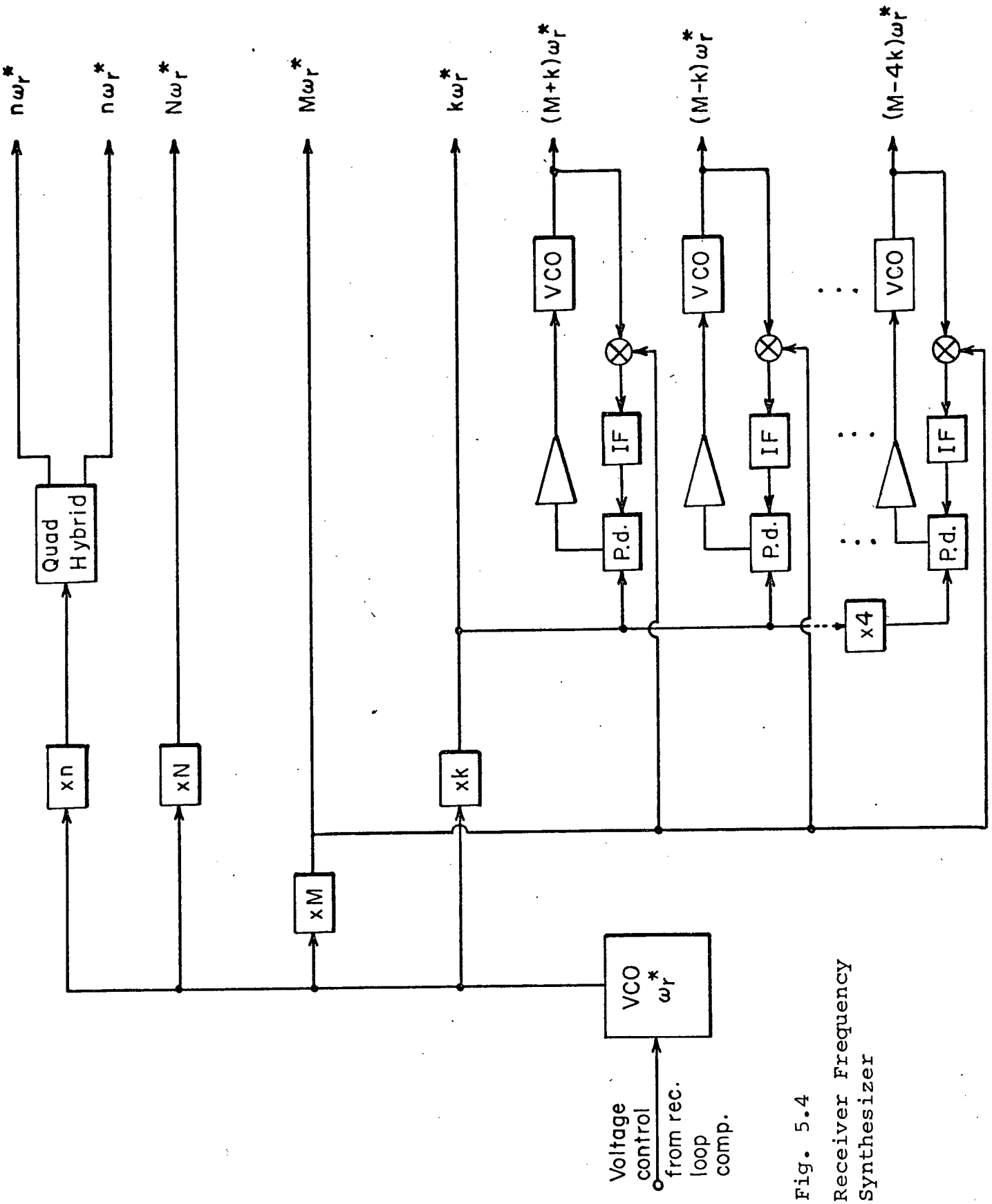

Fig. 5.4
Receiver Frequency Synthesizer

is likely that the spaceborne master oscillator in the transmitter and the effect of satellite motion will be less than the effects of changing parameters in the receiver VCO. There are several methods available for realizing an extremely stable VCO. Further analysis should be applied to determine the most appropriate approach for this receiver. The VCO output is used to synthesize all of the required signals in the receiver. The manipulations required to produce these signals are relatively straightforward as can be seen in Fig. 5.4. The tone demodulation references are generated with the aid of relatively simple phase locked loops which create the required offsets. For example a demodulation reference at $(M+k)\omega_r^*$ is generated as follows. The VCO output which is running at the desired frequency is mixed against M times the reference frequency. The difference is therefore at $k \times \omega_r^*$. This is amplified in an IF amplifier and compared against $k \times \omega_r^*$ in a phase detector. The output of the phase detector is then used in the usual way to control the VCO. The exact same circuitry is required to generate $(M-k)\omega_r^*$. In this case the VCO is constrained to operate below the first mixer reference rather than above it. In a similar way the other six demodulation references are generated.

5.3 Compatibility with the ATS-F System

The incremental phase correcting receiver just described can be implemented to be compatible with the existing ATS-F transmission format. The ATS-F system uses a 5 MHz master oscillator which is multiplied by a factor of 4,000 to produce a 20 GHz carrier or by 6,000 to produce a 30 GHz carrier. A 180 MHz tone is generated by multiplying the master oscillator output by a factor of 36. In terms of the system just described compatibility will be achieved if the following constraint is

fullfilled.

$$\omega_c = 4000\ \omega_r;\ \omega_r = 5\ \text{MHz},\ \omega_c = 20\ \text{GHz}$$
$$\omega_c = 6000\ \omega_r;\ \omega_r = 5\ \text{MHz},\ \omega_c = 30\ \text{GHz} \qquad (5.5)$$

Thus for operation at 20 GHz the various multiplication factors can be chosen as follows:

N = 3600, M = 375, and n = 25.

Fig. 5.5 shows a convenient synthesis technique for producing the three appropriate frequencies.

It would convenient to use similar multiplication factors for operation at 30 GHz. In this case a suitable set is as follows;

N = 5600, M = 375, and n = 25.

A suggested synthesis scheme for the 30 GHz operation is shown in Fig. 5.6. Note that this synthesizer shares a considerable number of components in common with the synthesizer proposed for 20 GHz operation.

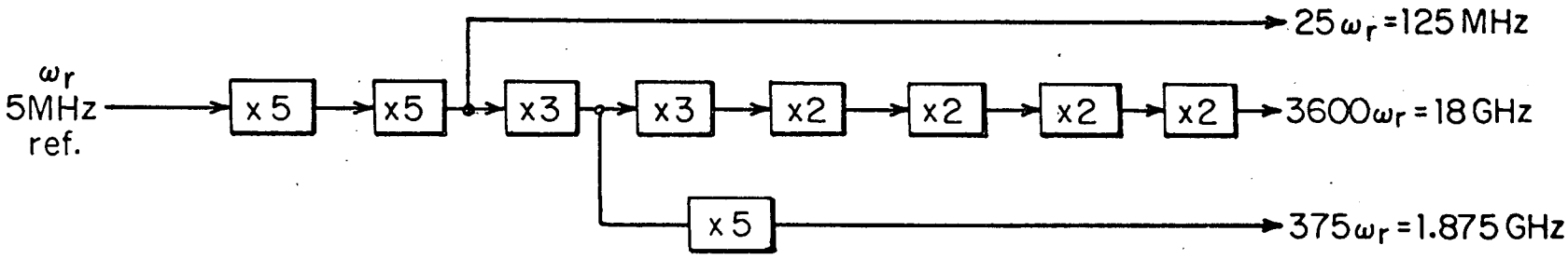

Fig. 5.5 20 GHz System Synthesizer

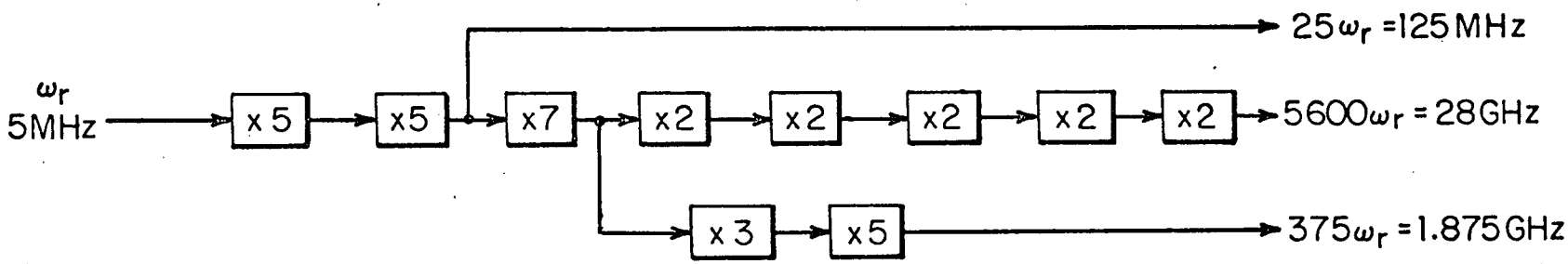

Fig. 5.6 30 GHz System Synthesizer

SECTION 6

DATA PROCESSING REQUIREMENTS

This chapter is concerned with the data processing requirements for a multitone channel characterization experiment as outlined in Section 3. The recording and interpretation of received data is considered in relation to other auxiliary data such as rainfall rate.

6.1 Processing of the Tone Responses

The experiment outline given in Section 3.2 calls for the processing of each tone to obtain amplitude and phase characteristics. Alternatively in-phase and quadrature components can be extracted. This latter approach is of course closely related but has the advantage that phase ambiguity problems are completely eliminated. Figure 6.1 illustrates the data collection procedure while Fig. 6.2 shows the way in which the data processing is carried out.

After phase and amplitude distortion by the channel, the received tones essentially represent the transfer function $H(f,t)$ sampled at frequencies $\{\omega_n/2\pi\}$ i.e.

$$r_n(t) = |H\left(\frac{\omega_n}{2\pi}, t\right)| \sin\left(\omega_n t + \gamma_n + \angle H\left(\frac{\omega_n}{2\pi}, t\right)\right) \quad (6.1)$$

Thus the required properties of $T_c(f)$ and $T_R(f,t)$ can be extracted from the phase and amplitude behavior of the received processes $\{r_n(t)\}$ after translation down to individual IF channels. We will assume here that the phase processes $\{\gamma_n\}$ have been incrementally corrected for oscillator drift effects so that from Eq. (3.28);

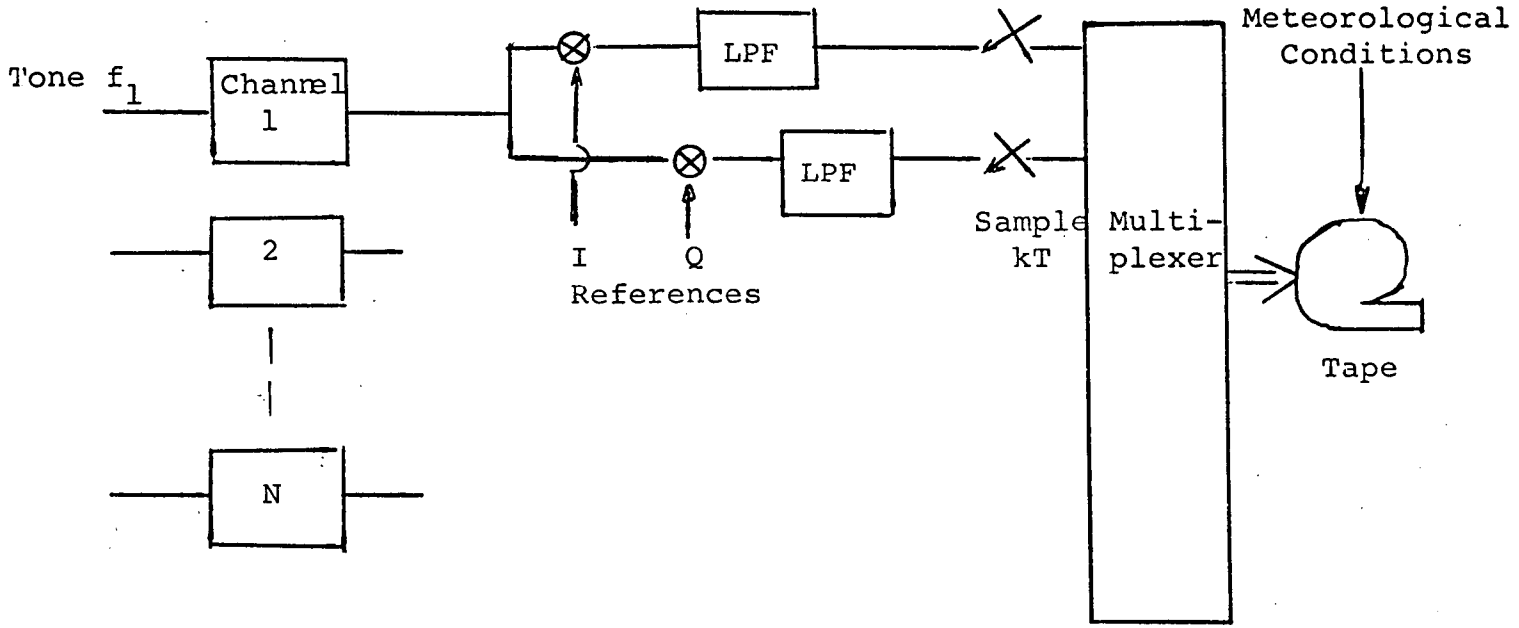

I = in-phase reference
Q = quadrature reference signal

Fig. 6.1. Data Collection

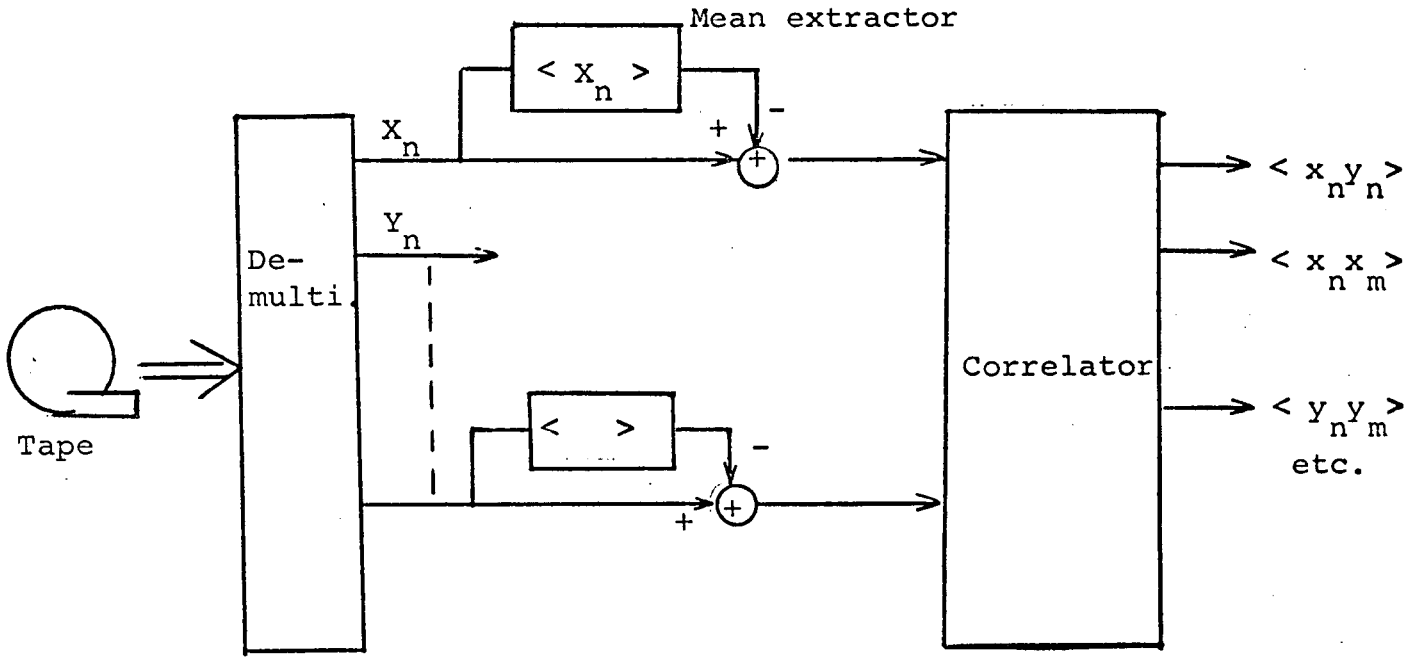

$$\langle x_n y_m \rangle = \frac{1}{K} \sum^{K} x_n(kT)\, y_n(kT-\tau)$$

Fig. 6.2. Processing of In-Phase and Quadrature Data

$$\gamma(f,t) = \phi(f,t) + \vartheta(f,t)$$

$$\simeq \phi(f,t) + \epsilon(f) \qquad (6.2$$

where $\epsilon(f)$ = nonlinear phase vs frequency component due to $T_c(f)$

$\phi(f,t)$ = random phase introduced by scattered signal component $T_R(f,t)$.

As shown in Fig. 6.1, the in-phase and quadrature components are extracted at each tone frequency, i.e.

$$X_n(t) = A_n(t) \cos \gamma_n(t)$$
$$Y_n(t) = A_n(t) \sin \gamma_n(t) \qquad (6.3)$$

and

$$A_n(t) = \left|H\left(\frac{\omega_n}{2\pi}, t\right)\right|$$

$$\gamma_n(t) = \angle H\left(\frac{\omega_n}{2\pi}, t\right) \qquad (6.4)$$

As previously discussed, $\{X_n(t)\}$ and $\{Y_n(t)\}$ are sets of stationary Gaussian processes; hence they are characterized by their means and cross covariances. This topic was discussed in detail in Section 2.3. The main distinction to be made here is the presence of additive noise generated at the receiver front end. The most interesting propagation conditions result in considerable attenuation of the signal, and as shown in Appendix B, the scattered signal may be 10 to 20 dB below the coherent or mean component; thus the scattered signal and receiver noise

component will often be comparable in power levels. Before proceeding with this aspect we write the observed I and Q components in terms of their mean and random components. i.e.

$$X_k(t) = \bar{X}_k(t) + x_k(t) + u_k(t)$$

$$Y_k(t) = \bar{Y}_k(t) + y_k(t) + v_k(t) \qquad (6.5)$$

where the mean components can be written,

$$\bar{X}_k(t) = R_e\left\{T_c\left(\frac{\omega_k}{2\pi},\ t\right)\right\}$$

$$\bar{Y}_k(t) = I_m\left\{T_c\left(\frac{\omega_k}{2\pi},\ t\right)\right\} \qquad (6.6)$$

and the random terms are,

$$x_k(t) = R_e\left\{T_R\left(\frac{\omega_n}{2\pi},\ t\right)\right\}$$

$$y_k(t) = I_m\left\{T_R\left(\frac{\omega_n}{2\pi},\ t\right)\right\} \qquad (6.7)$$

$u_k(t)$ = I noise in k^{th} IF channel (av. power = σ_u^2)

$v_k(t)$ = Q noise in k^{th} IF channel (av. power = σ_u^2)

It can be shown that the processes $\{u_k\}$ and $\{v_k\}$ are all independent of each other. Further individual time samples of each process will be approximately independent if the I and Q processes are sampled at the Nyquist rate (i.e. W samples/sec where W is the nominal IF filter bandwidth).

Note that in (6.6), the function $T_c(f,t)$ differs from previously definitions because of the influence of the phase incremental correction receiver which completely removes the slowly-varying linear phase vs frequency component from the coherent signal transfer function.

In the absence of other information pertaining to statistical properties of the channel, near otpimum estimates of means and covariances are provided by the following estimators;

Mean $\overline{X}$

$$\hat{\overline{X}}_k = \frac{1}{N} \sum_{n=1}^{N} X_k(n\Delta) \tag{6.8}$$

Covariance ($x_k(t)$ and $y_\ell(t)$)

$$\hat{R}_{xy}(f_k, f_\ell, \tau) \triangleq \hat{R}_{x_k y_\ell}(\tau)$$

$$= \frac{1}{N} \sum_{n=1}^{N} \left(X_k(n\Delta) - \hat{\overline{X}}_k\right) \left(Y_\ell(n\Delta - \tau) - \hat{\overline{Y}}_\ell\right) \tag{6.9}$$

Here the sampling interval is denoted by Δ and the total observation interval used in the estimate is $T = N\Delta$. It is also assumed that τ is some multiple of Δ. In the next section, the estimator performance is analyzed, and typical channel parameters are used to provide concrete examples.

6.1.1 Estimation Performance

Consider first the mean estimate given by Eq. (6.8). The statistical average of the estimate is,

$$E\{\hat{\bar{X}}\} = E\{\bar{X}_k + x_k(n\Delta) + u_k(n\Delta)\} = \bar{X}_k \tag{6.10}$$

while the variance is,

$$E\{(\hat{\bar{X}}_k - \bar{X}_k)^2\} = \frac{1}{N^2} E\{(\sum_n x_k(n\Delta) + u_k(n\Delta))^2\}$$

$$= \frac{1}{N^2} E\left\{(\sum_n x_k(n\Delta))^2\right\} + \frac{\sigma_u^2}{N} \tag{6.11}$$

with

$$E\{u(n\Delta)\ u(m\Delta)\} = \begin{cases} \sigma_u^2 & n=m \\ o & \text{otherwise} \end{cases}$$

Equation (6.11) can be further reduced to an expression containing the correlation function for $x_k(t)$; i.e. $R_{x_k}(\tau)$

$$\text{Var}\ (\hat{\bar{X}}_k) = \frac{1}{N^2} \sum_{n=1}^{N} (N-2n)\ R_{x_k}(n\Delta) + \frac{\sigma_u^2}{N} \tag{6.12}$$

Note that when $T=N\Delta$ is much larger than the correlation time, or width of $R_{x_k}(\tau)$, we can make the approximation,

$$\text{Var}\ (\hat{\bar{X}}_k) \simeq \frac{1}{N}\left[\sum_n R_{x_k}(n\Delta) + \sigma_u^2\right] \tag{6.13}$$

For a Doppler bandwidth of B, R_{x_k} will have a width of approximately 1/B, while the average power of $x_k(t)$ is given by

$$\sigma_x^2 \triangleq R_{x_k}(o)$$

Hence

$$\sum_n R_{x_k}(n\Delta) \simeq \sigma_x^2/\Delta B \tag{6.14}$$

Thus

$$\text{Var}\ (\hat{\bar{X}}_k) \simeq \frac{1}{N}\left[\frac{\sigma_x^2}{\Delta B} + \sigma_u^2\right] \tag{6.15}$$

Consider for example the range of parameters expected in the ATS-F experiment.[6.1].

Av. coherent power/tone = -110 dBm (no attenuation)

Carrier/noise power density = 48.8 dB/Hz.

For a 50 Hz IF bandwidth, i.e., $\Delta = 1/50$, we get,
Carrier/noise power = 31.8 dB.

Assuming a 12 dB attenuation and a scattered signal power 20 dB down from the carrier we arrive at a situation where the noise power σ_u^2, and the scattered signal power, σ_x^2, are both approximately equal. Expressing the performance as a fractional standard deviation:

$$\gamma = \left[\frac{\text{Var}\,(\hat{\bar{X}}_k)}{\bar{X}_k^2}\right]^{\frac{1}{2}}$$

$$\simeq \left[\frac{\sigma_x^2}{N}\ \frac{(\frac{1}{\Delta B} + 1)}{\bar{X}_k^2}\right]^{\frac{1}{2}} \tag{6.16}$$

With $B \simeq 1$ Hz we can solve for the $T = N\Delta$ which gives a reasonable quality estimate. Thus for $\gamma = 0.1$ we find

$$10^{-2} \simeq 10^{-2}/N\Delta B$$

since

$$\frac{\sigma_x^2}{\bar{X}_k^2} \simeq 10^{-2} \tag{6.17}$$

Therefore for the stated accuracy we need,

$$T = 1/B$$
$$= 1.0 \text{ sec.}$$

Note that the noise waveform contains an inherently larger number of degrees of freedom for a given T, and as a consequence its effect is averaged out much faster than the scattered signal contribution. As a result, the averaging time suggested above represents only an approximate guide, the choice of T to meet a given performance being strongly dependent on the true scattered/coherent power ratio.

In the second half of this section we consider the measurement accuracy attainable for an observation interval T when one is interested in implementing the covariance estimate given by Eq. (6.9). The expected value of $\hat{R}$ is computed as,

$$E\{R_{xy}(\tau)\} = \frac{1}{N} E\left\{ \sum_{n}^{N} [x(n\Delta) + u(n\Delta)][y(n\Delta-\tau) + v(n\Delta-\tau)] \right\}$$

$$\simeq R_{xy}(\tau) \qquad (6.18)$$

Since $E\{uy\} = E\{uv\} = E\{vx\} = 0$

Note that the frequency subscripts have been suppressed to avoid complicating the notation. It has been assumed here that the interval T is much larger than the correlation time (hence also the range of τ), and that the means $\overline{X}_k$ and $\overline{Y}_k$ are known exactly. In practice these quantities must be replaced (e.g. in Eq. (6.9)) by estimates which have non-zero error; thus the performance calculated below for known values, may be slightly optimistic.

The variance of $\hat{R}_{xy}$ is found from;

E

$$\text{var}\left\{\hat{R}_{xy}(\tau)\right\} = E\left\{\frac{1}{N^2}\left(\sum_n \left[x(n\Delta) + u(n\Delta)\right]\left[y(n\Delta-\tau)+ v(n\Delta-\tau)\right]\right)^2\right\}$$

$$- R^2_{xy}(\tau) \qquad (6.19)$$

For Gaussian variables $z_k, k = 1,4$ we can use the property,

$$E\left\{\prod_k z_k\right\} = E(z_1z_2)\ E(z_3z_4) + E(z_1z_3)\ E(z_2z_4) + E(z_1z_4)E(z_2z_3) \qquad (6.20)$$

Applying this to (6.19) and using an observation time T which is long compared with the correlation time we get,

$$\text{var}\left\{\hat{R}_{xy}(\tau)\right\} \simeq \frac{1}{N^2}\sum_{mn}\sum \left[R_x\left((n-m)\Delta\right)\sigma_u^2\right]\left[R_y\left((n-m)\Delta\right)+\delta\left((n-m)\Delta\right)\sigma_u^2\right]$$

$$+ \frac{1}{N^2}\sum_m\sum_n R^2_{xy}(\tau)$$

$$+ \frac{1}{N^2}\sum_m\sum_n R_{xy}\left((n-m)\Delta + \tau\right)\cdot R_{xy}\left((m-n)\ \Delta + \tau\right)$$

$$- R^2_{xy}(\tau) \qquad (6.21)$$

Assuming for example that,

$$R_x(\tau) = R_y(\tau)$$

$$R_{xy}(\tau) = R_{xy}(-\tau)$$

we get,

$$\text{var}\left\{\hat{R}_{xy}(\tau)\right\} \simeq \frac{1}{N}\left\{\sum_j R_x^2(j\Delta) + 2R_x(o)\sigma_u^2 + \sigma_u^4\right\}$$

$$+ \frac{1}{N}\left\{\sum_j R_{xy}(j\Delta-\tau)\ R_{xy}(j\Delta+\tau)\right\} \qquad (6.22)$$

This may be very roughly approximated by the expression;

$$\text{var}\left\{\hat{R}_{xy}(\tau)\right\} \simeq \frac{1}{N}\left\{\frac{(1+\rho)\ R_x^2(o)}{\Delta B} + 2R_x(o)\sigma_u^2 + \sigma_u^4\right\} \qquad (6.23)$$

where

$$\rho = \frac{R_{xy}(o)}{R_x(o)}$$

and

$$\Sigma\ R_x^2\ (j\Delta) \simeq \frac{R_x^2(o)}{\Delta B} \qquad B = \text{Doppler spread}$$

Following the previous definition of an RMS fractional error, we write,

$$\gamma^2 = \frac{\text{var}\left\{\hat{R}_{xy}(\tau)\right\}}{R_{xy}^2\ (\tau)}$$

$$\simeq \frac{1}{NR_{xy}^2\ (\tau)}\left[\frac{(1+\rho)\ R_x^2(o)}{\Delta B} + 2R_x(o)\sigma_u^2 + \sigma_u^4\right]$$

$$= \frac{1}{N}\left\{\frac{(1+\rho)}{\Delta B}\left(\frac{R_x(o)}{\sigma_u^2}\right)^2 + 2\left(\frac{R_x(o)}{\sigma_u^2}\right) + 1\right\}\Bigg/\left(\frac{R_{xy}(\tau)}{\sigma_u^2}\right)^2$$

(6.24)

Consider the following parameters, which were used previously.

$$B = 1 \text{ Hz}$$

$$1/\Delta = 50 \text{ Hz}$$

$$\frac{R_x(o)}{\sigma_u^2} = 1 \text{ (scattered power/noise power)}$$

$$R_{xy}(\tau) \simeq \frac{1}{10} R_x(o)$$

$$\rho \simeq 1/10$$

$$\gamma^2 \simeq \frac{1}{N} \left\{55 + 2 + 1\right\} 10^2$$

For $\gamma = 0.1$ we thus require

$$N = 5,800$$

or

$$T \simeq 100 \text{ secs.}$$

Similarly when estimating $R_x(\tau)$ and $R_y(\tau)$, the same formula can be used with ρ set equal to unity. For example when

$$\frac{R_x(\tau)}{R_x(o)} \simeq \frac{1}{10}$$

The result is almost exactly the same.

Note that when the scattered signal power level exceeds the average noise; i.e.

$$\frac{R_x(o)}{\sigma_u^2} > 1$$

equation (6.24) is closely approximated by;

$$\gamma^2 = \frac{1}{N}\left(\frac{R_x(o)}{R_{xy}(\tau)}\right)^2 \qquad (6.25)$$

i.e. the error introduced by the additive noise is significant. This is in fact true for even smaller values of $R_x(o)/\sigma_u^2$ due to the fact that all noise samples are independent while the signal is correlated over intervals of approximately 1/B.

6.1.2 Summary of Tone Processing

The in-phase and quadrature components of each tone response will be available in sampled form with sampling interval Δ. The quantities to be extracted for every T secs of data are;

(a) Mean I and Q values,

$$E\{X_k\} = R_e\{T_c(f_k)\}$$

$$E\{Y_k = I_m\{T_c(f_k)\} \qquad (6.26)$$

(b) Time-Frequency Covariance Properties

$$E\{x_k(t)x_\ell(t-\tau)\} = R_x(f_k, f_\ell; \tau)$$

$$E\{x_k(t)y_\ell(t-\tau)\} = R_{xy}(f_k, f_\ell; \tau)$$

$$E\{y_k(t)y_\ell(t-\tau)\} = R_y(f_k, f_\ell; \tau) \qquad (6.27)$$

These correlation functions along with the mean signal levels given by Eq. (6.26) allow complete characterization of the channel. In many examples of communications channels involving scattered signals, it has been found that the x and y components

have identical correlation properties and that certain symmetry in the cross correlation R_{xy} can be exploited. However because of the narrow beamwidths involved in a millimeter wave link, such relationships can not necessarily be assumed, and before the design of a suitable data link can proceed it is necessary to experimentally verify the expected parameter values and their relationships.

From the correlation processing we can obtain all required channel characteristics. For example the following parameters can be extracted.

(a) Attenuation versus frequency. The average in-phase and quad. processes indicate attenuation. As discussed previously, variation across the band gives rise to waveform distortion.

(b) Delay distortion. The components $\overline{X}_n$ and $\overline{Y}_n$ can be used to compute the phase shift across the band. Deviations from linear also distort the direct signal component.

(c) The two dimensional covariance functions R_{xx}, R_{xy} and R_{yy} can be used to determine the Doppler and multipath spreads imposed by the scattering medium. (See Ref. 6.2).

(d) Phase stability of the transmitter oscillator and satellite movement. The phase correction scheme allows these quantities to be separated from channel induced effects and measured if required.

The above parameters may be correlated with available meteorological data to verify that atmospheric models are useful in accurately predicting channel behavior. Then in turn, these

characteristics can be used to evaluate the distorting effect which the channel has on specific signaling waveforms and hence the corresponding short term error rate.

6.2 Collection and Processing of Auxiliary Data

The prevailing meteorological conditions obviously play a dominant role in determining the propagation conditions and resultant link performance. Consequently it is logical to undertake the sensing of certain meteorological parameters while the channel characterization experiment is being conducted, so that postulated couplings between atmospheric conditions and link properties can be verified. Furthermore if these two aspects do demonstrate strong correlation, there remains the prospect of direct prediction of link behavior based on the local meteorological history.

6.2.1 Meteorological Parameters of Interest

We first single out some of the parameters which have a direct bearing on millimeter wave propagation conditions. Consider for example the following observable quantities.

a) Rainfall rate; desired as a function of all space near beam intersections, but as a practical matter available only from a grid of spatial samples at ground level [6.3].

b) Atmospheric turbulence, in particular the atmospheric humidity levels. Again most readily available at ground level. [6.4].

c) Refractive Index profiles (vs height). These are of interest in determining beam refraction effects [6.5], and possible multipath propagation when low elevation angles are involved. [6.6].

In addition to the above categories it has been found that fog, cloud and snow have negligible effects on propagation at millimeter wavelengths.

The rainfall rate itemized in a), has a strong influence on attenuation. There has been a considerable amount of effort by others in this area [6.7, 6.8] and the basic relationships between rainfall rate and attenuation have been fairly well established. Similarly the mapping of rainfall rates over a wide spatial area to determine the potential of diversity paths through a rainstorm has been widely discussed and is currently under investigation using a dense rain gauge network [6.3, 6.9]. In light of these research efforts it does not seem profitable to consider an extensive rainfall gauge network implementation. It would still be desirable however to relate multipath and amplitude fluctuation data to the rainfall rate in the beam intersection volume and this can be simply satisfied using a line of gauges placed under the ground station beam. The characteristic structure of rainstorms tends towards cells of high rain intensity with dimension on the order of 1 km. Thus the spacing of the rain gauges should be 1 km or less [6.10].Fig. 6.3 illustrates the general configuration required. Rain gauges are currently available which will operate with high accuracy during rain rates of up to 10 inches/hour [6.11]. The electrical output consists of a continuous tone, the frequency of which is related directly to rain rate. The carrier offset frequency is sampled at each gauge output and recorded on tape for later processing, including the conversion from frequency to rain rate. Fig. 6.4 illustrates the processing involved. A similar configuration of rain gauges has already been implemented for the ATS-V experiment [6.12].

Atmospheric turbulence directly effects the amount of power scattered from the coherent beam and dictates the mean square amplitude and phase fluctuations of the signal. Unfortunately surface measurements of temperature pressure and humidity are far

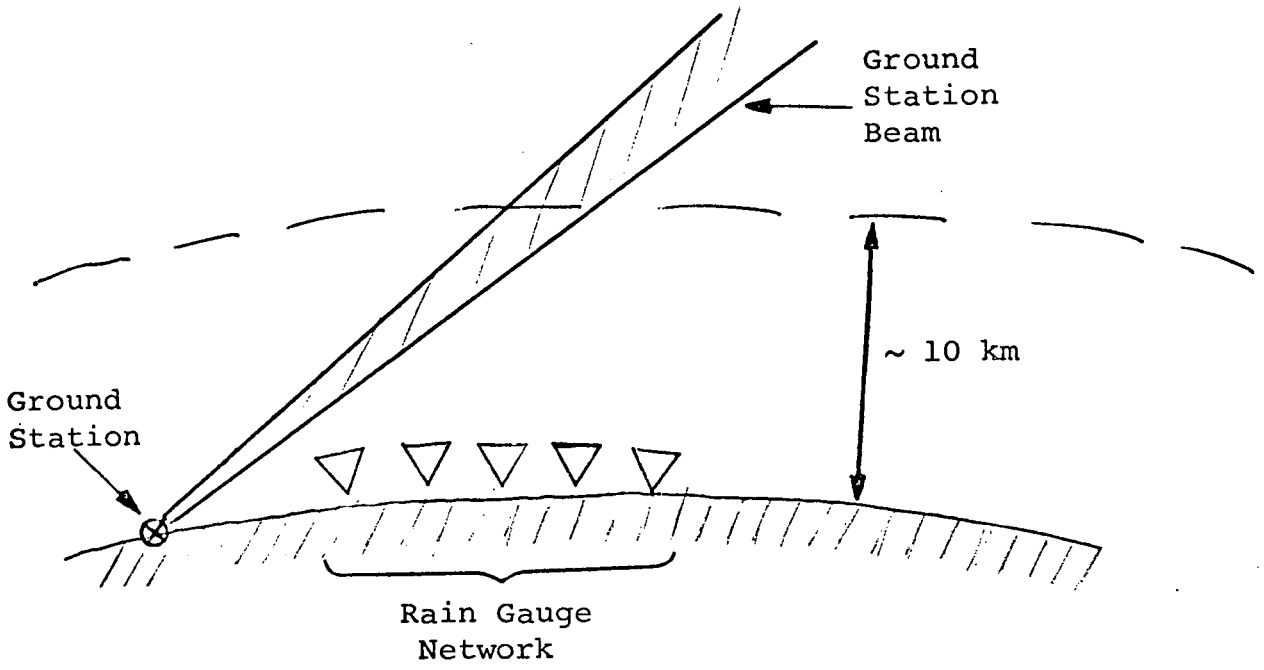

Gauge Spacing < 1 km

Total Number 10 - 20

Fig. 6.3. Rain Gauge Configuration.

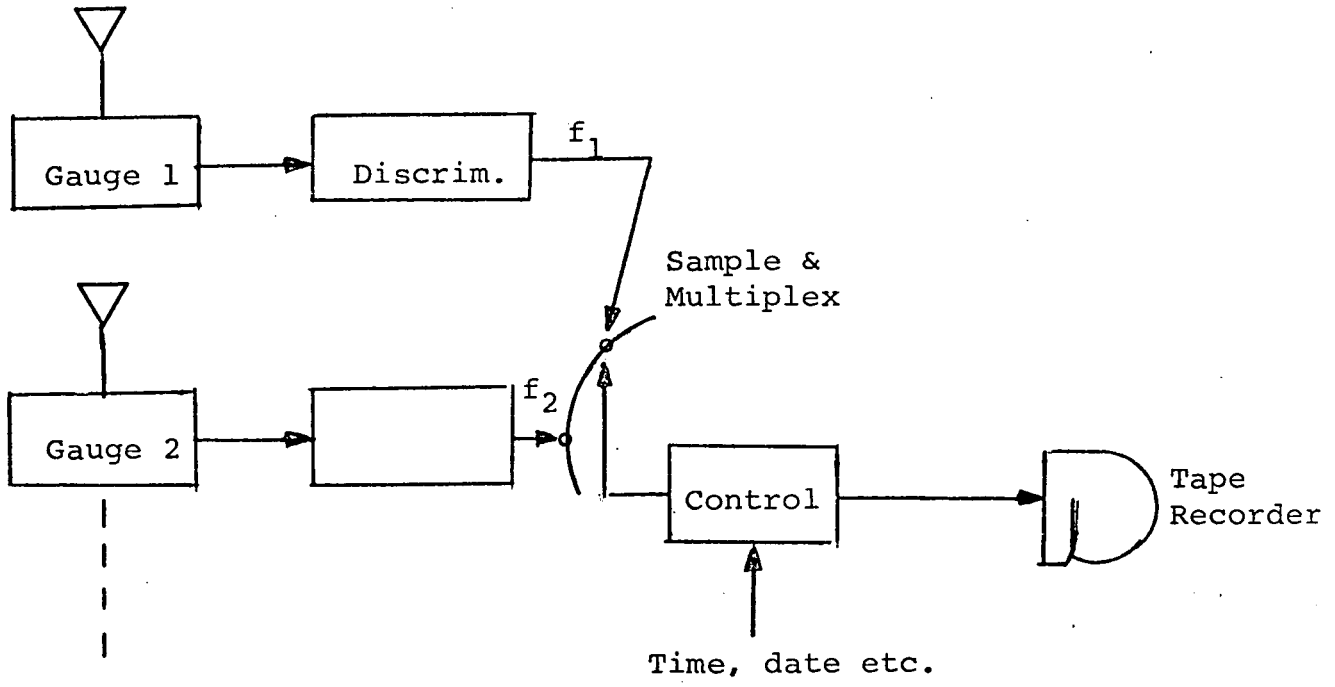

Fig. 6.4. Rain Gauge Data Acquisition.

from representative of atmospheric conditions at other altitudes. In general the complete profiles of temperature, pressure and humidity with altitude are necessary to establish the stability or relative turbulence of the atmosphere. These conclusions are largely substantiated by the results of various experiments where surface weather data was used. [6.13, 6.14]. In general the effects of high atmospheric turbulence are not severe, since the signal attenuation varies by only a few dB, and the link continues to operate under very high signal to noise conditions. This is in contrast to the high attenuation possible with rainstorms. Consequently it is not recommended that surface weather data be used in the experiment data reduction program, as the additional complications do not appear to be justified. This does not mean that bandwidth and multipath parameters are unimportant for propagation through the clear atmosphere but simply that the range of variation is not great and only loosely coupled to observable meteorological variables.

The third class of atmospheric data of interest is related to beam refraction effects which arise when the atmosphere becomes stratified into layers with different refractive index properties. In many instances these layers cover large horizontal areas so that vertical refractivity soundings provide a fairly complete picture of the total structure. These profiles are obtained from temperature pressure and humidity soundings. By utilizing a ray tracing program it is possible to examine the way a beam is distorted by the atmosphere and to investigate the possibility of multiple ray paths to the satellite. However it is well known that these refraction effects will be of minor importance in situations where the elevation angle exceeds 20^{o}, such as would be the case for an equatorial synchronous satellite linked to

most points in the North American continent. [6.5]. Consequently we will not pursue this topic further, but instead pass on to a brief discussion of the analysis of rainfall data.

6.2.2 Verification of Link Parameters Using Rainfall Data

Since rainfall causes the most severe link degradation and its gross properties are readily measured, we restrict further attention to this subject alone. The rainfall rate data can be utilized in two ways;

a) Prediction of satellite to ground link properties such as total attenuation, coherent/scattered power ratio and delay spread. These predictions would be based on the techniques used in Appendix A and B, and since the true channel parameters would be available by direct probing, correlation analysis of the predicted and measured data would indicate the validity of prediction of link characteristics based on surface weather data alone.

b) Interference Prediction. The intersection of antenna beams not associated with the same link will give rise to serious interference effects when a scattering medium such as a rainstorm is within the intersection volume. Predictions of the degree of interference can be made if the rainfall distribution is known.

These topics which involve link parameter predictions are implicitly developed in Appendices A-D where analytical expressions for the various parameters may be found.

SECTION 6

REFERENCES

[6.1] Ippolito, L.J., "The ATS-F Millimeter Wave Propagation Experiment," NASA X Document, X-751-71-460, October 1971, p 3.12.

[6.2] Gallager, R., "Characterization and Measurement of Time and Frequency-Spread Channels", MIT Lincoln Lab. Tech. Report 352, April 1964.

[6.3] Semplak, R.A., and H.E. Keller, "A Dense Network for Rapid Measurement of Rainfall Rate", BSTJ, Vol. 48, No. 6, July 1969, pp 1745-1756.

[6.4] F. Villars, and V.F. Weisskopf, "On the Scattering of Radio Waves by Turbulent Fluctuations of the Atmosphere", Proc. IRE, October 1955, pp 1232-1239.

[6.5] Crane, R.K., "Propagation Phenomena Affecting Satellite Communication Systems Operating in the Centimeter and Millimeter Wavelength Bands", Proc. IEEE, Vol. 59, No. 2, February 1971, p 185.

[6.6] Ruthroff, C.L., "Multiple-Path Fading on Line-of-Sight Microwave Radio Systems as a Function of Path Length and Frequency", BSTJ, Vol. 50, No. 7, September 1971, pp 2375-2398.

[6.7] Ref.[6.5], p 177.

[6.8] Godard, S.L., "Propagation of Centimeter and Millimeter Wavelengths Through Precipitation", IEEE Trans. on Antennas and Propagation, Vol. AP-18, No.4, July 1970, pp 530-534.

[6.9] Hogg, D.C., "Path Diversity in Propagation of Millimeter Waves Through Rain", IEEE Trans. Antennas and Propagation, Vol. AP-15, No.3, May 1967, p 410-415.

[6.10] Semplak, R.A. and R.H. Turrin, "Some Measurements of Attenuation by Rainfall at 18.5 GHz", BSTJ, Vol. 48, July 1969, No.6, pp 1767-1789.

[6.11] Ref.[6.3]

[6.12] Ippolito, L.J., "Effects of Precipitation on 15.3 and 31.65 GHz Earth Space Transmissions With the ATS-V Satellite", Proc. IEEE, Vol.59, No.2, February 1971.

[6.13] Weibel, G.E., and H.O. Dressel, "Propagation Studies in Millimeter-Wave Link Systems", Proc. IEEE, Vol.55 No. 4, April 1967, p 509.

[6.14] Straiton, A.W. et.al., "Amplitude Variations of 15 GHz Radio Waves Transmitted Through Clear Air and through Rain", Radio Science, Vol. 5, No. 3, March 1970, p 554.

SECTION 7

CONCLUSIONS

This section summarizes the results achieved during the study effort. The analysis of channel characteristics carried out in this program has attempted to extend and refine the propagation channel model for K-band satellite-to-ground links. This augmentation of the channel characteristics is, in part, based on recently derived experimental data and, in part, on a more detailed definition of typical communication systems parameters hypothesized for K-band satellite-to-ground links. In a similar manner the report considered measurement techniques to derive channel characteristics using an experimental spacecraft. Again, the design philosophy which is evolved in this report is based in part on recent experimental experience and in part on advances in the state-of-the-art in component technology.

7.1 Channel Characterization and Measurement Approach

Channel characterization and measurement approach are discussed in detail in Section 2. A relatively simple model for the channel is derived. This model is specifically appropriate for the analysis of communication and/or navigation systems operating through the propagation medium. The emphasis in the discussion is placed on the effect of the channel characteristics on generalized received signals, rather than on the physical interactions which give rise to the channel properties. A measurement philosophy is derived based on the simple channel model. The rather general discussion of Section 2 is augmented by detailed analyses which are contained in Appendix A and

Appendix B. These latter discussions attempt to tie together the discussions available in the open literature so that some insight into the relative magnitudes of the effects to be observed can be derived.

It was found, for example, that satellite-to-ground K-band links may not conform to the generalized channel models derived or assumed in the open literature. Note that there is a move toward narrower beamwidth antennas at K-band frequencies and above. It was found in this report that for narrow beamwidths the channel is not WSSUS as assumed in most theoretical discussions (See for example Ref. 2.2 and 2.7). Further, examination of the effect of narrow-beam antennas on channel characteristics uncovered a source of frequency dependence in the deterministic portion of the channel transfer function.

The channel model derived in this report, and hence, the experimental measurement technique suggested , is valid in the region from 15-90 GHz. At 90 GHz, however, multiple scattering should become significant, and thus, the random scattering effects may become important and predominate over deterministic effects despite narrow beamwidths.

7.2 Measurement Techniques

Sections 3 and 4 considered two basic measurement techniques for extracting channel data. In particular, section 3 analyses the multi-tone technique which has been implemented for ATS-5 and ATS-F. An incremental phase direction scheme is explored to augment the basic multi-tone channel probing approach. This technique is compatible with the receiver demodulation technique currently employed in the ATS hardware. The incremental phase

correction approach provides a little more data about the channel scattering characteristics. It is shown that the investigated incremental phase correction scheme will provide adequate performance for the K-band satellite-to-ground link only if the combined effects of satellite oscillator instability and satellite motion could be tracked out. Chapter 3 concludes with a discussion of phase-locked loop techniques for incremental phase correction. In particular, the second and third order digital phase-locked loops are discussed which provide extremely narrow bandwidths. It is shown that such techniques will provide the necessary performance; however, detailed analysis to determine the exact level of system complexity and the applicability to the current satellite configuration have not been carried out at this time.

The multi-tone approach analyzed and discussed in section 3 does not provide data in a format which is directly usable by communication and navigation design engineers. Furthermore, it is shown that significant receiver complexity and processing is required by this technique to derive adequate data. Thus, in Section 4 we consider a more direct channel measurement approach. In particular, section 4 considered pulsed channel measurement techniques. It is interesting to note that although the pulse techniques appear to be more straightforward, more detailed analysis shows that these techniques suffer from essentially the same problems as were considered for the multi-tone approach, namely oscillator stability and satellite motion. Furthermore, there is a problem in the pulsed system concerning signal-to-noise ratio. The problem arises because the satellite transmissions must consist of extremely short (sub-nanosecond) pulses and these are difficult to generate at high power levels

in the spacecraft environment. CW waveforms are generally considered to be more desirable in such an environment. Furthermore the received pulses cannot be combined coherently at the receiver unless a highly complex receiver system is constructed. Thus, the results of this study reaffirm the conclusion that multi-tone processing, with all its drawbacks, remains optimum for K-band satellite-to-ground link channel measurement.

7.3 Hardware and Data Processing Considerations

Sections 5 and 6 consider equipment designed for channel measurement and data processing requirements, respectively.

The equipment configurations described in Section 5 are based in part on experience obtained by NASA personnel with current equipment, and in part on improvements in the state-of-the-art of solid-state components. An all solid-state multi-tone channel prober transmitter is shown which relies heavily on feedback compensation techniques to assure the stable transmission of the prober waveform. An IMPATT oscillator is phase-locked in the transmitter to a suitably multiplied carrier reference frequency. The stability of the output is directly related to the stability of this reference signal. The second loop which includes a frequency discriminator is used to create the tone modulation. Again, the output of the transmitter is demodulated through the frequency discriminator and the resulting demodulating waveform is compared against the desired waveform. In this case the desired waveform is a simple sinusoid at the fundamental tone modulation frequency. In general, the feedback approach employed in the transmitter design somewhat reduces individual component performance requirements. A receiver design is described which is compatible with the feedback stabilized

transmitter. This receiver design also provides incremental phase correction. The receiver is furthermore compatible with the transmitter configuration currently employed in the ATS-F system provided a special frequency reference synthesizer subsystem is used. This latter device is also described in detail in Section 5.

Section 6 deals with detailed processing requirements for the multi-tone channel measuring system. The discussion emphasizes the use of in-phase and quadrature processing rather than amplitude and phase detection techniques. An analysis is provided to demonstrate the advantages of the in-phase/quadrature approach. Of course, the hardware changes required to convert from amplitude/phase to in-phase/quadrature are trivial.

Using the processing techniques described in Section 6 the following channel characteristics can be extracted:

a) Attenuation vs. Frequency and Delay Distortion
   These characteristics characterize the non-scattering distortion properties of the propagating medium.

b) The Two-Dimensional Covariance Functions R_{xx}, R_{xy} and R_{yy}
   These correlation functions characterize the scattering components of the medium.

c) Phase Stability of the Transmitter Oscillator and Effect of Satellite Movement.
   These characteristics constitute the third component in the K-band satellite-to-ground channel model.

Section 6 also presents a discussion of the utility of various meteorological monitoring techniques, in particular rain gauge data systems are discussed in some detail. It is shown that a

relatively simple rain gauge configuration will provide adequate data to correlate observed channel characteristics with meteorological effects.

7.4 Summary of Results and Recommendations

The study reconsidered the channel characterization of K-band satellite-to-ground links. Several channel measurement techniques were considered for the purpose of collecting new channel data. Emphasis was placed on variations of the multi-tone probing technique and some variations of a pulsed probing technique. It was found that the multi-tone technique is preferred because the state-of-the-art in component technology is not sufficient to support a pulsed techniques. Problems, in particular, were found with respect to available power levels and with respect to available signal bandwidths with the pulsed techniques considered.

The recommeded multi-tone technique is slightly modified relative to the approach implemented for ATS-5 and ATS-F. Specifically, it is still uncertain whether an incremental phase correction technique be used to track out the effect of transmitter oscillator instability and satellite motion. If this could be done, then the multiple tones could be demodulated in such a way that actual phase differences among tones can be extracted if desired. It is noted, however, that direct phase measurements were not recommended. It was found that in-phase and quadrature demodulation of the tone components provided a small advantage.

The transmitter design which is recommended reflects the latest technological advances. The approach will supply superior performance in the spacecraft environment. Since the transmitter design is all solid-state, it should provide a significant improvement in

reliability relative to the current design. It is noted that the current design is based on technology available in the mid-1960's.

Some small component improvements are required to realize the transmitter as described in this report. In particular a small increase in power level above that which is available off-the-shelf at the present time is required. It is expected that since the state-of-the-art of IMPATT oscillators is advancing rapidly at this time that higher powers will be available shortly.

It is difficult to evaluate the robustness of the conclusions derived in this report. Nonetheless it is stated that the most vulnerable area concerns the selection of the channel measurement technique. In particular, it is noted that given a significant advance in the state-of-the-art of digital logic components and RF high-power switching techniques, an alternate channel measurement technique would have been proposed. In such a case, the pseudo-random noise probing technique is more desirable. This technique does not suffer from signal-to-noise ratio limitations as does the pulse techniques of section 4. However, to implement the PRN approach, a bit rate on the order of 2 GHz is required. This certainly cannot be purchased off-the-shelf at the present time, nor is such performance anticipated in the near future. Furthermore, RF switch gear which could be used to create a phase shift keyed modulator is similarly unavailable at this time. Such switch gear would have to provide 100 picosecond switching transients in order to be useful. It is possible to realize a PRN channel prober which operates at roughly 500 megabits per second, however such a rate is not sufficiently faster than proposed microwave data links to provide relevant performance information.

Several developments are recommended at the present time to ensure successful deployment of the equipment designed in this study. First it is recommended that an effort be made to improve the stability of the space qualified stable reference oscillators. For the system under consideration in this report, we are particularly concerned with stability over intervals on the order of 100 seconds or less. We are less concerned with very long term stability.

Next is recommended that an effort be undertaken to develop space qualified IMPATT oscillators designed to operate in the region above 20 GHz.

Finally, it is recommended that an effort be expended to develop efficient frequency synthesizer techniques for use with the proposed spacecraft transmitter portion of the channel prober system.

Appendix A

RAIN SCATTERING EFFECTS FOR THE LOS MILLIMETER WAVE SATELLITE LINK

A.1 Description of the Scattering Process

A.1.1 General Discussion

The discussion here will be limited to propagation through rain. Some of the properties of typical raindrops, which are assumed to be approximately spherical, are listed below.

Diameter	1 - 3 mm
Drop density	15 - 3000/m^3
Rain rate	5 - 100 mm/hr.

Considering a range of frequencies from 15 GHz (λ = 2 cm) to 94 GHz (λ = 0.3 cm) it is apparent that the drop diameters will usually be less than a wavelength in diameter, while average spacings

$$d = (\text{Density})^{-3} \text{ meters}$$

will be significantly greater than a wavelength with the exception of the highest drop densities at the lowest frequency.

This latter conclusion is important because it allows the analysis to proceed in terms of independent scattering, i.e., the field scattered from any single drop can be studied without reference to other drops.* This does not preclude the possibility of multiple scattering of energy. However, it simply allows the

*Frequently it is possible to express the average scattered intensity as the sum of the intensities from individual scatterers, but for a bistatic antenna configuration this assumption must be examined carefully.

analysis to proceed in terms of radiation fields with near field effects neglected. Note that the mutual spacing required for independent scattering is on the order of 3 times the particle radius (rather than a function of wavelength).

Other media that are of interest at the higher frequencies, such as fog and clouds, also satisfy the criterion for independent scattering.

A.1.2 Field Scattered From a Dielectric Sphere

The solution for the field which results when a plane wave is incident on a lossy dielectric sphere can be found in spherical coordinates. (See Ref. [A1]).

The solutions are expressed in terms of the wave functions;

$$\psi_{e_{0n}} = \begin{cases} \cos\phi \\ \sin\phi \end{cases} P_n(\cos\theta) Z_n(kR) \qquad \text{(A.1)}$$

where $\{P_n(\cos\theta)\}$ are the Legendre polynomials, and

$$Z_n(kR) = \begin{cases} j_n(kR) = \sqrt{\frac{\pi}{2kR}}\, J_{n+1/2}(kR) \quad ; \quad R \le a \\ h_n^{(2)}(kR) = \sqrt{\frac{\pi}{2kR}}\, H^{(2)}_{n+1/2}(kR) \quad ; \quad R \ge a \end{cases} \qquad \text{(A.2)}$$

$H^{(2)}$ = Hankel function of second kind

J = Bessel function of first kind.

a = Radius of the sphere.

For large arguments,

$$j_n(kR) \simeq \frac{1}{kR} \cos\left(kR - \left(\frac{n+1}{2}\right)\pi\right)$$

$$= \frac{1}{2kR}\left[(-j)^{n+1} e^{jkR} + (j)^{n+1} e^{-jkR}\right] \qquad \text{(A.3)}$$

and

$$h_n^{(2)}(kR) \simeq \frac{1}{kR}(-j)^{n+1}e^{jkR} \tag{A.4}$$

The field at any point in space is the sum of two components;

$$\vec{E} = \begin{cases} \vec{E}_i + \vec{E}_s & R > a \\ \vec{E}_i + \vec{E}_t & R < a \end{cases} \tag{A.5}$$

$\vec{E}_s$ = scattered field
$\vec{E}_t$ = transmitted field (inside sphere).

The incident field can be expressed in spherical coordinates as;

$$\vec{E}_i = \hat{i}_x E_0 e^{j(wt - kz)}$$

$$= E_0 e^{jwt} \sum_{n=1}^{\infty} (-j)^n \frac{2n+1}{n(n+1)} (\underline{m}_{0_n} + j\underline{n}_{e_n}) \tag{A.6}$$

In the far field ($k_2R >> 1$) with $1/R^2$ terms neglected;

$$\underline{m}_{0_n} = -\hat{i}_\theta \frac{1}{\sin\theta} j_n(kR)P_n(\cos\theta)\sin\phi$$

$$-\hat{i}_\phi j_n(kR)\frac{dP_n(\cos\theta)}{d\theta}\cos\phi \tag{A.7}$$

$$\underline{n}_{e_n} = \hat{i}_\theta \frac{[kRj_n(kR)]'}{kR}\frac{dP_n(\cos\theta)}{d\theta}\cos\phi$$

$$-\hat{i}_\phi \frac{1}{\sin\theta}\frac{[kRj_n(kR)]'}{kR}P_n(\cos\theta)\sin\phi \tag{A.8}$$

where $k = k_2$

$\hat{i}_\theta \hat{i}_\phi$ are unit vectors

$[f(x)]'$ denotes derivative w.r.t. x.

The scattered field is of the same form,

$$\vec{E}_s = E_0 e^{jwt} \sum (-j)^n \frac{2n+1}{n(n+1)} \left(a_n^s \underline{m}_{0n}^{(2)} + jb_n^s \underline{n}_{en}^{(2)}\right) \quad (A.9)$$

$\underline{m}_{0n}^{(2)}$ and $\underline{n}_{en}^{(2)}$ are computed from the expressions for $\underline{m}_{0n}$ and $\underline{n}_{en}$ using $h_n^{(2)}$ in place of j_n, while the coefficients a_n^s and b_n^s are computed from boundary conditions. It is apparent from the expression for $\vec{E}_s$ along with the far field approximation for $h_n^{(2)}(kR)$ that the scattered field is in the form of propagating spherical waves.

A.1.3 Description of Received Field

For a plane wave $\vec{E}_i$ incident on a spherical particle, the resultant field observed at some distance from the scatterer can be expressed as (Ref. [A2])

$$\vec{e} = \vec{E}_i + \vec{S}(n,a,\theta)\vec{E}_i \left[\frac{e^{-jkR}}{jkR}\right] \tag{A.10}$$

where $k = \frac{2\pi}{\lambda_0}$

R = distance to observer

$\vec{S}$ = scattering matrix

a = particle radius

θ = scattering angle

n = refractive index.

The two by two scattering matrix $\vec{S}$ gives a description of the scattered field at angle θ, for each polarization component (in the plane of scattering and orthogonal (see Fig. A.1)). For particles large in terms of a wavelength the components of $\vec{S}$ are computed from a Mie series (i.e., Eq. (A.9) with boundary conditions). When $\frac{2\pi a}{\lambda}$ is much less than unity, Rayleigh scattering prevails and there is no scattering angle dependence. If a single scattering model is valid, the total received signal can be computed from a summation over all particles. If $\vec{e}_\ell$ is the field contribution from particle ℓ, the total field is

$$\vec{E}_R = \vec{E}_i + \sum_\ell \vec{S}_\ell(n,a,\theta)\vec{E}_i \frac{e^{-jkR_\ell}}{jkR_\ell} \tag{A.11}$$

(See Fig. A.2).

The entries in the summation of Eq. (A.11) can be rearranged into two groups, i.e., those within the first Fresnel zone and those outside of this zone.

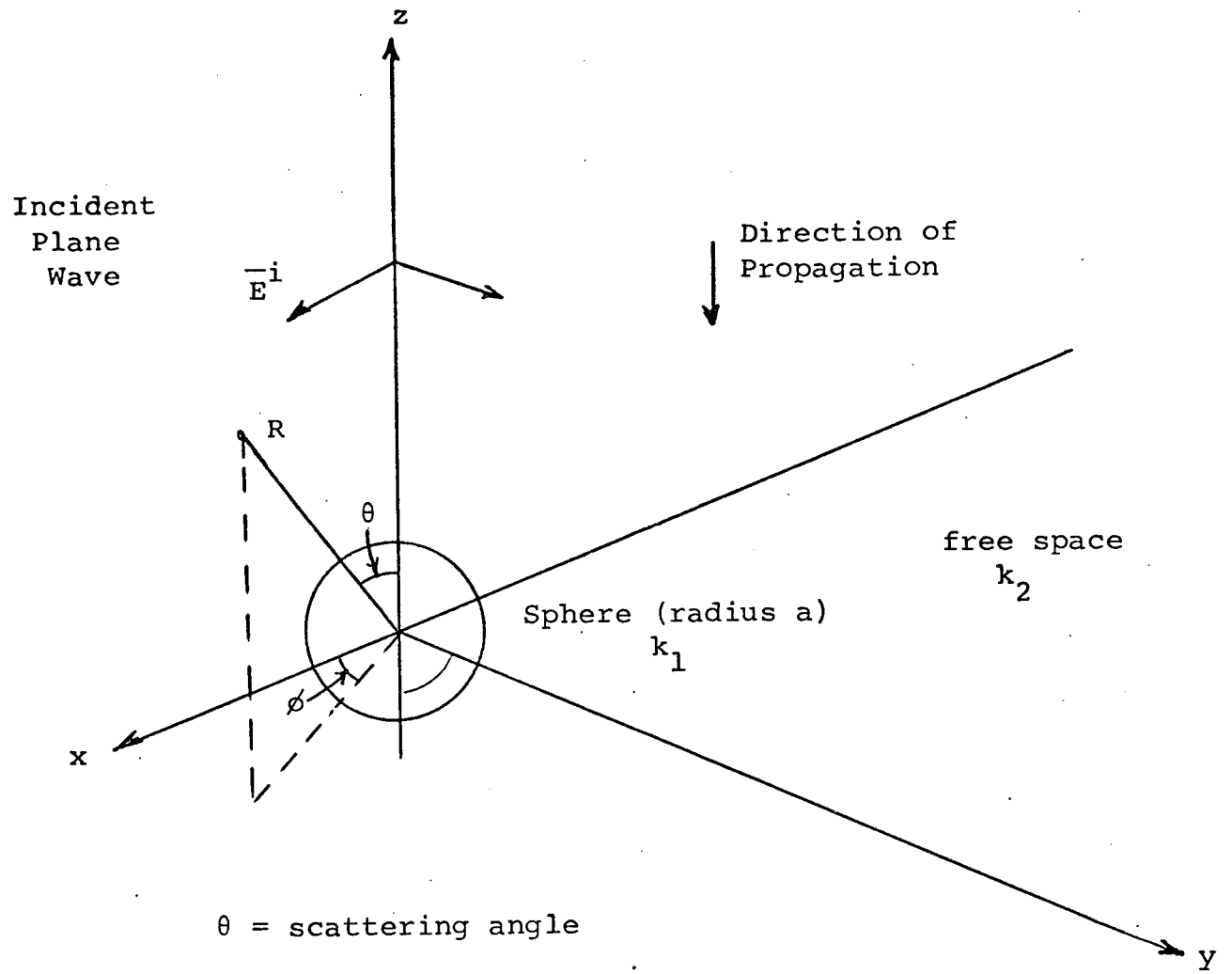

Fig. A.1 Coordinate System for Scattering from a Sphere

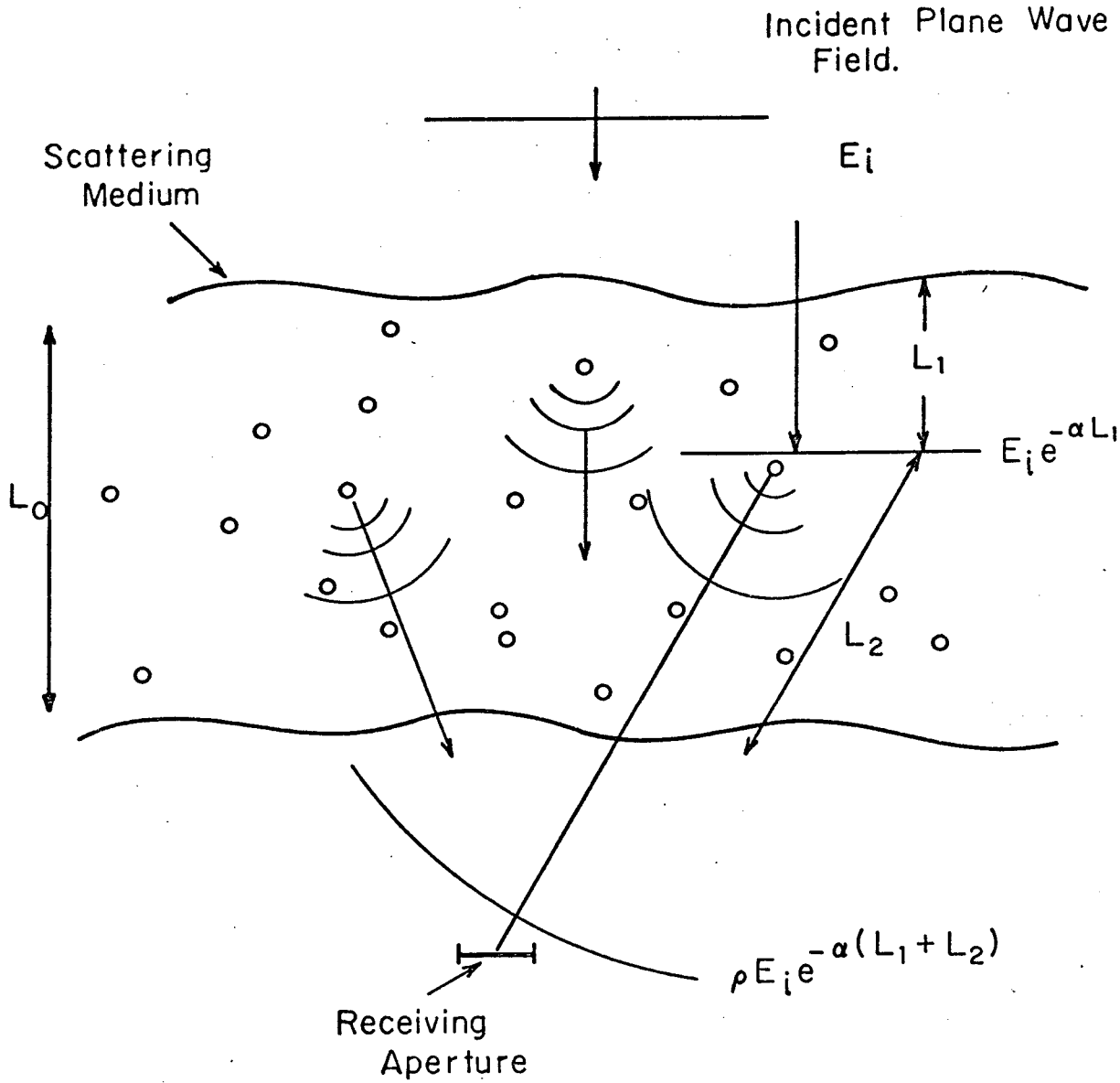

Received Field $\vec{E}_R = \vec{E}_i e^{-\alpha L_0} + \sum_{\ell} \vec{e}_\ell$

Fig. A.2 Single Scattering Model for Rain.

Thus

$$\vec{E}_R \simeq \vec{E}_i + \sum_m^M \frac{\vec{S}_m(n,a,\theta)\vec{E}_i}{jkR_m} + \sum_\ell \vec{S}_\ell(n,a,\theta)\frac{\vec{E}_i e^{-jkR_\ell}}{jkR_\ell}$$

$$= \left[1 + \sum_m^M \frac{\vec{S}_m}{jkR_m}\right]\vec{E}_i + \sum_\ell \vec{S}_\ell \frac{\vec{E}_i e^{-jkR_\ell}}{jkR_\ell} \qquad \text{(A.12)}$$

(coherent term) (incoherent term)

where the gross approximation has been made that all scatterers within the first Fresnel zone radiate coherently. Thus the first term above represents coherent radiation while the second corresponds to incoherent terms. The individual terms must of course be weighted by the antenna response (to plane waves) when computing the terminal voltage, e.g., for a linearly polarized antenna the voltage is;

$$V_R = G_R\{E_c + \sum_\ell g_R(\alpha)\frac{S_\ell(\theta)E_i e^{-jkR_\ell}}{jkR_\ell}\} \qquad \text{(A.13)}$$

where E_c is the coherent component,

$$\vec{E}_c = [1 + \sum_m^M \frac{\vec{S}_m}{jkR_m}]\vec{E}_i \qquad \text{(A.14)}$$

and $g_R(\alpha)$ is the receiving antenna response to a plane wave such that

$$g_R(0) = G_R \qquad \text{(A.15)}$$

Energy is removed from the incident wave by both absorption and scattering. These two components are accounted for in Eq.(A.14) by recognizing that the refractive index n is complex.

Consider first the nature of the coherent signal, i.e., contributions from within the first Fresnel zone. The summation over m in Eq.(A.16) represents a complex constant which modifies both the phase and magnitude of the original incident field $\vec{E}_i$. This results in:

(a) An effective attenuation due to the intervening scattering medium (loss of energy from absorption and scattering).

(b) A phase shift.

The discrete distribution of scatterers which contributes to the coherent signal can thus be replaced with a uniform lossy medium having an equivalent refractive index;

$$n_e = n_{er} + jn_{ei} \tag{A.16}$$

where n_{ei} accounts for the losses introduced (see Fig. A.3).

At first sight it might appear that the phase and amplitude of the coherent component fluctuate with the variation in number of scattering particles present. This is in fact true, but the effect is not very significant as is shown in Section B.2.4. This topic is postponed temporarily because conclusive arguments require estimates of rain drop densities and these are contained in Appendix B. For most purposes we can safely assume the coherent signal equivalent refractive index to be time invariant.

Outside of the Fresnel zone the scattered contributions to the received field tend to be incoherent, i.e., the parameter R_ℓ modulo λ is uniformly distributed over λ. That is to

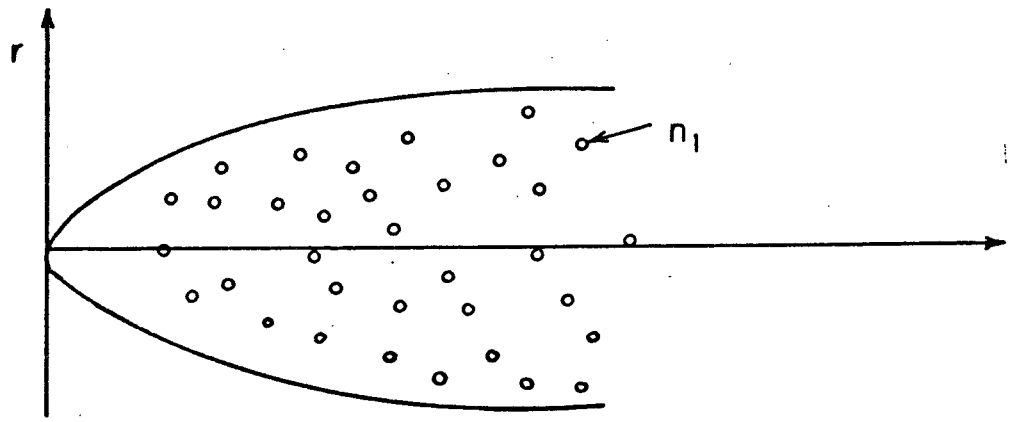

(a) Original Medium

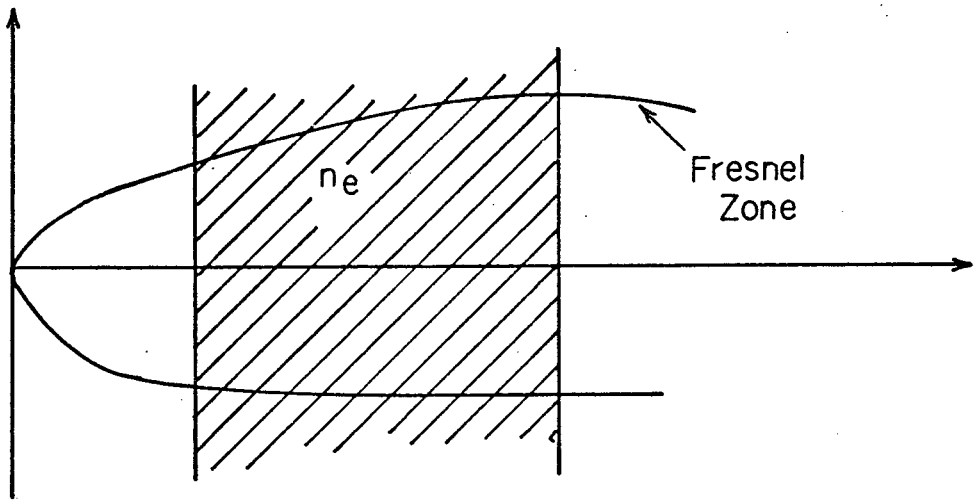

(b) Equivalent Medium

Fig. A.3 Equivalent Propagation Medium for Rain

say,

$$R_\ell = N\lambda + v \tag{A.17}$$

where v is uniformly distributed on the interval $[0,\lambda]$, and λ is the wavelength. Because the particles are in constant motion, the relative phase introduced by each is constantly changing and variable over 2π radians. Consequently the superposition of these incoherent components gives rise to a signal with deep fading characteristics and average power determined by the sum of the individual scattered power levels. The fading rate is determined by the velocity of the particles and the geometry in question, while the increased path length from transmitter to receiver via a scatterer gives rise to the multipath phenomenon.

To determine the relative importance of the incoherent and coherent fields one must examine the specific system geometry in question. It is easily seen that the coherent contribution is derived from an integration over the first Fresnel zone, while the incoherent component is found by integrating over the remaining volume within the antenna beam. For millimeter wavelength antennae the Fresnel zone can be comparable to the 3 dB beamwidth. The current trends indicate future emphasis on higher frequency bands and larger diameter antenna structures, so that the effect being discussed will tend to become more pronounced. A more detailed analysis of the statistical properties to be encountered is deferred until the next section which does not use the rather simplistic approach of dividing the scattering region into coherent and incoherent zones.

A.1.4 Statistical Properties of the Rain Scattering Transfer Function

The lowpass complex field response to a sinusoid of frequency f is given in one form by Eq.(A.11). (The carrier component $e^{j2\pi ft}$ has been suppressed in this formulation.) i.e.,

$$\vec{E}_R = \vec{E}_i + \sum_{\ell} \vec{S}_\ell(n,a,\varphi)\ \vec{E}_i\ \frac{e^{-j\frac{2\pi f}{c}\cdot R_\ell}}{(j\frac{2\pi f}{c})\ R_\ell} \qquad (A.18)$$

Including the antenna gain pattern $g(\alpha)$ and neglecting depolarization effects, the complex received voltage can be expressed in terms of the transmitter terminal voltage as

$$V_R = G'_R\ V_T \left\{1 + \sum_{\ell} g_R(\alpha_\ell)\ S_\ell(n,a,\varphi_\ell)\ \frac{e^{-j\frac{2\pi f R_\ell}{c}}}{(j\frac{2\pi f}{c})R_\ell}\right\} \qquad (A.19)$$

where the constant G_R includes all required proportionality constants. The subscript ℓ denotes the ℓ'th scattering particle with α_ℓ equal to the angle subtended by the scatterer with the transmitter-receiver path. (i.e., $\varphi = 180 - \alpha$). Note that the quantity S_ℓ will implicitly be a function of frequency because of the diameter/wavelength change in particles as a function of frequency. This aspect will really only be of great significance when the particle diameters are a significant portion of a wavelength. In this section we suppress the implied frequency dependence.

The equivalent transfer function can be written in an alternative integral form;

$$H(f) = G_R\left\{1 + \int g_R(\alpha)\ n(\vec{r},\alpha)\ \frac{e^{-j\frac{2\pi f}{c}}}{(\frac{2\pi f}{c}R)}\ d\vec{r}\ \right\} \qquad (A.20)$$

where

H = transfer function

$\vec{r}$ = position vector

R = Distance receiver to scatterer

ΔR = Distance from transmitter to receiver minus the line of sight path length

n = impulsive distribution function

G_R now includes the linear phase term corresponding to line of sight propagation. As a first approximation we assume $n(\vec{r},\alpha)$ is a function of space only, i.e., the particle scattering pattern is broad compared with the antenna beamwidth. The distribution function is random in nature since it corresponds to the instantaneous distribution of scattering particles. It has mean and covariance properties expressible as

$$E\{n(\vec{r})\} = \bar{n} \tag{A.21}$$

and

$$E\{(n(\vec{r}_1) - \bar{n})\ (n(\vec{r}_2) - \bar{n})\} = \sigma_0\ \delta(\vec{r}_1 - \vec{r}_2) \tag{A.22}$$

Time variation of V_R and n can be included but this is not necessary to illustrate the principles being discussed. In addition we note that $n(\vec{r})$ and $g(\alpha)$ are approximately real, so that the in-phase and quadrature components of $H(f)$ are found to be

$$\begin{aligned} X(f) &= \mathrm{Re}\{H(f)\} \\ &= G_R\left\{1 + \int g_R(\alpha)\ \frac{n(\vec{r})\ \cos(2\pi f \Delta R/c)}{\frac{2\pi f}{c} R}\ d\vec{r}\right\} \end{aligned} \tag{A.23}$$

with

$$\bar{X}(f) = E\{X(f)\}$$

$$= G_R\left\{1 + \bar{n}c \int g_R(\alpha) \frac{\cos(2\pi f\Delta R/c)}{2\pi fR} d\vec{r}\right\}$$

Similarly,

$$Y(f) = E\{Y(f)\}$$

$$= G_R\left\{ 1 + \int g_R(\alpha) \frac{n(\vec{r}) \sin(2\pi f\Delta R/c)}{2\pi fR/c} d\vec{r}\right\}$$

$$\bar{Y}(f) = G_R\left\{1 + \bar{n}c \int g_R(\alpha) \frac{\sin(2\pi f\Delta R/c)}{2\pi fR} d\vec{r}\right\}$$

If we define

$$\Delta n(\vec{r}) = n(\vec{r}) - \bar{n}$$

the I and Q components $x(f,t)$ and $y(f,t)$ defined in Section 2.3.1 can be written for a given instant of time as,

$$x(f,t) = G_R \int g_R(\alpha)\, \Delta n(\vec{r}) \frac{\cos(2\pi f\Delta R/c)}{2\pi fR/c} d\vec{r} \qquad (A.24)$$

$$y(f,t) = G_R \int g_R(\alpha)\, \Delta n(\vec{r}) \frac{\sin(2\pi f\Delta R/c)}{2\pi fR/c} d\vec{r}$$

The complete time and frequency covariance functions for x and y are difficult to evaluate because of the need for time-frequency correlation properties of $\Delta n(\vec{r})$ and these are generally not known. However, the frequency correlation functions can be established

Let

$$x(f_1) = x(f_1,t)$$

$$y(f_2) = y(f_2,t)$$

Then

$$R_x(f_1,f_2) = E\{x(f_1)\ x(f_2)\} \tag{A.25}$$

$$R_{xy}(f_1,f_2) = E\{x(f_1)\ y(f_2)\} \tag{A.26}$$

$$R_y(f_1,f_2) = E\{y(f_1)\ y(f_2)\} \tag{A.27}$$

These functions can be evaluated from (A.24) using (A.22)

$$R_x(f_1,f_2) = G_R \int g_R^2(\alpha)\ \sigma_o \left[\frac{\cos 2\pi f_1 \Delta R/c}{2\pi f_1 R/c}\right]\left[\frac{\cos 2\pi f_2 \Delta R/c}{2\pi f_2 R/c}\right] d\vec{r} \tag{A.28}$$

$$R_{xy}(f_1,f_2) = G_R \int g_R^2(\alpha)\ \sigma_o \left[\frac{\sin 2\pi f_1 \Delta R/c}{2\pi f_1 R/c}\right]\left[\frac{\cos 2\pi f_2 \Delta R/c}{2\pi f_2 R/c}\right] d\vec{r} \tag{A.29}$$

$$R_y(f_1,f_2) = G_R \int g_R^2(\alpha)\ \sigma_o \left[\frac{\sin 2\pi f_1 \Delta R/c}{2\pi f_1 R/c}\right]\left[\frac{\sin 2\pi f_2 \Delta R/c}{2\pi f_2 R/c}\right] d\vec{r} \tag{A.30}$$

Clearly these functions involve arguments such as $(f_1 + f_2)$ and so are non-stationary in frequency. However the sum frequency components will be rapidly oscillating with respect to ΔR and may not be important. To further illustrate the behavior of the functions involved, consider a one-dimensional version of the problem, i.e., using the Fresnel approximation let

$$\Delta R \approx \frac{x^2}{2Z} \tag{A.31}$$

(See Fig. A.4 for notation) Note also that variations in R are relatively slow compared with other terms under the integrals. The covariance functions therefore involve integrals approximately of the form:

$$R_x(f_1,f_2) = A_1 \int g_R(\frac{x}{Z_o}) \cos(\pi f_1 x^2/c) \cos(\pi f_2 x^2/c)\, dx \tag{A.32}$$

In particular we find that

$$R_x(f_1,f) = A_1 \int g_R(\frac{x}{Z_o}) \cos^2(\pi f n^2/c)\, dx \tag{A.33}$$

$$R_{xy}(f,f) = A_2 \int g_R(\frac{x}{Z_o}) \sin(\pi f_1 x^2/c) \cos(\pi f_2 x^3/c)\, dx$$

$$R_y(f,f) = A_3 \int g_R(\frac{x}{Z_o}) \sin^2(\pi f_1 x^2/c)\, dx$$

The functions $\sin kx^2$ and $\cos kx^2$ are sketched in Fig. A.5 . Clearly if g_R is narrow compared with the first Fresnel zone we have

$$R_x(f,f) \neq R_y(f,f)$$

and

$$R_{xy}(f,f) \neq 0 \tag{A.34}$$

This result is important in the discussion at the end of Section 2.

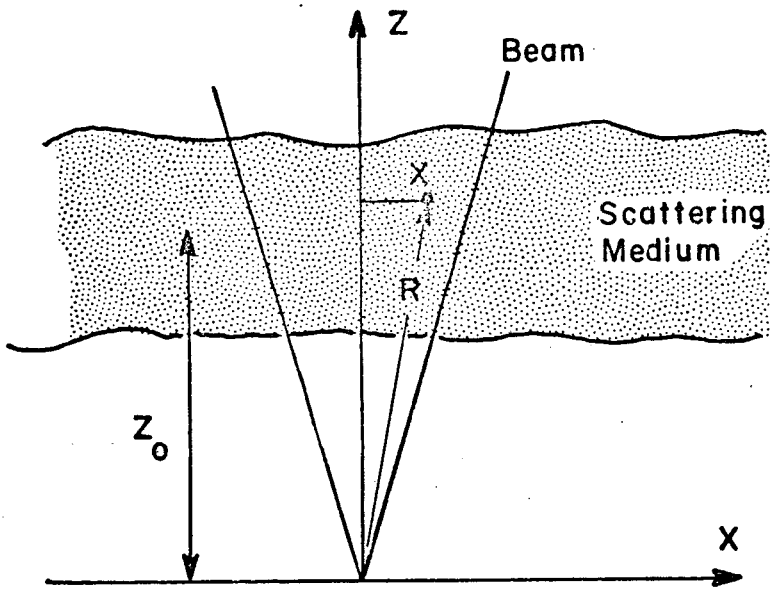

Fig. A.4. One-dimensional Scattering Model

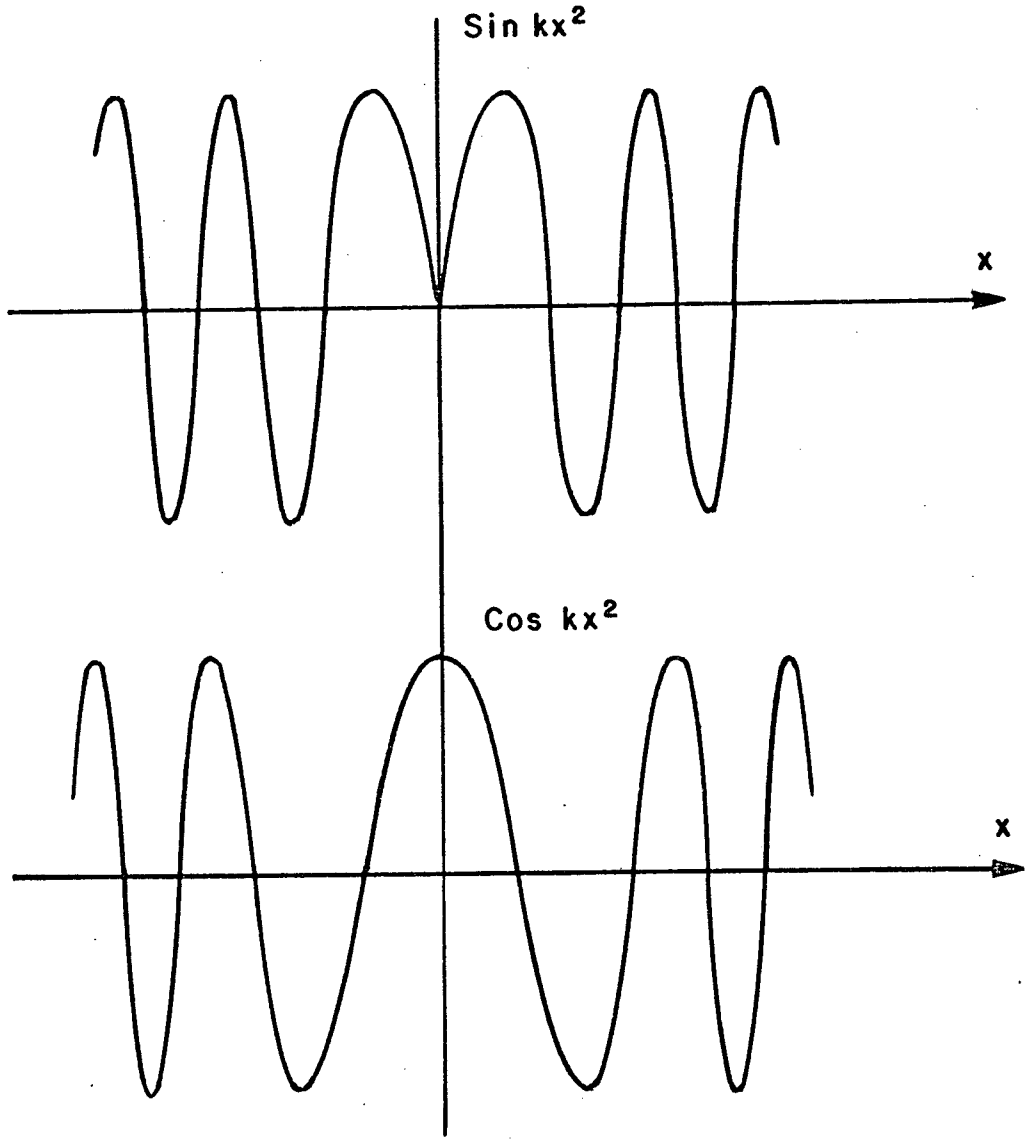

Fig. A. 5. Integral Weighting Functions

REFERENCES

[A1] Stratton, Electromagnetic Theory, pp 564-573.

[A2] Van der Hulst, H.C., Light Scattering by Small Particles, Wiley, N.Y. 1957, P32.

[A3] Feller W., An Introduction to Probability Theory and Its Applications, Vol. I, Wiley, N.Y., 1957, P228.

[A4] Mondre, E., Correlation Analysis and Scintillation for 15 GHz Line of Sight Propagation Channels, NASA Tech. Note, NASA TN D-5613, P5.

[A5] Middleton, Introduction to Statistical Communication Theory, McGraw Hill, 1960, P418.

Appendix B
PREDICTION OF CHANNEL CHARACTERISTICS

B.1 Introduction

The transmission medium between satellite and receiver will be subject to marked variations with changing weather conditions. Rather than distinguishing between different climatic conditions and their associated probability of occurrence, we shall simply choose examples which might intuitively be construed as worst case situations. Since the communication error rate will be strongly influenced by these abnormal low probability events anyway, they will be the most interesting as far as channel characteristics are concerned, i.e., the basic system design will include a suitable margin for fading effects. Below this fading level the error rate will be very high, while above it the error rate will be perhaps several orders of magnitude smaller.

The two effects to be considered are rain scattering and atmospheric turbulence. The former will be the real culprit in terms of worst case system performance but the latter is included because it will be the dominant scattering mechanism most of the time. Where appropriate some attention will also be given to ionospheric effects and scattering from cloud particles.

B.2 Scattering From Rain

As discussed in Appendix A the response to a transmitted sinusoid can be decomposed into the sum of a time varying

C2

coherent component and an incoherent component. Alternatively we can think of the received signal as the sum of a time invariant specular component plus a random contribution.

The following assumptions and approximations will be used in the analysis.

(a) A single scattering model is sufficiently accurate.

(b) Both the incident and first order scattered component fields will suffer from attenuation due to absorption and further scattering.

If the intensity of the incident wave is I_i, and the distance propagated through the scattering medium is Z (see Fig. B.1), then from Ref. [B-1],

$$I_{SPEC}(Z) = I_i e^{-\gamma Z} \tag{B.1}$$

where I_{SPEC} = intensity of "specular" component (mean coherent field)

γ = extinction constant

Note that

$$\gamma = \gamma_{ab} + \gamma_s \tag{B.2}$$

where γ_{ab} accounts for energy losses due to absorption, while γ_s indicates scattering losses. It can be computed by averaging the scattering cross section $\sigma(\theta)$ over a sphere enclosing the scatterer. $\sigma(\theta)$, which describes the power scattered in direction θ per unit solid angle for a unit volume of scatterers, is itself derived from the scattering matrix $S(n,a,\theta)$

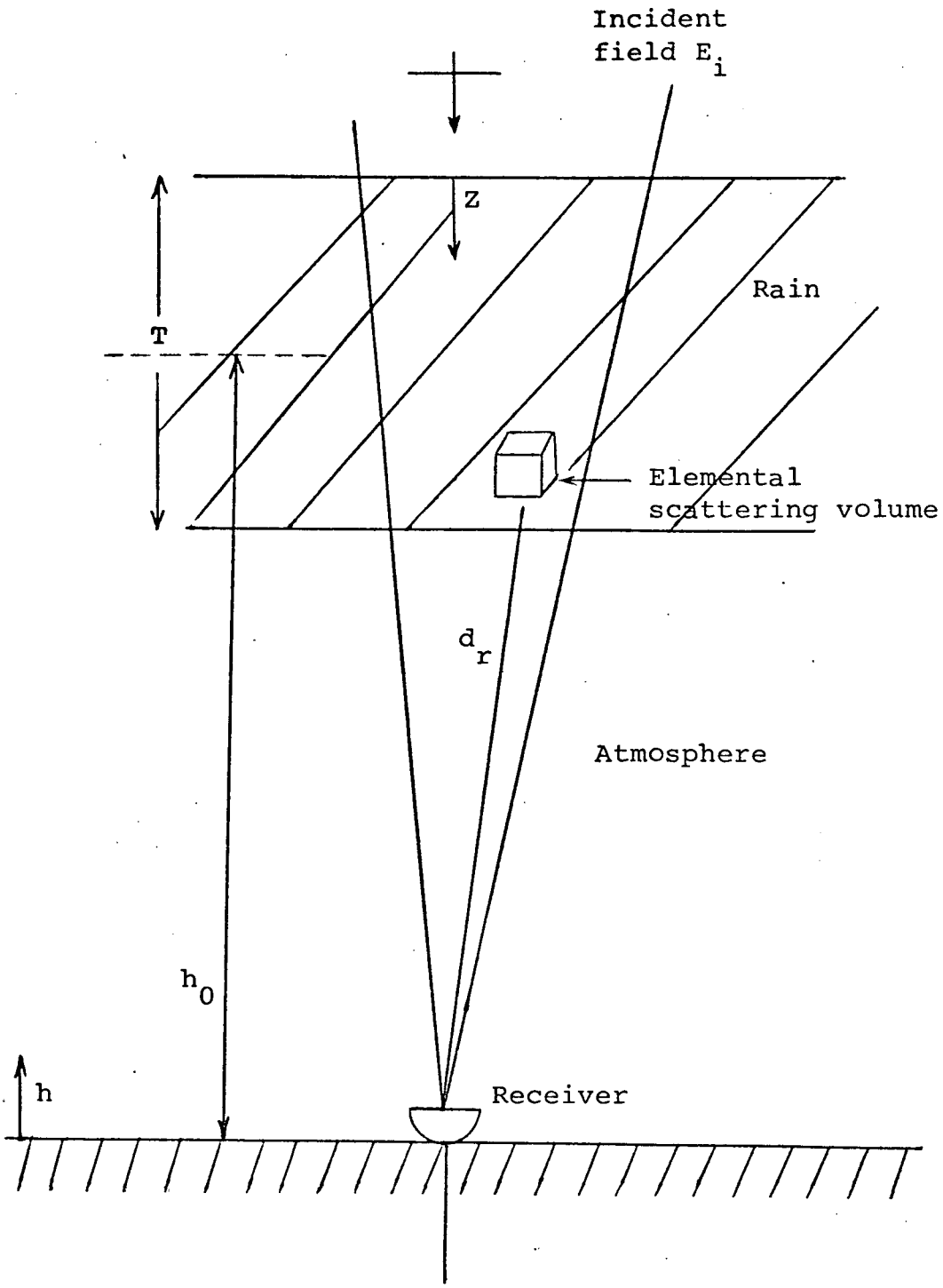

Fig. B.1 Rain Scattering Geometry

(Ref. [B-1]). An averaging over the drop size distribution is also required. Thus for a total rain layer thickness of T we have an emerging field intensity,

$$I_{SPEC} = I_i e^{-\gamma T}$$

Neglecting further free space attenuation due to spherical wave propagation, this will be the strength of the specular signal at the receiving aperture. The received power from the unscattered component is therefore;

$$P_{SPEC} \simeq A_e I_i e^{-\gamma T} \qquad A_e = \text{equivalent antenna area}$$

$$= \left(\frac{G_{or}\lambda^2}{4\pi}\right) I_i e^{-\gamma T} \tag{B.3}$$

Consider now the scattered component of the field. At any point in the scattering medium, the intensity of the field incident on a particle is roughly,

$$I_i' = I_i e^{-\gamma z}$$

The power scattered from a particle then undergoes further attenuation as it crosses the medium to the receiver, due to both absorption and secondary scattering. Assuming none of these losses are regained through multiple scattering, the wave from the particle reaches the receiver with an intensity which is reduced by a factor;

$$e^{-\gamma(T-z)}$$

Thus for a unit volume of scatterers d_r meters from the receiver, the flux density at the antenna aperture is,

$$\left[\frac{I_i e^{-\gamma z}\sigma(\theta)}{4\pi d_r^2}\right] e^{-\gamma(T-z)} \qquad \text{(B.4)}$$

Hence the total average scattered power is obtained by integrating over the antenna power gain pattern G_r, i.e.,

$$G_r(\theta) = g_r(\theta)G_{or} \qquad \text{with} \qquad g_r(0) = 1$$

Then,

$$P_{SCAT} = \int_{vol} \left[\frac{I_i e^{-\gamma T}\sigma(\theta)}{4\pi d_r^2}\right]\left(\frac{\lambda^2 G_{or}}{4\pi}\right) g_r(\theta)\, du \qquad \text{(B.5)}$$

Power density

Antenna equiv. area

Note that this integral form could not be used if strong multiple scattering was in evidence. Strictly speaking the integration volume only covers the region outside the first few Fresnel zones, but generally we shall over-estimate the scattered power levels by using the complete beam intersection with the rain volume.

B.2.1 Scattered/Specular Power Ratio

Let us assume that we wish to find,

(i) The specular component power level P_{SPEC}

(ii) The ratio of scattered to unscattered power $\eta = P_{SCAT}/P_{SPEC}$.

Consider (ii) first using Eqs. (B.3) and (B.5).

$$\eta = P_{SCAT}/P_{SPEC}$$

$$= \int_{vol} \frac{\sigma g_r(\theta)}{4\pi d_r^2} \, du \qquad (B.6)$$

Here it has been assumed that σ is approximately independent of θ. Also

$$d_r \simeq (h_0 + \frac{T}{2} - z) \qquad (B.7)$$

for narrow beamwidths. The integration volume is determined primarily by the layer dimensions and the function $g_r(\theta)$. As a first approximation let the integration volume be cylindrical with diameter determined by the beam thickness at the center of the layer.

Thus

$$\int g(\theta) \, du \simeq \frac{T\pi(\epsilon_r h_0)^2}{4} \qquad (B.8)$$

where ϵ_r is the 3 dB beamwidth.

$$\eta \simeq \frac{\sigma T \epsilon_r^2}{16} \qquad \text{(B.9)}$$

But

$$\sigma = \frac{\pi^5}{\lambda^4} |K|^2 Z$$

$$\simeq \frac{\pi^5}{\lambda^4} Z \qquad \text{(Ref. [B-2])}$$

Hence

$$\eta = \frac{\epsilon_r^2 \pi^5 T Z}{16 \lambda^4} \qquad \text{(B.10)}$$

For example consider the ATS-F experiment with the following parameters,

$$\epsilon_r = 4 \times 10^{-3} \text{ rad.} \qquad (0.23^\circ \text{ BW})$$

$$T = 4 \times 10^3 \text{ meters}$$

$$Z = 46 \times 10^{-14} \text{ m}^6/\text{m}^3 \qquad (46 \times 10^4 \text{ mm}^6/\text{m}^3)$$

This choice of Z corresponds to a 6"/hr. rainfall rate (see [B-3]) when the average drop size distribution is assumed to be that used by Laws and Parsons. The accompanying attenuation [B-3] at 20 GHz is 10 dB/Km and about 20 dB/Km at 30 GHz. Then the ratio η computed using Eq.(B.10) is,

$$\eta = \frac{1.84\ \pi^5 10^{-15}}{\lambda^4} \qquad (\lambda \text{ in meters})$$

Thus for f = 30 GHz,

$$\eta = 5.8 \times 10^{-5}$$
$$= -42 \text{ dB}$$

This ratio is of course smaller for lower rainfall rates (smaller Z) or lower frequency.

The total attenuation effect on the specular signal as itemized in (i), can readily be obtained from theoretical and experimental evidence relating attenuation to the parameter Z or rainfall rate [B-3, B-4]. Note that rainfall rates which give rise to more than 10 dB total attenuation through the atmosphere can be expected to occur less than 0.1% of the time at frequencies of 30 GHz. The example computed involves a 4 Km thickness for the rain layer and a total of 40 dB attenuation, thus indicating that we are indeed dealing with an extreme case.

We conclude this subsection by noting two assumptions that could possibly be violated.

(a) When a Rayleigh scattering cross section is not appropriate (i.e., $\frac{2\pi a}{\lambda} > .1$) the equivalent Z may be significantly larger for a given drop size distribution and rainfall rate due to strong forward scattering. This would be important at higher frequencies such as 90 GHz.

(b) Multiple scattering may occur at the high frequency bands which would change the scattered power level slightly.

(c) Experimental results for line of sight terrestrial links often involve larger beamwidths and larger paths which could conceivably give rise to a significant scattered signal.

We now consider the signal dispersion effects which result from multipath scatter propagation.

B.2.2 Multipath Spread Due to Rain Scattering

Consider now the dispersion in arrival time of a short transmitted pulse due to the variety of different scattering paths constituent in the total scattered signal. When single scattering predominates the delay introduced by each scatterer can be computed from its spatial coordinates. Here we capitalize on the symmetry of the antenna beams and use r to denote distance from the transmitter-receiver center line, and h to denote height above the earth.

The delay introduced into an individual scattering path relative to line of sight can be expressed as,

$$\xi(r,h) = (D_1 + D_2)/c - \tau_0 \qquad \text{(B.11)}$$

where D_1 = distance to transmitter
D_2 = distance to receiver
τ_0 = line of sight transit time

Thus

$$\xi = [D_1 + (h^2 + r^2)^{1/2}]/c - \tau_0$$

$$\simeq \frac{r^2}{2hc} \qquad \text{(B.12)}$$

Since

$$(h^2 + r^2)^{1/2} \simeq h + \frac{r^2}{2h}$$

The scattering elements have a broad scattering pattern so that the maximum delay experienced will be primarily determined by the receiving antenna beamwidth rather than the elements themselves.

The following calculation is for the value of ξ computed at the 3 dB antenna beamwidth, and will correspond roughly to the 1/2 power value of the delay power spectrum, which specifies average power as a function of delay.

Let

$$\theta_{1/2} \simeq \frac{2r}{n}$$

$$= .23^{o} \qquad \text{(3 dB beamwidth at 20 GHz)}$$

and

$$h = 10 \text{ Km.}$$

Then

$$\xi_{1/2} = \frac{h\theta_{1/2}^2}{8c}$$

$$= 0.061 \times 10^{-9} \text{ sec.} \qquad \text{(B.13)}$$

Because the scattering medium is limited to the lower portion of the atmosphere, we would not expect h to exceed 10 Km, so that the above figure represents a bound on the expected multipath, at least for a homogeneous medium-single scatterer model. Substantial increases in multipath spread would occur for a propagation path at low elevation angles (hence allowing a larger value of h), or for multiple scattering situations.

B.2.3 Doppler Spread Due to Rain Scattering

The constant and random movement of the scatterers gives rise to a spectral broadening of any transmitted signal. Expressions for the Doppler shift in frequency due to motion of a single particle give a rough indication of the degree of spreading involved. Consider a scatterer at position (r,h) moving with velocity $\vec{v}$. Using small angle approximations we can easily derive the following equations for Doppler shift in terms of velocity components either transverse or parallel to the transmitter receiver center line (see for example [B-6]). For the transverse component v_r,

$$f_r \simeq \frac{rv_r}{\lambda_0 h} \qquad \text{(B.14)}$$

But for the parallel component v_h,

$$f_h \simeq \frac{2r^2 v_h}{\lambda_0 h^2} \tag{B.15}$$

Using $\theta = \frac{2r}{h}$ we find that

$$f_r \simeq \frac{v_r \theta}{2\lambda_0}$$

$$f_h \simeq \frac{v_h \theta^2}{2\lambda_0}$$

Since the height of the scatterer is not a parameter (within the range of these approximations), we compute worst case Doppler shifts using only the 3 dB antenna beamwidth. Furthermore we compute the Doppler shift per unit velocity (1 meter/sec) since even typical velocities are difficult to predict. Thus

$$\theta_{1/2} = 3.8 \times 10^{-3} \text{ rad} \qquad (.23^{\circ})$$

$$\lambda_0 = 1.5 \text{ cm} \qquad (20 \text{ GHz})$$

$$f_h/v_r \simeq 1.26 \times 10^{-1} \qquad \text{Hz/meter/sec}$$

$$f_h/v_h \simeq 4.8 \times 10^{-4} \qquad \text{Hz/meter/sec}$$

Vertical velocities of 10 meters/sec or less might be typical, while the RMS horizontal velocity (v_r) due to turbulence will be on the order of several meters/sec. Based on the above

calculations then, we would predict a Doppler spread of about 1 Hz. Because there is a collection of contributing scatterers each with different velocity and different spatial position, we get a continuum of Doppler shifts at any instant.

B.2.4 Coherent Propagation Through Rain

Here we refer to all energy derived from a spatial region encompassing the first few Fresnel zones, and include both scattered and unscattered signals. It is assumed that the individual scattered signals have identical phase, so that phase and amplitude fluctuations of the total signal in time and frequency, are derived from variable instantaneous number and size distributions.

When single scattering is appropriate the equivalent medium refractive index can be represented as in Section A.1.3,

$$n_{eq} = n_R - jn_I$$

To proceed with the evaluation of n_{eq} as a function of frequency one needs to assume forms for drop size and number distributions which adequately describe the range of distributions to be encountered. The actual computation is quite involved and beyond the scope of this study so we will merely rely on the results of other workers in this area. In particular consider the work of Crane [B-7] who evaluated n_{eq} using measured (convective) rainstrom drop size distributions. At $18^{o}C$ in the region of 20 - 30 GHz he found that the refractivity $(n_R - 1)\ 10^6$ was approximately linear,

$$N = (n_R - 1)\ 10^6$$

$$\simeq \begin{cases} 7.0 - 0.3\ (f - 20) & \text{Rain rate 8"/hr.} \\ 1.2 - 0.05\ (f - 20) & \text{Rain rate 2"/hr.} \end{cases}$$

with f in GHz. The effective phase shift experienced at the receiver is computed from,

$$\phi = \frac{f(n_R - 1)\ x}{c} \qquad \text{cycles}$$

where x = thickness of rain layer. For example consider a 5 Km thickness. Then,

$$\phi(f) = 0.016\ fN \qquad \text{cycles}$$

$$= \begin{cases} 0.016f(7.0 - 0.3\ (f - 20)) & \text{8"/hr.} \\ 0.016f(1.2 - 0.05\ (f - 20)) & \text{2"/hr.} \end{cases}$$

again with f in GHz. Several points are evident from these expressions.

(a) At any frequency, fluctuations in instantaneous rain rate from 2"/hr. to 4"/hr. give rise to phase variations of several cycles.

(b) The linear phase shift with frequency gives rise to a time varying group delay. The change in delay in changing from 2"/hr. to 8"/hr. rain rate is approximately 0.1 nsec.

B

(c) The quadratic phase vs. frequency behavior gives rise to distortion effects, i.e., a short pulse transmitted through the medium is spread in time (see Ref. [B-7]).

Similarly one can predict the variation of attenuation with frequency and rain intensity using the imaginary component of the refractive index n_I. With linear approximations to Crane's data (Fig.B.3 Ref. [B-7]) the following rough guidelines can be used;

Attenuation at 20 GHz

$$= \begin{cases} 25 \text{ dB/Km} & \text{at} \quad 8\text{"/hr.} \\ 7 \text{ dB/Km} & \text{at} \quad 2\text{"/hr.} \end{cases}$$

Attenuation gradient at 20 GHz

$$\simeq \begin{cases} 2 \text{ dB/Km/GHz} & \text{at} \quad 8\text{"/hr.} \\ 0.4 \text{ dB/Km/GHz} & \text{at} \quad 2\text{"/hr.} \end{cases}$$

As in the case of quadratic phase versus frequency, the variable attenuation across the band will cause pulse distortion.

Generally speaking the instantaneous fluctuations in n_{eq} will not be as extreme as the 2"/hr. to 8"/hr. examples shown above. Since both n_R and n_I can be shown to bear an approximately linear relationship to the number of contributing raindrops, we can gauge the RMS variation by drop number variations. Assume for example that the number of drops is a

Poisson variable. Then, if M is the average number of drops which gives rise to a particular average rainfall rate, the RMS spread in n_R is proportional to $\sqrt{M}$. However one must be careful to obtain the correct proportionality constant. The instantaneous phase, assuming a linear relationship, is,

$$\phi = \alpha m \qquad m = \text{instantaneous number of drops in volume}$$

Then

$$(\Delta\phi)_{RMS} = \overline{[(\phi - \bar{\phi})^2]}^{1/2}$$

$$= \alpha\overline{[(m - M)^2]}^{1/2}$$

$$= \alpha\sqrt{M}$$

where $\bar{\phi} = \alpha M$

Eliminating α we obtain the expression

$$(\Delta\phi)_{RMS} = \bar{\phi}/\sqrt{M}$$

The average number of raindrops in the volume of interest will be quite large. For example a rain rate of 2"/hr. corresponds to a raindrop density of approximately;

$$\rho \simeq 10^{-4} \text{ drops/cc}$$

At an altitude of 10 Km the $\lambda/4$ Fresnel zone has a diameter of about 15 meters so that for a 5 Km thick layer of rain, the total volume is,

$$V \simeq 5 \times 10^3 \times \pi \times 49 \text{ cu.m.}$$

Thus

$$\begin{aligned} M &= \rho V \\ &\simeq 10^{-4} \times 7.5 \times 10^5 \times 10^6 \\ &\simeq 10^8 \end{aligned}$$

Hence

$$(\Delta\phi)_{RMS} \simeq \bar{\phi} \times 10^{-4}$$

This is a small fraction of a cycle. We can readily conclude that any observable fluctuations in amplitude and phase with time for the coherent component, will be due to inhomogeneity in the medium structure rather than density variations as predicted using a Poisson distributed scatterer model.

B.3 Propagation Through the Atmosphere

The atmosphere gives rise to two distinct propagation phenomena. These are:

(a) Scattering of energy from the refractive index inhomogeneities which result from minute pressure, temperature and humidity fluctuations,

(b) Distortion of the transmitted signal because of the weak frequency dependence of the mean refractive index.

It should be noted that the atmosphere can be modelled as a layer with an exponential decrease in refractive index as a function of height. The refractivity value at ground level is on the order of 300 N units, i.e., the refractive index is,

$$n = 1 + 300 \times 10^{-6}$$

Superimposed on this trend we have random fluctuations which give rise to scattering. The RMS variation is typically several N units.

The next few subsections contain estimates of various parameters of interest, most of which have been obtained directly from the literature on this subject.

B.3.1 Amplitude Scintillation

The amplitude fluctuations of a CW plane wave source after propagation through a turbulent atmosphere, have been computed by several investigators, using the theory presented in [B-9]. For example Lane [B-10] predicts the scintillation fading for a path through the atmosphere at the zenith angle using two different models. The magnitude of the received carrier can be thought of in terms of a fixed mean component A_0 and a random component δA. The parameter usually computed from Tatarski's equations is,

$$\overline{x^2} = \overline{[\log A_1/A_0]^2}$$

$$\approx \overline{(\delta A)^2}/A_0^2 \qquad \text{for } \overline{x^2} << 1$$

where

$$A_1 = A_0 + \delta A \ .$$

Generally attention is centered on the fading level corresponding to an amplitude reduction of $(\delta A)_{RMS}$ which corresponds to the RMS value of X for weak scintillation.

Using the formulae given in Tatarski and two different models for the structure of the stmosphere, Lane [B-10] has computed typical fading levels. At 35 GHz we find

L = fading depth relative to signal without turbulence

$$\approx \begin{cases} \pm 0.9 \text{ dB} & \text{Model 1} \quad \text{(eq.(4)[C-10])} \\ \pm 2.2 \text{ dB} & \text{Model 2} \quad \text{(eq.(5)[C-10])} \end{cases}$$

Experimental results at 10 GHz reported by Crane [B-11] indicate a general confirmation of these figures.

B.3.2 Multipath Spread Due to Turbulence

It was demonstrated in section B.2.2 that the multipath spread for rain can be computed directly from geometrical considerations, using the 3 dB antenna beamwidth to gauge the width of the delay power spectrum. For atmospheric turbulence the situation is somewhat different since the scattered energy received is confined to a cone much narrower than the beamwidth. Hence we would expect a multipath spread considerably less than the value computed in B.2.2.

REFERENCES

[B-1] Van der Hulst, H.C., Light Scattering by Small Particles, Wiley, New York, 1957, pp. 11-13.

[B-2] Kerr, D. E., Propagation of Short Radio Waves, Rad. Lab. Series, McGraw Hill, New York, 1951, Vol. 13.

[B-3] Crane, R. K., "Propagation Phenomena Affecting Satellite Communication Systems Operating in the Centimeter and Millimeter Wavelength Bands," Proc. IEEE, Vol. 59, No. 2, February 1971, pp. 176-184.

[B-4] Altschuler, E. E., et al, "Atmospheric Effects on Propagation at Millimeter Wavelengths," IEEE Spectrum, July 1968, pp. 83-90.

[B-5] Evans, H. W., "Attenuation on Earth-Space Paths at Frequencies up to 30 GHz," ICC 1971 Conference Proceedings, pp. 27-1 to 27-5.

[B-6] Application of Wideband Signals for Propagation Interference Measurement, Final Report, SIGNATRON, Inc., July 1970, p. 4.4.

[B-7] Crane, R. K., "Coherent Pulse Transmission Through Rain," IEEE Trans. AP, Vol. AP-15, No. 2, March 1967, pp. 252-256.

[B-8] Van der Hulst, H.C., Light Scattering by Small Particles, Wiley, New York, 1957.

[B-9] Tatarski, V. I., Wave Propagation in a Turbulent Medium, McGraw-Hill, New York, 1961.

[B-10] Lane, J. A., "Scintillation and Absorption Fading on Line of Sight Links at 35 and 100 GHz," IEE Conf. on Tropospheric Wave Propagation, Pub. No. 48, 1968.

[B-11] Crane, R. K., See [B-3] above.

APPENDIX C

DELAY POWER SPECTRUM ESTIMATES FOR INTERFERING BEAMS

C.1 Delay Power Spectrum Calculations

For a scattering cross section $\sigma(\theta)$, the average received power for any ellipsoidal range shell can be expressed as;

$$Q(\tau)\, d\tau = P_t \int_{V(\tau)} \frac{\eta G_t G_r \sigma(\theta)}{d_1^2 d_2^2} \frac{\lambda^2}{(4\pi)^3}\, dv \qquad (C.1)$$

where $V(\tau)$ = volume corresponding to a delay shall

P_t = transmitter power

σ = scattering cross section/unit volume

η = depolarization and absorption loss

G_t, G_r = antenna gain functions

d_1, d_2 = distance to scatterer from receiver and transmitter, respectively

θ = scatter angle.

Figure C-1 shows some of the parameters involved. The antenna beam patterns can be expressed as the product of their maximum gains, G_{0t} and G_{0r}, with a renormalized pattern function. Assuming axial symmetry around the beam center line the antenna beam patterns can be expressed as a function of the angle subtended with the antenna center line (α), i.e.,

$$G_t(\alpha) = G_{0t} g_t(\alpha) \qquad (C.2)$$

(similarly for G_r, the receiving antenna). For example when g_t is Gaussian shaped;

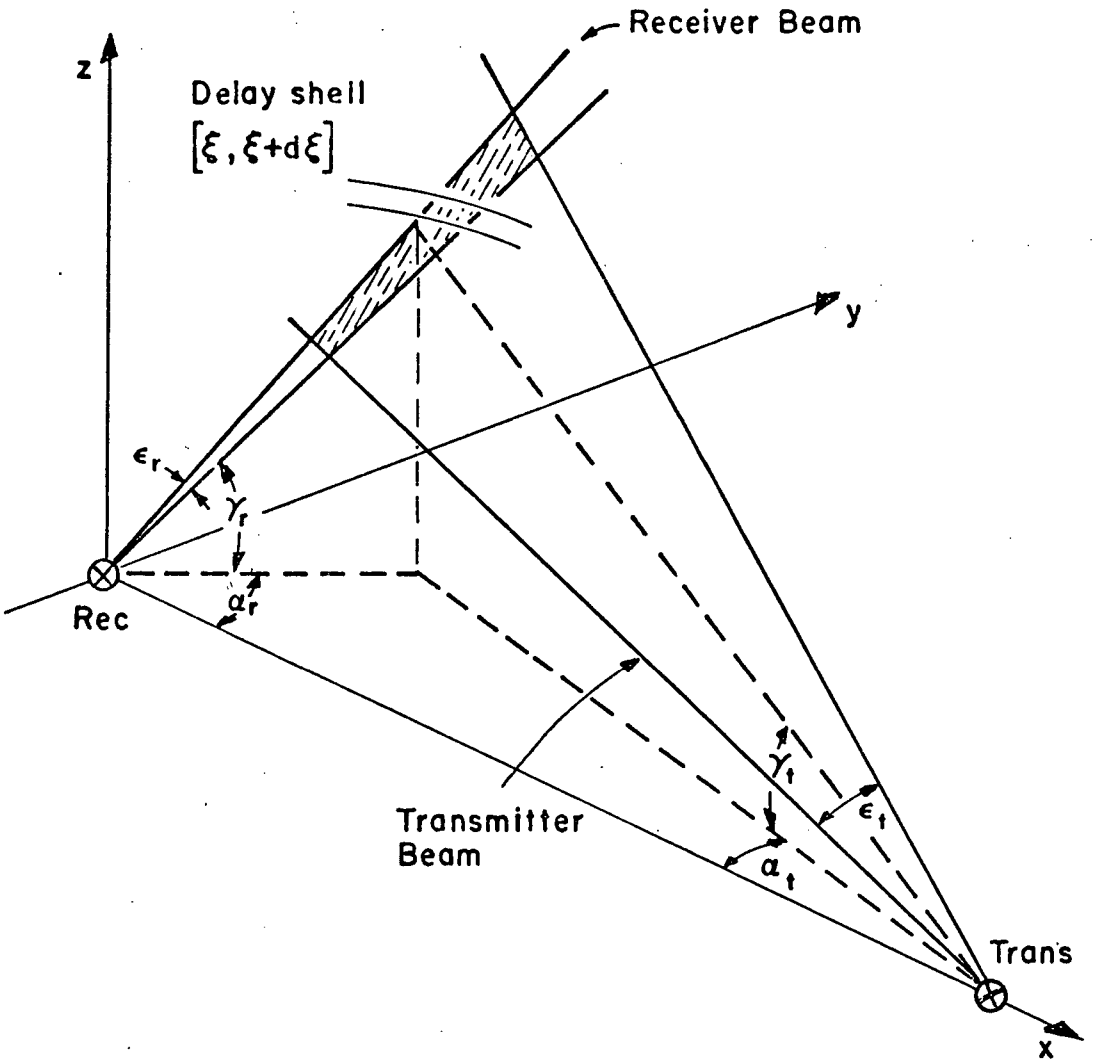

Fig. C.1 Beam Intersection Geometry

$$g_t(\alpha) = e^{-\alpha_t/\sigma_t^2} \tag{C.3}$$

with a 3 dB beamwidth given by

$$\epsilon_t = \sigma_t/0.6 \ . \tag{C.4}$$

Note that in Fig. B1 the receiving and transmitting azimuth and elevation pointing angles are denoted by α_r, γ_r and α_t, γ_t.

C.2 Simplified Integration Procedure

Equation (C-1) is difficult to evaluate unless some simplifications are made. In particular we choose the following approximation (refer to Fig. C-2.) For the volume $V(\varepsilon)$ of interest it will be assumed that the integral Eq. (C-1) is simply the integral of a constant, i.e., the receiver beamwidth is sufficiently narrow so that changes in quantities such as σ, d_1, d_2, and G_t are negligible since the receiver beamwidth is on the order of 0.5°. Hence,

$$Q(\varepsilon)\, d\varepsilon = A_0 \int_{V(\varepsilon)} \frac{\eta G_t G_r \sigma}{d_1^2 d_2^2}\, dv$$

$$\approx A_0 \left[\frac{\eta G_t \sigma}{d_1^2 d_2^2}\right] \int_{V(\varepsilon)} G_r\, dv \tag{C.5}$$

Furthermore the receiving antenna beamwidth is sufficiently narrow so that the volume $V(\varepsilon)$ in question can be approximated by the intersection of parallel planar surfaces at ε and $\varepsilon + d\varepsilon$, with the receiving antenna beam. Initially we shall consider the distribution of power as a function of distance along the receiving antenna center line, i.e., let

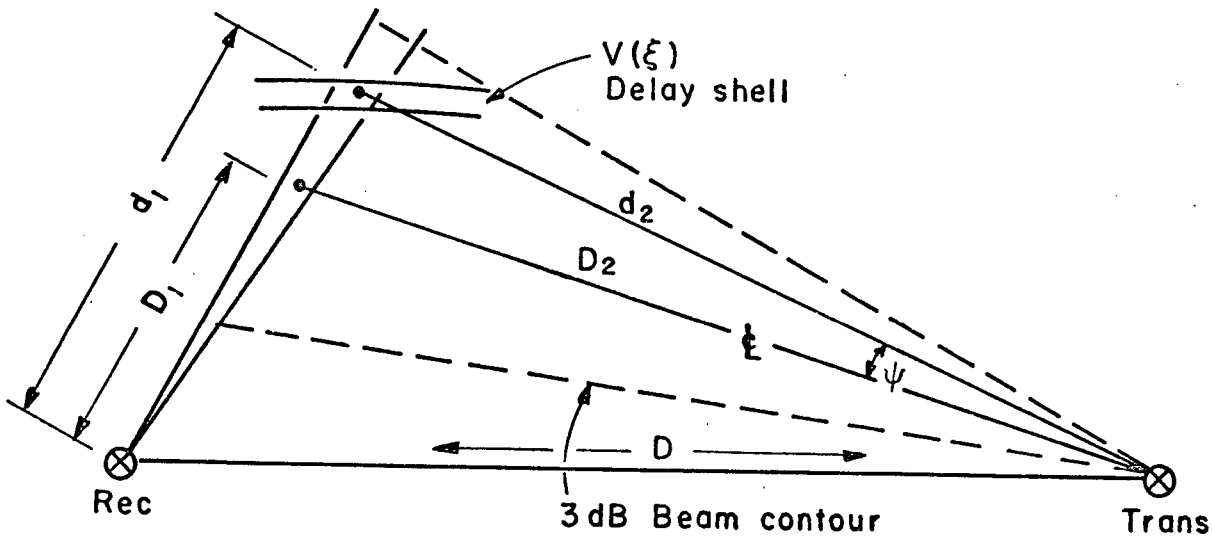

Fig. C.2 Delay Shell Intersection

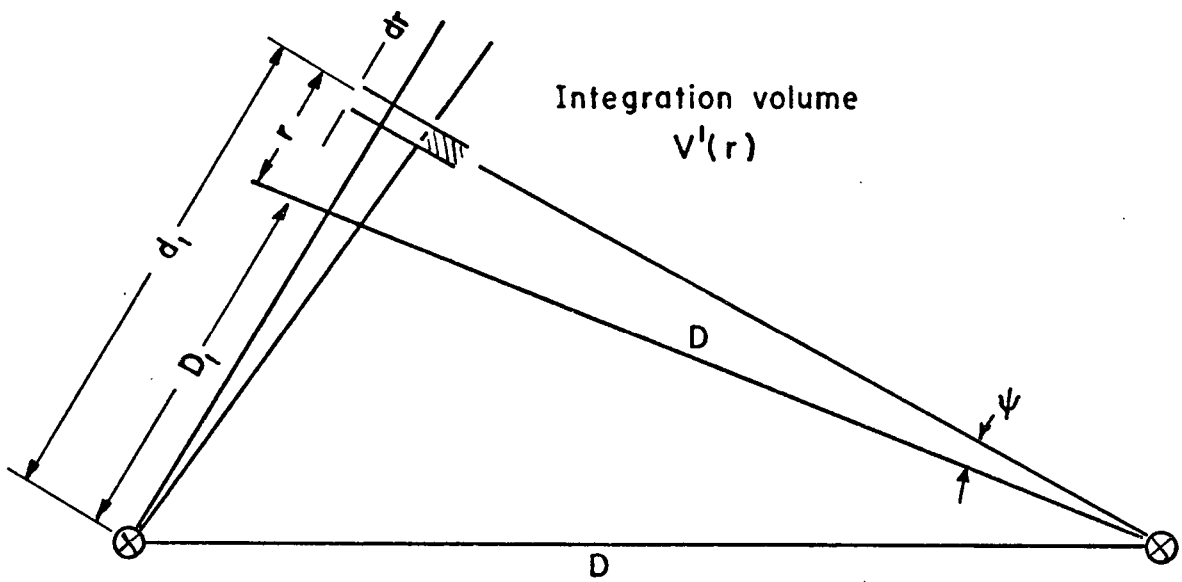

Fig. C.3 Integration Geometry

$$d_1 = D_1 + r$$

then we can compute a function

$$P(r)\,dr = A_0\left[\frac{\pi G_t \sigma}{d_1^2 d_2^2}\right] \int_{V'(r)} G_r\,dv \qquad (C.6)$$

much more easily than $Q(r)$. $V'(r)$ denotes the new integration volume shown in Fig.C.3. But

$$\int_{V'(r)} G_r\,dv = dr \iint G_t e^{-(\rho/d_1)^2/\sigma_t^2}\,\rho\,d\rho\,d\phi$$

$$= dr\ 2\pi G_t \int_0^\infty \rho\, e^{-\frac{\rho^2}{d_1^2\sigma_t^2}}\,d\rho$$

$$= dr\ \pi G_t (d_1\sigma_t)^2 \qquad (C.7)$$

Returning to Eq.(C.6) we therefore find;

$$P(r) = \frac{P_t\lambda^2}{(4\pi)^3} G_{0t}G_{0r}\pi(0.6d_1\theta_r)^2 \cdot \left\{\frac{\eta(r)e^{-\psi^2/\sigma_r^2}\sigma(r)}{d_1^2 d_2^2 10^3}\right\} \qquad (C.8)$$

with
- r d_1 and d_2 in Kms
- λ $\sigma(r)$ in meters
- ψ = angle separation from transmitting beam center line.

Note that it is possible to obtain a rough estimate of $Q(\xi)$ from $P(r)$ using a derived relationship between r and ξ, but its validity will be restricted to situations where the ξ plane almost intersects the beam at a right angle.

The angle ψ can be expressed in terms of r and β (see Fig. C.4).

$$\frac{r \sin (\pi - \beta)}{D_2 - r \cos (\pi - \beta)} = \tan \psi \qquad \text{(C.9)}$$

$$\psi = \tan^{-1} \left\{ \frac{r \sin \beta}{D_2 + r \cos \beta} \right\}$$

Furthermore the antenna gains G_{0t} and G_{0r} can easily be expressed in terms of their beamwidths when the beamwidth is on the order of a few degrees or less.

$$G(\psi) = G_0 e^{-\psi^2/\sigma^2} \qquad \text{(C-10)}$$

For a radiation efficiency e;

$$G_0 = \frac{e\, G(0)}{\iint_R G(\psi)\, dA/4\pi R^2}$$

But

$$\iint_R G(\psi)\, dA \simeq \int\int G\left(\frac{r}{R}\right) \rho\, d\rho\, d\phi$$

$$= 2\pi \left(\frac{R^2 \sigma^2}{2}\right) G_0$$

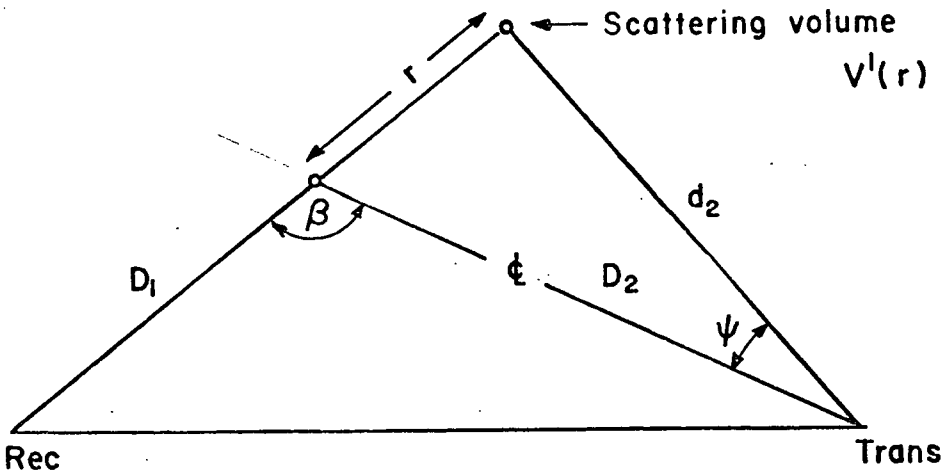

Fig. C.4 Parameters for Evaluation of ψ

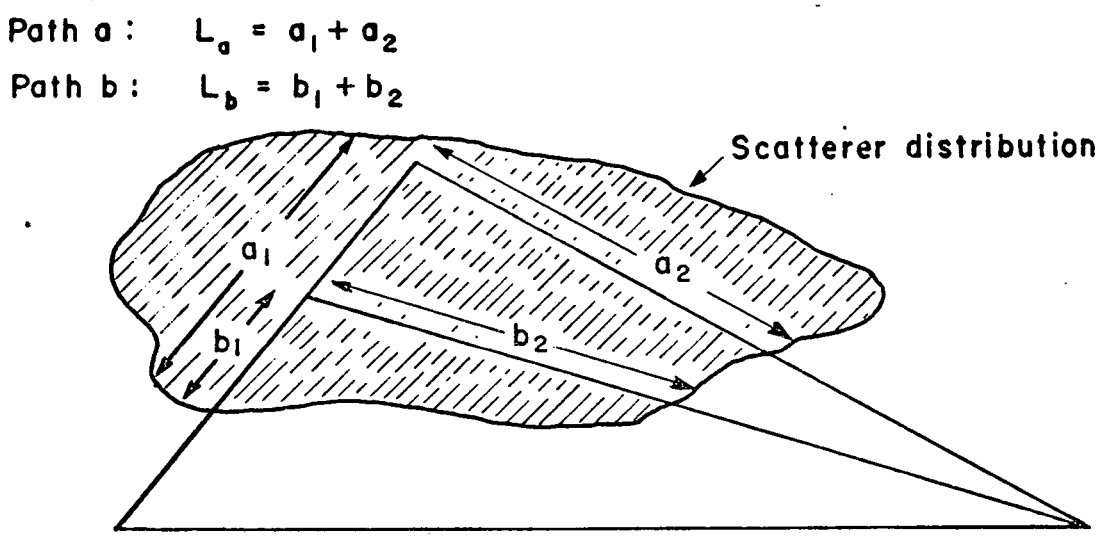

Fig. C.5 Differential Attenuation

For an efficiency of 0.6 this yields,

$$G_0 = \frac{0.6}{\sigma^2/4}$$

$$= 6.66/\epsilon^2 \qquad \text{(C.11)}$$

where ϵ is the half power beamwidth and

$$\sigma = 0.6\,\epsilon \qquad \text{(C.12)}$$

Returning to Eq.(C.8) with $P_t = 1$, we find that,

$$P(r) = \frac{\lambda^2}{64\pi^2}\left[.36\left(\frac{6.66}{\epsilon_r}\right)^2\right]\left\{\frac{\eta(r)e^{-\psi^2/2\sigma_r^2}\sigma(r)}{d_2^2\ 10^3}\right\}$$

$$= .25 \times 10^{-4}\ \frac{\lambda^2 e^{-\psi^2/2\sigma_r^2}}{\epsilon_r^2\ d_2^2}\sigma(r)\eta(r) \qquad \text{(C.13)}$$

C.3 Polarization and Absorption Loss

In general the polarization decoupling loss will be a complicated function of the antenna pointing angles. However the differential effect over the common volume will be quite small and here will be neglected completely. The power levels computed in this program will be based on minimum coupling loss, but corrections can easily be made to take into account the depolarization effect.

The field incident at any point in the scattering volume will be attenuated relative to that which would exist in the absence of scatterers due to both absorption and scattering. Both effects have an exponential behavior with increasing path length for a uniform scattering medium, and will be lumped together. (see Fig. C.5)

Let

A = attenuation coefficient dB/Km

then the intensity of the incident field I in terms of the free space intensity I_0 can be written,

$$I = I_0 e^{-aL} \tag{C.14}$$

L = total path length through scattering medium

$a = (\frac{2.302}{10})A$ attenuation constant.

When the scattering medium is uniform and encloses the beam intersection completely;

$$L = d_1 + d_2 - D_1 - D_2$$

$$= r + d_2 - D_2 \tag{C.15}$$

Thus

$$\frac{I}{I_0} = e^{-.23A(r + d_2 - D_2)} \tag{C.16}$$

C.4 Scattering Cross Sections

Assuming a single scattering model is valid, the scattering cross section σ for the two most important scattering mechanisms can be expressed as;

(i) Rayleigh (rain) scattering

$$\sigma = \frac{\pi^5}{\lambda^4} |K|^2 Z \qquad (C.17)$$

with $|K| \simeq 1$

(ii) Atmospheric Turbulence

$$\sigma = \frac{128\pi^6}{\lambda^4} (0.033\ c_n^2 (\frac{4\pi}{\lambda} \text{Sin}\ \frac{\theta}{2})^{-11/3}) \qquad (C.18)$$

where θ = the scattering angle (change of ray direction at the scatterer).

These expressions can be used in Eq. (C.13) and the profile of power versus r is computed directly. With an approximately linear relationship between delay and r the resultant function P(r) can be interpreted in terms of power versus delay. Alternately when linearity cannot be assumed, more involved transformations can be performed.

C.5 Description of the Program SCATER

This program computes path loss (includes antenna gains), the power profile P(r) from Eq. (C.13), and transforms r into the equivalent differential delay τ relative to the intersection point of the two beams. The required input variables are listed below. All are in Kms or degrees unless noted.

(a) Frequency (f_o in GHz), Receiver beamwidth (BW), and a parameter ISIG;

$$\text{ISIG} = \begin{cases} 0 & \text{Rayleigh cross section (eq. (C.17))} \\ 1 & \text{Atmospheric turbulence cross section (eq. (C.18))} \end{cases}$$

Note that in the program the following parameters are fixed.

$$Z = 10^{-14}$$

$$K = 1.0$$

$$c_n^2 = 10^{-14}$$

(b) Spacing (D), Bearing angle to Nth-Sth line of transmitting site (BEAR), beamwidth of transmitting beam (EPS)

(c) Scan coordinates. Radius (R), azimuth (ALPH), height of intersection (ZO).

On completion the program reverts to a point where it accepts a new set of scan coordinates (i.e., (c)). Input of zero intersection height causes return to monitor.

The total path loss in dB. is computed from the sum of the samples of P(r). Corrections can be made to this value for absolute attenuation (for the beam intersection path) and variations in the cross section parameters c_n^2 and Z.

C.6 Delay Power Spectrum and Path Loss Calculations

The orthogonal baseline configuration previously considered was examined in terms of its delay power profile and path loss. These quantities were computed for different intersection points in the proposed scan volume with the following fixed parameters.

f_o = 7.8 GHz
BW = 0.5^o
D = 90 and 180 Km
ϵ = 1.45^o
Z0 (intersection ht.) = 7.0 Km

The resulting path loss values as a function of scan radius R, are shown in Figs. C.6 and C.7. The former is with the atmospheric turbulence scattering cross section, Eq.(C.18), while Fig. C.7 applies to a Rayleigh scattering medium (Eq.(C.17)).

In the absence of differential attenuation effects (ATT = 0.), it was found that the power profiles P(r) (Eq.(C.13))were approximately Gaussian in form. i.e., P(r) is determined almost entirely by the transmitting beam radiation pattern. Thus we can approximately represent P(r) as;

$$P(r) \simeq f(\gamma_r, \alpha_r, \gamma_t, \alpha_t)\ g_t(\psi(r))$$

i.e., a constant times the antenna beam pattern, where f( ) is a function of the antenna pointing angles only.

The following points are also of interest concerning the behavior of path loss.

(a) Along the great circle scan, path loss varies only with the change of common volume length for Rayleigh scattering and therefore follows an approximate cosecant law with respect to the receiving antenna elevation

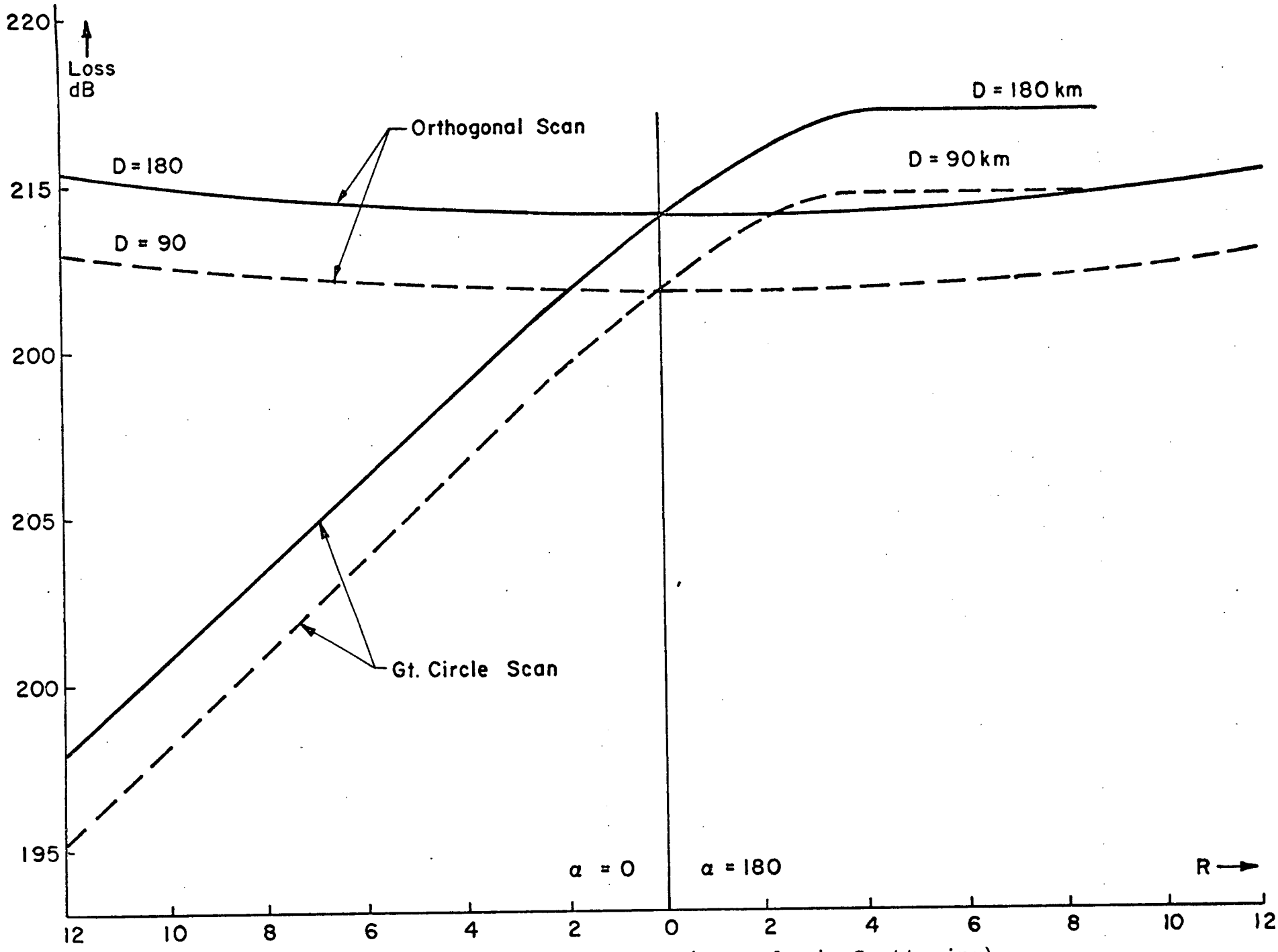

Fig. C.6. Path Loss vs Scan Coordinate R (Atmospheric Scattering)

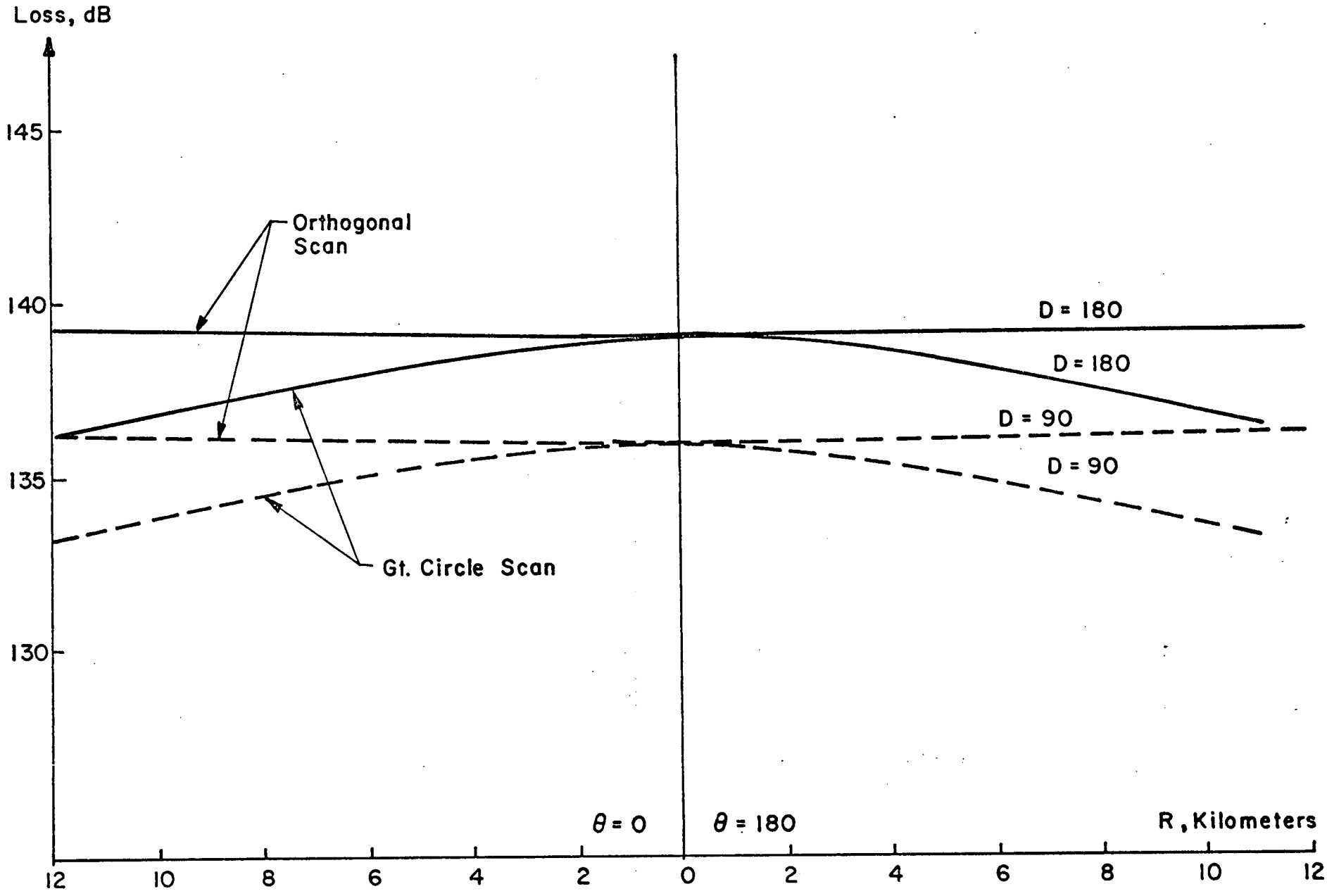

Fig. C.7 Path Loss vs Scan Coordinate R (Rain Scattering)

angle λ_r. For atmospheric turbulence there is a strong scattering angle dependence so that in the forward scatter mode losses are very much reduced. In the orthogonal scan configuration the scattering angle changes only slightly. (see Fig. C.6) Furthermore, there is no change of volume length L across the scan which accounts for the constant loss characteristic with a Rayleigh cross section.

(b) Choice of antenna spacing D.

There are two ways of approaching this choice. One is for fixed transmitting antenna beamwidth ϵ_t, and the other is for an illuminated volume at the receiver of fixed vertical extent. i.e., the beam thickness of the transmitting antenna at the receiver is given by;

$$\Delta h \simeq D\epsilon_t \qquad \text{(see Fig. C.8)}$$

This determines the vertical extent of the scan volume. Consider variation of path gain with ϵ_t fixed assuming that the receiver beam is pointed in a vertical direction.

$$\begin{aligned} \text{Gain} &\alpha \text{ Common Vol. x } D^{-2} \\ &\alpha \Delta h \cdot D^{-2} \\ &\alpha D^{-1} \end{aligned}$$

Hence the 3 dB improvement in Figs. C.6 and C.7 when the distance is changed from 180 Km to 90 Km. For fixed Δh;

$$\begin{aligned} \text{Gain} &\alpha \Delta h \text{ x } D^{-2} \text{x Antenna Gain} \\ &\alpha D^{-2} \text{x } \epsilon_t^{-2} \\ &\alpha D^{-2} \text{x } D^2 \\ &\alpha \text{ const.} \end{aligned}$$

Therefore the path loss can be maintained at a constant value as long as the beamwidth ϵ_t can be reduced sufficiently.

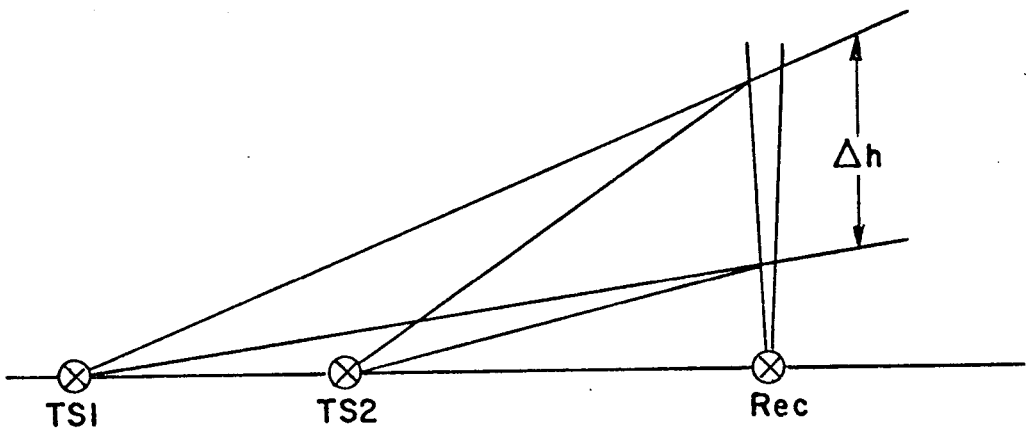

Figure C.8 Common Volume Dimensions

C.7 Conclusions for the Proposed Bistatic Interference Experiment

In designing an interference experiment there are two possible philosophies.

a. Restrict the E.S. antenna beam elevation to greater than say 30^{o} (see Fig. C.9) and measure interference through main lobe coupling or through coupling of the E.S. sidelobes with the TS beam. This represents a direct simulation of satellite link interference. The ES radiation pattern can be modeled (see Fig.C.10)by the sum of an omnidirectional pattern and a pencil beam.

b. Recognize that sidelobe interference contributions while not as strong as main lobe effects, will occur more frequently. Hence use the E.S. main lobe over the complete range of elevation angles 0 - 90^{o}, as a probing tool. This results in higher signal levels than would be available using the sidelobes for the same measurement as in a. (This approach has been used by Crane.*)

The previous analysis and work by others, notably Crane, tends to support the following points.

(i) The principal interference mechanisms will be rain, atmospheric turbulence and ducting.

---

* Predictions of Transhorizon Field Strengths Using Modeling Techniques, Lincoln Lab. TN.

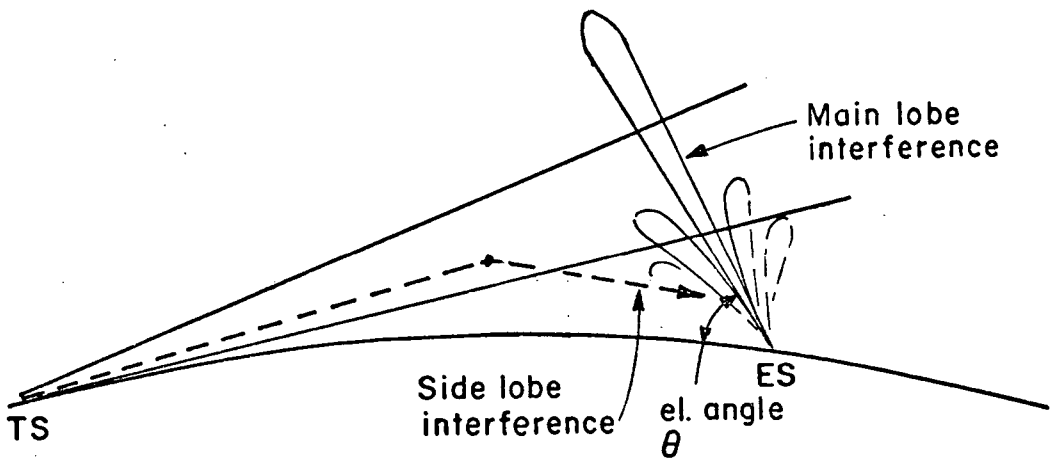

Fig. C.9 Antenna Beam Configuration

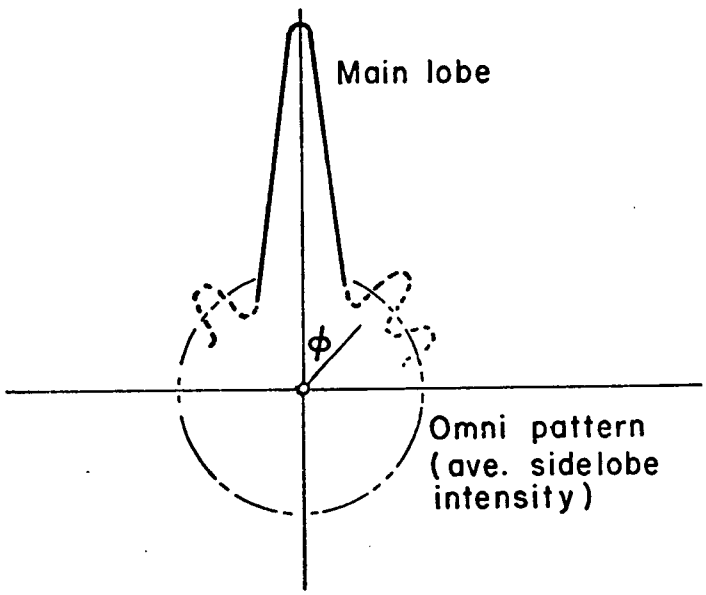

Fig. C.10 ES Beam Pattern

(ii) There is a 60 - 70 db difference between the interference signal levels for rain and atmospheric turbulence for scattering through the main lobe (assuming E.S. elevation angles greater than 30^{o}).

(iii) Power contributed through the sidelobes will be important and will frequently exceed the CCIR recommended levels. All three mechanisms in (i) will be competitive, for low scattering angle, forward scatter situations. (i.e., if they do contribute significantly it will be from a preferred direction and elevation angle).

(iv) At times ducting through the sidelobes can exceed main lobe rain scattered signal levels.

Thus it can be seen that the real discrimination problem will be one of two kinds: Distinction between rain inside the main lobe and ducting through the sidelobes (Fig.C.12),or alternatively between rain, atmospheric turbulence and ducting, all through the sidelobes (see Fig.C.11).Note that (iii) indicates the prime advantage of a bistatic measurement over monostatic radar. In particular, ducting into the sidelobes will be a major interference contributor, but this mechanism is not readily observable with a monostatic configuration. On the other hand, without an absolute delay reference the actual location of the dominant scattering medium will be unknown, and Doppler discrimination techniques which generally require such knowledge, will be ineffective.

The exceptions, which fortuitously match our discrimination requirements are;

(1) Ducting as opposed to rain scattering, will exhibit low Doppler shifts and spreads.

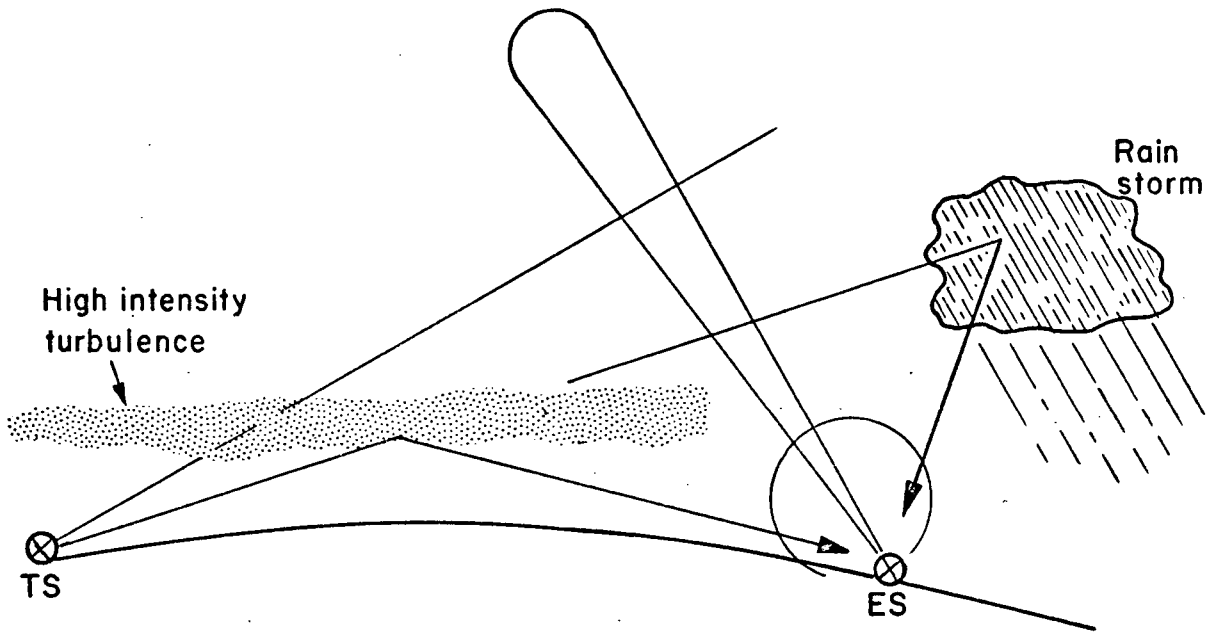

Fig. C.11 Turbulence-rain storm geometry.

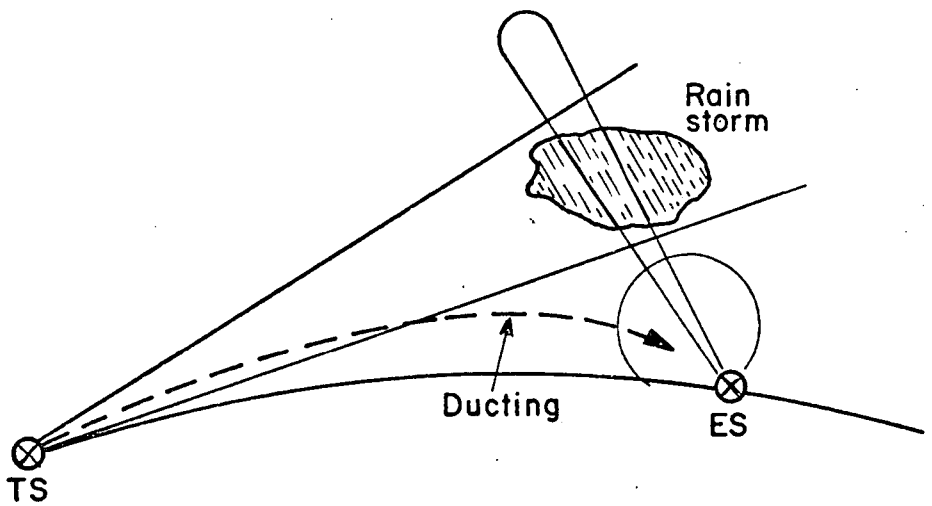

Fig. C.12 Ducting - rain storm geometry.

(2) Along and transverse to the great circle path, forward scatter from atmospheric inhomogeneities will result in negligible Doppler spreads (similarly for ducting) while rain is predominantly vertical in motion, and will contribute signals with substantial Doppler spreading. (Note that for sidelobe interference, the common volume is the intersection of a TS beam with an omni beam.)

Conclusions. The orthogonal TS configuration originally proposed should be reduced to a single ES-TS pair. It would be desirable to have an E.S. beam steerable down to 0^{o} elevation. In its normal operating mode (elevation greater than 30^{o}) it would be used to map rain intensity distributions, while in a forward scatter mode (elevation $\simeq 0^{o}$) it would give higher signal levels for investigation of sidelobe interference.

APPENDIX D

INTERFERENCE EXPERIMENT CONFIGURATION DESIGN

D.1 Outline of the Material Presented

In view of the fact that the reader may not desire to follow the detailed analysis and design procedure presented, this Appendix has been organized in a slightly unorthodox way. Section D.2 contains an outline of the various parameters involved for each mechanism (Section D.2.1) followed directly by a discussion concerning choice of configuration parameters (Section D.2.2). A detailed description of the program and computed data is then available in Section D.3.

D.2 General Objectives

In choosing a suitable geometrical configuration, the basic objectives of the experiment must be kept in mind.

(i) The accumulation of valid experimental data for the interference coupling between a simulated communications satellite link and terrestrial microwave relay systems. (Provides justification for use of bi-static system over monostatic radar).

(ii) Verification of the extent to which meteorological history for a given region can be used to predict interference levels by extrapolating the results of direct coupling measurements.

To achieve the second of these goals, it is necessary to make a correct assessment of the mechanism causing the interference and to obtain as much information as possible about its characteristics for correlation with observed meteorological parameters. Thus the system must be capable of carrying out the following functions.

(a) Identification of the scattering mechanism with some degree of certainty.

(b) Measurement of parameters which will be important in characterizing the interference effects. e.g., average power levels, Doppler spreading and multipath spreading in the case of wideband communication systems.

(c) Measurement of spatial structure of the scattering medium or equivalent parameters which can be related directly to meteorological data.

In summary then, the system must perform an identification and subsequent mapping of a spatial region which corresponds to realistic beam intersection geometries. (See Fig. D.1.)

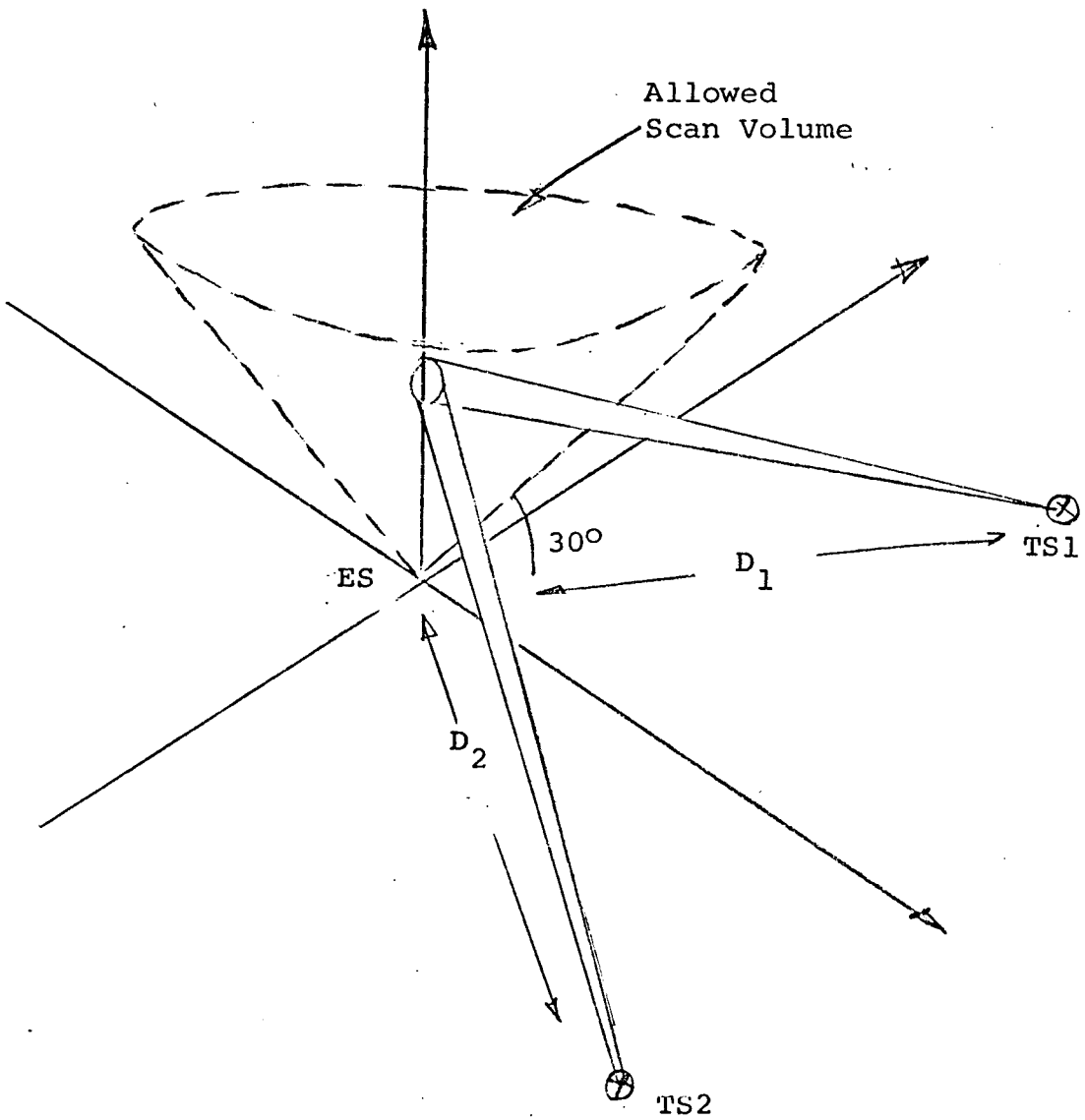

Fig. D.1 Intersection Geometry.

The spatial zone of interest will be defined arbitrarily in terms of an elevation angle greater than 30^{o}. Very low elevation angles may be particularly useful in the investigation of specific mechanisms, however(see Appendix C) to facilitate the mapping of a large spatial region without excessive duplication of equipment, it appears essential to use the ES antenna in a scanning mode. This would provide a high degree of flexibility and also allow the extraction of large amounts of data from relatively rare but important events, such as high intensity rainstorms. A fixed beam experiment is restricted in the sense that only an isolated spatial region is sampled, with a resultant lack of confidence in the predicted long term statistics.

It is interesting to note in passing that a scattering cross section mapping experiment as outlined above would also provide useful information for characterization of the satellite to ground line of sight link; i.e., given a complete description of the spatial structure of the medium and estimates of defining parameters, the influence of the scattering medium for a line of sight configuration could be found. With such an approach long term statistics could be built up from the experimental data.

D.2.1 Important Interference Mechanisms

The most important scattering mechanisms that will be encountered and which must be separated, can be grouped as follows;

(a) Precipitation in the form of columnar or convective rain showers, snow, hail shafts.

(b) Scattering from homogeneous turbulent atmospheric inhomogeneities.

(c) Ducting effects and partial reflection mechanisms involving large scale horizontal statification of the atmospheric refractive index.

(d) Reflections from aircraft and birds.

Table D.1 MECHANISM ATTRIBUTES

	(a) Precipitation	(b) Turbulence	(c) Stratification	(d) Aircraft
Power vs. scattering angle β	No scattering angle dependence	Strong β dependence e.g., β-11/3	Scattered energy centered around reflection or duct primary ray.	
Doppler shift and spread	Predominant vertical motion Marked variation in v_z due to drop distribution	Horizontal motion due to winds, with superimposed turbulence	Slow movement Low Doppler effects	High horizontal velocities. High Doppler shift.
Delay spread	Most severe delay spread	close to max. delay spread	Tendency towards narrow delay spreading.	Min.delay spread
Wavelength Dependence	λ^{-4}	$\lambda^{-1/3}$	Variable	Variable
Associated meteorological variables	Rain gauges Drop size measurements	Wind speed	Refractive index profiles	

Table D.1 lists some of the attributes of interest for each mechanism group. Ideally one would like to select an arrangement of terrestial station antennas, TS1, TS2 ... etc., in a way that when all were intersecting the ES beam at a single point in space, individual TS beams were particularly sensitive to different attributes. (see Fig. D.1) This would allow identification of the existing mechanism for the mutual intersection volume in question.

D.2.2 Configuration Parameters

If attention is restricted to a scanning ES beam concept such as illustrated in Fig. D.1, the remaining system parameters to be selected are as follows.

(a) Number of transmitting stations TS1, TS2... etc.

(b) Location of each in terms of distance D and angle θ.

(c) Beamwidth of terrestrial stations (ϵ).

(d) Frequencies of operation (f_o)

(e) Probing signal bandwidth (W)

Note that the receiving antenna (ES) beamwidth is assumed to be representative of a real satellite terminal (e.g., 0.5^o at 8 GHz). Similar considerations should dictate the choice of transmitting site beamwidths.

A computer program described in Section D.3 was used to give a preliminary evaluation of proposed configurations and the insight gained from sample calculations will now be presented.

(a) Number of transmitting sites. This choice is dominated by the desire for simplicity. We should choose the minimum number required to give an unambiguous identification of the scattering medium and also to allow the ES to scan the full volume proposed (i.e., the scan cone in Fig. D.1).

(b) Variation with D. Our analysis has demonstrated that over the scan volume of interest the spatial resolution and vertical to horizontal Doppler component discrimination capabilities are only weakly affected by choice of D. The primary consequence of increasing D for a fixed beamwidth ϵ, is the reduced power level at the common volume.

A further consideration is the use of movable TS beams to allow variation in the intersection altitude (and hence scanning over a larger vertical extent.) If D is too large, shadowing effects due to earth curvature place a bound on the lower limit of the scan volume.

(c) Beamwidth of terrestrial stations. The beamwidth should be representative of those used in microwave links. A wider beam gives a more extensive scan capability with lower demands on pointing accuracy and fewer adjustments of the TS beams to cover a given volume. (Note that 1.45^{o} beamwidth corresponds to a beam thickness of 2.3 Km at D=90 Km). The power levels expected for a given spatial resolution cell will be reduced as the inverse square of the beamwidth because of reduced antenna gain.

(d) Frequencies of operation. The different scattering mechanisms exhibit wavelength dependences which could be profitably used in their identification (using a multiple wavelength system). However the added complexity might be undesirable for an initial system design. This applies only to discrimination capabilities; accumulation of data at various frequencies would be useful but preferably over different observation periods.

(e) Probing signal bandwidth. The analysis in Section D.3 demonstrates that for the scan volume proposed, the spatial resolution is determined almost entirely by W the bandwidth.

(i.e., it is almost independent of D the TS-ES spacing). From the example given in Table D-2. it is seen that 10 MHz bandwidth allows 190 meter resolution (D = 180 Km) in the extreme forward scatter mode, and 16 meter resolution in the extreme backscatter mode. As discussed, the received power levels are directly related to the volume in a spatial resolution cell, so that reduced resolution might be desirable if backscatter measurements are important. Alternatively a variable bandwidth scheme could be implemented, with resolution tailored to the scan position.

A Proposed Configuration

Based on the previous comments it appears that an orthogonal system of the form shown in Fig. D.2 should be implemented. The parameters D (spacing), ϵ (beamwidth) and W (bandwidth) cannot be determined without a more detailed study of signal levels. (See Appendix C).

Despite the fact that backscatter measurements will be quite difficult to implement, they will still provide data which is unique in terms of building up statistical knowledge of interference. Simply in terms of scanning the cone of interest (see Fig. D.2), third antenna located at point B would be desirable, but it must be recognized that the time involved in a complete volume scan would be unrealistic anyway; hence the best strategy would seem to involve a broad scan in the forward scatter mode, with occasional limited sampling of backscatter conditions.

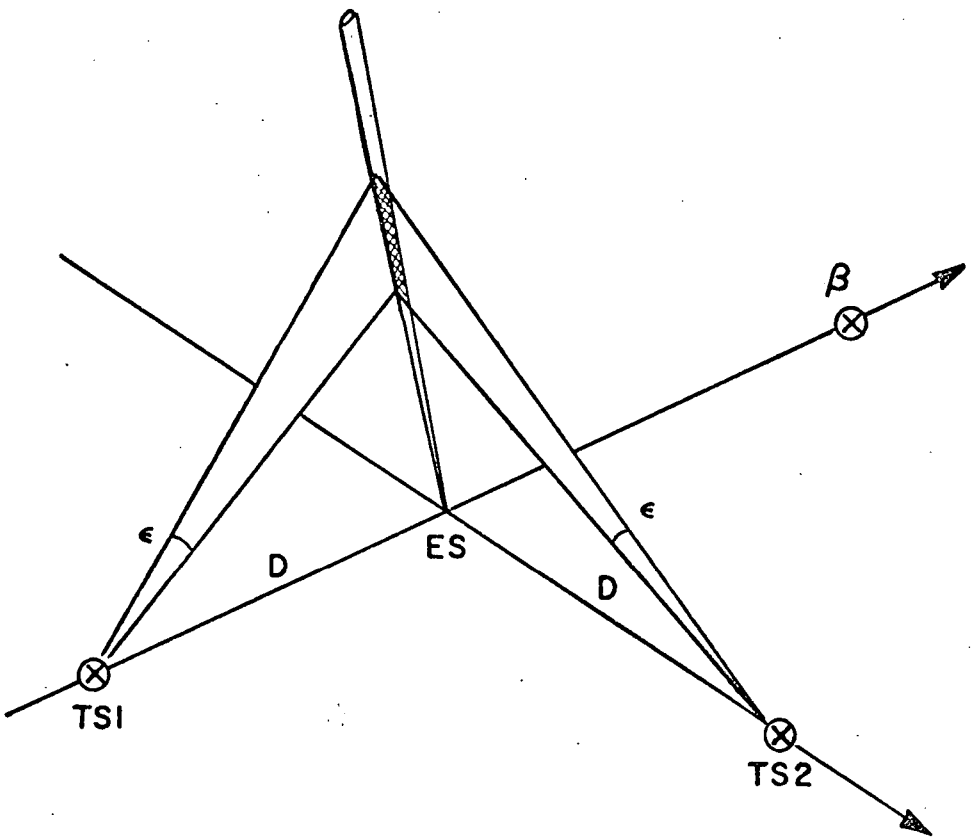

Fig. D.2 Proposed Configuration.

D.3.1 Description of the Configuration Analysis

Consider an array of terrestrial transmitting antennas which have beams intersecting a narrow satellite earth station beam (ES) (See Fig. D.3). The terrestrial beams are denoted by TS1 to TS4 for the system under consideration. The coordinate system is centered on ES while all azimuthal angles are measured with reference to an arbitrary line such as the Nth-Sth line. Each terrestrial station TS_n is located according to its radius D_n and angle θ_n. (See Fig. D.4 for details of the currently configured RIPP experiment.)

The five beams are assumed to intersect at a point determined by parameters (R, α, h) in a cylindrical coordinate system. (See Fig. D.3.) A common intersection point for all beams is somewhat artificial in terms of a real system network, but is necessary for mechanism identification and to avoid over complication of the analysis. SIGNATRON has a computer program (SCAN) which gives a quick estimate of the delay and Doppler parameters for each coupling between the ES beam and terrestrial beam.* The following assumptions are made:

(i) The ES beam is of neglibible width compared with terrestrial station beams. (Pencil beam).

(ii) The volume common to both beams is completely and uniformly filled with elemental scatterers, i.e. The scattering cross section is not a function of space.

*Note that interference between terrestrial stations such as a T1 - T2 beam intersection can be analyzed using conventional tropospheric scattering prediction methods with the appropriate parameters. This will be considered if time permits.

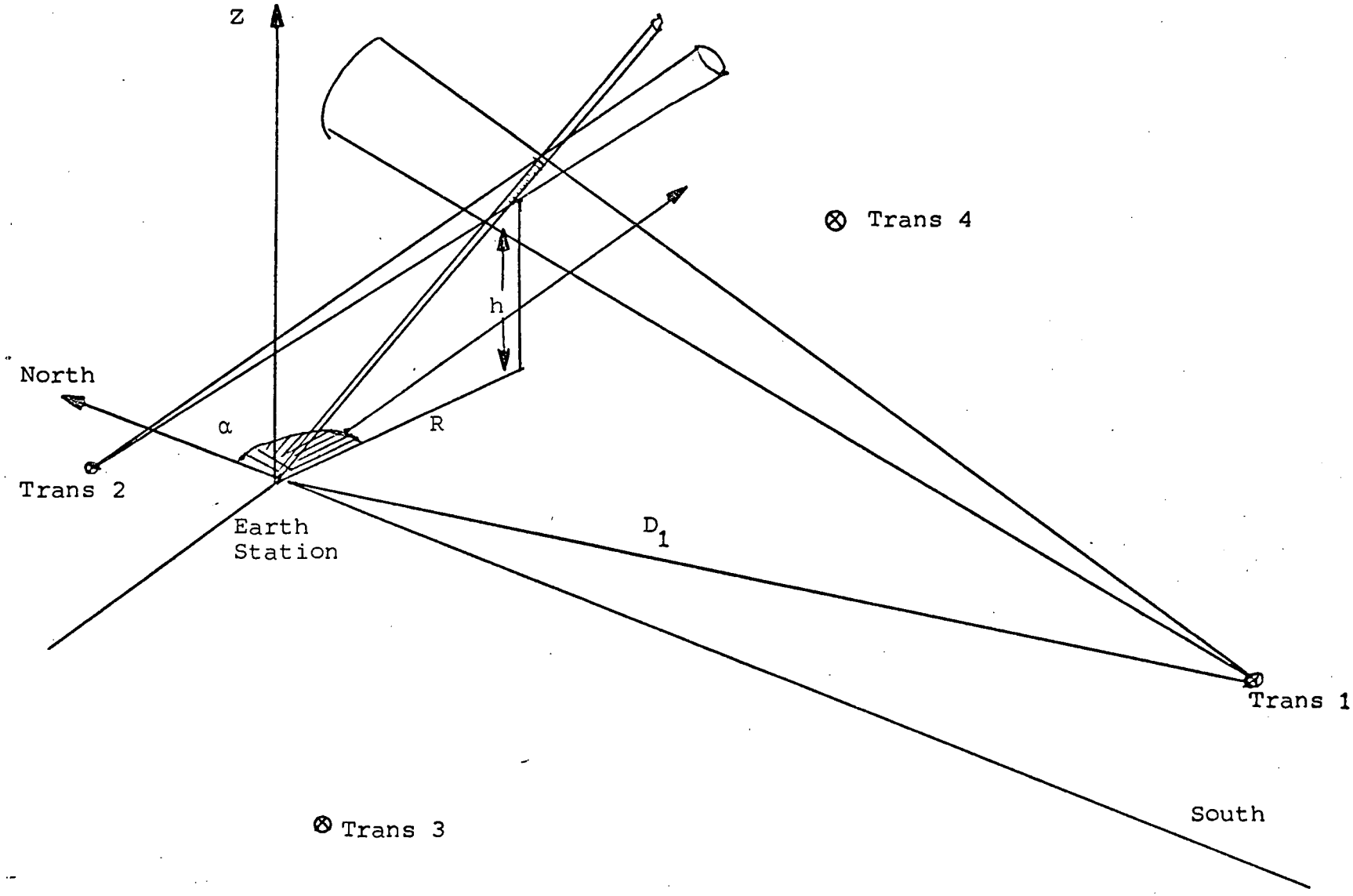

Fig. D.3 Antenna Pointing Coordinate System

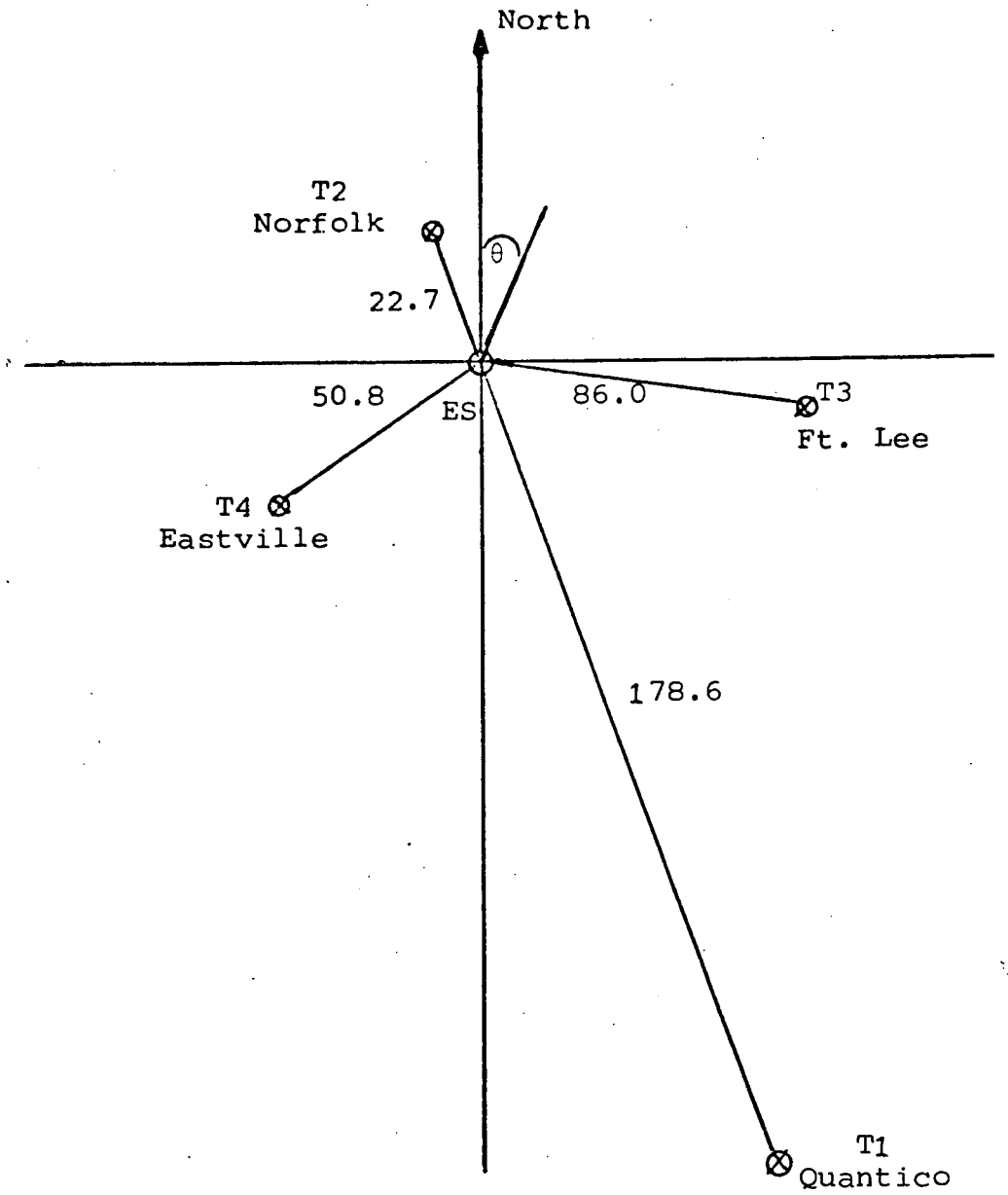

Fig. D.4 Current RIPP Configuration

Transmitter	D	Q
1. Quantico	178.6	152.2
2. Norfolk	22.7	332.7
3. Ft. Lee	86.0	99.9
4. Eastville	50.8	237.9

E

(iii) The gross parameters computed are found without considering the weightings due to scattering cross section, inverse path length etc. Only the intersection of the 3 dB antenna patterns is of interest.

D.3.2 Parameters Computed

Figure D.5 shows a detailed perpective of the common volume. The following parameters were computed for the upper and lower intersection points.

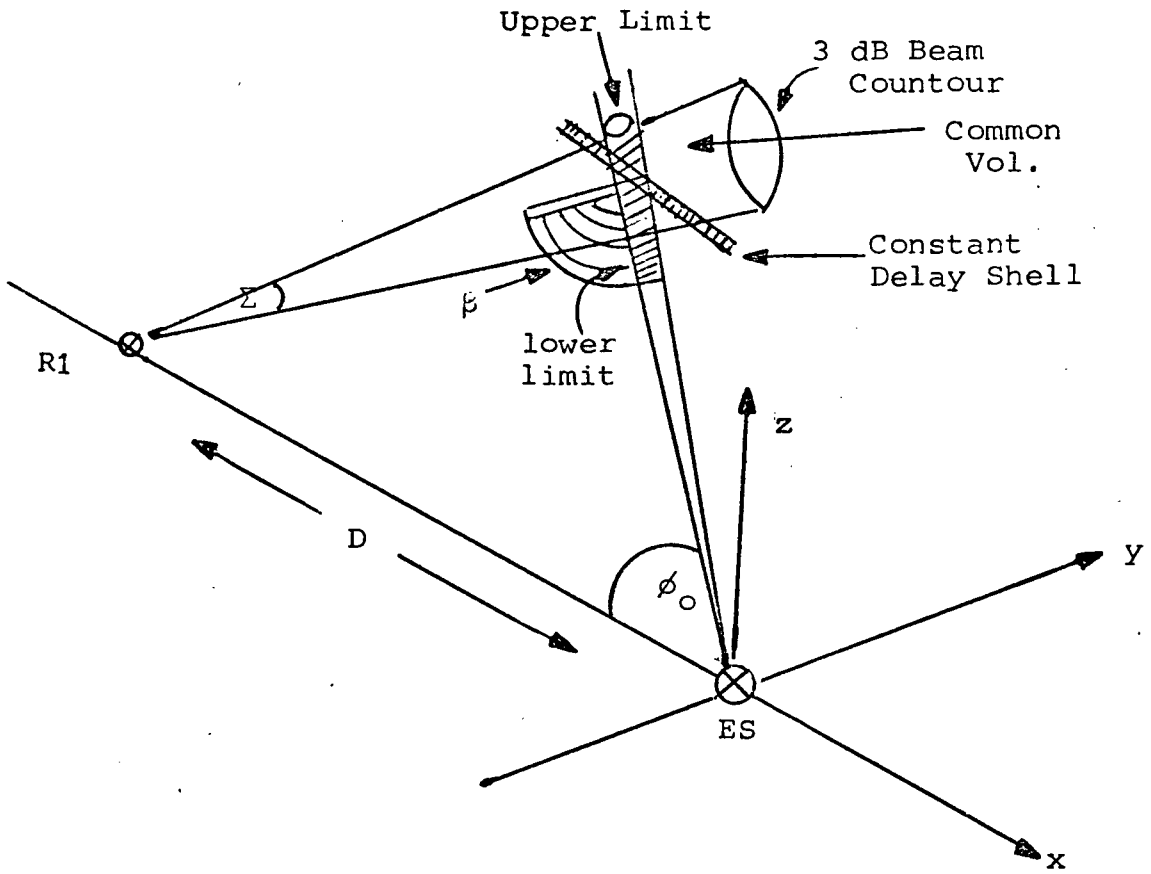

Fig. D.5 Common Volume Geometry

f_x, f_y, f_z — Frequency shift in Hz per unit velocity (meter/sec) for x,y and z components of scatterer velocity.

ξ — Path delay. (μsec.)

L — Volume length in Kms.

ℓ — Diameter of ES beam at common volume mid point

In addition the differential delay spread across the volume was computed from the upper and lower delays. i.e.,

$$\tau = \xi_u - \xi_\ell \tag{D.1}$$

One should note that for a fixed temporal resolution $\frac{1}{W}$, the corresponding spatial resolution can be found approximately from,

$$\Delta L \simeq \left(\frac{L}{\tau}\right) \frac{1}{W} \tag{D.2}$$

This assumes a linear relationship between delay and distance along the common volume cylinder, which is only approximately true. Furthermore, the slope of the ellipsoidal delay surface relative to the ES beam ultimately determines the characteristics of a spatial resolution cell.

In utilizing the Doppler coefficients f_x, f_y, f_z, two points are of concern. First the (x,y,z) coordinate system is relative to the chord joining the ES and terrestrial station. Thus, for a network of terrestrial antennas the appropriate transformations of x and y components must be made. The second point is that at each location in the common volume there will generally be a spectrum of velocities for each direction. Hence there will be a corresponding spectrum of

Doppler shifts. The coefficients above should therefore only be interpreted in terms of Doppler sensitivity at a given point.

The program operates in the following manner:

(a) Read parameters $R, \alpha, z_o, f_o, \epsilon, \theta, D$

r, α, z_o = intersection coordinates

f_o = frequency in GHz

ϵ = terrestrial station beamwidth

D, θ = coordinates of terrestrial station

(b) Compute intersection coordinates in an (x,y,z) frame

$$x = r\text{Cos}(\alpha-\theta)$$
$$y = r\text{Sin}(\alpha-\theta) \qquad \text{(D.3)}$$
$$z = z_o$$

(c) Compute path lengths to center point (see Fig. D.6)

$$D_1 = (r^2 + z_o^2)^{\frac{1}{2}}$$
$$D_2 = [(D - x)^2 + y^2 + z^2]^{\frac{1}{2}} \qquad \text{(D.4)}$$

(d) Find coordinates of upper and lower intersection points.

$$\beta = \text{Cos}^{-1}\left[\frac{D_1^2+D_2^2-D^2}{2\,D_1D_2}\right] \qquad \text{(D.5)}$$

(scattering angle at common volume center)

$$\phi_o = \text{Tan}^{-1}(z_o/r) \qquad \text{(D.6)}$$

$$d_u = D_2\text{Sin}(\epsilon/2)/\text{Sin}(\beta-\epsilon/2) \qquad \text{(D.7)}$$

$$d_\ell = D_2\text{Sin}(\epsilon/2)/\text{Sin}(\pi-\beta-\epsilon/2)$$

$$r_{u\ell} = (D_1 \pm d_{u,\ell})\ \text{Cos}\ \phi_o \qquad \text{(D.8)}$$

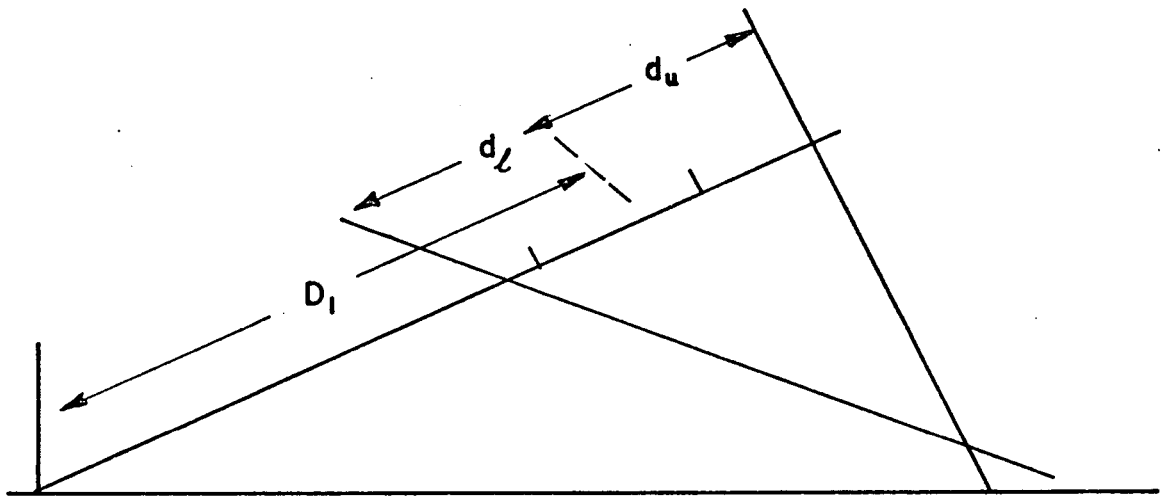

Fig. D.6 Intersection Geometry

Hence

$$x_{u,\ell} = r_{u,\ell} \cos(\alpha-\theta) \tag{D.9}$$

$$= (D_1 \pm d_{u,\ell}) \cos \phi_o \cos (\alpha-\theta)$$

$$y_{u,\ell} = r_{u,\ell} \sin(\alpha-\theta) \tag{D.10}$$

$$= (D_1 \pm d_{u,\ell}) \cos \phi_o \sin(\alpha-\theta)$$

$$z_{u,\ell} = (D_1 \pm d_{u,\ell}) \sin \phi_o \tag{D.11}$$

(e) Calculate the delay and Doppler components for upper and lower intersection points using the formulae above for D_1 and D_2, i.e.,

$$D_{1u} = D_1 (x_u, y_u, z_u) \qquad \text{etc.}$$

Then for both upper and lower points;

$$\xi = \frac{D_1+D_2-D}{c} \tag{D.12}$$

$$f_x = -\frac{f_o}{c} \left(\frac{x}{D_1} - \frac{(D-x)}{D_2}\right) \tag{D.13}$$

$$f_y = -\frac{f_o}{c} \left(\frac{1}{D_1} + \frac{1}{D_2}\right) y \quad ; \quad f_z = -\frac{f_o}{c} \left(\frac{1}{D_1} + \frac{1}{D_2}\right) z$$

The delay spread τ is indicated by,

$$\tau = \xi_u - \xi_\ell \tag{D.14}$$

In addition the total volume length and diameter are computed from

$$L = d_u + d_\ell \tag{D.15}$$

$$\ell = D_1 \times (BW)$$

where BW is the beamwidth of the ES beam.

D.3.3 Evaluation of the Current RIPP Configuration

A preliminary examination of possible configurations has indicated that an orthogonal system of antennas would simplify matters and yet still be sufficiently general. For this reason the scans shown in Fig. D.7 were evaluated using the current site configuration as a tentative example. The intersection point was moved along the dotted lines corresponding to scan A and scan B at heights 10 Km and 3 Km (Freq. 3.67 GHz, B Widths TS1, TS2, TS3, TS4 1.8°, ES, 0.62°.

Table D.2 contains the results. The Doppler coefficients at the upper and lower edges of the common volume were found to be within 10% of each other almost without exception. Hence the table contains only the upper common volume Doppler coefficients.

From a detailed study of the table one can draw the following broad conclusions.

(a) The volume resolution ΔL specified in Eq. (D.2) will be of the same order of magnitude as the beam resolution ℓ (see Eq. (D.15)) when the bandwidth W is about 5 MHz. For example, in a backscatter mode (see Fig. D.8a), this bandwidth gives $\Delta L \simeq 40$ meters (ES 30° elevation angle) while in the forward scatter mode (see Fig. D.8b), $\Delta L \simeq 130$ meters. An excessively small value of ΔL compared with ℓ does not serve any useful purpose; on the contrary it is detremental in the sense that the measurement signal to noise is proportional to $\Delta L \times \ell$. The volume resolution shows little dependence on spacing D for a backscatter mode and only minor variation with D in the forward scatter mode. In the backscatter mode the system performs almost as a monostatic radar would, so that bandwidth and resolution ΔL can be traded directly.

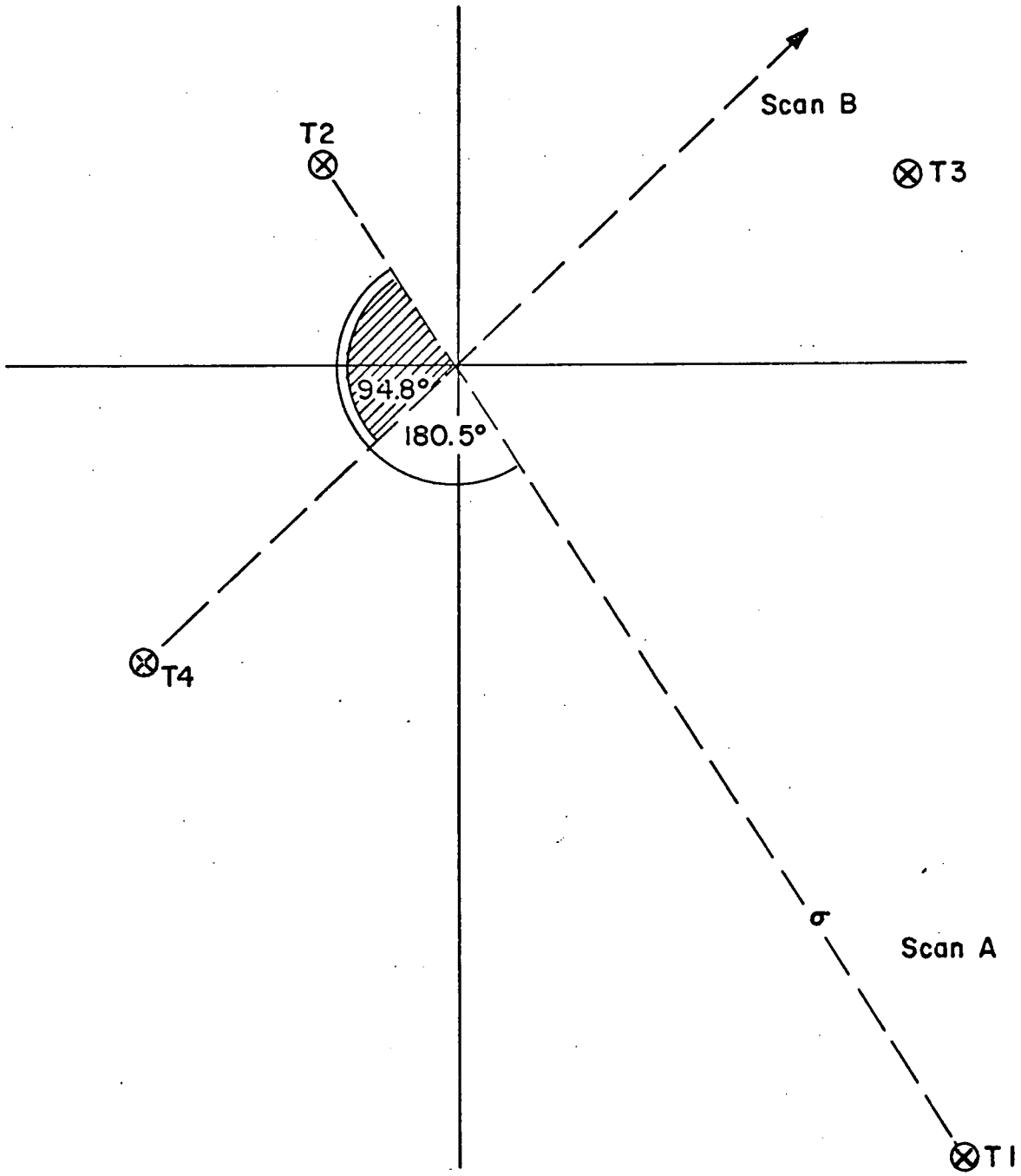

Figure D.7 Scan Patterns

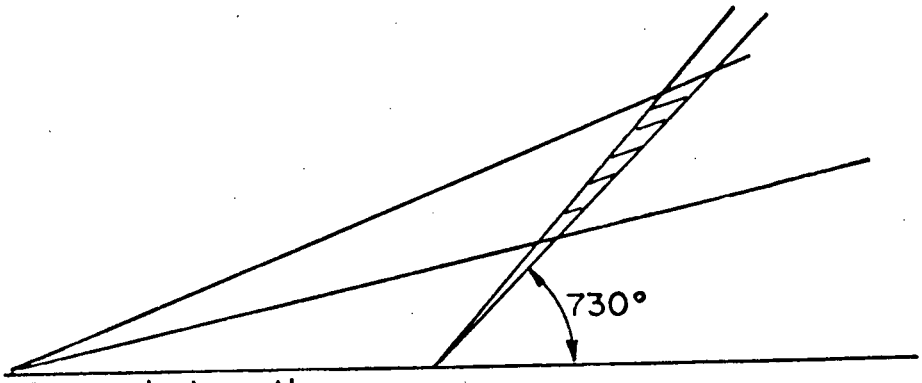

a. Backscatter Mode

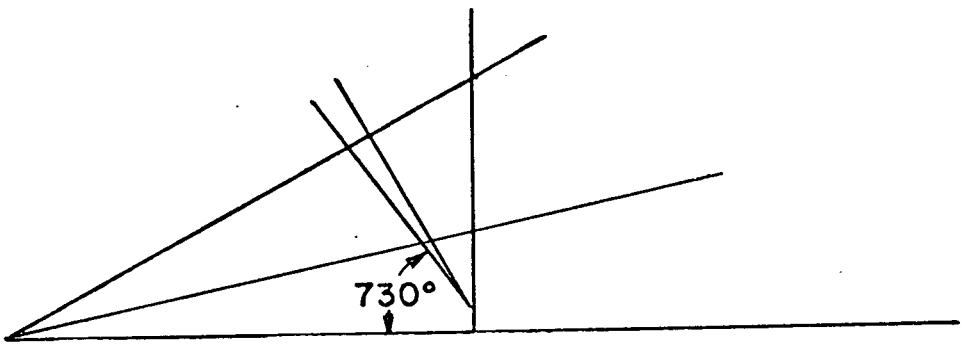

b. Forward Scatter Mode

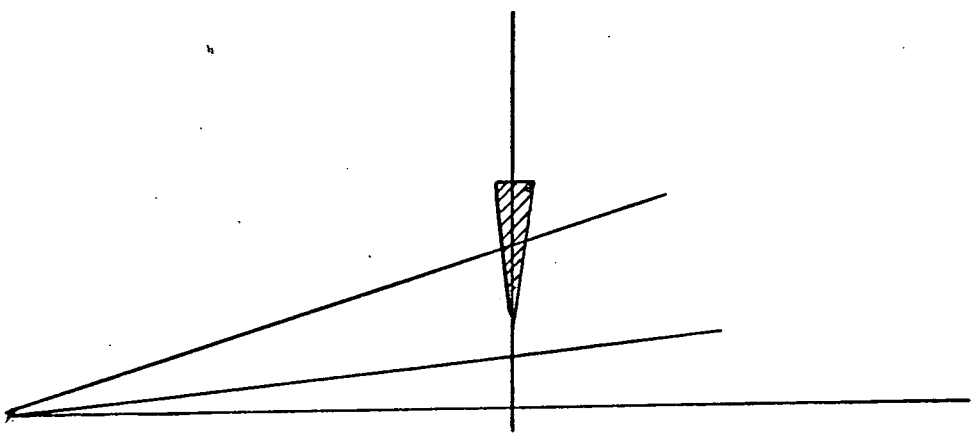

c. Vertical Mode

Fig. D.8 Great Circle Paths

TABLE D-2

Scan: A Intersection ht: 10km

Intersection		Antenna 1						Antenna 2					
R	α	f_x	f_y	f_z	τ	L	ℓ	f_x	f_y	f_z	τ	L	ℓ
22.7	332	23.4	.11	-5.7	114.	17.8	.26	-11.4	0.	-17.2	1.61	.34	.26
8.25	332	20.0	.07	-10.3	44.6	7.99	.14	2.16	0.	-16.6	1.69	.55	.14
2.0	332	14.6	.022	-12.9	24.5	5.87	.11	8.53	0.	17.5	3.11	.74	.11
2.0	152	9.8	0.	-12.9	16.1	5.61	.11	13.7	-.03	-16.8	5.18	1.0	.11
8.25	152	4.41	0.	-10.3	9.07	6.64	.14	19.4	-.09	-13.4	11.7	1.9	.14
20.	152	1.25	0.	-6.4	4.5	9.94	.24	22.8	-.15	-8.5	39.3	5.9	.24
40.	152	.32	0	-4.0	2.33	14.0	.44	23.9	-.18	-5.1	158.	23.8	.44

TABLE D-2 (continued)

Scan: A Intersection ht: 10km

Intersection		Antenna 1						Antenna 2					
R	α	f_x	f_y	f_z	τ	L	ℓ	f_x	f_y	f_z	τ	L	ℓ
22.7	332	18.7	11.3	-6.2	25.9	4.5	.27	11.9	-16.1	-7.1	10.5	2.1	.27
8.25	332	16.8	7.2	-10.9	16.7	3.3	.14	12.5	-9.7	-11.9	7.54	1.75	.14
2.0	332	13.6	2.16	-13.6	11.6	2.84	.11	12.2	-2.9	-14.5	6.75	1.67	.11
2.0	152	10.7	-2.15	-13.6	8.9	2.7	.11	11.8	2.9	-14.5	6.51	1.65	.11
8.25	152	7.31	-7.2	-11.1	6.63	2.66	.14	11.2	9.8	-11.9	6.67	1.66	.14
20.0	152	5.12	-11.4	-7.2	5.7	2.5	.24	10.2	15.6	-7.8	8.1	1.82	.24
40.	152	3.4	-15.1	-4.8	6.36	2.22	.44	8.2	19.7	-4.9	13.1	2.4	.44

TABLE D-2 (Continued)

Scan: A Intersection ht: 3.0 Km

Intersection		Antenna 1						Antenna 2					
R	α	f_x	f_y	f_z	τ	L	ℓ	f_x	f_y	f_z	τ	L	ℓ
22.7	332	24.4	0.13	-1.98	360.0	55.3	.25	-12.3	0.	-13.8	0.36	.095	.25
8.25	332	23.7	0.11	-4.5	117.0	18.0	.095	.44	0.	-6.86	.44	.88	.095
2.00	332	19.0	.061	-10.6	36.1	6.9	.039	5.29	0.	-12.1	1.38	0.73	.039
2.00	152	5.44	0.	-10.6	10.1	6.6	.039	18.9	-.069	-11.8	5.67	1.03	.039
8.25	152	0.73	0.	-4.6	3.31	15.0	.095	23.7	-.13	-5.5	25.8	3.93	.095
20.0	152	0.13	0.	-2.2	1.40	30.1	.21	24.3	-.16	-2.8	118.0	17.8	.21
40.0	152	.025	0.	-1.37	0.7	46.4	.43	24.4	-.19	-1.69	723.	109.	.43

TABLE D-2 (Continued)

Scan: A Intersection ht: 10 Km

Intersection		Antenna 3						Antenna 4					
R	α	f_x	f_y	f_z	τ	L	ℓ	f_x	f_y	f_z	τ	L	ℓ
22.7	332	19.3	12.0	-2.0	27.1	4.69	.25	12.2	-17.1	-2.26	10.0	2.05	.25
8.25	332	19.1	10.2	-4.6	20.1	3.7	.095	13.0	-13.6	-4.9	7.02	1.69	.095
2.0	332	16.3	5.72	-10.8	13.5	2.95	.039	12.8	-7.3	-11.1	6.02	1.62	.039
2.0	152	8.06	-5.7	-10.8	6.51	2.8	.039	11.7	7.35	-11.1	5.48	1.60	.039
8.25	152	5.14	-10.3	-4.71	4.91	2.95	.095	11.2	13.6	-4.97	5.91	1.61	.095
20.0	152	4.51	-12.3	-2.34	5.05	2.62	.21	10.3	16.8	-2.53	7.68	1.76	.21
40.0	152	3.32	-15.4	-1.46	6.06	2.21	.43	8.34	20.1	-1.51	12.7	2.41	.43

TABLE D-2 (Continued)

Scan: B Intersection ht: 10 Km

Intersection		Antenna 1						Antenna 2					
R	α	f_x	f_y	f_z	τ	L	ℓ	f_x	f_y	f_z	τ	L	ℓ
50.8	238	10.8	-15.5	-3.0	23.7	5.8	.56	6.5	22.7	-4.5	30.2	4.7	.56
20.	238.	11.3	-12.4	-6.2	19.8	5.62	.24	9.81	18.4	-9.2	8.73	1.52	.24
1.0	238	12.1	-1.3	-13.0	19.7	5.62	.11	11.2	1.72	-17.3	4.0	.85	.11
20.	58	12.9	12.4	-6.2	23.0	5.81	.24	7.3	-19.0	-9.5	7.3	1.3	.24
50.	58	12.6	15.4	-3.0	28.2	6.3	.55	3.0	-23.3	-4.7	25.9	4.0	.55

TABLE D-2 (Continued)

Scan: B Intersection ht: 10 Km

Intersection		Antenna 3						Antenna 4					
R	α	f_x	f_y	f_z	τ	L	ℓ	f_x	f_y	f_z	τ	L	ℓ
50.8	238	20.6	-11.4	-3.4	55.8	8.9	.56	-12.2	0.	-14.6	1.27	.32	.56
20.0	238	20.2	-9.07	-6.8	30.3	5.11	.24	.63	0.	-9.4	1.39	1.45	.24
1.0	238	13.0	-.92	-13.8	11.1	2.8	.11	10.7	0.	-14.8	5.87	1.60	.11
20.0	58	3.7	9.7	-7.3	4.6	2.6	.24	23.0	0.	-7.3	46.0	7.0	.24
50.	58	.92	15.0	-4.5	5.2	1.9	.55	24.1	0.	-3.8	221.	33.2	.55

TABLE D-2 (Continued)

Scan: B Intersection ht: 3.0 Km

Intersection		Antenna 1						Antenna 2					
R	α	f_x	f_y	f_z	τ	L	ℓ	f_x	f_y	f_z	τ	L	ℓ
50.8	238	10.8	-15.8	-.93	23.5	5.84	.55	6.6	23.0	-1.37	29.3	4.6	0.55
20.0	238	11.2	-13.6	-2.05	19.4	5.6	.22	10.3	19.9	-3.0	7.8	1.4	.22
1.0	238	11.9	-3.9	-12.	18.6	5.61	.034	12.4	4.4	-13.4	2.84	.73	.034
20.0	58	13.0	13.6	-2.0	22.9	5.8	.22	7.7	-20.6	-3.1	6.4	1.18	.22
50.	58	12.7	15.6	-.94	28.1	6.3	.54	3.0	-23.7	-1.4	25.0	3.9	.54

TABLE D-2 (Continued)

Scan: B Intersection ht: 3.0 Km

Intersection		Antenna 3						Antenna 4					
R	α	f_x	f_y	f_z	τ	L	ℓ	f_x	f_y	f_z	τ	L	ℓ
50.8	238	20.8	-11.6	-1.02	56.7	8.9	0.55	-12.4	0.	-13.	.33	.09	.55
20.0	238	21.1	-9.9	-2.2	33.9	5.6	.22	.057	0.	-3.2	.40	4.0	.22
1.0	238	15.1	-2.7	-12.2	12.0	2.8	.034	8.33	0.	-12.5	4.01	1.62	.034
20.	58.	3.0	10.5	-2.3	3.8	2.8	.22	24.3	0.	2.5	142.0	21.4	.22
50.	58	.90	15.2	-1.3	4.9	1.9	.54	24.4	0.	-1.29	960.	144.	.54

(b) The total delay spread τ becomes excessive for backscatter modes of operation. This is only important however if the spatial resolution ΔL is correspondingly reduced to a value much less than ℓ, which causes a severe loss in signal strength. A large value of τ is not too difficult to handle if a tapped delay line processor with sliding taps is implemented. Furthermore, it may be true that only a portion of the delay range corresponds to an interesting spatial region.

(c) The ability to distinguish between vertically and horizontally induced Doppler effects is highly desirable, due to the predominance of z velocity components in rain, and x and y components in aircraft and atmospheric turbulence. The ratio of f_x/f_z is maximized by choosing to operate in a backscatter mode, while it is minimized by operating in a forward scattering mode. Ratios of about 8:1 are possible in extreme cases. In the vertical mode (Fig. D-8c) horizontal and vertical velocity components cannot be distinguished, although a transverse velocity v_y will give zero contribution. (This is approximately true for all Great Circle Paths).

(d) For the orthogonal path geometry shown in Fig. D.9, all three Doppler coefficients are found to be of the same general magnitude. There may be some advantage however in using both the great circle and orthogonal geometries in obtaining sensitivity to both of the orthogonal horizontal velocity components.

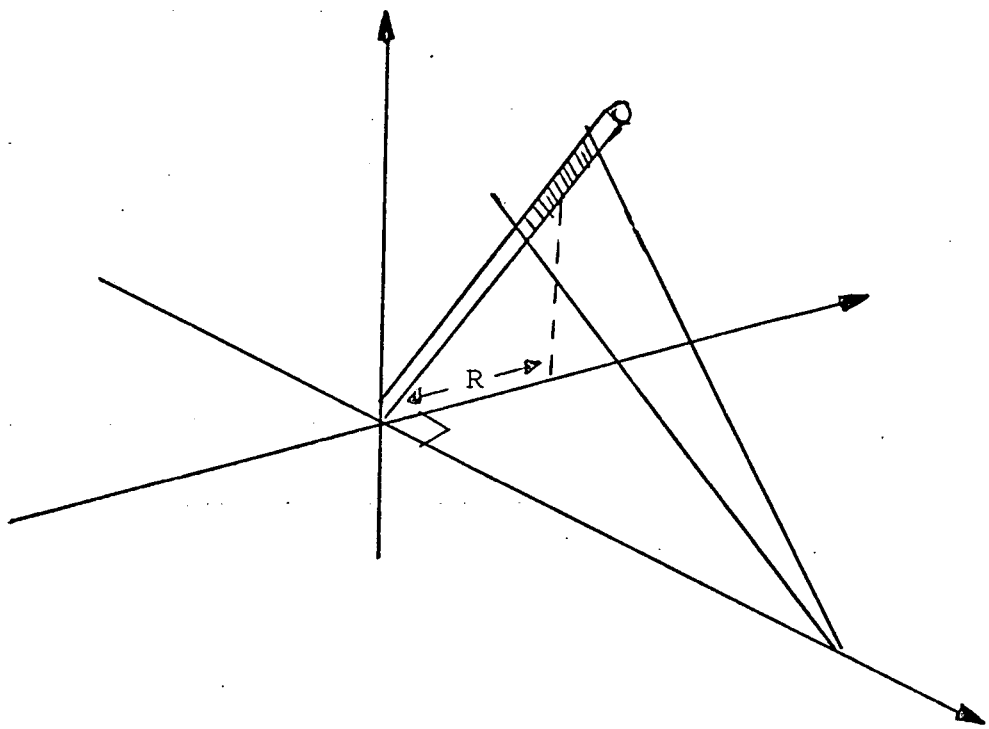

Fig. D.9 Orthogonal Mode

D.3.4 Evaluation of an Orthogonal Configuration

As a test case the sample configuration shown in Fig. D.10 was run. Two different values of D show the sensitivity involved in selection of this parameter.

Parameters of interest are,

$D = 180, 90$ Km

$\epsilon = 1.45^{\circ}$ Transmitting beam widths

$BW = 0.5^{\circ}$ ES Beamwidth

$h = 7.0$ Km Intersection height

r was varied over a range corresponding to a minimum ES evaluation angle of 30°. The results are shown in Table D-3.

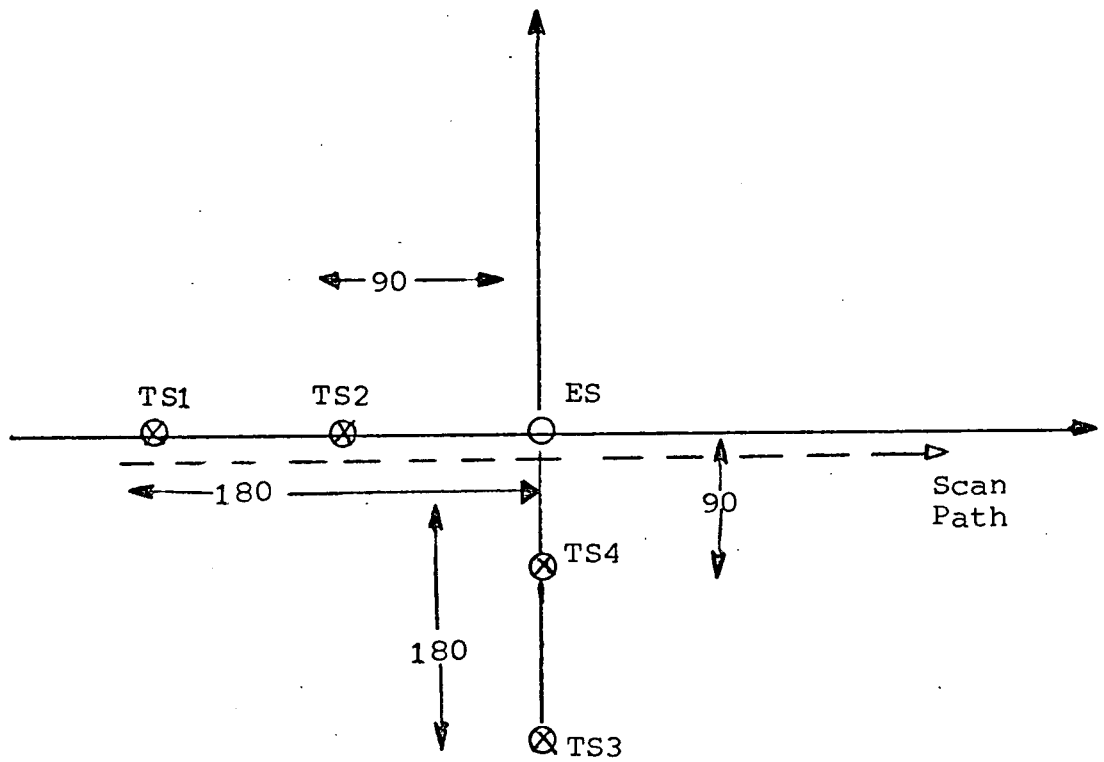

Fig. D.10 Orthogonal configuration.

TABLE D-3

Scan: A Intersection ht: 7.0 Km

Intersection		Antenna 1						Antenna 2					
R	α	f_x	f_y	f_z	τ	L	ℓ	f_x	f_y	f_z	τ	L	ℓ
12.	0	3.5	0.	-14.5	4.15	7.9	.12	3.41	0.	-15.8	2.11	3.42	.12
8.0	0.	6.4	0.	-18.5	5.8	6.33	.093	6.31	0.	-19.7	2.95	2.9	.093
4.0	0	13.1	0.	-23.9	9.02	5.02	.07	13.0	0.	-25.	4.63	2.41	.07
1.0	0	22.3	0.	-27.1	13.6	4.56	.062	22.2	0.	-28.1	7.07	2.26	.062
1.0	180.	29.6	0.	-27.1	18.3	4.66	.062	29.6	0.	-28.1	9.6	2.37	.062
4.0	180.	38.9	0.	-23.9	28.0	5.49	.07	38.8	0.	-24.8	15.0	2.88	.07
8.0	180.	45.5	0.	-18.4	44.8	7.56	.093	45.5	0.	-19.3	24.7	4.12	.093
12.0	180.	48.4	0.	-14.4	64.6	10.3	.12	48.4	0.	-15.2	36.9	5.84	.12

f = 7.8 GHz

TABLE D-3 (Continued)

Scan: A Intersection ht: 7.0 Km

Intersection		Antenna 3						Antenna 4					
R	α	f_x	f_y	f_z	τ	L	ℓ	f_x	f_y	f_z	τ	L	ℓ
12.	0	25.9	24.5	-14.3	16.5	4.6	.12	25.6	26.2	-15.3	8.9	2.33	.12
8.	0	25.9	21.0	-18.3	16.1	4.57	.093	25.8	22.1	-19.3	8.6	2.31	.093
4.	0	26.0	13.6	-23.9	15.9	4.56	.07	25.9	14.2	-24.9	8.34	2.30	.07
1.	0	26.0	3.87	-27.1	15.8	4.56	.062	25.9	4.01	28.1	8.24	2.3	.062
1.	180	26.0	-3.8	-27.1	15.8	4.56	.062	25.9	-4.01	-28.1	8.24	2.3	.062
4.	180.	26.0	-13.6	-23.9	15.9	4.56	.07	25.9	-14.2	-24.9	8.34	2.3	.07
8.	180.	25.9	-21.0	-18.3	16.1	4.57	.093	25.8	-22.1	-19.3	8.6	2.31	.093
12.	180.	25.9	-24.5	-14.3	16.5	4.58	.12	25.6	-26.2	-15.3	8.96	2.33	.12